Development of a Current Limiter Using Vacuum Arc Current Commutation

Phase 2: Maximizing the Current Rating of a Single 72-kV Device Using a Minimum Amount of Parallel Capacitance

---

EL-1221
Research Project 564-3

Final Report, October 1979

Prepared by

WESTINGHOUSE ELECTRIC CORPORATION
Research and Development Center
1310 Beulah Road
Pittsburgh, Pennsylvania 15235

Principal Investigator
C. W. Kimblin

Authored by
C. W. Kimblin
J. G. Gorman
F. A. Holmes
P. R. Emtage
J. V. R. Heberlein
R. E. Voshall

Prepared for

Electric Power Research Institute
3412 Hillview Avenue
Palo Alto, California 94304

EPRI Project Manager
J. W. Porter
Electrical Systems Division

ORDERING INFORMATION

Requests for copies of this report should be directed to Research Reports Center (RRC), Box 50490, Palo Alto, CA 94303, (415) 961-9043. There is no charge for reports requested by EPRI member utilities and affiliates, contributing nonmembers, U.S. utility associations, U.S. government agencies (federal, state, and local), media, and foreign organizations with which EPRI has an information exchange agreement. On request, RRC will send a catalog of EPRI reports.

NOTICE

This report was prepared by the organization(s) named below as an account of work sponsored by the Electric Power Research Institute, Inc. (EPRI). Neither EPRI, members of EPRI, the organization(s) named below, nor any person acting on their behalf: (a) makes any warranty or representation, express or implied, with respect to the accuracy, completeness, or usefulness of the information contained in this report, or that the use of any information, apparatus, method, or process disclosed in this report may not infringe privately owned rights; or (b) assumes any liabilities with respect to the use of, or for damages resulting from the use of, any information, apparatus, method, or process disclosed in this report.

Prepared by
Westinghouse Electric Corporation
Pittsburgh, Pennsylvania

ABSTRACT

Phase 1 showed the feasibility of developing a current limiter using vacuum arc current commutation. In concept, the electrodes of a vacuum device would be separated during the fault current rise, and the subsequent application of a transverse magnetic field would cause the arc current to commutate into a parallel capacitor and ultimately into a parallel current limiting resistor. The feasibility of commutating at arc current levels to 8.5kA was demonstrated. However, the parallel capacitance was prohibitively large at 300μF.

The objective of Phase 2 has been to increase the commutation current of a single 72kV device while also reducing the value of the parallel capacitance. The program has been largely experimental in nature, although a parallel theoretical effort has provided device and circuit guidelines. A total of 14 prototype vacuum devices were designed, built and evaluated, and the major parameters varied were device geometry, characteristics of the parallel circuit, electrode actuation speed, waveshape of the applied transverse magnetic field, point on wave of electrode separation, and the use of series connected vacuum interrupters. Progress can be determined by comparing the commutation levels with Phase 1. For the earlier 15kV circuit, the commutation level increased to 14.5kA for a parallel capacitance of 50μF. In particular, commutation levels of 12kA (50μF) were observed in circuits where the transient recovery voltage of 50kV approximated the transient associated with a 72kV circuit. Here, the necessary conditions of rapid electrode separation were approximated by actuation to 2cm in 1.4ms. Analysis involving assumptions about the actuator and sensor characteristics indicates that the present device could reduce by half the fault currents associated with 72kV/10kA and possibly 72kV/15kA circuits. A Phase 3 program is recommended aimed at further improving the device performance, and in particular at developing a concept for a 145kV fault current limiter.

EPRI PERSPECTIVE

PROJECT DESCRIPTION

As power systems grow, short-circuit currents also grow, which increases the stresses on the system and the cost of newly installed equipment. In addition, it can overstress existing equipment, necessitating costly change-out. This Phase 2 report describes the progress made in the development of a device that would limit the magnitude of short-circuit current in the event of a fault. It was preceded by EPRI report EL-393, which described the Phase 1 effort; it is expected that another report will be issued at the conclusion of Phase 3.

PROJECT OBJECTIVES

The goal of Phase 1 of this project, which started in July, 1975, and culminated in December, 1976, was to demonstrate the principle of vacuum arc fault current commutation. This was achieved at modest current and voltages (i.e., 8.5 kA and 15 kV) but required a prohibitively large parallel capacitor (300 μf). The objective of Phase 2 was to increase the current that can be commutated while reducing the amount of capacitance required to 50 μf or less, and to do this under conditions which simulate a practical 72-kV circuit. The period of Phase 2 was from January, 1977, until June, 1979.

PROJECT RESULTS

The goals outlined for Phase 2 were achieved. The parallel capacitance required was reduced to 50 μf, and the current commutation level was increased to 14.5 kA at voltages representative of a 72-kV application. An important feature of this concept is that it operates much like a conventional circuit breaker, i.e., it is a multishot device that does not require a bypass switch. The concept should also prove useful for dc circuit breaker applications.

Phase 3 has as its goal a further increase in performance and a conceptual design for a prototype 145-kV device that can be used to evaluate device application and cost. Phase 3 is expected to be completed in May, 1980.

J. W. Porter, Project Manager
Electrical Systems Division

ACKNOWLEDGMENT

The authors gratefully acknowledge the assistance and contributions of the many participants in this program. Dr. P. G. Slade of the Power Interruption and Lamp Technology Department provided valuable guidance and technical consultation during the course of the program. Mr. S. J. Cherry and Mr. P. O. Wayland of the Westinghouse Industrial and Government Tube Division manufactured the sealed vacuum devices, and took an active interest in the design of the devices. Mr. J. J. Bonk of the Westinghouse Transmission and Distribution Systems Engineering group assisted in the analysis of circuit transients and in the determination of device ratings. Mr. R. T. Innis of the Westinghouse Distribution Apparatus Division provided expertise in the application of capacitors to current limiting devices. We also thank Messrs. B. W. Powell, E. R. Hardy, R. P. Sabol and M. Mastorovich for their technician assistance during the experimental stages of this study, and Ms. K. Burkhart for typing the final report. Ms. L. Massaro is acknowledged for assistance in assembling the final report. We wish especially to thank Dr. N. Hingorani, Mr. R. E. Kennon, and Mr. J. W. Porter of EPRI for their valuable suggestions and guidance during the course of this program. We also gratefully acknowledge the helpful comments of the Utility Advisors: Mr. P. L. Kolarik, Mr. O. Compton, Mr. L. Long, Mr. L. Edwards, and Mr. R. C. St. Clair.

CONTENTS

APPENDICES

FIGURES

FIGURES (Continued)

FIGURES (Continued)

FIGURES (Continued)

FIGURES (Continued)

FIGURES (Continued)

FIGURES (Continued)

FIGURES (Continued)

LIST OF TABLES

LIST OF TABLES (Continued)

SUMMARY

There is a stated need by the Electric Utilities for fast acting current limiting devices which insert appreciable impedance into power circuits. Insertion of this impedance during the initial rise of fault current reduces the fault current peak, and simplifies the interruption requirements of conventional circuit breakers. Reduction of the fault current peak also reduces the electromagnetic forces which would otherwise damage circuit components such as power transformers. line traps, bus structures, disconnect switches, and breakers.

In a program with the Electric Power Research Institute, we are developing a current limiter using vacuum arc current commutation. We are presently reporting our progress in Phase 2 of this program which is concerned with maximizing the current rating of a single 72kV device using a minimum amount of parallel capacitance.

In the concept for current limitation which was developed in Phase 1, the electrodes of a vacuum device are separated during a fault current rise, and a stable vacuum arc burns in the metal vapor evaporated from the electrodes. When the electrodes have been rapidly separated to a spacing of 2 to 3 centimeters, a magnetic field is applied transverse to the arc path. This field causes arc instability with a resulting rapid rise in the arc voltage. In the presence of a parallel capacitor, this causes current diversion (commutation) from the vacuum device. After the vacuum arc is extinguished the circuit current continues to flow into the capacitor, and ultimately flows through the parallel current limiting resistor. The resistive drop results in high voltages being impressed across the vacuum device electrodes. However, the arc does not reignite since vacuum arcing devices are associated with a rapid dielectric recovery. This approach to a current limiter is attractive because (a) the continuous current is carried by an in-line device (b) the device is not polarity sensitive (c) the apparatus for causing a forced arc extinction can be isolated from line potential and (d) high voltages can be withstood by relatively short electrode spacings. This simplifies the actuator mechanism.

At the end of Phase 1 we had demonstrated the feasibility of commutating from the vacuum device into the parallel capacitance at arc current levels to 8.5kA.

However, the parallel capacitance for this current level was prohibitively large (300μF). Further, the feasibility was demonstrated in circuits with recovery voltages of peak value $\leq$ 15kV whereas operation of a fault current limiter in a practical 72kV circuit would result in peak recovery voltages of $\geq$ 50kV. In addition, the transverse field was usually applied 4ms after the instant of electrode part. This was necessitated by the relatively slow speed actuators available for the experiments, and the consequent long time period to attain the required electrode separation of 2 to 3cm. Other features of Phase 1 were the use of prototype vacuum devices with ceramic envelopes of $\leq$ 18cm diameter, and the application of magnetic fields with fast risetimes to an essentially constant value. Despite these restrictions, Phase 1 provided a solid framework for proceeding with Phase 2. High speed movies of arc-magnetic field interactions, together with a theoretical interpretation of the interactions, laid a good foundation for relating the magnitude of fault current which could be commutated from the vacuum device to parameters such as the magnetic field strength B, the rate of change of magnetic field strength $\dot{B}$, the magnitude of the parallel capacitance, and the electrode spacing at the instant of field application.

The objective of Phase 2 has been to increase the commutation current while also reducing the value of the parallel capacitance. Further objectives have been to simulate the conditions which would be observed in a practical fault current limiter operating in one phase of a 72kV circuit; namely with electrode separation to 2cm in 1.5ms or less, and with recovery voltages of about 50kV.

Four principal steps were involved in the experimental program:

- Step #1. Continuation of Phase 1, using different electrode geometries.
- Step #2. Experiments with oscillatory magnetic fields in low voltage ($\leq$ 15kV) circuits.
- Step #3. Experiments with oscillatory magnetic fields in low voltage ($\leq$ 15kV) circuits with a conventional vacuum interrupter in series with the transverse field device.
- Step #4. Use of oscillatory magnetic fields and series vacuum interrupter in practical circuits.

In Step #1 the magnetic field rose in an essentially linear manner to a constant value. The rate of rise of field was higher than in Phase 1, and the ceramic envelopes were 18cm or 23cm in diameter. The peak recovery voltage was limited to 15kV, and the speed of electrode separation was slow (2cm in 4ms). When a 50μF parallel capacitor was used, the current commutation limit was less than 9kA.

In Step #2 a large transverse magnetic field was made to oscillate at high frequency. The interaction of the arc with the field caused oscillations in the current in the parallel circuit, and the arc was observed to extinguish when the arc current oscillated through zero. The peak recovery voltage was still limited to 15kV, and the speed of electrode separation remained somewhat slow (2cm in 3ms). With a 50μF parallel capacitor, the current commutation limit was 10kA.

In Step #3 a conventional vacuum interrupter was connected in series with the limiter to help withstand the recovery voltage. The transverse magnetic field was made to oscillate, and the peak recovery voltage was still limited to 15kV. With a 50μF parallel capacitor, the current commutation limit was 14.5kA. With a 25μF parallel capacitor, the limit was 9kA.

In Step #4 the ceramic envelopes were 30.5cm in diameter, and the separation to 2cm in $\leq$ 2ms was achieved by moving both electrodes. The test circuits were arranged to give recovery voltages of 50kV after current interruption; a conventional vacuum interrupter again being connected in series with the limiter to help withstand the recovery voltage. When an oscillatory magnetic field was used together with a 50μF parallel capacitor, the current commutation limit was 12kA.

The final Phase 2 concept for a current limiting system involves a vacuum limiter in series with a conventional vacuum interrupter. When a fault is detected, the electrodes of both devices are rapidly separated to a distance of 2cm in 1.5ms, and a high frequency oscillating magnetic field is applied transverse to the electrode axis of the limiter. In the presence of a capacitor in parallel with the series-connected devices, the arc current is forced to fluctuate. At a current zero, the arc will extinguish in the series-connected devices, and the circuit current will continue to flow into the capacitor and ultimately through the parallel current limiting resistor.

In developing a rating for the present current limiting system, we have made assumptions concerning the sensor characteristics and the availability of an actuator capable of separating electrodes to 2cm in 1.5ms following the sensor signal. Here it must be emphasized that the present experimental program has only simulated this electrode separation by moving each of the two electrodes in the prototype devices. This provides an accurate representation of the arcing conditions, but in practice a more sophisticated actuator would be required with movement of only one electrode. In developing a rating, we have also chosen to consider the fault current limiter applied at either the transformer secondary terminals

of a 72kV system, or in the bus tie breaker position. We have further assumed that the fault current limiter is capable of commutating at current levels to 14.5kA; the highest level attained in Phase 2 for a parallel capacitance of 50μF. For these particular circuit studies, we conclude that the limiter would be effective in reducing by half the potential fault current in circuits of between 72kV/10kA and 72kV/15kA rms available current.

We consider that the fault current commutation limit, and reliability, could both be improved by additional experimental and theoretical investigations. A further goal would be reduction in the magnitude of the parallel capacitance. We further consider that the present current limiting system should be evaluated as a module for a 145kV device, with two of the modules connected in series for 145kV operation.

Our specific recommendations for future work on this vacuum-arc current limiter concept involve three parallel efforts.

- Experimental evaluation of additional prototypes.
- Analysis to determine the recovery voltage associated with a 145kV module and the overall 145kV rating.
- Conceptual design of a prototype 145kV three-phase current limiting device.

With respect to a conceptual three-phase design, we recommend the layout of an overall 145kV current limiting device. This device would be designed to meet the rating developed from the research evaluation of prototypes, and also the circuit analysis. The layout should be performed by personnel who are familiar with the packaging of capacitor banks and vacuum apparatus. However, research personnel would have to cooperate in selecting the type of vacuum devices required for 145-kV duty. For example, it may be reasonable to use two of the 72-kV devices connected in series. This would involve two transverse field devices and two conventional interrupters. Alternatively, it may be advantageous to use a single transverse field device in series with three conventional interrupters. The layout should include the transverse field devices, the series vacuum interrupters, the magnetic field coils and associated power supplies, the capacitor banks, the insulators, and the mounting platform. Reasonable assumptions would have to be made concerning the space and power required by the sensors and high speed actuators. The layout should include all the necessary power supplies and control circuitry for a functioning device.

This recommended continuation program would terminate with a final report which would summarize the progress, provide specifications which would permit the design and fabricating of a high-speed actuator, and contain a specific design of a prototype 145kV three-phase CLD having an established objective rating. This prototype design would also permit a cost estimate from which the economic feasibilities of this approach could be evaluated.

Section 1

INTRODUCTION

The present document is the Final Report in Phase 2 of our Vacuum Arc Current Limiter Program with the Electric Power Research Institute. The Phase 1 program was concerned with determining the feasibility of developing a current limiter using vacuum arc current commutation. This Phase 1 program has been fully documented (1). The Phase 2 program is concerned with maximizing the current rating of a single 72kV device using a minimum amount of parallel capacitance.

The technique for current limitation which was developed in Phase 1 is summarized in Figure (1-1). The electrodes of a vacuum device will be separated during a

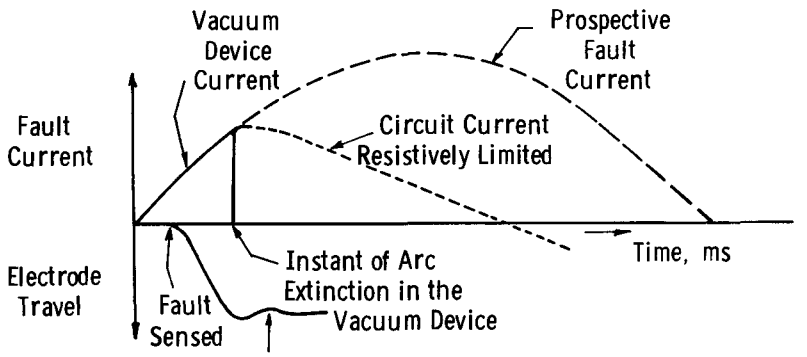

(a) Time Sequence of current commutation process

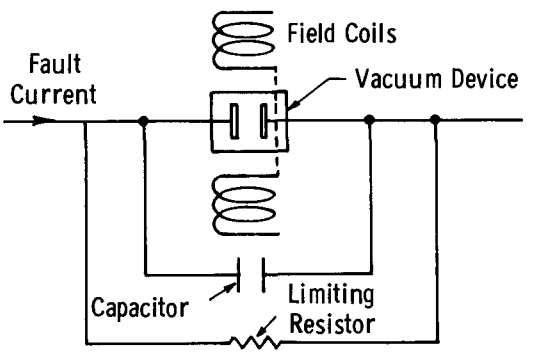

(b) Schematic of the Current Limiting Device

Figure 1-1 The technique of using transverse magnetic fields to force current commutation and limitation.

fault current rise, and a stable vacuum arc will burn in the metal vapor evaporated from the electrodes. When the electrodes have been rapidly separated to a spacing of 2 to 3 centimeters, a magnetic field will be applied transverse to the arc path. This field causes arc instability with a resulting rapid rise in the arc voltage. In the presence of a parallel capacitor, this causes current diversion (commutation) from the vacuum device. After the vacuum arc is extinguished the circuit current continues to flow into the capacitor, and ultimately flows through the parallel current limiting resistor. The resistive drop results in high voltages being impressed across the vacuum device electrodes. However, the arc does not reignite since vacuum arcing devices are associated with a rapid dielectric recovery.

At the end of Phase 1 we had demonstrated the feasibility of commutating from the vacuum device into the parallel capacitance at arc current levels to 8.5kA. However, the parallel capacitance for this current level was prohibitively large (300μF). Further, the feasibility was demonstrated in circuits with recovery voltages of peak value $\leq$ 15kV whereas operation of a fault current limiter in a practical 72kV circuit would result in peak recovery voltages of $\geq$ 50kV. In addition, the transverse field was usually applied 4ms after the instant of electrode part. This was necessitated by the relatively slow speed actuators available for the experiments, and the consequent long time period to attain the required electrode separation of 2 to 3cm. Other features of Phase 1 were the use of prototype vacuum devices with ceramic envelopes of $\leq$ 18cm diameter, and the application of magnetic fields with fast risetimes to an essentially constant value.

The objective of Phase 2 has been to increase the commutation current while also reducing the value of the parallel capacitance. Further objectives have been to simulate the conditions which would be observed in a practical fault current limiter operating in one phase of a 72kV circuit; namely with electrode separation to 2cm in 1.5ms or less, and with recovery voltages of about 50kV.

Four principal steps were involved in the experimental program:

- Step #1. Continuation of Phase I, using different electrode geometries.
- Step #2. Experiments with oscillatory magnetic fields in low voltage ($\leq$ 15kV) circuits.
- Step #3. Experiments with oscillatory magnetic fields in low voltage ($\leq$ 15kV) circuits with a conventional vacuum interrupter in series with the transverse field device.
- Step #4. Use of oscillatory magnetic fields and series vacuum interrupter in practical circuits.

A schematic diagram of the current limiting device that results from this work is shown in Figure 1-2. The principal differences from Phase 1 are the use of larger diameter prototypes devices, the application of an oscillating magnetic field, and the presence of a series connected vacuum interrupter.

Section 2 of this Phase 2 report deals with the theory of current commutation from vacuum arcs subjected to transverse magnetic fields. The theory first deals with the influence of a linearly rising magnetic field, and a detailed description of the subsequent arc structure and current flow appears in Appendix A. Section 2 then continues with a phenomenological description of arc/circuit interactions in the presence of an oscillating transverse magnetic field. A circuit analysis re-

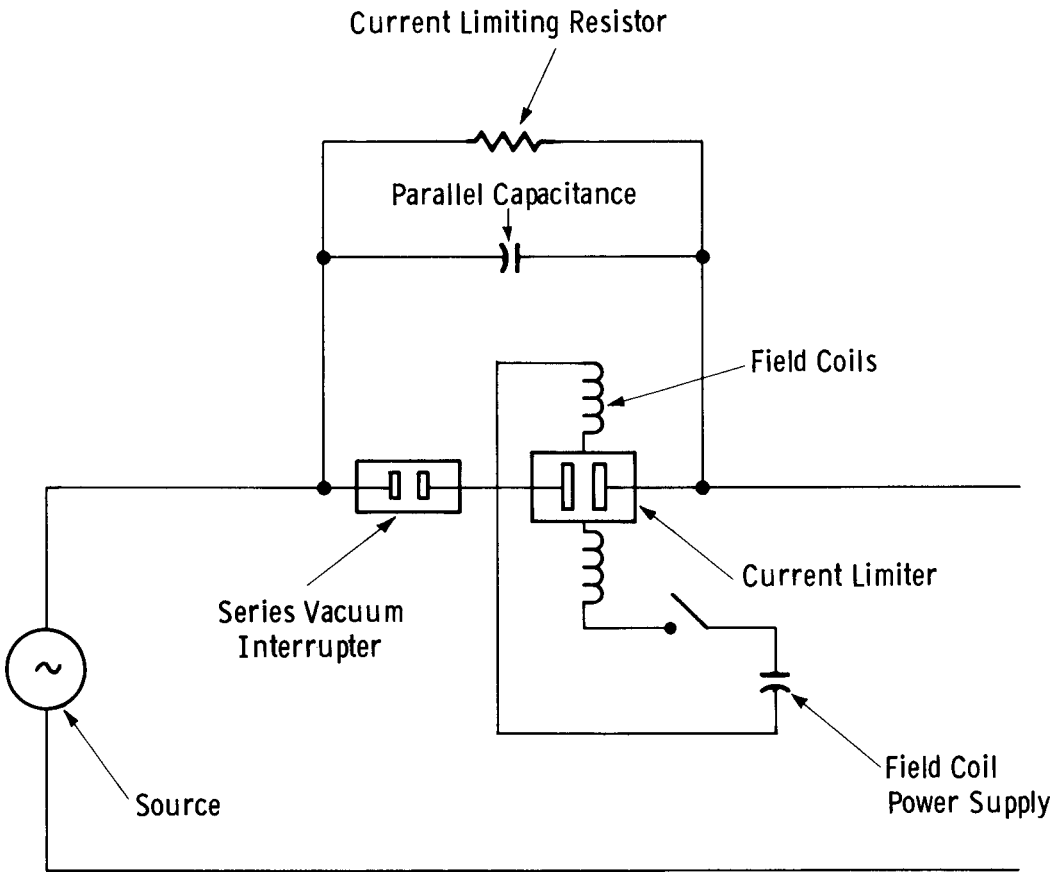

Figure 1-2. Single phase representation of a vacuum current limiter resulting from Phase 2.

lated to the current oscillations appears in Appendix B, and an empirical model for the arc voltage in the presence of an oscillating field appears in Appendix C.

Section 3 provides an overall description of the experiments conducted during Phase 2. Subsection 3-1 gives details of the experimental apparatus, and in particular describes the parallel capacitors, repulsion coil actuators, magnetic field coils, demountable arc chamber, and, in Table 3-1, the prototype vacuum devices. This table should prove of particular value to the reader. The table summarizes the physical characteristics of each prototype, and the experimental program performed on each prototype. Further, the table references the appropriate Subsections in Section 4 which deal with the experimental results for the particular prototype. Section 3 concludes with Subsection 3-2 which provides a brief description of the experimental parameters investigated.

Section 4 provides an extensive description of the experiments performed on the fourteen prototypes and presents the results of those experiments. The material is arranged in essentially chronological order, with experimental data obtained on the first prototypes preceding data appropriate to later prototypes. Experiments which do not lend themselves to this format, but which are worthy of record, appear in Appendix D. The Subsections of Section 4 which relate to step #3 of the Phase 2 program, and which are consequently of most interest, are 4-3.2, 4-4, 4-7 (oscillating field), 4-4.2, 4-7 (series interrupter) and 4-6, 4-8, 4-9, 4-10 (high speed actuation).

Section 5 essentially condenses the experimental data of Section 4 into results of value for a 72kV device. In this Section, each parameter of significance is allocated two paragraphs. The first is a statement concerning our conclusion or recommendation concerning the particular parameter. The second contains possible qualifiers to that statement, together with cross-references to places in the text which support the statement.

Section 6 is concerned with the potential rating of the present vacuum arc current limiter. It is shown that the rating not only involves the maximum current which can be commutated from the device, but also involves assumptions concerning the sensor trip setting, the sensor discrimination time, and the actuator speed. The overall electrical circuit also has to be considered with due consideration of both symmetric and asymmetric faults. Subsection 6-5.4 is concerned with the fault current limiter applied at either the transformer secondary terminals of a 72kV system, or in the bus tie breaker position. For these particular circuit studies, the limiter is effective in reducing by half the potential fault currents in circuits of between 72kV/10kA and 72kV/15kA rms available current.

The overall conclusions from this Phase 2 program appear in Section 7, and recommendations for future work at 145kV appear in Section 8. Here the overall current limiting module resulting from Phase 2 would be used in a series connected system for fault current limiting in 145kV circuits.

Section 2

THEORY OF CURRENT COMMUTATION

2-1 INTRODUCTION

The following section contains both the basic theory of an arc in a transverse magnetic field, and a phenomenological description of the extinction of high current arcs.

The first part of the theory, Section 2-2, describes the physics of an arc in a constant magnetic field, and the extinction of arcs by a uniformly increasing magnetic field. The second part, Section 2-3, concerns the extinction of an arc by an oscillating magnetic field.

A detailed calculation of the structure of an arc in a transverse magnetic field is presented in Appendix A. This calculation has led to a substantial revision of our previous estimate of the field at which current extinction begins, and to various other changes. The arc theory that was presented in our final report on Phase I has therefore been rewritten in Section 2-2, to allow both a coherent presentation of the theory as a whole and a comparison with experimental results that are now available.

The basic theory holds for arcs in which the initial current is less than 5-8kA. At higher currents, commutation cannot be achieved by a uniformly increasing magnetic field, and it is found that a current continues to flow even when the magnetic field is large, provided that the arc voltage is sufficiently great.

The phenomenological theory of Section 2-3 proceeds from the observed arc voltage as a function of magnetic field, and is applied primarily to arcs in which the initial current exceeds 6kA. It is shown that the introduction of oscillations in the magnetic field gives rise to an oscillatory voltage that can drive high current arcs to extinction.

2-2. PLASMA PHYSICS OF CURRENT COMMUTATION

2-2.1 The Hall Field

The interelectrode space in a diffuse vacuum arc is filled with a highly conductive neutral plasma emitted by the cathode spots, which are sources of both ions and electrons. A transverse magnetic field can cause extinction when the magnetic force is strong enough to force the interelectrode plasma out of contact with one or both of the electrodes.

The essential element of the theory is the Hall field E_H, see Figure 2-1a, which is the transverse electric field needed to maintain current flow across magnetic lines of force in a plasma that is almost free of collisions (see Appendix A). If the electron current density is j_x and the magnetic field B_z, the Hall field is

$$E_H = -j_x B_z / ne \qquad (2\text{-}1)$$

where n is the density of electrons.

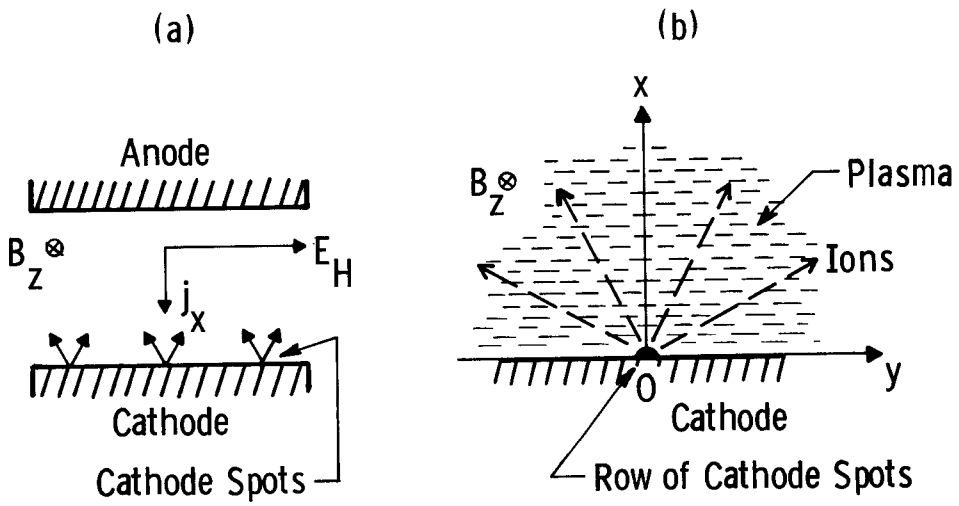

Figure 2-1. (a) Electrode configuration, showing fields and currents. (b) "Rigid" plasma in a magnetic field.

We can show that this field is independent of both distance and current in the case of a plasma emitted radially from a cathode spot, assuming that the electron current is radial (it is shown in Appendix A that this presumption does not hold,

but we retain it here so as to estimate the average strength of the Hall field). Suppose, for simplicity, that ions and electrons are emitted isotropically into a hemisphere; at a distance r from a spot that emits a current $-I_e$ of electrons one has

$$j = -I_e/2\pi r^2 \quad .$$

Associated with the electrons is a current I_i of ions; let their mean velocity be u_i and their mean charge $\bar{Z}$. Then, from the condition of electrical neutrality within the plasma, we find

$$n = \bar{Z}n_i = I_i/2\pi r^2 e u_i \quad .$$

Therefore, Eq. (2-1) yields

$$E_H = \frac{I_e}{I_i} u_i B_z \quad . \tag{2-2}$$

But the ratio of electron to ion current, I_e/I_i, is constant for a given cathode material, and is roughly equal to 10 for most materials (2). The mean Hall field therefore depends on the magnetic field alone, and is independent of the total current and of distance from the cathode.

Most of the mass of the plasma is made up of the ions, and the envelope of the plasma is determined by the ion trajectories. The total transverse force on an ion is the sum of Lorentz and Hall forces, which act in opposite directions

$$F_i = \bar{Z}e(-u_i B_z + E_H) = \bar{Z}e u_i B_z \left(\frac{I_e}{I_i} - 1 \right) \quad . \tag{2-3}$$

i.e., the total force on the ions is, on average, equal to the Amperian force on the current, and is opposite in sense to the Lorentz force on the ions. The Hall force exceeds the Lorentz force by the factor $I_e/I_i \simeq 10$; even when the current density is not uniform, we may expect the mean Hall field to dominate the plasma structure.

Finally, we note that the Hall field, being an electric field, gives rise to an alignment of the cathode spots, an effect qualitatively different from the effects expected from magnetic forces alone. In the case of Cu we have (2) $I_e/I_i = 11$ and (3) $\bar{Z} = 2$, the ion energy being 30 eV/unit charge; therefore, $E_H = 35$ V/cm when $B_z = 0.05$T, which is a typical value. This transverse field is large, and if the cathode spots were to remain spread over the cathode, as in Figure 2-1a,

the Hall field would cause a variation in sheath potential as one moved across the cathode. However, there is only one sheath potential, of approximately 20V, at which the cathode spots can burn stably. It follows that the cathode spots can be expected to lie on or near that line, parallel with B, on which the voltage is 20V. This is the line 0 in Figure 2-3b (ion trajectories are shown as straight lines in this sketch, because the regions of greatest curvature have not yet been determined).

It has been found that the Hall field constrains all, or most, of the cathode spots to lie near a single line of force across the cathode. The initial position of this line, when the magnetic field is first applied, is probably such that it passes through the center of gravity of the current distribution on the cathode. Thereafter, as is usual in a vacuum arc, the spots move in the retrograde sense (i.e., opposite to the direction of the Amperian force on the current) until either the arc is extinguished or they reach the side of the cathode.

2-2.2 The Plasma Configuration and the Threshold Field

The shape of the plasma in a magnetic field is calculated in Appendix A, and the result is shown in Figure 2-2. There is a dense region near the plasma boundary that results from the reflection of ions by the boundary, and all reflected ions lie between the boundary and the curve marked "reflection envelope". We expect, therefore, that the plasma in a magnetic field will contain a bright luminous column extending from the cathode and bent in the forward direction, i.e. in the direction of the Amperian force on the total current.

An observed plasma structure is shown in Figure 2-3, and is similar to the calculated picture. The observed plasma is, however, markedly more diffuse than is calculated, probably as a result of interionic collisions and of irregularities in the distribution of cathode spots.

The greatest height reached by the plasma in a field B_z is, from Eq. (A.14),

$$d_H = 1.43 \frac{I_i}{I_e} \frac{V_i}{u_i B_z} \quad , \tag{2-4a}$$

where V_i is the voltage that accelerates the ions into the plasma. The general form of this result follows directly from the Hall force of Eq. (2-3). If an ion on the outer boundary of the plasma is acted on by the force F_i at right angles to its motion, it moves in a circle of diameter d_i, where

$$d_i = \frac{2Mu_i^2}{F_i} = 4 \frac{I_i}{I_e} \frac{V_i}{u_i B_z} \quad , \quad \left(I_e >> I_i\right) \quad . \tag{2-4b}$$

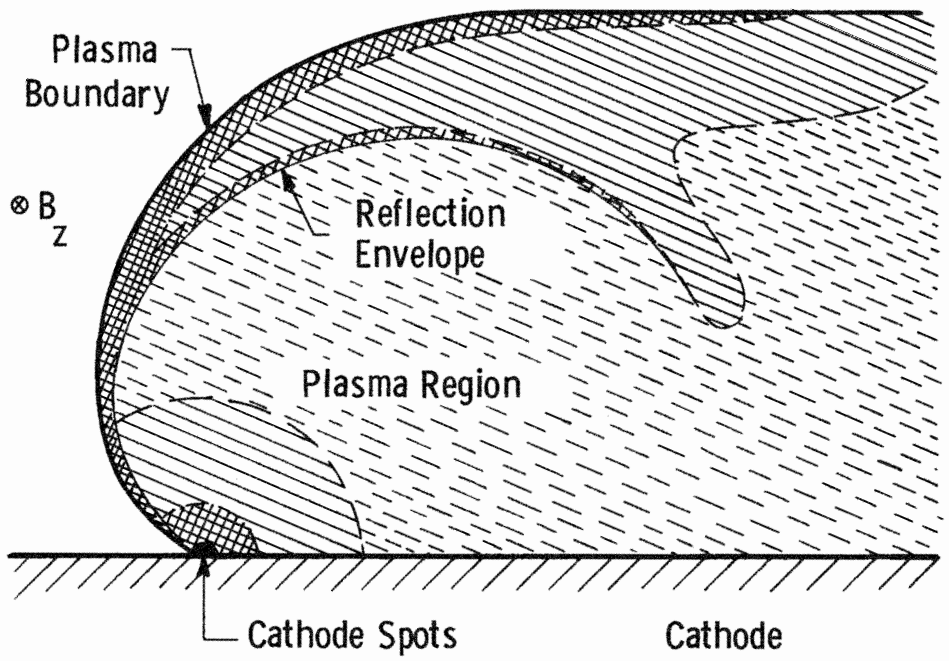

Figure 2-2. Calculated plasma structure, with hatching to indicate the density. The anode, which is omitted, either intersects the plasma before it reaches its greatest height, or is just above the upper boundary.

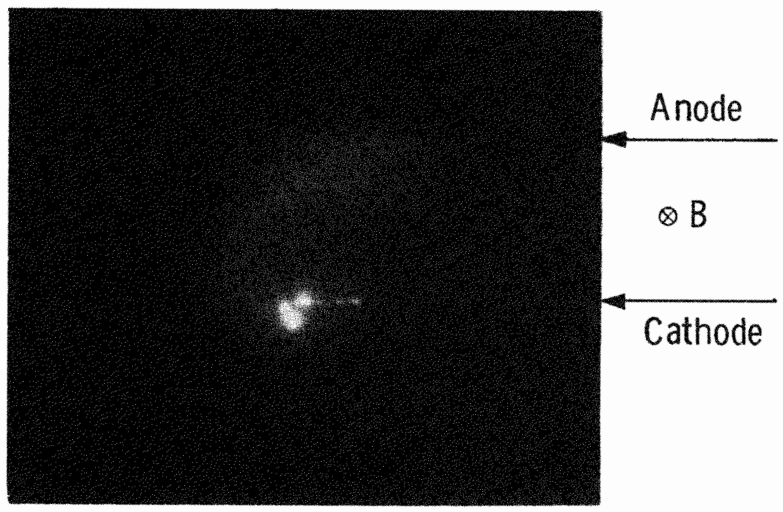

Figure 2-3. Observed plasma structure in a magnetic field of 0.03T; the electrode separation is 2cm.

This argument gives the algebraic form of the plasma height correctly, but with a large numerical error that results from the extreme non-uniformity of the current distribution; the entire electron current is in fact confined to a thin shell on the outer edge of the plasma (see Appendix A).

The threshold field B_c for the beginning of arc extinction occurs when the height d_H of the plasma is equal to the separation d_o of the electrodes. In the case of Cu electrodes, where V_i = 30V, $\bar{Z}$ = 2, and I_e/I_i = 11, Eq. (2-4a) yields

$$B_c = 0.034/d_o \quad , \tag{2-5}$$

where B_c is measured in Tesla and d_o in centimeters.

An extension of this result to rapidly rising magnetic fields is given in Eq. (A-16). When B_z increases at a rate $\dot{B}$ it is found that the threshold field is increased according to the relation

$$B_c(\dot{B}) = B_c + \tau_f \dot{B} \tag{2-6}$$

where $\tau_f = 2d_o/u_i$ is the mean time of flight of the ions from cathode to anode, and B_c is given by Eq. (2-5).

Observed values of B_c are compared with theory in Figure 2-4. The calculation appears to underestimate the effect of rapid rates of increase in the field.

The above mechanism, in which the arc is separated from the anode by a relatively large magnetic field, is the principal means of arc extinction. A low field mechanism does exist, when the line of spots marches in the retrograde sense across the cathode, over the edge, and then beneath it, thereby separating the plasma from the anode. This low field mode of extinction has been observed, and is most effective at low currents; we shall not consider it hereafter.

2-2.3 Current Extinction

Current extinction begins when the field reaches the threshold value given by Eq. (2-5). During extinction the current and ion density vary rapidly with time, so the plasma diameter need not be the steady-state diameter of Eq. (2-4a).

To find the diameter of a time-dependent arc one must return to Eq. (2-1) for the Hall field. On equating the force on the ion due to this field with the centrifugal force, as was done in deriving Eq. (2-4b), one finds

$$d_p \sim M_i u_i^2/ZeE_H \sim V_i en(t)/B(t)j(t) \quad .$$

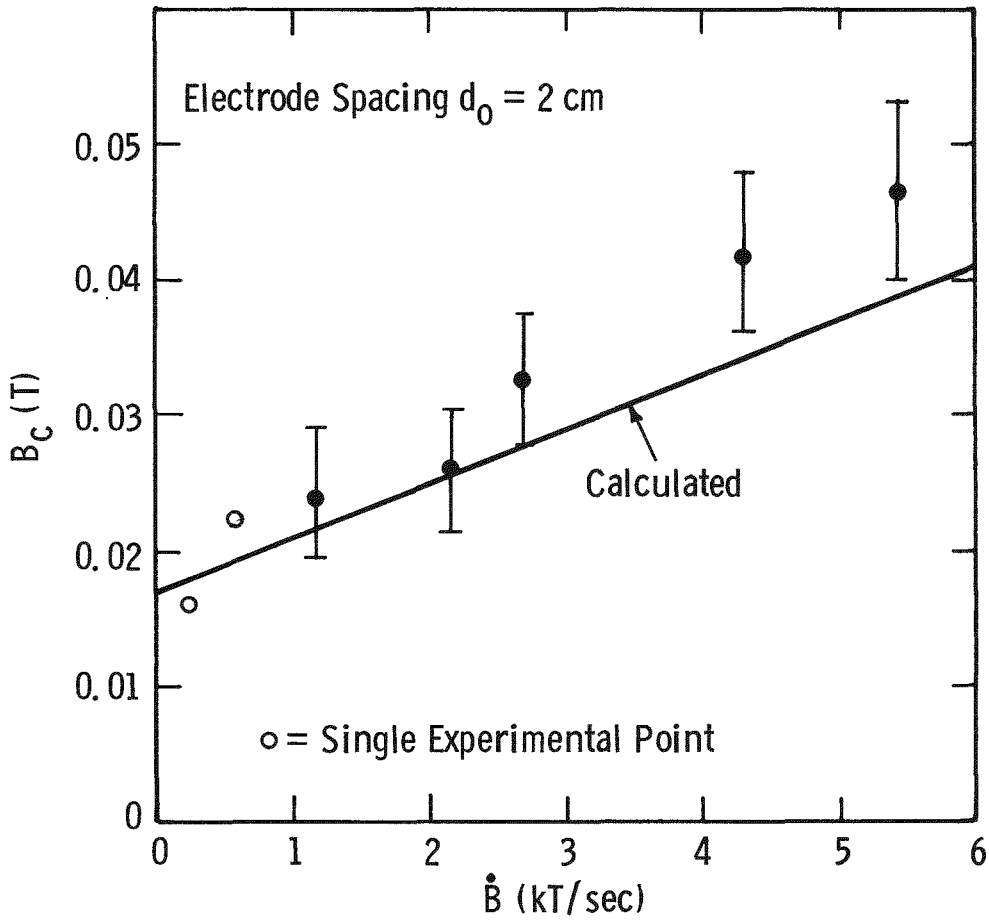

Figure 2-4. Dependence of the threshold field, B_c, on the rate of rise of field, $\dot{B}$.

This expression can be reduced to Eq. (2-4) for d_i, the steady-state diameter, if $n(t) \sim j(t)$ at all times. However, the electron density, $n(t)$, is determined by the ion density, and ions near the anode at time t were emitted at time $t - \tau_f$, where $\tau_f \simeq 2d_o/u_i$ is the time of flight of the ions. The electron density therefore corresponds to the current at time $t - \tau_f$, i.e.,

$$n(t) = \frac{dn}{dj}\, j(t - \tau_f) \quad .$$

Therefore, if I(t) is the total current

$$d_p = d_o \frac{I(t-\tau_f)}{I(t)} \frac{B_c}{B(t)} \quad . \qquad (2\text{-}7)$$

Note, for currents independent of time, that $d_p = d_o$ when $B = B_c$, in agreement with the definition of the threshold field B_c in Eq.(2-5).

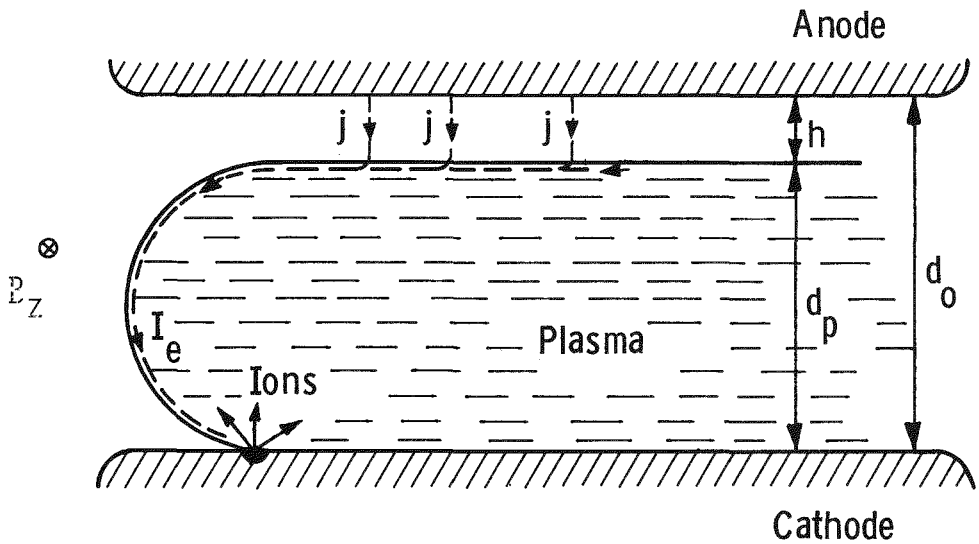

Fig. 2-5. Sketch of plasma during extinction.

The plasma configuration during extinction is sketched in Figure 2-5; the leading edge of the plasma is curved until it reaches a height d_p at the point of closest approach to the anode. Thereafter, the plasma has a straight boundary more or less parallel with the anode, and there is a gap of height

$$h = d_o - d_p \tag{2-8}$$

between anode and plasma. The current has to flow across this gap, and the resultant voltage serves to commutate the arc current into a parallel network.

The trailing edge of the plasma has been taken to be parallel with the anode because this is the only available equilibrium of the system. If the plasma bent further towards the anode, the gap h would disappear, and no substantial voltage could be developed in the system, while if the trailing edge bent away from the anode the electron current would not be able to cross the increased gap and a large space charge would develop upon the trailing edge of the plasma.

The voltage that commutates the current into the external circuit is developed across the gap between plasma and anode. During most of the turn-off the current density across the gap is high, and the voltage is the space-charge-limited voltage given by Child's equation for a vacuum diode

$$V_{SCL} = Aj^{\frac{2}{3}}h^{\frac{4}{3}} \quad , \tag{2-9}$$

where $A = 5690\ V/(amp)^{\frac{2}{3}}$, j is the mean current density within the gap, and h is measured in cm. The peak current density j, which will be needed later in calculating the maximum heating of the anode, is calculated in Appendix A, see Eq. (A-18); its value is

$$j = \frac{3\sqrt{3}}{4} \frac{I}{\ell d_o} \quad , \tag{2-10}$$

where I is the total current and ℓ is the length of the active line of spots on the cathode.

We will now calculate the current waveform during current commutation, taking into account the effect of the parallel circuit. Consider first the case where the external circuit is of very low impedance. The gap h must now be small, since otherwise, from Eq. (2-9), a large voltage would develop across it and a current greater than I_o, the initial current, would flow in the external circuit. Accordingly, we may set $d_p = d_o$ in Eq. (2-7). We approximate the magnetic field as increasing linearly with time during current extinction.

$$B(t) = B_c + \dot{B}t \quad ,$$

t being measured from the time the field reaches the threshold value B_c, and then solve Eq. (2-7) to first order in τ_f under the condition $d_p = d_o$. The result is

$$I(t) = I_o e^{-2t^2/t_s^2} \tag{2-11}$$

where the switch-off time t_s is given by

$$t_s^2 = 4\tau_f B_c/\dot{B} = 5.72 \frac{M_i}{ZeB} \frac{I_i}{I_e} \quad . \tag{2-12}$$

Here M_i is the mass of the ions.

We shall now show, in a typical case, that t_s is little affected by an external circuit of finite impedance. Note that during current extinction we can set limits on the plasma diameter d_p; it must lie between d_o and d_i, d_i being the steady-state diameter of Eq. (2-4a), because Eq. (2-7) yields $d_p > d_i$ when the current is decreasing with time, while if d_p were to exceed d_o the gap h would vanish and no driving voltage could be developed. If d_p is close to d_i we have an essentially stationary condition and the arc current varies only slowly with time, while if d_p is close to d_o the arc current turns off as in Eq. (2-11). By way of example, take I_o = 5kA, d_o = 2cm, ℓ = 10cm, $\dot{B}$ = 650 T/sec, and let the parallel circuit be a capacitance C = 10μF. If the current falls according to Eq. (2-11), then $I = \frac{1}{2} I_o$ at t = 12μsec; at this time the charge on the capacitor from the diverted current gives rise to a voltage of 1200V, which must equal V_{SCL}. The current density in the gap is now 125A/cm^2, so from Eq. (2-9) we find h = 0.029cm. But, at this time, the calculated value of the steady state plasma diameter d_i is 1.56cm, so $d_o - d_i$ = 0.44cm. Therefore, it is indeed the case that $h = d_o - d_p \ll d_o - d_i$, so the condition $d_p \simeq d_o$ is a satisfactory approximation during turn-off. A more careful calculation, including both capacitance C and associated stray inductance L_C, shows that t_s is increased by less than 10% provided C > 10μF and L_C < 20μH.

Figure 2-6 shows a comparison of observed and calculated switch-off times, t_s, for values of $\dot{B}$ up to 6000 T/sec. The observed times obey the predicted rule $t_s \sim 1/\dot{B}^{1/2}$ reasonably well, but are about 30% greater than the calculated times.

Note that the switch-off time, t_s, as defined above, is <u>not</u> the total time for current extinction; rather, it is the time in which most of the current reduction occurs, i.e., the interval in which the current falls from 94% to 6% of its initial value. The extinction time is greater than t_s and is not readily calculable, since its value depends to some extent on the instability time of low current arcs.

<u>Voltage</u>

These theoretical considerations indicate that the external circuit has little effect on the process of current extinction, provided its impedance is not unreasonably large. In the short time of current extinction we may take it that the total current into the limiter and its associated circuits remains constant at I_o. The current between the electrodes, I(t), is then given by Eq. (2-11) after switch-off has begun, and the current flowing into the associated parallel circuit is I_o-I(t). Also, the parallel resistor has little effect until the voltage has become large, so we need take account only of the parallel capacitance C and stray inductance L_C. At

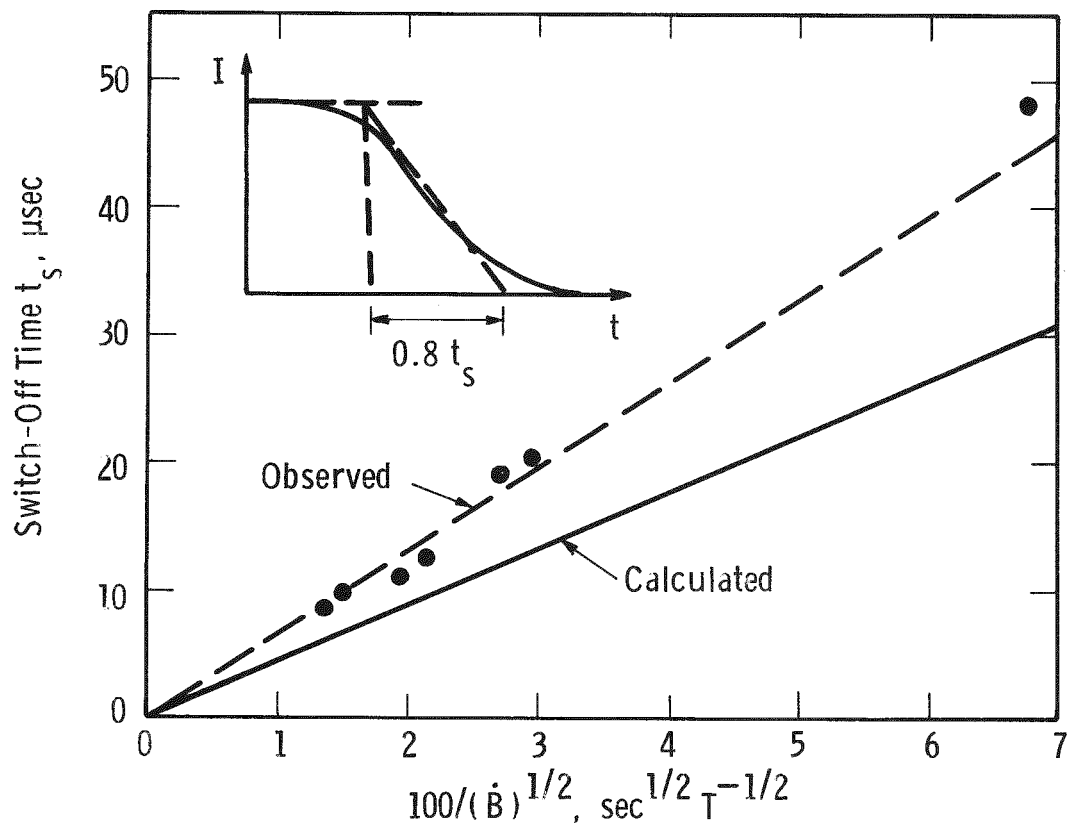

Figure 2-6. Dependence of the switch-off time, t_s, on the rate of rise of field, $\dot{B}$.

time t, the voltage demanded by this external circuit is

$$V = -L_C \frac{dI}{dt} + C^{-1} \int_0^t [I_o - I(t')]dt' \quad , \tag{2-13}$$

where I(t) is given by Eq. (2-11). The calculated evolution of arc current and voltage with time are shown in Figure 2-7, for the case of a 5kA arc with $\dot{B}$ = 1500 T/sec, C = 25μF, and L_C = 1.5μH; the calculated switching time t_s is 15μsec.

The voltage generated during extinction is not intrinsic to the arc in the above theory. Rather, the arc current falls in a manner that is governed by the magnetic field, and the space charge region of the arc generates whatever voltage is demanded

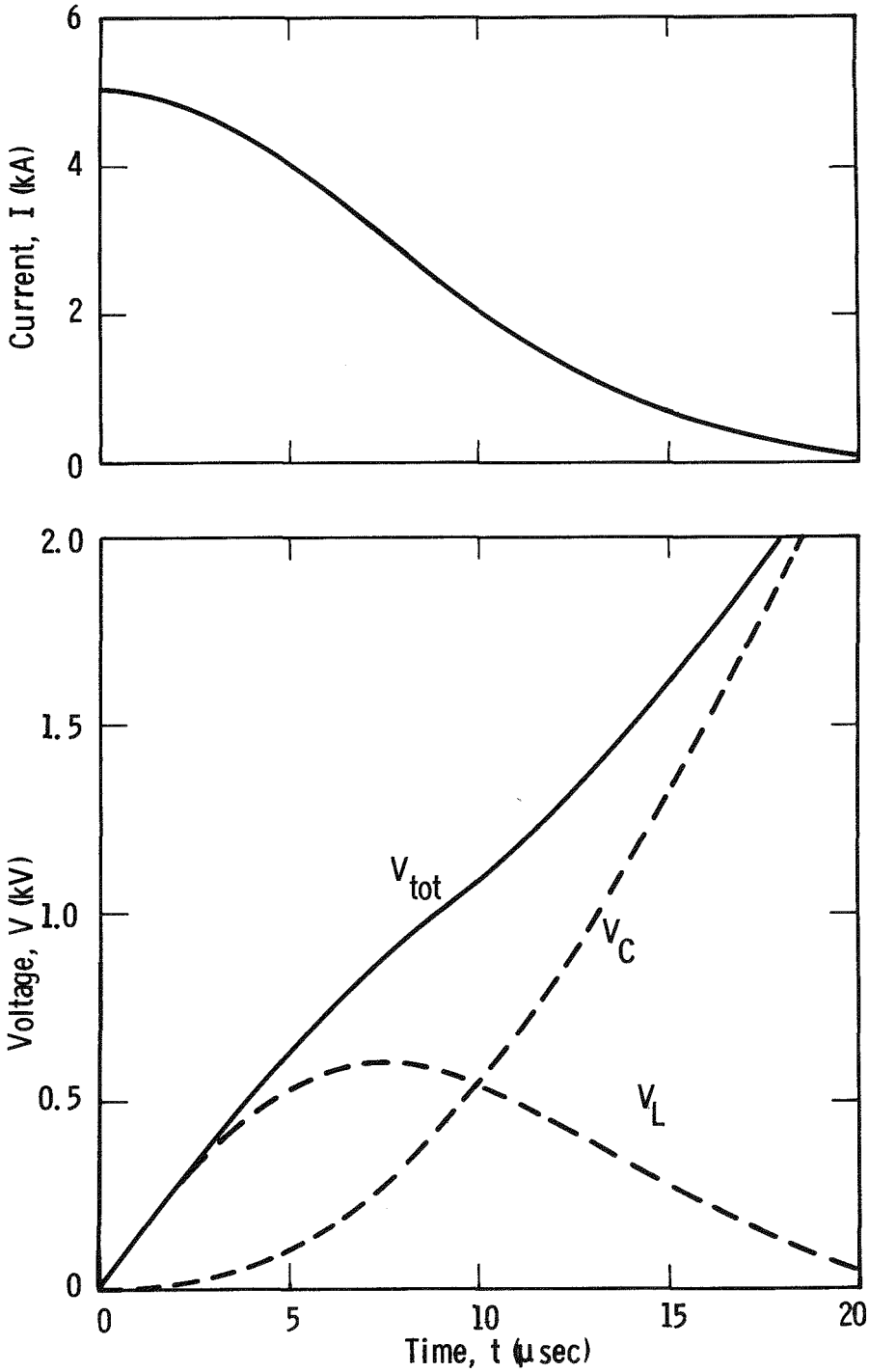

Figure 2-7. Calculated evolution of arc current and voltage with time, from the onset of extinction; I_o = 5kA, C = 25μF, L_c = 1.5μH, $\dot{B}$ = 1500 T/sec.

by the external circuit. This point is illustrated in Figure 2-8, which shows current and voltage traces for two extinctions with similar values of I_0 and $\dot{B}$, but with different external inductances. The decrease in current is very similar in the two cases, though the peak voltages during extinction are 4kV in one case and 1.5kV in the other.

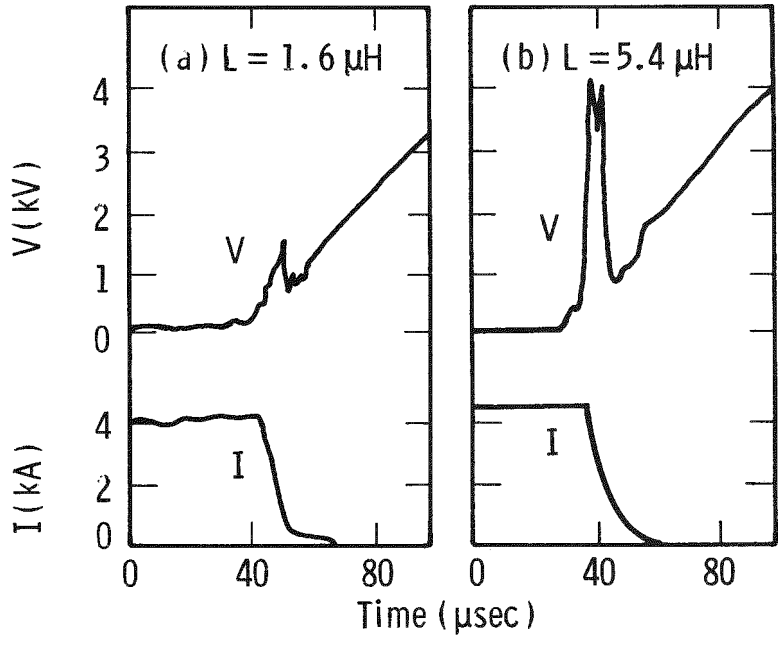

Figure 2-8. Observed similarity of current extinctions despite different voltages due to different external inductances, (a) L = 1.6μH and (b) L = 5.4μH. In both cases $\dot{B}$ = 4300 T/sec. and C = 50μF.

The onset of the extinctions in Figure 2-8 is sharp, with a discontinuity in the rate of change of current instead of the smooth variation of Figure 2-7. Such behaviour is associated with large values of $\dot{B}$, 4300 T/sec. in this case; it can be seen from Figure 2-4 that current extinction does not then begin until B is well above B_c, so there is a strong driving force on the current as soon as interruption begins.

2-2.4 Discussion

Successes of the Theory

The above theory gives a good description of the smooth extinction of an arc in a monotonically increasing magnetic field. The observed and calculated arc structures agree reasonably well, and we have calculated the threshold field, the extinction time, and the arc voltage with errors of less than 30%.

We have not, however, given any description of the limitations of this method of current commutation. The mechanism by which failure occurs at high currents was not anticipated and is not yet understood; we can do no better than to indicate the difficulties.

Expected Mechanism of Failure

When current flows across a high magnetic field and the voltage is moderate, plasma must span almost all of the interelectrode space, because a voltage of 80kV is required to drive an electron across a plasma free gap of 1cm in a field of 0.1T. Further, there is no mechanism by which a voltage-free plasma can carry a current across a high magnetic field; it is easy to show, from Eq. (A-13), that the ion momentum must become large if the current is to flow across a magnetic field much greater than the threshold field. A region within which some ions are accelerated to high energy is therefore required for failure to occur, and this region cannot be the cathode sheath because the plasma potential is positive.

We know of no mechanism by which a large voltage can be generated within the body of the cathode plasma; it was therefore expected that failure would result from the formation of an anode spot as a result of heating during extinction. An anode spot is a source of ions, and a high voltage between anode and plasma can supply the necessary energetic ions. From Eq. (2-4a), the voltage required is

$$V \simeq V_i (B/B_c)^2, \quad B \gg B_c \quad , \tag{2-14}$$

where B_c is the threshold field and V_i the voltage that accelerates the ions of a cathode spot, V_i = 30V; it has been presumed that the ratio I_e/I_i is the same for anode and cathode spots. From an estimate of the anode heating it was concluded that currents as high as 15kA could be interrupted smoothly, provided that the current density to the anode was uniform.

Observed Mechanism of Failure

A residual current of a few hundred amps often flows after most of a high current extinction is completed. This residual current can persist for many tens of microseconds, with subsequent reignition of the arc when the voltage becomes high, as shown in Figure 2-9a. At currents above 8kA the current usually does not become small, and there is no region of residual current, as is shown in Figure 2-9b.

The residual current results from the continued activity of a few spots on the cathode, for the following reasons: (i) The displacement current due to ions in the interelectrode space has been calculated, and found too small to sustain a residual current for more than 5μsec. (ii) Reignition does not occur if the residual current stops before a large voltage has developed, which indicates than an electrode is still active. (iii) The initial current is too low to ignite an anode spot, and if the anode were active we would expect prompt reignition of the main arc current rather than a lengthy residual current.

It is therefore possible for a current that originates on the cathode alone to persist across a high magnetic field, provided that the voltage is large, though the mechanism is not known. For this reason we anticipated that high current failures, without a region of very low current, also arose from a reorganization of the cathode plasma rather than from the development of anode activity; this expectation is confirmed by the fact that a subsequent forced current zero generally results in extinction.

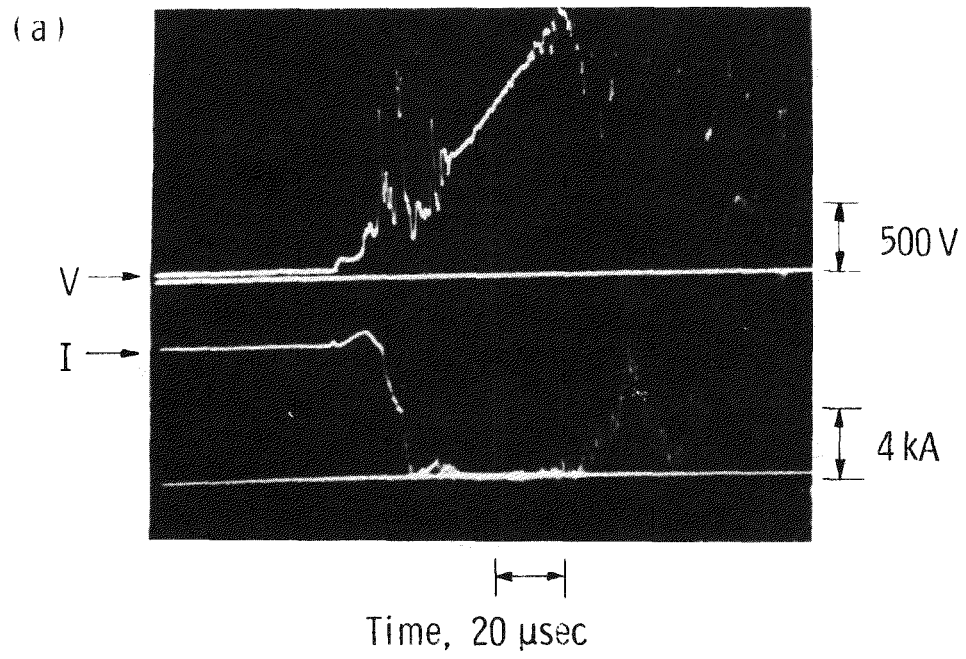

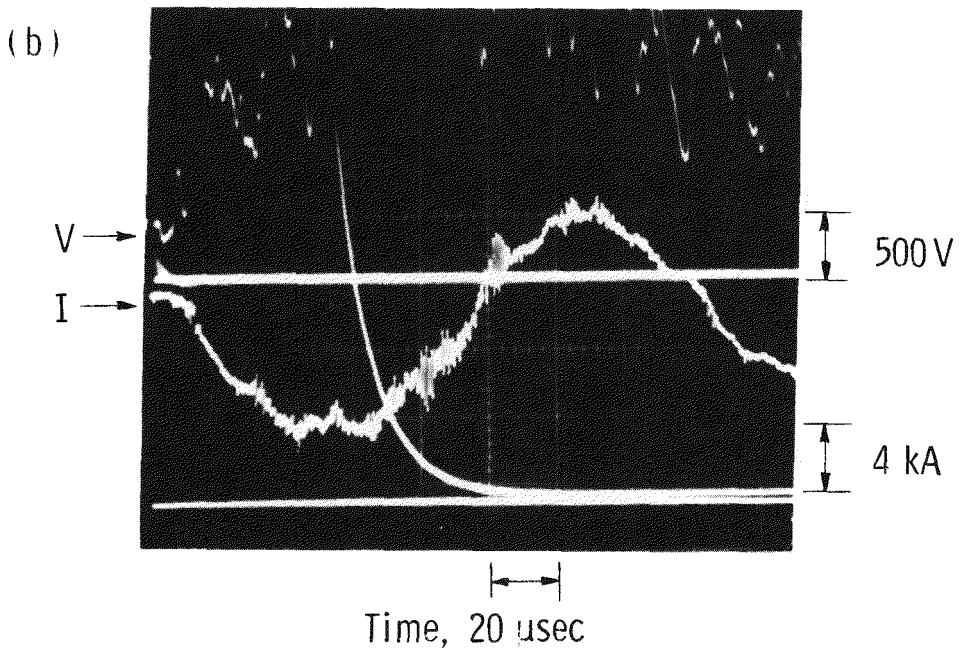

Figure 2-9. Principal types of failure. (a) Residual current leading to reignition (b) The current never becomes small.

2-3 PHENOMENOLOGICAL DESCRIPTION WITH AN OSCILLATING MAGNETIC FIELD

2-3.1 Introduction

When we are commutating relatively small currents or operating with a heavily damped magnetic field, the current in the sealed device is usually forced directly to zero. This is called a Mode 1 type of commutation and is illustrated in Figure 2-9. When we are using an oscillating magnetic field and are operating near the limit of the device, the arc current may fail to fall directly to zero and the current will subsequently increase. The arc current may then oscillate back towards current zero with a successful commutation on the second attempt. This is called a Mode 4 commutation and is illustrated in Figure 2-10. This process may continue a third time with the current oscillations growing until a commutation is achieved.

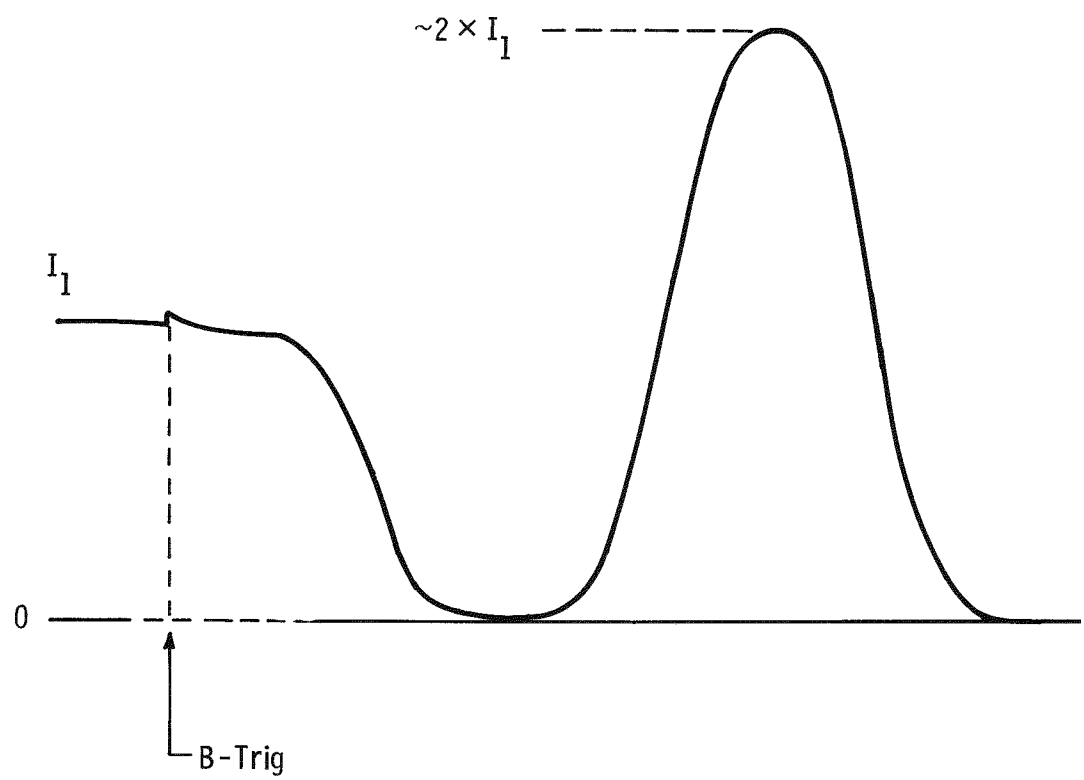

Figure 2-10. Illustration of a Mode 4 commutation.

The oscillograms of Figure 2-11 illustrate two experiments where the current was forced toward zero three times before successful commutation was achieved. These two oscillograms are not unusual and we have occasionally seen four and five excursions before successful commutation is achieved. Greater than five excursions usually leads to a failure.

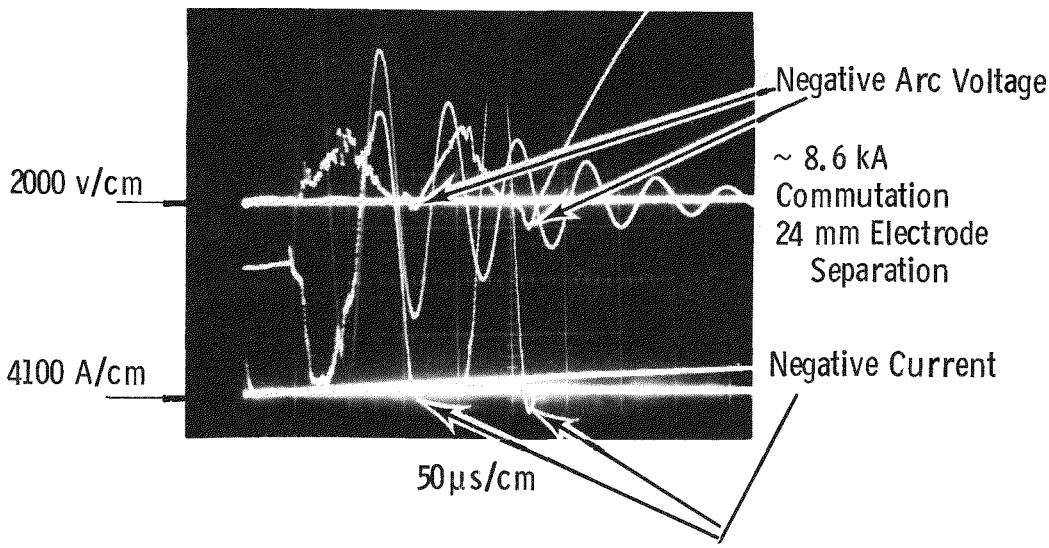

2-11 (a). 8.6kA Commutation.

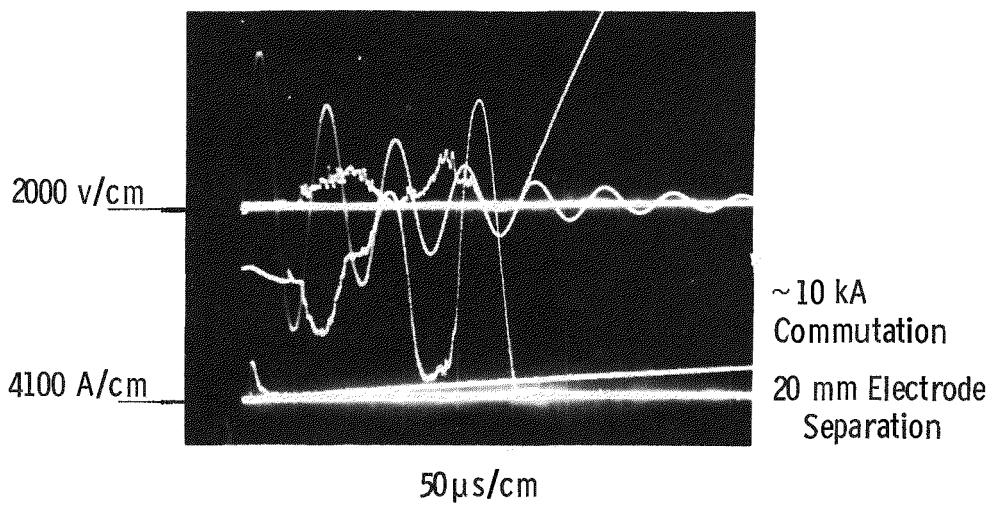

2-11 (b). 10kA Commutation.

Figure 2-11. Selected oscillograms from experiments with Prototype #5 showing increasing current oscillation leading to successful commutation; C_2 = 100μF, and B = 7200 T/S.

In Figure 2-11 (a) the current crosses zero after the second excursion and again after the third excursion. The arc voltage also changes sign. The final commutation takes place from a negative current. We have analyzed the two oscillograms of Figure 2-11 with the objective of approaching an understanding of this oscillatory phenomenon. The technique used to understand the increase of current oscillation was to set up a differential equation for the external circuit and measure the observed arc voltage. The differential equation was solved numerically using the observed arc voltage to calculate the evolution of current as a function of time. There was good agreement between calculated and observed current as illustrated in Figures 2-12 and 2-13. The details of this calculation appear in Appendix B.

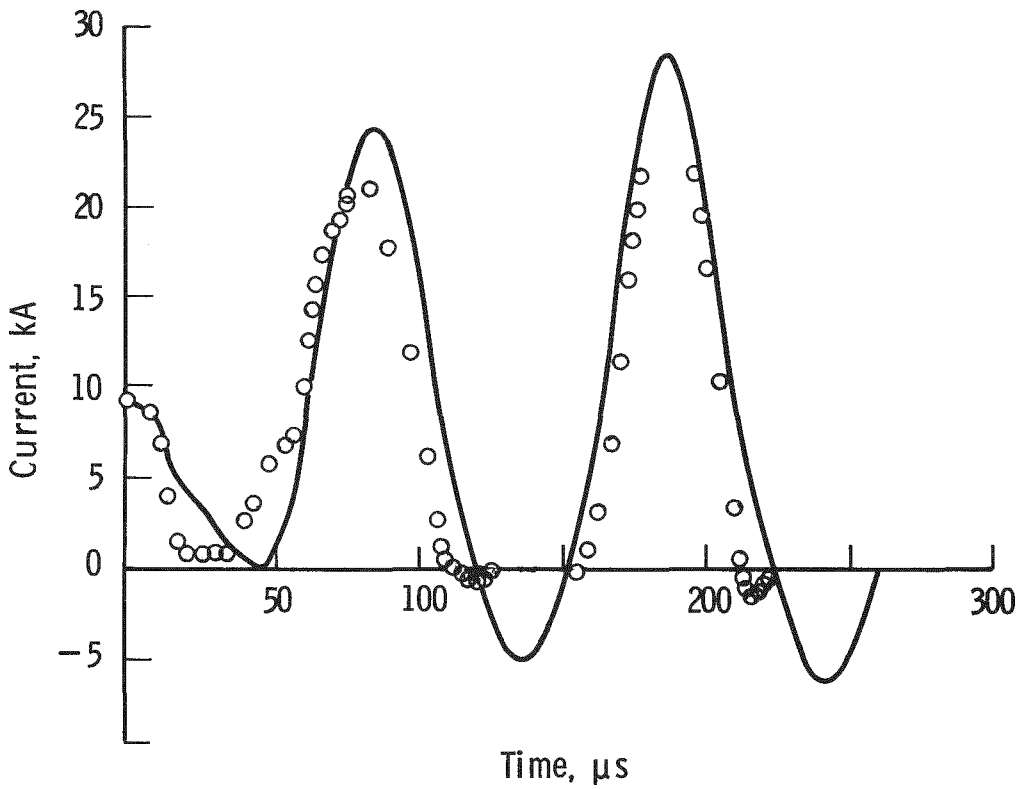

Figure 2-12. Comparison of experiment (o) with circuit analysis (solid line) for an 8.6 kA commutation C_2 = 100 μF and L_2 = 1.5 μH.

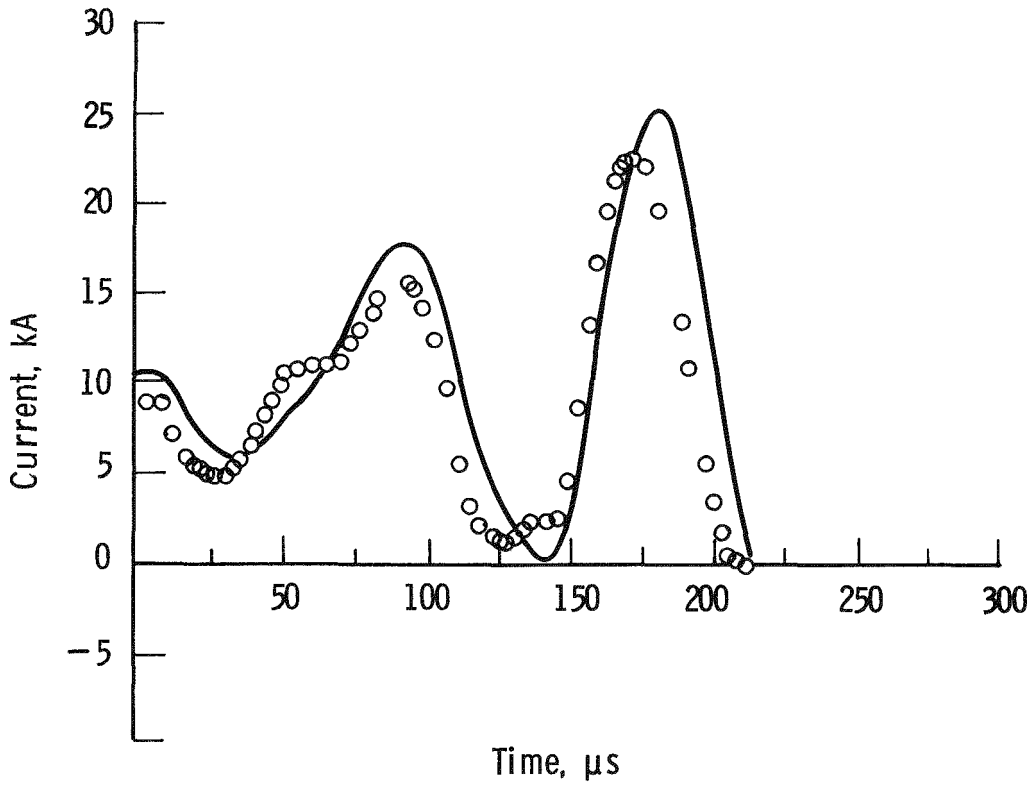

Figure 2-13. Comparison of experiment (o) with circuit analysis (solid line) for a 10kA commutation, C_2 = 100μF, and L_2 = 1.5μH.

2-3.2 Empirical Model

The voltage associated with continued current flow across a high field is a voltage intrinsic to the arc, unlike the voltage generated in a smooth extinction. In the absence of any adequate theory, we expect that the voltage will be of the order of that given in Equation 2-14. When d_o = 2cm, and B = 0.2 T, we find V ∿ 3kV.

A regression analysis of the arc voltage data from the two oscillograms shown in Figure 2-11 appears in Appendix C. The calculations show that the observed arc voltage is not a consistent function of current and each model selected fits the data almost as well if the arc current is neglected. The equation which gives the best fit to a logarithmetic transformation of the data has an exponent on B of nearly unity. However, applying an equation of the form

$$V_a = KB^2 \qquad (2\text{-}15)$$

accounts for almost 70% of the variance for a given oscillogram and because of the better agreement with what one would expect from the theory we suggest using an equation of this form to model the arc voltage. We suggest a value for K in equation 2-15 of approximately 3.5×10^4, hence

$$V_a = 3.5 \times 10^4 B^2 \quad . \tag{2-16}$$

From a limited amount of data, the actual value for K in equation 2-15 could lie between 2.5×10^4 and 5×10^4 depending on the arc length associated with continued current flow across a high magnetic field and the magnitude of the current prior to the application of the magnetic field. As an example, the best value for K for the upper oscillogram of Figure 2-11 is 4.6×10^4 or

$$V_a = 4.6 \times 10^4 \tag{2-17}$$

and for the lower oscillogram

$$V_a = 2.8 \times 10^4 \tag{2-18}$$

Equation 2-17 is compared with the arc voltage data in Figure 2-14 and a similar comparison of equation 2-18 with arc voltage data appears in Figure 2-15. Comparing equation 2-17 with 2-18 serves as a rather dramatic example of the difficulty of developing a universal equation for arc voltage when there is continued current flow. In both oscillograms of Figure 2-11 the electrode separation, electrode design, external circuit, magnetic flux density, etc. are all the same. The only significant difference is the magnitude of current prior to the application of the magnetic field. The initial arc current in the upper oscillogram is 8.6kA and in the lower oscillogram is 10kA.

We have run experiments with the magnetic flux density, B, oscillating at several different frequencies and with external circuits resonant at various frequencies. In all cases the general form of the arc voltage equation, 2-15, appears to be valid.

2-3.3 Discussion

There is very good agreement between theory and experimental observation when the arc follows a smooth extinction. When the arc does not follow a smooth extinction we may see the arc current increase. Once this has occurred, the voltage associated with continued current flow across a high magnetic field is a voltage intrinsic to the arc. At this point, the theory has reduced utility and we must resort to empirical techniques to obtain useful information. The interaction between the current limiting

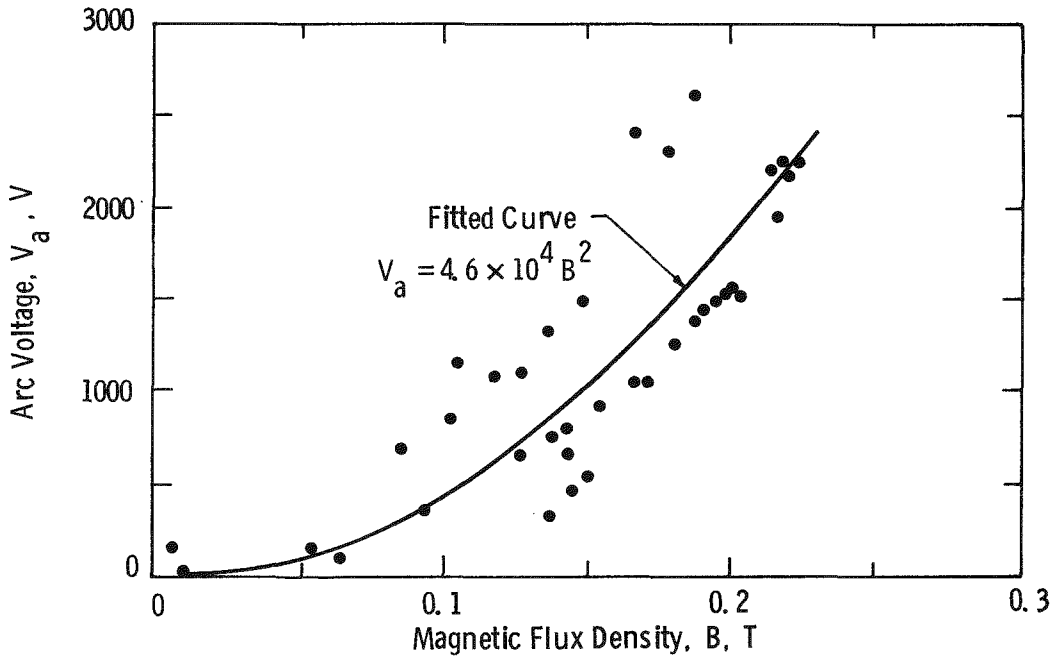

Figure 2-14. Plot of the arc voltage data from the upper oscillogram in Fig. 2-11.

device and the external circuit is well understood and given the arc voltage, we can calculate the arc current as a function of time.

In section 2-3.2 and Appendix C we treat the arc voltage as the dependent variable and use regression techniques to develop an empirical equation for arc voltage as a function of magnetic flux density. This equation applies, strictly speaking only for the experimental condition studied. Different electrode design or electrode separation would yield a somewhat different coefficient in the equation, but the form of the equation is useful for predicting how a current limiter will behave in a somewhat different circuit. Further, equation 2-16 is useful for predicting the current oscillation when the magnetic flux density, B, oscillates at a frequency other than the frequency used in this experiment.

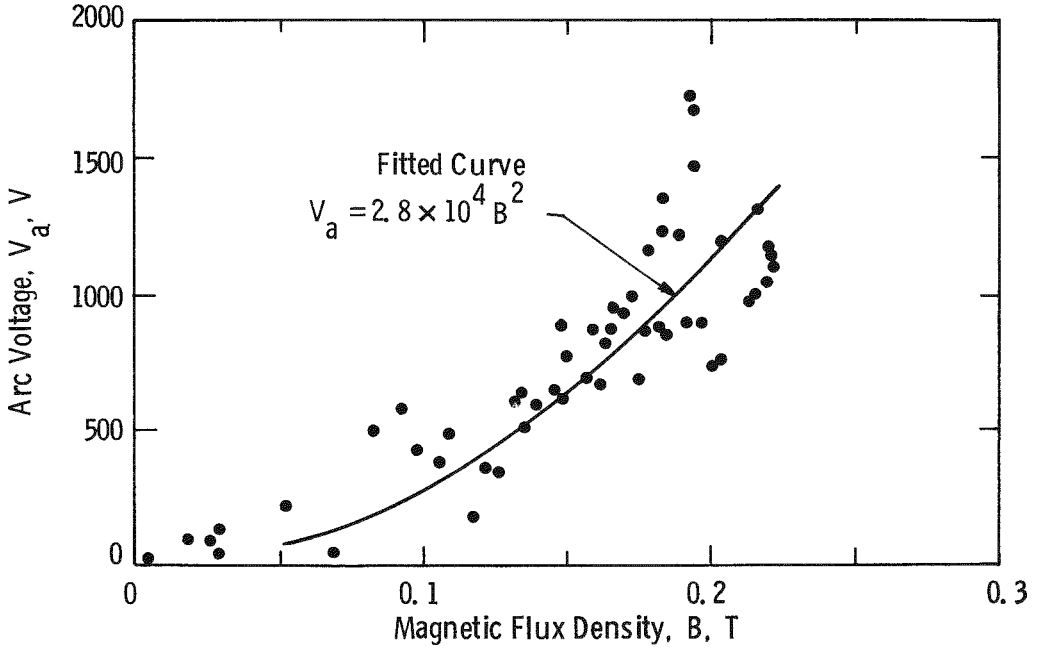

Figure 2-15. Plot of the arc voltage data from the lower oscillogram in Fig. 2-11.

Section 3

DESCRIPTION OF EXPERIMENTS

3-1 APPARATUS

3-1.1 Capacitor Banks

The basic high power test facility at the Westinghouse R&D Center consists of a capacitor bank capable of storing a maximum energy of 2×10^6 Joules, six air core inductors and appropriate instrumentation. This high current capacitor bank can be used to produce an oscillatory current when discharged through the inductors and the test device. We use this equipment to simulate a symmetric fault in a 60Hz circuit. We can select any appropriate capacitance up to 43,200μF at 10kV or 10,800μF at 20kV and combine the inductors in series or parallel to select any desired inductance to achieve a desired circuit impedance. Further, we can select capacitance and inductance to oscillate at frequencies other than 60Hz. A photograph taken inside of the capacitor bank room showing some of the capacitors and some of the inductors (reactors) appears in Figure 3-1.

A typical schematic of one of the current limiter experiments appears in Figure 3-2. A selection of 5400μF of capacitance and 1.25mH of inductance is used to supply the simulated symmetric fault current.

In Figure 3-2, the parallel capacitance consists of 54 0.88μF capacitors, and the assembly is shown in Figure 3-3. This capacitor bank was used in the high recovery voltage experiments of Sections 4-7 through 4-9, and was used for recovery voltages up to 50kV. These capacitors are housed in a separate room for personnel safety. They are connected to the vacuum device by one or more coaxial cables to minimize inductance.

3-1.2 Actuators and Actuator Power Supplies

The repulsion coil actuator has proven to be a reliable, moderately fast actuating device. An example of one is shown in Figure 3-4. Repulsion coil actuators are described in detail in reference (1) Many of the commutation experiments with sealed devices have used as many as five of these actuators at one time. Figure

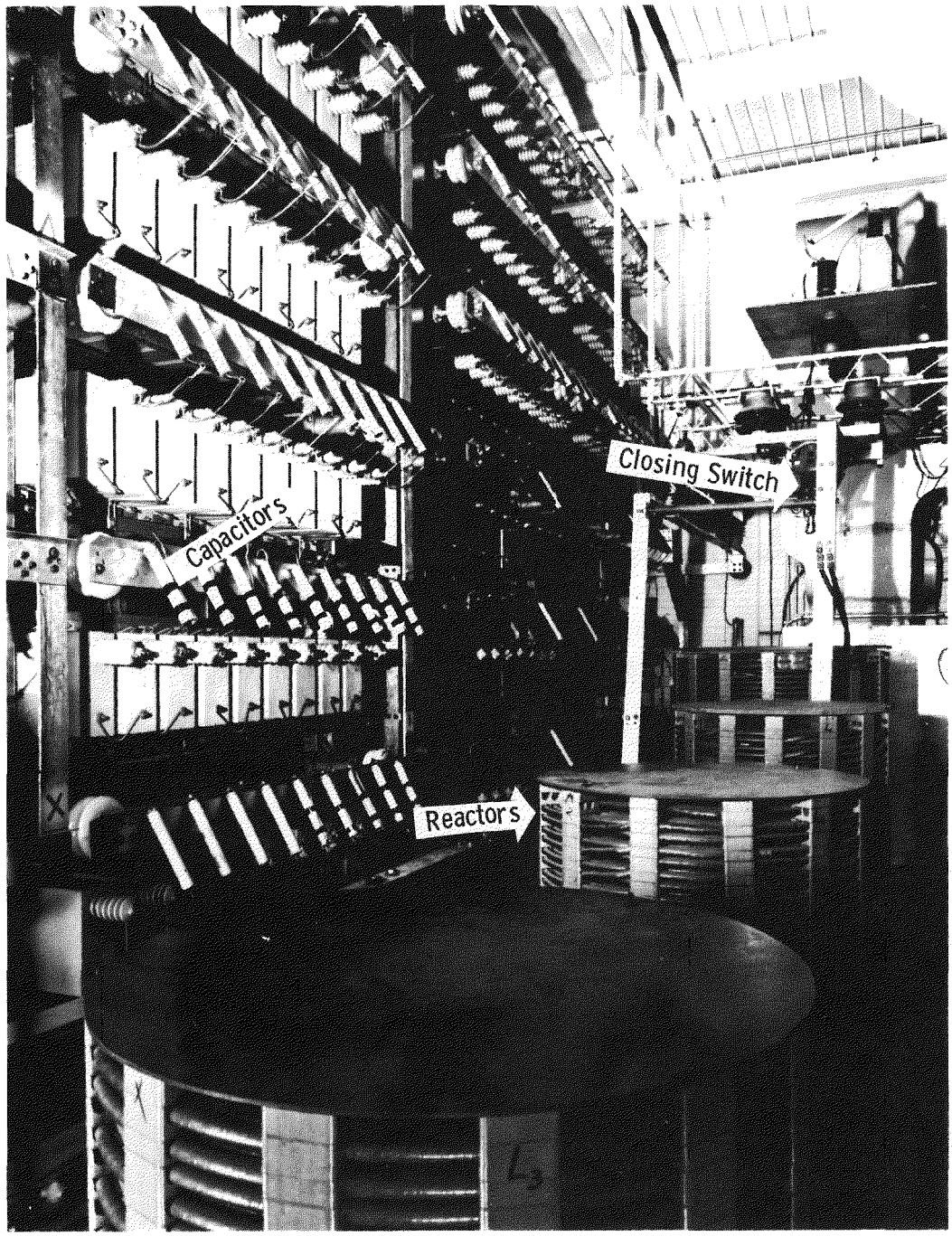

Figure 3-1. Capacitor Bank Room. Shown are one of the four banks of the capacitors, current limiting reactors, and closing switch (upper right).

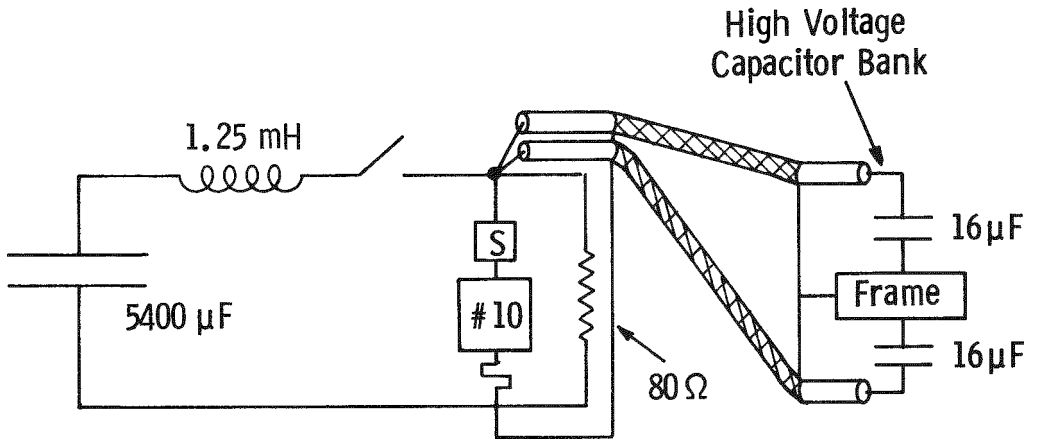

Figure 3-2. Schematic of experiments with Prototype #10 connected to 32µF of the high voltage capacitor bank.

3-5 is a schematic showing where each of these actuators were used. Actuators 1 and 2 in Figure 3-2 were used to operate the current limiting device and Actuator 3 was used to operate the series connected vacuum interrupter. Additional vacuum interrupters are needed to isolate the L and C_1 part of the circuit; because of the speed requirement, repulsion coil actuators were needed to operate these devices also. These two repulsion coil actuators are labelled 4 and 5 in Figure 3-5.

For effective use in a current limiting device the contacts of the vacuum device must be parted to the required spacing as rapidly as possible. In order to accomplish rapid operation, current must be delivered to the coils as rapidly as possible. We chose a capacitor discharge power supply design to deliver the current. A schematic of one of the capacitor discharge power supplies appears in Figure 3-6. A further refinement used in one of the power supplies was to use two stages of capacitors. A two-stage actuator power supply is shown schematically in Figure 3-7. The small 110µF capacitor is charged to a high voltage (usually 3000V) and the initial rate of rise of current is very large because of the high voltage. As the current is built up rapidly to the desired level, the 110µF capacitor is discharged and the switching diode turns on. The 2000µF capacitor which has been charged to a moderate voltage delivers the current for the acceleration period

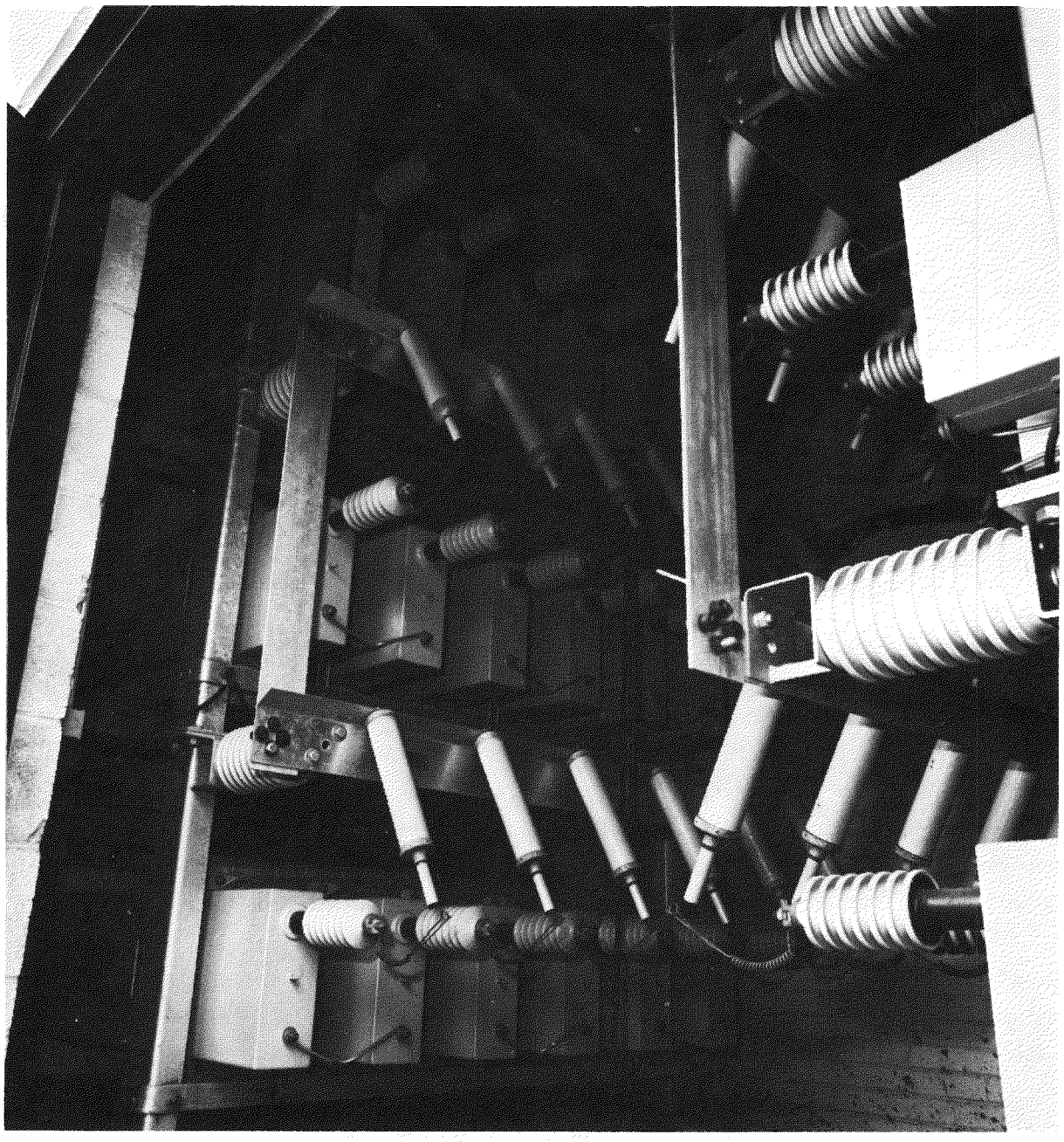

Figure 3-3. High voltage parallel capacitor bank. Photograph shows two of the three banks of capacitors.

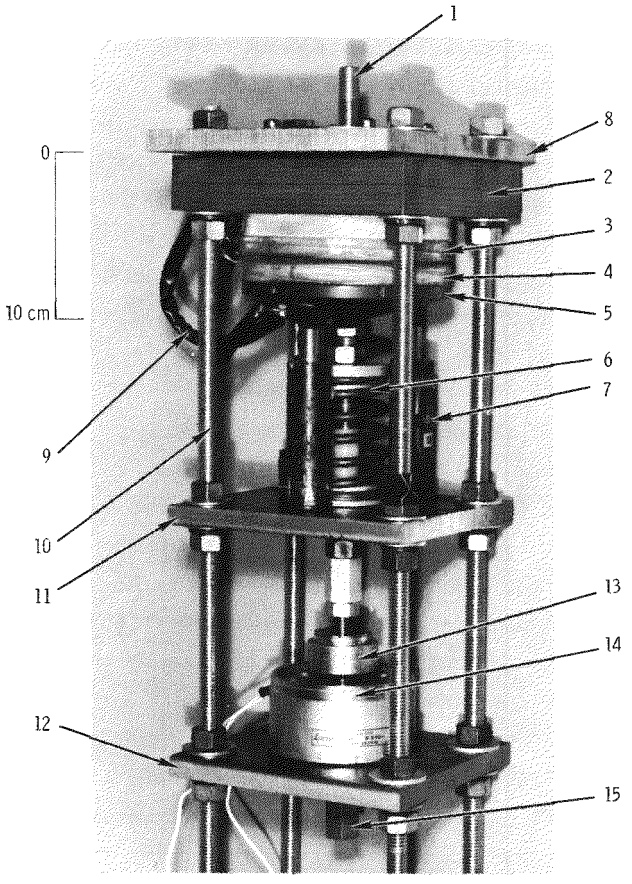

1. Main drive shaft
2. Spacer plate (micarta)
3. Fixed repulsion coil
4. Movable repulsion coil
5. Movable coil drive plate (micarta)
6. Reclosing spring
7. Shock absorber (3 total)
8. Main support plate
9. Electric leads to coils
10. Main tie rod (4 total)
11. Shock absorber support plate
12. Latch support plate
13. Latch armature
14. Latch field coil assembly
15. Connection for travel indicator (not shown)

Figure 3-4. A Repulsion Coil Actuator.

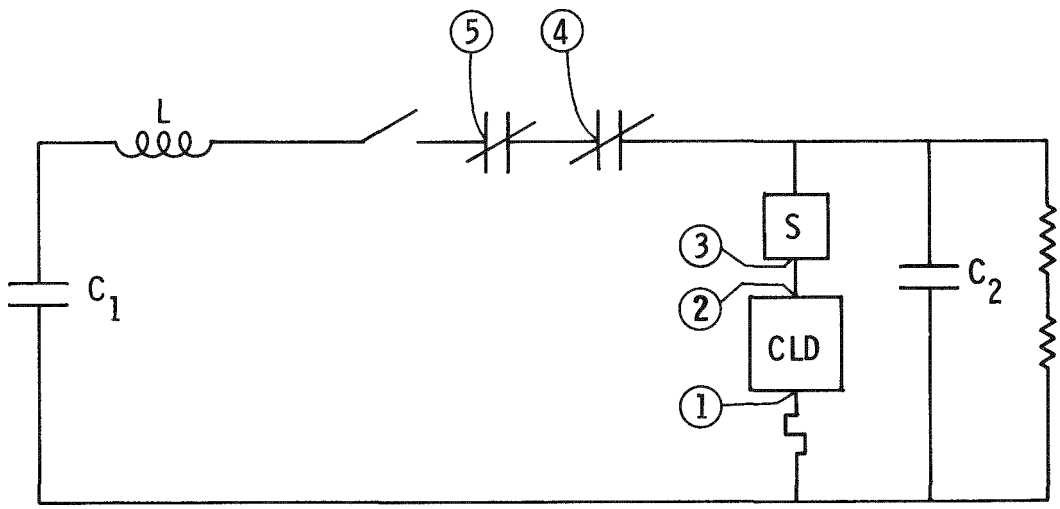

Figure 3-5. Schematic of the test circuit showing where each of the five repulsion coil actuators are used.

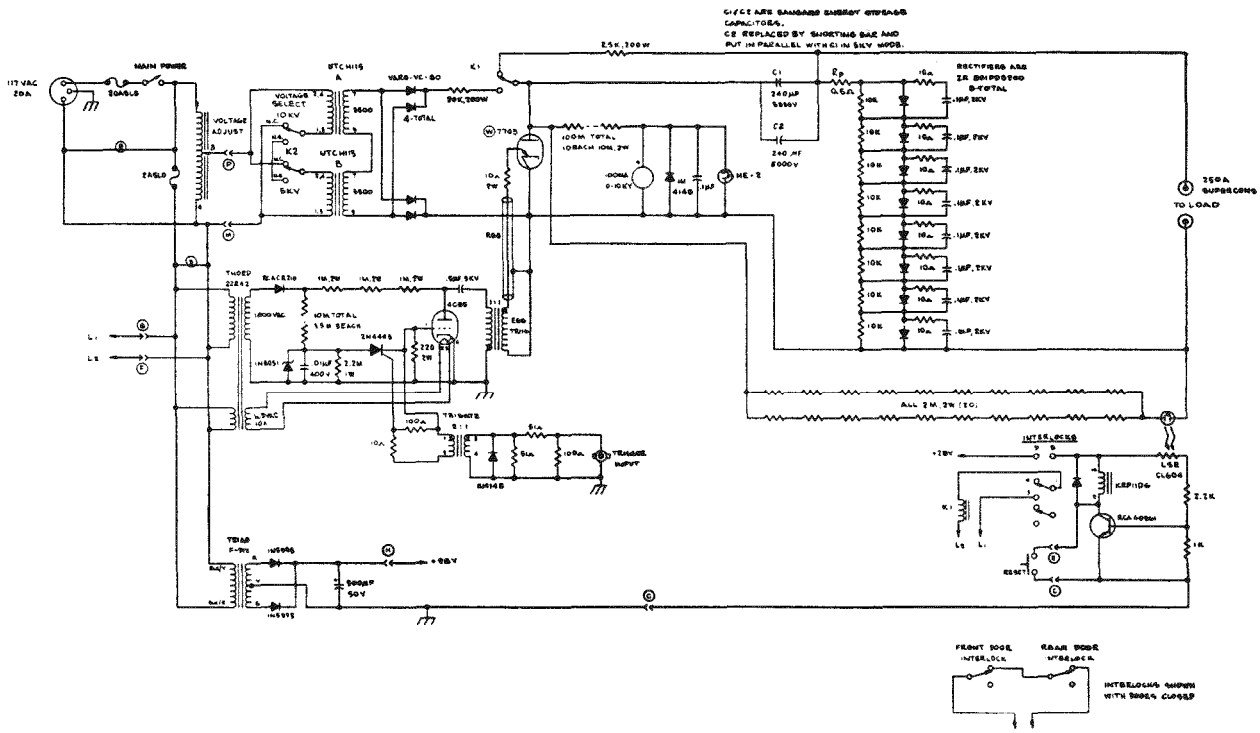

Figure 3-6. 5 kV, 6 kJ actuator power supply with energy discharge capacitors.

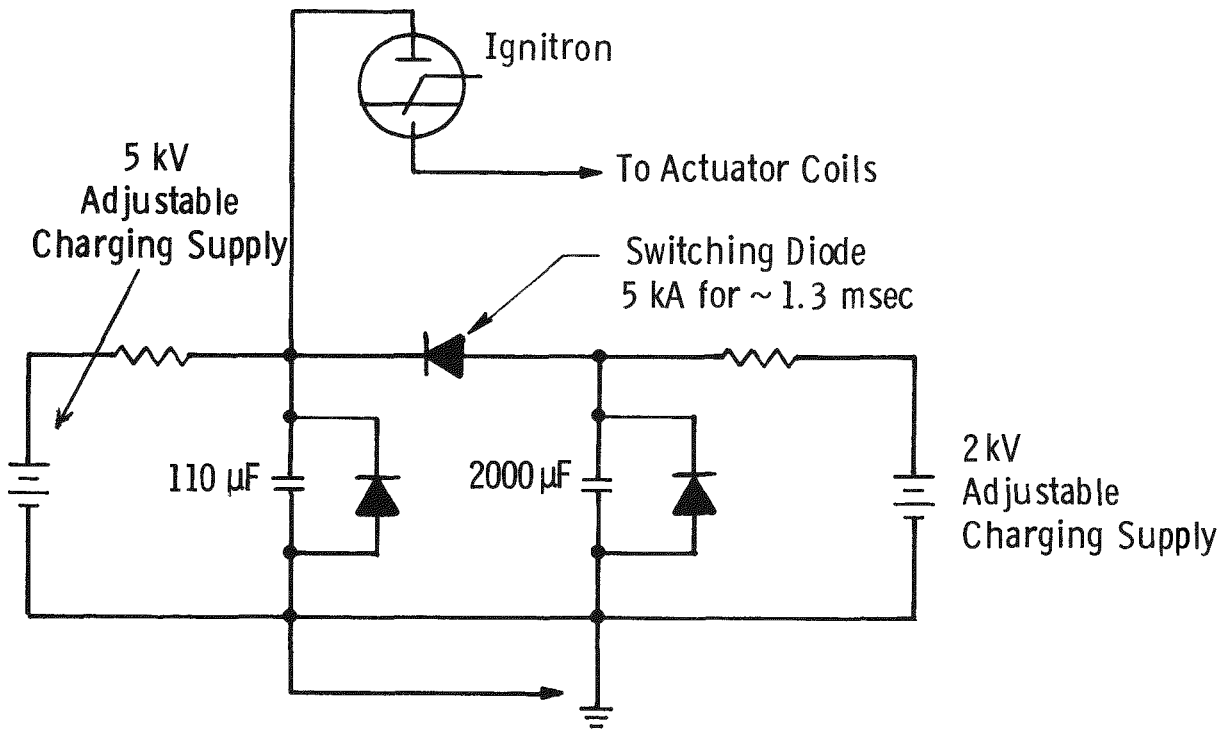

Figure 3-7. Two-stage fast actuator power supply.

which is approximately one millisecond. There was no need for further development work on fast actuators during Phase II of this project; hence, only one two-stage actuator power supply was constructed. Each of the other four repulsion coil actuators used power supplies similar to the one shown in Figure 3-6.

3-1.3 Magnetic Field Coils and Power Supplies

Magnetic field coils were mounted adjacent to the sealed vacuum device oriented to produce a transverse magnetic field across the axis of the vacuum device. Figure 3-8

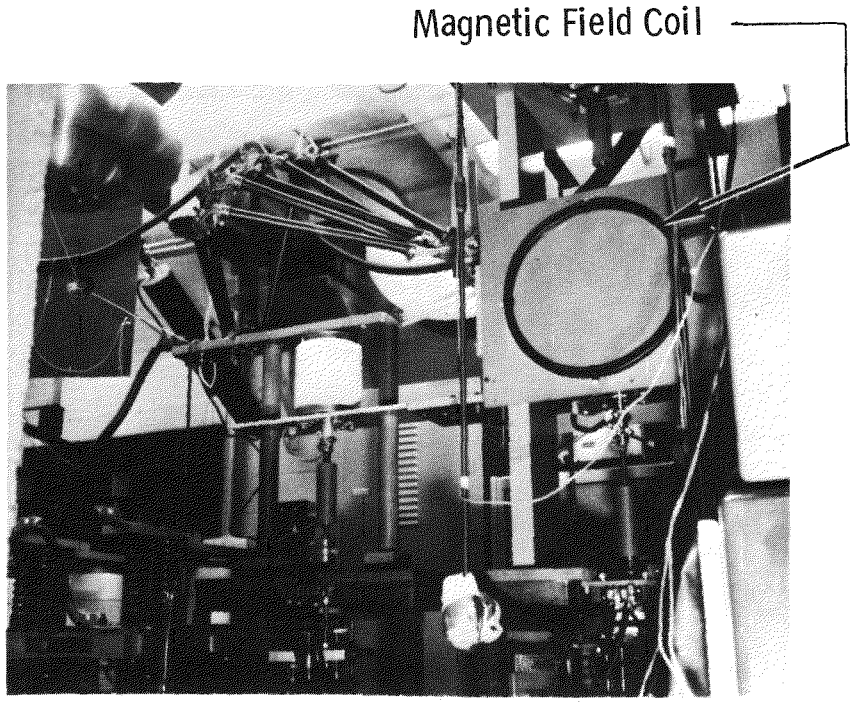

Figure 3-8. Typical current limiter experiment showing one of the two magnetic field coils. The current limiting device is inside the Micarta box with the magnetic field coils.

shows the magnetic field coils in a typical experiment. These were two turn coils each connected to a separate capacitor discharge power supply. The current in each coil was 33kA and the voltage was 8kV. The coils used only two turns to reduce inductance, to permit a rapid increase of current and a large rate of change of magnetic field, $\dot{B}$. The coils were 37.5cm in diameter, separated by 36cm. The inductance of these coils was 8μH.

A schematic of one of the two identical capacitor discharge power supplies appears in Figure 3-9. These supplies could not be connected electrically in parallel since they would have been damaged by the large circulating current. Further they could not be connected electrically in series since they would be damaged by the voltage. We, therefore, connected each supply to a separate coil and triggered them at the same time. Even though the supplies are limited in the current they can deliver, the separate coils present a lower inductance and we were therefore able to increase $\dot{B}$. This approach has two disadvantages: the impedance of one coil was not large enough and excessive currents could have been drawn if the capacitors of the power supply had been charged to the full value (10kV). Furthermore, the two circuits would not oscillate at exactly the same frequency causing the magnetic flux produced by one coil not to remain synchronized with the other for long time periods.

We also investigated using one power supply to deliver current to both coils connected electrically in series. This has the advantages of a better impedance match and a guarantee that the current in each coil is identical. However, experimental results showed that there is a slight advantage to using two independent supplies, and nearly all experiments were performed with this arrangement.

At the beginning of Phase II the magnetic field power supplies were equipped with electrolytic capacitors, and diodes were connected directly across the capacitors to prevent voltage reversal. A schematic appears in Figure 3-10. The resulting field waveshape was a rapid rise followed by a slow decay to zero. We later replaced the electrolytic with new energy storage capacitors, and placed a resistor R_p in series with the diodes; see Figure 3-9. This resistor limits the current through the diodes and hence provides protection. We have used this modified supply to generate two types of oscillating fields: (a) with the resistor and diodes connected the field oscillates at about 5kHz with a logarithmic decrement of 0.97, (b) with the resistor and diodes out of circuit the field oscillates at about 5kHz with a logarithmic decrement of 0.27. In both cases the ignitron Ⓦ type 7703 can conduct current in the reverse direction. The configuration with the diodes and resistor out of the circuit produced the best performance of the sealed device and was used for most of the experiments with sealed devices during Phase II.

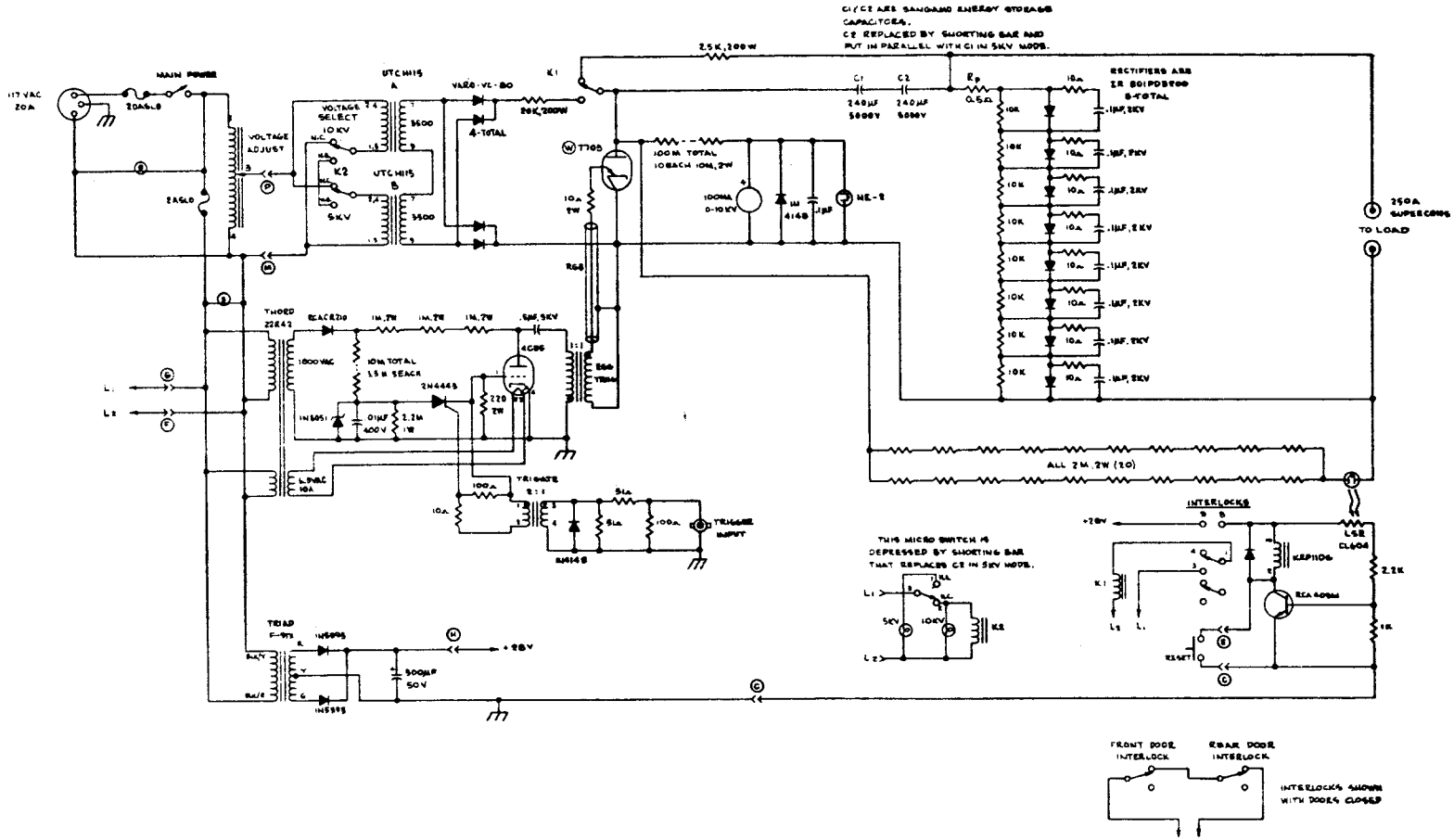

Figure 3-9. 10 kV, 6 kJ magnetic field coil power supply with energy storage capacitors.

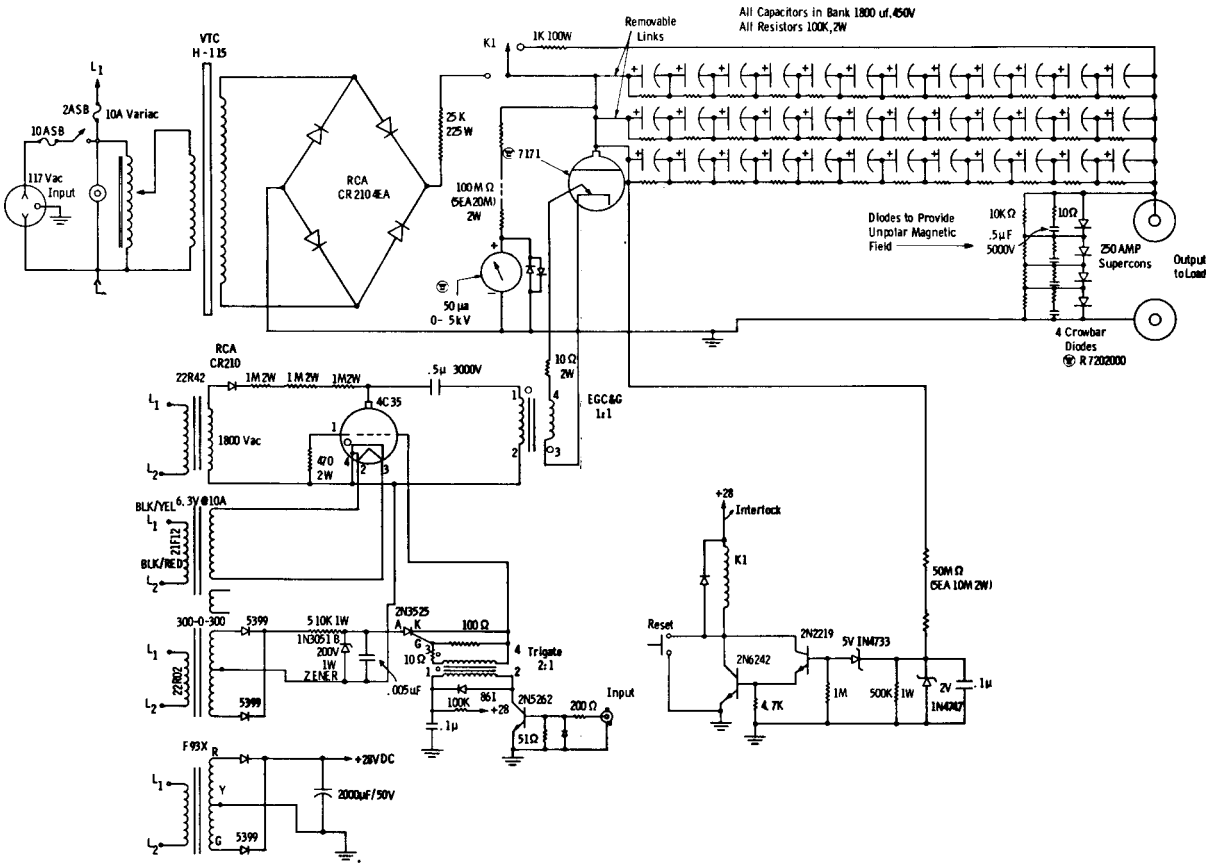

Figure 3-10. 5000 V, 5.6 kJ magnetic field coil power supply with electrolytic capacitors.

3-1.4 Description of the Demountable Arc Chamber and Outline of Experiments

The demountable arc chamber allows arc observation at the instant of application of the transverse magnetic field using high speed cinematography. A schematic of the chamber is shown in Fig. 3-11 and a more detailed description appears in ref.(1)

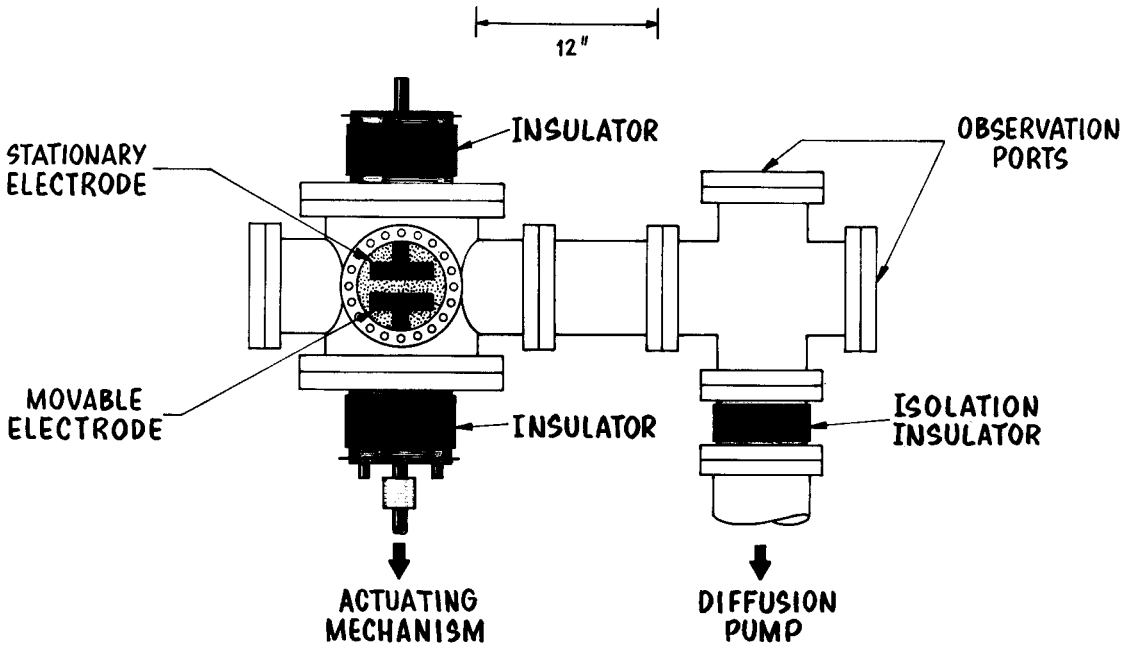

Fig. 3-11. Schematic of the large demountable arc chamber

The magnetic field coils were arranged such that the field was directed out of the plane of the paper. A cylindrical quartz liner inside the metal chamber minimized the interaction between the arc and the chamber walls. The circuit was set up to give a single 50Hz current halfwave, and the transverse magnetic field was applied at current crest. The rate of rise of the field was 140mT in approximately 850μs. The contacts were all made of CLR material, and the geometries were (1) cup contacts, 10cm diameter, [ref. (4)]; (2) cup contacts, 10cm diameter, with 5cm cuts in the side wall (see Fig. 3-12); (3) concave bar contacts, 5cm x 10cm (see Fig. 3-13); (4) convex bar contacts, 5cm x 11.2cm (see Fig. 3-14). The concave bar contacts were utilized with three different orientations with respect to the applied magnetic field: parallel, perpendicular, and with an angle of 45^{o}. The cup contacts with cuts and the convex bar were oriented such that the cuts and the bar, respectively, were parallel to the applied magnetic field. With the exception of the convex bar

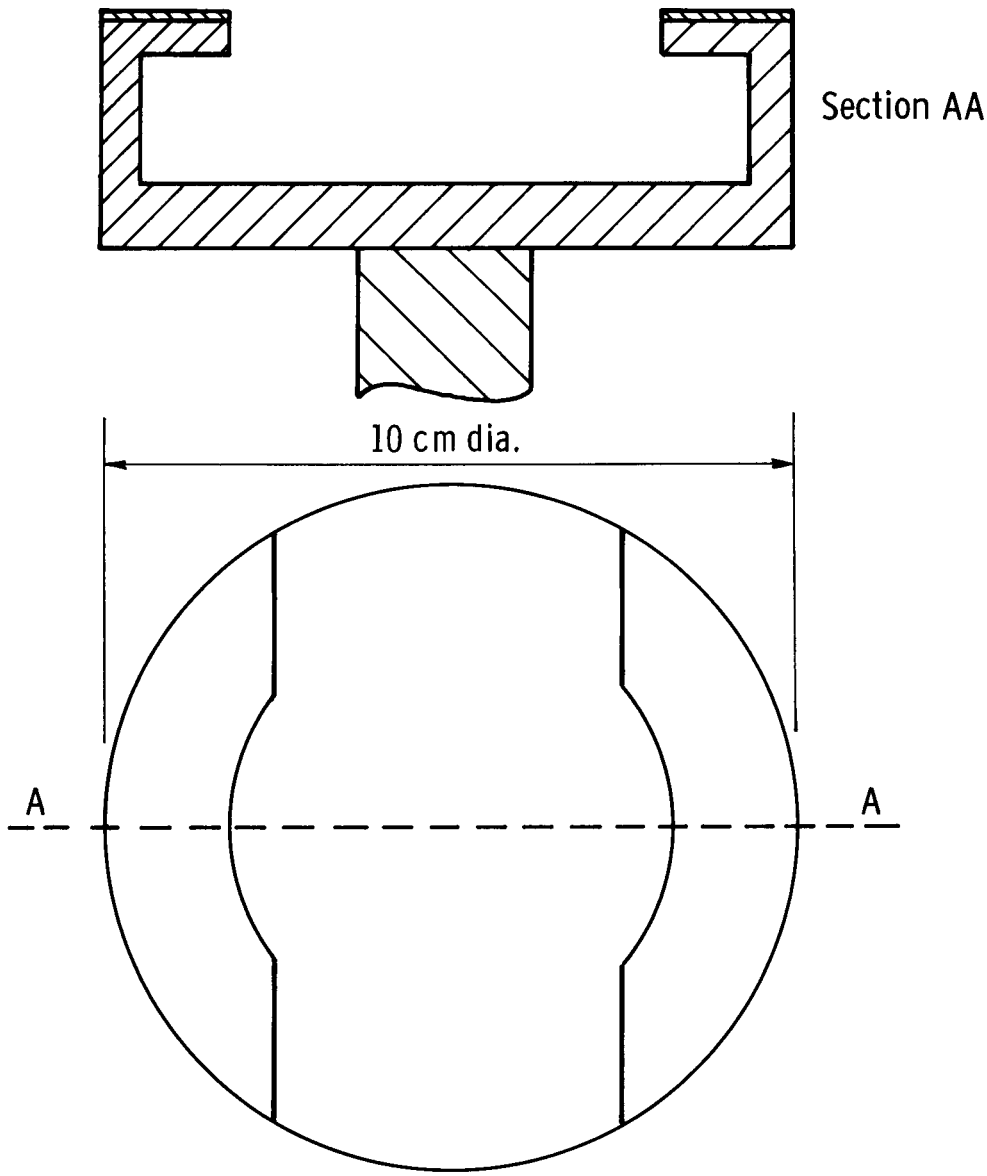

Fig. 3-12. Schematic of cup contacts with 5cm. cut

contacts, the actuation speed was 4.4m/s giving a gap of 22cm at the instant of B-field application. For the convex bar, the contacts were separated slowly to 24mm using the keep alive technique (reference (1). In some of these experiments, the arc was subjected to a weak axial magnetic field ($\sim$ 30mT) before and during the application of the transverse magnetic field.

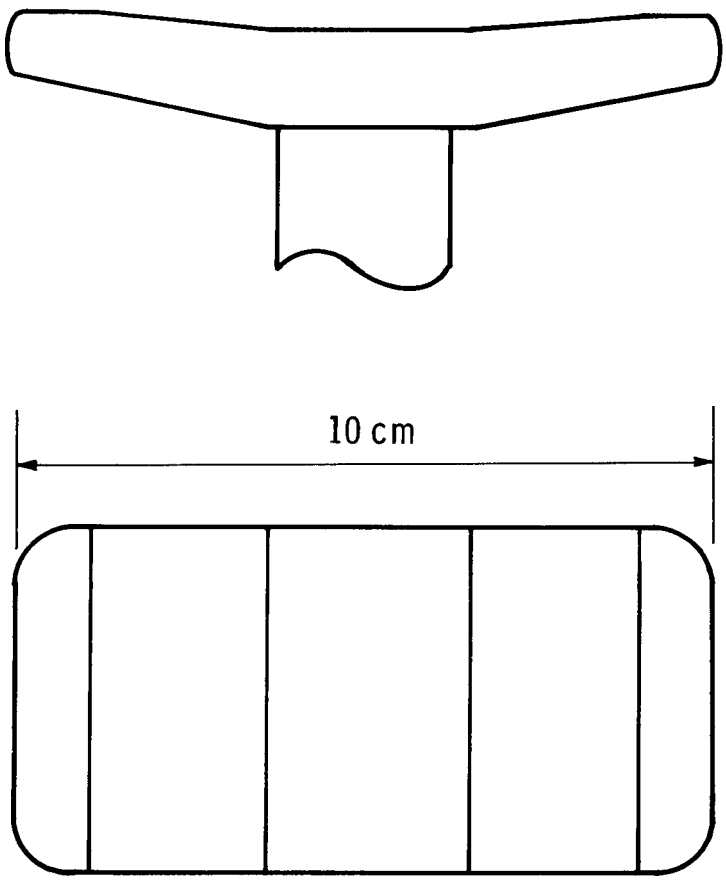

Fig. 3-13. Schematic of concave bar contact

Two high speed movie cameras recorded the arc appearances from two directions; parallel and perpendicularly to the applied magnetic field. Arc voltage, arc current and total circuit current were observed with two oscilloscopes. The triggering of one oscilloscope was delayed until shortly before the triggering of the magnetic field in order to give better time resolution during the commutation process. The arcs were photographed at current levels in the range 1 - 12kA.

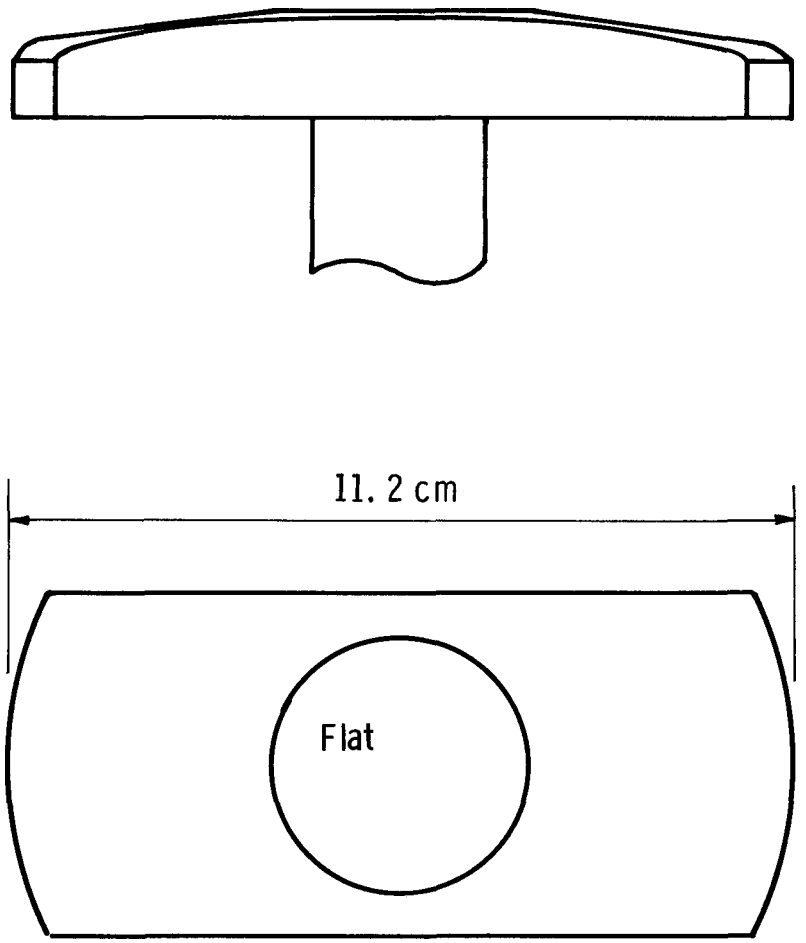

Fig. 3-14. Schematic of convex bar contact

3-1.5 List of Prototypes

The prototype sealed devices that were built and tested during Phase II are listed in Table 3-1. A brief description of each device and the purpose for which it was built are given under the various column headings of the table. The 18cm diam. devices were 30cm long, measured on the outside flange to flange, with the exception of prototype #7 which was 34cm long. The 23cm diam. and 30.5cm diam. prototypes were all 36cm long. In the last column of the table, reference is made to the subsections of Section 4 in which the various experiments carried out with each of the prototype devices are described in detail.

TABLE 3-1

Summary of Sealed Devices Tested
During Phase II

Prototype Number	External Ceramic Diameter	Internal Shielding	Electrodes	Purpose	Ref. to Section 4
1.	18cm	None	11.5cm diam., Bruce profile, CLR material	• Observed residual current • $B,\dot{B},C$ dependence established	4-1
2.	23cm	None	14cm diam., Bruce profile, CLR material	• Comparison with 1. to show effect of increased electrode diam. • Lifetime at 10kA	4-3 4-3
3.	18cm	None	11.5cm diam., Bruce profile, Cu-Bi material	• Comparison with 1. to check effect of Cu-Bi on remanent current • Effect of higher $\dot{B}$	4-3
4.	18cm	Bellows electrode isolated from endplate	11.5cm diam., Bruce profile, CLR	• Comparison with 1. to see if remanent current associated with endplates • Effect of B waveshaping	4-3 4-4
5.	23cm	None	Bar with two end mating "flats" (15cm x 7cm, CLR)	• High current commutation with large area bars which touch at two points • Oscillating magnetic field	4-4
6.	23cm	None	15cm diam., cup geometry, CLR	• Oscillating magnetic field • Diffuse arc plasma at high currents	4

TABLE 3-1 (Continued)

7.	18cm	Shielded end-plates, shielded external ceramic	Large area bar (28cm x 5cm) CLR Material	• Solenoidal field applied to large area bars	4-5
8.	23cm	None	15cm diam. stationary Bruce profile electrodes with a third low mass arc initiation electrode; CLR	• Fast electrode separation • Short arcing times	4-6.1 4-8.2
9.	23cm	Improved bellows shield	15cm diam., cup geometry, CLR	• Oscillating magnetic field (15kV/50kV circuits) • Diffuse arc plasma at high current • Series vacuum interrupter	4-6.2 4-7.1
10.	30.5cm	None	15cm diam., Bruce profile CLR material	• Series interrupter • Oscillating magnetic field	4-7.2 4-7.3

11.	30.5cm	Bellows shields (both electrodes movable)	15cm diam., cup geometry CLR	• Evaluation of cup electrodes in larger diameter ceramic • Oscillating magnetic field (15kv/50kV circuits) • Series interrupter • Faster electrode separation via two actuators	4-8.2
12.	30.5cm	"	" Device equipped with welded bellows	"	4-9
13.	30.5cm	"	• Two 15cm diam. stationary Bruce profile electrodes; CLR • Two 5cm diam. movable bridging electrodes;CLR • Steel electrode stems	• Oscillating magnetic field • 50kV circuits • Series interrupter • Faster electrode separation via two actuators	4-10
14.	30.5cm	"	Similar to Pro. #12 but with • reduced weight cup electrodes • steel electrode stems (overall 40% weight reduction) • (CLR material on arcing surfaces)	" (Same as above)	4-10

As a general guide, the four main variations of parameters were as follows.

Step #1 - For prototypes #1, 2, 3, 4

- linearly rising B-field to constant B_{max}
- relatively slow speed actuation (2cm in 4msec)
- low recovery voltage (<15kV).

Step #2 - For prototypes #5, 6, 7, 9, tests were run with

- oscillating B-field
- moderate speed actuation (2cm in 3msec)
- low recovery voltage (<15kV).

Step #3 - For prototypes #9, 10 tests were run with

- parameters of Step #2 but with
- series vacuum interrupter

Step #4 - For prototypes #8, 9, 10, 11, 12, 13, 14, tests were run with

- oscillating B-field
- high speed actuation (2cm in <2msec)
- high recovery voltage (∿50kV)
- series vacuum interrupter

3-1.6 Saturable Reactors

The use of a saturable reactor in series with the CLD suggests itself from the similarity of our current commutation to that of the current counterpulse technique used in d.c. switching (5, 6). In effect the reactor does not change the circuit impedance until the current in the CLD is reduced to a low value. Then the unsaturated cores present a large inductance which slows the rate of change of current as a current zero is approached. In principle this gives the vacuum device a longer period for deionization once a current zero is reached.

During Phase II, we tested prototype #9 with a saturable reactor (see Sect. 4-6). These tests produced uncertain results. However, we consider that the use of a saturable reactor should be tried again. To this end we give a brief description of this reactor here and describe the experiments we performed on the saturable reactor itself in Appendix D-3.

The saturable reactor consisted of five cylindrical cores. Each core was wound from a 0.1mm strip of silicon steel. Each core had a 2.5cm inner diameter, a 10cm outer diameter, and was 10cm long. The cores were stacked on a 2cm diameter copper rod with electrical insulation between the individual cores and with insulation between the cores and copper conductor. The calculated flux change, from minus saturation to plus saturation for this reactor was 0.08 Wb or 0.08 V-sec.

3-2 PARAMETERS FOR INVESTIGATION

Many parameters were varied to increase the magnitude of the fault current that could be limited by vacuum arc current commutation in a 72kV circuit. The parameters that were investigated can be grouped into the catagories of device parameters, circuit parameters and operational parameters. At the start of the Phase 2 Program, the need for variation and optimization of such device parameters as envelope diameter, electrode diameter and configuration, internal shielding, etc., was clearly evident. Also clear, at that time, was the need to investigate the characteristics of the parallel circuit parameters and especially to aim at reducing the parallel capacitance. Less clearly seen were possible variations in the operational parameters.

The device parameters that were investigated included:

a.) The diameter and length of the sealed devices.
b.) The size and shape of the electrodes.
c.) The spacing of the arcing gap.

The circuit parameters investigated were:

a.) The capacitance in the parallel circuit.
b.) The magnitude and rate of rise of the transverse magnetic field.
c.) Oscillating magnetic field.
d.) The use of a series vacuum interrupter.
e.) High recovery voltages.
f.) Properties of a saturable reactor.
g.) The effect of a spark gap in series with either the parallel capacitor or resistor.

The operational parameters were:

a.) Time of B-field application following electrode separation.
b.) Point on current wave of electrode separation.
c.) Opening speed.
d.) Use of two B-fields.

Section 4

EXPERIMENTAL RESULTS

Introduction

Before describing the experimental results in detail, a chronology of the experimental program will be useful. The objectives of the various experimental series, the reasons for taking a particular approach, and the new experimental findings will be reviewed. Figure 4-1 will serve as a framework for this résumé. In this figure, the 14 Prototype devices built and tested in Phase II are shown as circled numbers. (See Table 3-1 for a listing of these Prototypes.) The horizontal position of a circle indicates the quarterly period during Phase II in which the Prototype was tested. The height of the circle above the base line indicates the current limiting capability of the Prototype when a capacitance of 50 μF was used in the parallel circuit.

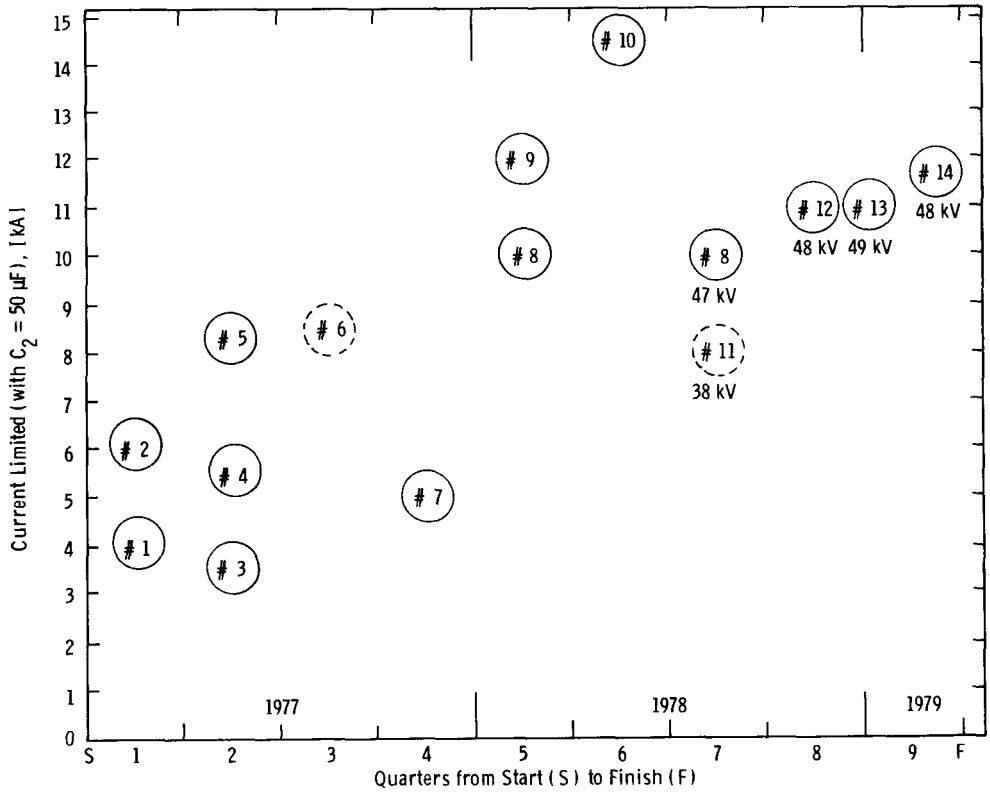

Figure 4-1. Prototype Performance During Phase II

Phase II started on January 1, 1977, following the completion of Phase I. The final two devices tested in Phase I were 23 cm diameter prototypes equipped with numerous internal ceramic shields. We encountered major problems with the shield attachments as discussed in Appendix D of the Phase I Final Report. The first two devices tested in Phase II were deliberately designed without internal ceramic shields. Rather the overall length of the devices was increased from 22 cm to 30 cm in order to reduce the probability of arcing from end plate to end plate. Prototype #1 contained 11.5 cm diameter Bruce profile electrodes within an 18 cm diameter ceramic envelope, and prototype #2 contained 14 cm diameter Bruce profile electrodes within a 23 cm diameter ceramic envelope.(See Table 3-1)

The objective of the first quarter test series was to investigate the commutation process in order to aid the design of future, higher current prototypes. We obtained high speed oscillograms showing the modes of commutation, and we determined the effect on commutation of (a) rate of rise of magnetic field, field magnitude, and the field duration, (b) parallel capacitance, (c) lead inductance and (d) electrode diameter. Further, the longer external ceramic provided a marked increase in reliability and life (more than 150 tests on the 23 cm diameter device with currents ranging up to 12 kA with no deterioration in commutation ability).

The tests revealed the presence of a residual current of several hundred amperes which can persist for several tens of microseconds following the main current collapse. The experimental series also identified two primary modes of current commutation. Mode 1 was a rapid collapse of the current. Here we frequently observed a residual current of several hundred amperes which persisted for several tens of microseconds and which could lead to arc reignition. Mode 4 involved an induced oscillation of the arc current which forced a current zero. The maximum commutation current at the end of the first quarter was 10.5 kA for a parallel capacitance of 200 μF. However, for a parallel capacitance of 50 μF, the results are shown in Figure 4-1.

The objectives of the second quarter were to understand and enhance the two modes of commutation in order to obtain similar commutation levels at reduced capacitance. We therefore performed a series of experiments on an additional three prototype sealed devices #3, 4, 5. Prototype #3 was almost identical with #1 but was equipped with Cu-Bi electrodes. This non-refractory electrode material actually decreased the commutation ability. Prototype #4 was also similar to #1, but the end flange was isolated from the electrode stem. The residual current was still observed with this flange isolated, and this showed that the residual current flowed between the

arcing electrodes. Tests with this prototype also showed the advantage of using rapid rates of rise of magnetic field with high peak values. The most interesting test series was performed with Prototype #5, which contained concave bar electrodes within a 23cm diameter ceramic envelope. Here we deliberately enhanced the mode 4 commutation by oscillating the applied magnetic field. In all previous experiments we had used the linearly rising field to a constant value. Commutation currents of 10kA were attained with a parallel capacitance of 100μF.

This experimental series showed that (a) CLR is a better electrode material than Cu-Bi for current limiter applications, (b) large area electrodes are beneficial, (c) the magnetic field should have a rapid rate of rise of ∿ 8000 T/sec for mode 1 commutation, (d) oscillation of this magnetic field can increase the mode 4 commutation ability, and (e) electrodes for producing parallel arcs within a single ceramic envelope require careful design. The experimental series also showed marked progress in the commutation ability. At the end of Phase I, in December of 1977, the commutation limit was 8.5 kA for a parallel capacitance of 200 to 300 μF. We were now achieving this order of commutation level for a parallel capacitance of 50 μF (see Figure 4-1). These commutations were achieved in an a.c. circuit where the dV/dt following arc extinction is similar to the dV/dt which would be observed in a practical transmission circuit for the same capacitance. The peak of the recovery voltage in a 72 kV application will certainly be significantly higher than the 15 kV peak used in these experiments. However, the immediate current zero phenomena are comparable.

The major development in the second quarter was the observation of enhanced current commutation using modulation (oscillation) of the applied transverse magnetic field. Our future experiments exploited this phenomenon in combination with improved prototype designs.

During the third quarter, we tested Prototype #6 using oscillating transverse magnetic fields. The commutation limit exceeded 8.5 kA, but the actual limiting value was not determined since the device went to atmospheric pressure during the test series. Subsequent experiments were performed with Prototypes #4 and #5 which had previously been subjected to extensive commutation experiments. Prototype #5 was used to investigate the possible effect on commutation level of tuning both the magnetic field circuit and the parallel external circuit. The ratio of the external circuit frequency to the magnetic field frequency was varied from two to six, and the commutation level was observed to be insensitive to this ratio over the given range.

We gained additional information concerning the interaction of oscillating magnetic fields with vacuum arcs by observing current commutation from devices connected in series. The commutation levels of Prototypes #4 and #5 were determined separately using oscillating magnetic fields, and these prototypes were then operated in series with a single capacitor across the two devices. Simultaneous application of oscillating transverse magnetic fields caused a 33 percent improvement over the current commutation ability of each device individually.

During the third quarter, we also approached an understanding of the oscillatory phenomena by analyzing the interaction between the arc, the magnetic field, and the external circuit. We were unable to predict the transient arc voltage behavior in the presence of an oscillatory magnetic field, and it was therefore necessary to read the transient arc voltages from high speed oscillograms. With these voltages as input data, the resulting circuit analysis showed a reasonable and self-consistent arc current behavior. In particular the arc current passed through zero.

Prototype #7 was equipped with large bar electrodes positioned along the long axis of an 18 cm diameter ceramic envelope. The design of the electrodes necessitated slow electrode separation using the d.c. keep alive technique, and oscillating magnetic fields were applied at electrode separations of 2 cm. The commutation ability was 4.4 kA (26 μF) and 7.3 kA (100 μF) and these levels were higher than observed in previous 18 cm devices. However, there was no major improvement in performance. This prototype was also subjected to experiments where a low d.c. field was applied immediately prior to application of the main oscillating magnetic field. The low field was intended to align the cathode spots, but this field did not improve commutation ability. This technique was not pursued further.

The alignment of the electrodes in Prototype #7 permitted large area electrodes to be enclosed within an 18 cm diameter ceramic. The commutation ability was somewhat better than with previous 18 cm diameter devices. However, the extent of the improvement was inconsistent with the increase expected from area considerations. Rather the data suggested that high commutation ability is associated with both large electrode area and large ceramic diameter. This conclusion was tested when Prototype #10 was evaluated. The electrodes in Prototype #10 are similar in design to those used in Prototypes #2 and #8, but the diameter of the external ceramic was increased from 23 cm to 30.5 cm.

During the fifth quarter Prototype #7 was evaluated with faster electrode separation (2.3 cm in 4.2 ms) and without a keep alive current. The commutation limit

was 7.7 kA (100 μF) which slightly exceeded the commutation limit of 7.3 kA (100 μF) observed with slow electrode separation (2 cm in 25 ms). In both cases, the commutation ability was inferior to that observed with Prototypes #8 and #9.

Since Prototype #8 was equipped with a third low mass movable electrode, commutation experiments could be performed with rapid electrode separation. In particular, true fault current limitation was observed, with the oscillating magnetic field applied during the a.c. current rise. The commutation limit was 8.5 kA (50 μF). This prototype received further evaluation.

Prototype #9 was tested with a single parallel 50 μF capacitor placed across both the prototype and a series connected conventional vacuum interrupter. The peak current commutated had a value of 12 kA which represents a 40 percent increase in commutation ability over previous circuit arrangements. High current commutations of 5.4 kA (12 μF) and 8.6 kA (26 μF) were also observed without the series interrupter. Prototype #9 was also used for preliminary evaluation of saturable iron cores.

In all previous Phase I and Phase II experiments, the initial rate of rise of the recovery voltage was accurately simulated. However, the peak recovery voltage was deliberately maintained at the low value of 15 kV. An analysis in the fourth quarter showed that the actual recovery voltage peak would be approximately 50 kV for a 72 kV/15 kA circuit with a 50 μF capacitor. This value was confirmed by more rigorous calculations performed in the fifth quarter. In particular, we made a preliminary evaluation of Prototype #9 using 50 kV recovery voltages. The circuit was by no means optimized, and yet 4 kA was commutated with a parallel capacitance of 32 μF. The extensive experimental series of the fifth quarter showed the value of a) cup electrode geometries, b) series vacuum interrupters, and c) bridging electrodes for rapid electrode separation. Further, the series gave initial experience with saturable iron cores and high voltage circuits. The data were used in the tests on Prototype #10, and provided guidelines for designing the five prototypes built in 1978.

Design parameters resulting from 1977 experiments can be summarized as follows. Prototype #7 contained large area bar electrodes which were oriented along the axis of the 18 cm diameter ceramic. The maximum commutation current was 7.7 kA (100 μF), and this maximum was comparable with the value observed for other 18 cm diameter devices (#1, 3 and 4). In order to optimize commutation ability, we considered that future prototypes should be manufactured with larger diameter (23 or 30.5 cm) ceramics. Further, the bar electrode geometry should be abandoned in favor of the disk and cup geometries.

Prototype #8 demonstrated true current commutation with current transfer to the parallel R C network during the current rise. When we applied the magnetic field 2.2 ms after the start of current we commutated 8.5 kA (50 μF). Here the small electrode was only separated by a distance of 1.2 cm from the opposing electrode. It is probable that this commutation level would have been exceeded if a higher speed actuator had been used. For example, Prototype #8 commutated a crest current of 10 kA (50 μF) when the bridging electrode was withdrawn 2 cm in 2.2 ms. By contrast, Prototype #6 commutated a crest current of 8.5 kA (50 μF) when the electrodes were separated to 2 cm in 4 ms. The conclusions from experiments with Prototype #8 were a) that the effect of high speed electrode separation should be investigated further and b) that a bridging electrode may prove a feasible technique for lowering the effective electrode mass.

Experiments with Prototype #9 showed the value of connecting a single 50 μF capacitor across both the prototype and a series connected conventional interrupter. The peak commutated current had a value of 12 kA which represents a 40 percent improvement over previous tests with cup electrodes (Prototype #6). The experiments also confirmed the significance of the cup electrode design, with record currents of 5.4 kA (12 μF) and 8.6 kA (26 μF) being commutated without the series vacuum interrupter.

Finally, the preliminary experiments in the 50 kV circuits indicated a variety of circuit problems which were corrected. For example, all future high voltage tests were performed in the test cell which is located in close proximity to the 48 μF high voltage capacitor bank.

During the sixth quarter Prototype #10 was first evaluated in low voltage circuits where the recovery voltage was limited to less than 20kV. The initial tests were performed without a conventional vacuum interrupter in series with the current limiter device, and the highest currents commutated were 8.3kA (50μF) and 7.7kA (26μF). We had anticipated higher commutation currents from a 30.5cm diameter device, and we attribute the relatively poor performance to initial manufacturing problems associated with the processing of a large volume device. The device apparently contained sufficient residual gas to facilitate arc reignition at relatively low recovery voltages. We did, however, observe vigorous current oscillations with current reversal.

Prototype #10 was then evaluated in a low voltage circuit with a conventional vacuum interrupter connected in series. There was a considerable increase in performance to 14.5 kA (50 μF) and 9 kA (26 μF). These currents represented the highest commutation levels to date, and future prototypes were built with 30.5 cm diameter ceramic envelopes. Subsequent experiments with Prototype #10 involved the use of spark gaps in series with either the parallel capacitor or parallel resistor with the objective of enhancing the current oscillation.

The final experimental series with Prototype #10 involved commutation studies in a high voltage 50 kV circuit. Experimental difficulties were encountered in minimizing the inductance of the parallel circuit and in synchronizing the operation of the circuit components. However, the commutation current in the high voltage circuit was increased from the previous level of 4 kA (32 μF) with Prototype #9 to 7.5 kA (32 μF) with Prototype #10.

In order to use the large diameter prototypes at high rates of change of magnetic field, with high peak values, we used an individual power supply with each of the two field coils. This magnetic field arrangement was slightly better than energizing series-connected coils from a single supply. We also determined that the commutation ability did not increase with an increase in electrode separation from 2 cm to 2.5 cm.

These tests indicated that Prototype #11 should be tested with an electrode spacing of 2 cm, with an individual power supply for each of the field coils, with a series vacuum interrupter, and in a high voltage circuit in which the frequency of the parallel circuit is at least twice the magnetic field frequency.

During the seventh quarter all of the experimental data were obtained with high recovery voltages (40 to 50 kV) following commutation, and with a conventional vacuum interrupter in series with the CLD. Prior to performing these experiments, the overall circuit received extensive modification to permit full use of the H.V. capacitor bank in parallel with the CLD. Prototype #10, equipped with 15 cm diameter Bruce profile electrodes in a 30.5 cm diameter ceramic, successfully commutated currents as high as 7.5 kA (32 μF) with a recovery voltage of 45 kV. Prototype #11, equipped with 15 cm diameter, cup electrodes in a 30.5 cm diameter ceramic, also successfully commutated currents as high as 7.8 kA (48 μF) with a recovery voltage of 38 kV. This was not a limit. However, the bellows failed due to contact with the electrode stem.

In order to study the effect of short arcing times on commutation ability, Prototype #11 had been equipped with two movable electrodes. We had planned to actuate

the two electrodes simultaneously, but this plan was aborted due to the bellows failure. Instead we substituted the previously tested Prototype #8. This prototype contains a light movable "bridging" electrode which passes through a stationary 15 cm diameter Bruce profile electrode. The opposing electrode has a similar Bruce profile geometry, and this more massive electrode is also mounted on a bellows. We actuated the two electrodes of the 23 cm diameter prototype simultaneously, and achieved a gap spacing of 20 mm in 1.5 ms. With electrode separation during the initial current rise we commutated 10 kA (48 μF) with a recovery voltage of 47 kV. With electrode separation near current crest, the commutation level was significantly reduced to 6 kA. The preliminary conclusion was that rapid electrode separation does not adversely affect the commutation level when the current at contact part is only several thousand amperes. However, there were indications that the commutation level decreases for contact part at currents $\geq$6 kA. These high speed phenomena were investigated further using Prototypes #13 and #14.

During the eighth quarter, Prototype #12 was tested. Prototype #12 contained 15 cm diameter cup geometry electrodes within a 30.5 cm diameter ceramic. Two actuators were used to give a maximum electrode separation of 2 cm in a minimum time of 2.2 ms. All experiments were performed in a high voltage circuit with 48 μF of parallel capacitance and a series connected vacuum interrupter. The prototype was associated with high arc voltage and low voltage withstand which indicated poor internal vacuum. However, despite a resulting erratic performance, a commutation level of 11 kA (48 kV) was observed at an electrode spacing of 2 cm. This commutation level was achieved even though the field was applied 2.8 ms following electrode separation at a current level of 13 kA. This indicated that the initial columnar arc (7) may not adversely affect the commutation ability.

These experiments contradicted previous tentative conclusions concerning the effect of electrode separation at high currents. With Prototype #8 the commutation ability decreased. However, with Prototype #12, the commutation level of 11 kA was achieved following electrode part at 13 kA. However, the time of field application following electrode part was significantly longer for Prototype #12. The faster electrode separation permitted by Prototypes #13 and #14 helped to resolve this difference in performance.

During the ninth and final quarter of Phase II, Prototypes #13 and #14 were tested. Prototype #13 contained 15 cm diameter stationary Bruce electrodes spaced 20 mm apart within a 30.5 cm diameter ceramic. Passing through holes in the centers of the stationary electrodes were two 5 cm diameter movable bridging electrodes. Smaller

diameter stems made of stainless steel were used to give a maximum opening separation of the bridging electrodes of 20 mm in 1.4 ms. All experiments were performed in a high voltage circuit with 48 μF of parallel capacitance and three different types of series connected vacuum interrupters were used. With high speed opening on a rising 60 Hz current wave which gave a low separation current, a commutation level of 9 kA (46 kV) was obtained. Maintaining the rapid separation speed but at a higher separation current, a commutation level of 8 kA (31 kV) was observed. These data supported the conclusions reached with Prototype #12 that the commutation level was not adversely affected by the current level at contact separation, i.e., by the initial columnar arc expected at the higher separation current.

In a second series of experiments using Prototype #13, a commutation level of 11 kA (49 kV) was observed. Several beneficial factors that may have been responsible for this improved performance include a) the use of a series vacuum interrupter provided with an axial magnetic field that prevents anode involvement and thus a more rapid recovery voltage withstand and b) a voltage grading method that helped divide the recovery voltage between the two vacuum devices.

Prototype #14 was similar to Prototype #12 but with stainless steel stems and cup electrodes of reduced mass. The electrodes were separated to 20 mm in 1.8 ms (Prototype #12 required 2.2 ms). A commutation level of 12 kA (48 kV) was observed. This level was achieved under the same conditions described in the previous paragraph for Prototype #13.

Additional experiments with Prototype #14 at the 10 kA (47 kV) level showed that this device also was not sensitive to the level of separation current.

4-1 RESIDUAL CURRENT AND COMMUTATION MODES; PARAMETRIC STUDIES WITH SEALED DEVICES

4-1.1 Experimental Setup and Sample Data

A schematic of the circuit used to study current commutation from prototypes #1 and #2 is shown in Figure 4-2. The transverse magnetic field (B-field) was produced by discharging a capacitor into the two coils disposed on either side of the vacuum device as shown in the schematic. The coils have eight turns each; they are 27 cm in diameter and are separated by 34 cm. The peak value of the B-field and its time rate of change, $\dot{B}$, were parameters varied during these tests.

The contacts of the vacuum device were separated by means of the repulsion coil actuator. The average velocity of separation ranged up to 6 m/sec. The arcing gap length at the time of current commutation was varied from 17 to 33 mm.

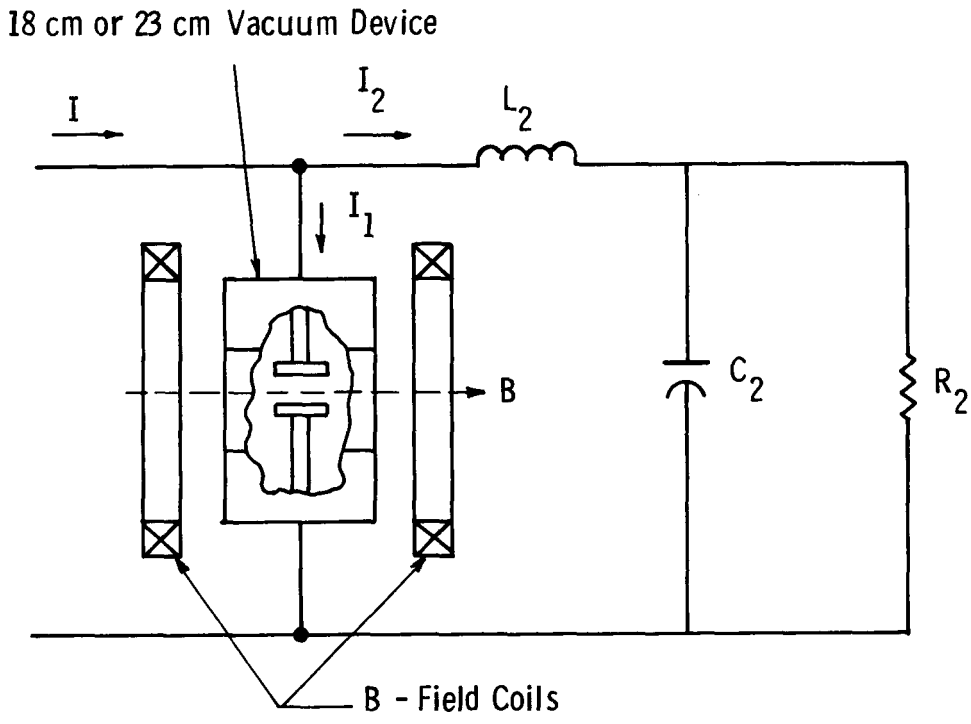

Figure 4-2. Schematic of the circuit used to study current commutation from the vacuum device into R_2.

The parallel circuit is composed of L_2, C_2 and R_2 as seen in Figure 4-2. The capacitance, C_2, was either 14, 50 or 200 μF; the inductance, L_2, was varied from a minimum of about 1 μH (due to the inductance of the loop comprising the capacitor and the vacuum device) to about 5.5 μH; R_2 was either 1.15Ω or 2.3Ω, and the value was selected to prevent the recovery voltage across C_2 from exceeding 12 kV.

Single loops of 60 Hz current were supplied from our high power test facility. Shortly after the start of current flow, the contacts of the vacuum device were parted creating a metal vapor arc between the separating contacts. As sketched in Figure 4-3, the circuit current, I, and the current through the vacuum device, I_1, were nearly identical up to the time the B-field was triggered. In general, the timing of the B-field trigger was chosen to be at or near the crest of the 60 Hz wave for experimental convenience. On the time scale used for Figure 4-3, the device current, I_1, drops instantly to zero while the circuit current is controlled by the parallel network with a typical decay to zero as shown. When the circuit current reaches zero, a back up breaker also experiences a current zero, and current ceases to flow.

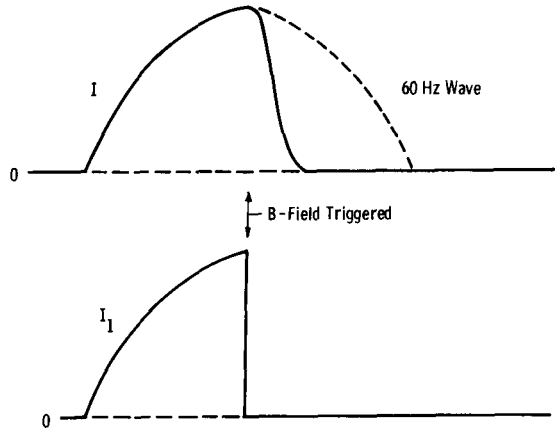

Figure 4-3. The circuit current, I, and the current, I_1, through the vacuum device; the B-field was triggered (and current commutation occurred) at or near the crest of the 60Hz wave for experimental convenience.

The way in which I_1 decays to zero is a major objective of these studies. The most common mode of current decay, defined previously as Mode 1, is shown in Figure 4-4. Here, with data taken from a fast time sweep, we can see the essential details of the current decay. A slight pip on the current trace marks the beginning of the rising B-field. Some 10 to 40 μsec later, depending on the magnitude of B, the threshold magnetic field is reached and the current starts to decay rapidly. For purposes of analysis, we have identified the time t_e by the graphic construction shown in Figure 4-4. The current switch-off time, t_s, is approximately 1.2 t_e when the current decay follows a Gaussian curve. For values of current well below the limit, for a given set of parameters, the current waveshape follows the solid line, i.e., it goes to zero promptly. When I_1 is raised, we observed a tailing of the current as shown by the dotted line in Figure 4-4. If this tailing starts at 200 A or so it seems to decay to zero in times of the order of several multiples of t_e. If this tailing or residual current starts at a level of more than 200 A, it does not decay but persists for an uncertain time and then increases again. Under most circumstances this current rises to approximately the circuit current level and commutation has not been accomplished.

Under some conditions, however, this reignition leads to an oscillation of the current in the device which results in a successful commutation. This Mode 4 commutation is depicted in Figure 4-5. The initial current decay is similar to Mode 1

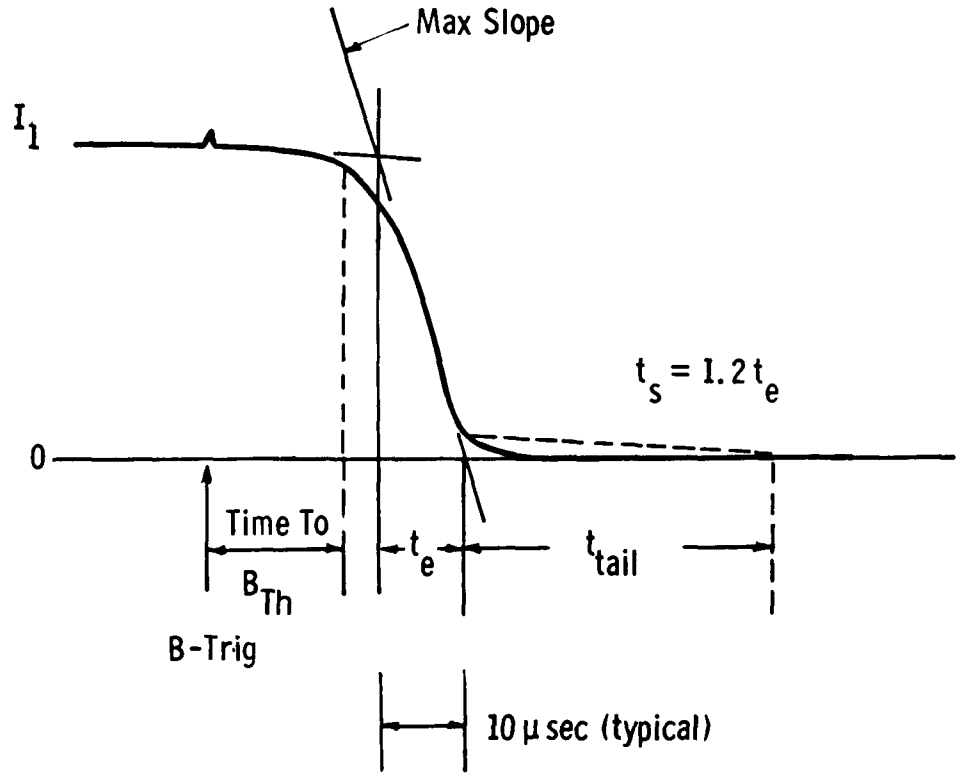

Figure 4-4. Details of the Mode 1 current decay.

but the residual current hovers for a time. Then I_1 increases to approximately twice the circuit current value and decays again to zero. The period of this current oscillation is related to the period of the parallel circuit. Evidently the capacitor, C_2, continues to charge up during the time I_1 is hovering at a low value. Then a reignition of the arcing leads to a large current flow which discharges C_2. The ensuing oscillation creates a current zero and permits the arc in the device to extinguish. This leads to a successful current commutation. The practicality of using this mode and its optimization was studied in later experiments.

Representative oscillograms of the current through Prototype #1 and the voltage across it are shown in Figure 4-6. The parallel capacitor, C_2, was 50 μF. Successful commutation via Mode 1 is seen for the 3 kA and 4 kA cases while the 5 kA case shows a failure from the residual current.

Figure 4-7 shows an example of current commutation via Mode 4. Here again, the capacitance value C_2 is 50 μF.

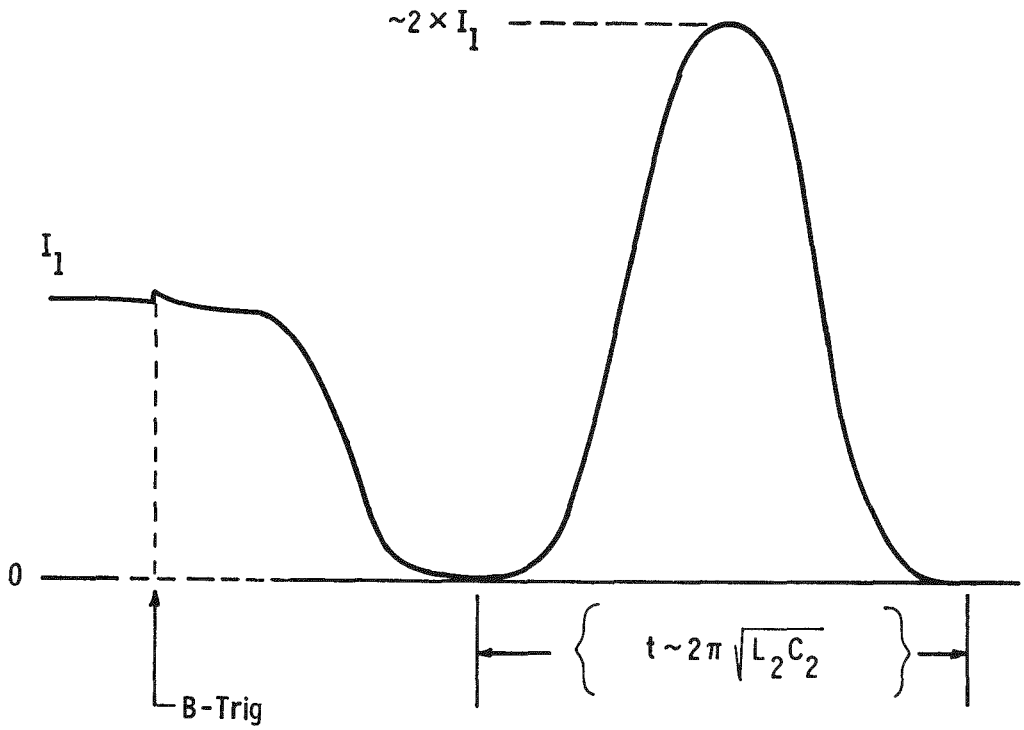

Figure 4-5. Mode 4 current commutation.

The upper trace of Figure 4-8 shows the device current and the recovery voltage for Prototype #2 with C_2 = 200 μF. Here the commutated current is 10.5 kA, although the mode of commutation cannot be identified on this 1ms/div. timescale. The lower trace shows the contact separation, d, and the circuit current.

4-1.2. Conclusions

These experiments revealed several new aspects. (1) The high speed oscillograms allowed us to make more detailed comparisons with theoretical predictions which appear in Section 2, (2) a further mode of current commutation was found, Mode 4, (3) we became aware that residual current can flow after most of the current has been commutated from the device, and that ways must be found for dealing with this effect, and (4) we succeeded in building devices that exhibit a comparatively long life. In particular, Prototype #2 underwent 150 tests with currents ranging up to 12 kA and did not show any deterioration in commutation ability.

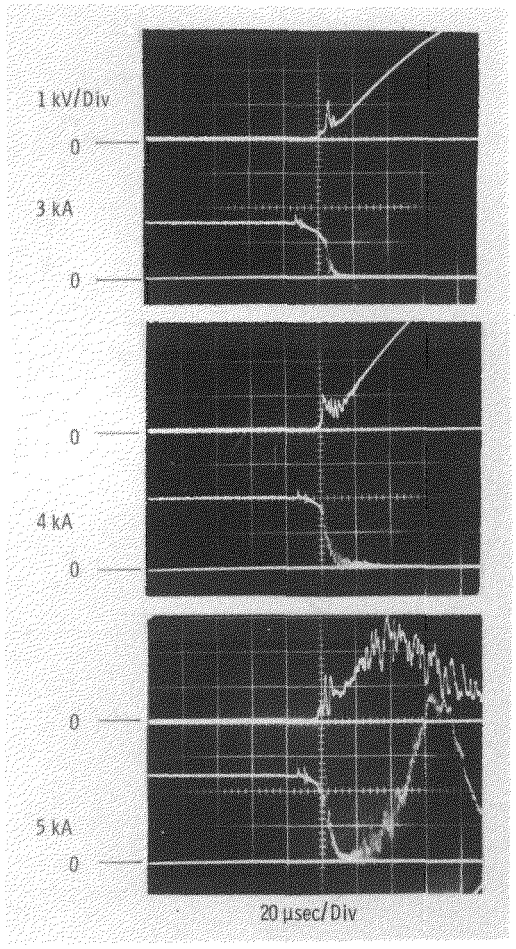

Figure 4-6. Representative oscillograms taken with Prototype #1; C_2 = 50µF, d = 2cm.

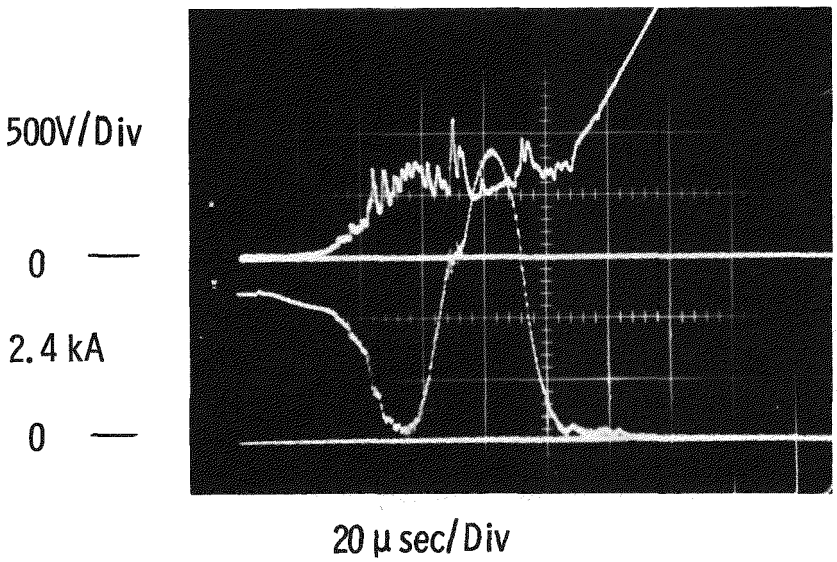

Figure 4-7. An example of Mode 4 current commutation from Prototype #1; C_2 = 50µF d = 2cm.

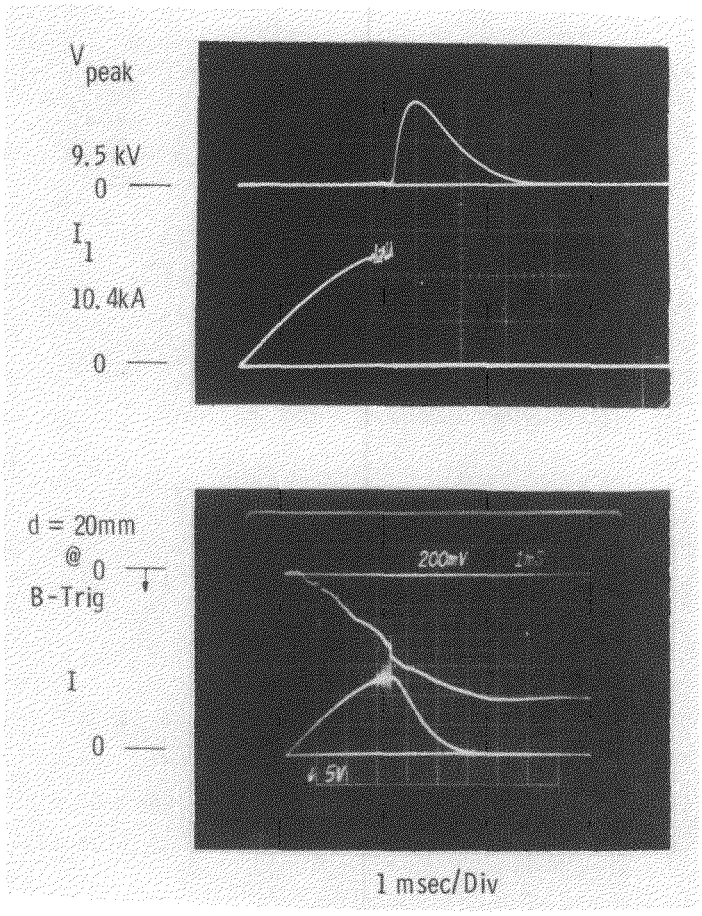

Figure 4-8. Current commutation from Prototype #2; upper picture shows the device current and recovery voltage; lower picture shows the contact separation and the circuit current; C_2 = 200μF.

In addition to the above findings, a series of parametric studies were made at this time. The details of these studies can be found in Appendix D-1. They are summarized below:

- Both B_{max} and B should be large to achieve maximum performance. It was possible that the apparent large B_{max} effect may actually be due to longer duration of the magnetic field.
- The performance of the vacuum device improved beyond the theoretical optimum $\dot{B}$ where the optimum is based on anode heating considerations. In fact, at five times the optimum $\dot{B}$, the performance was continuing to increase. This illustrated that the mode of failure to commutate was not excessive anode heating.
- Increased parallel circuit capacitance increased preformance. It seemed probable that the faster rising voltage with small capacitance caused reignition from the residual current.

- Larger diameter electrodes increased the device performance.
- We would expect only a modest increase of performance with a further reduction of external circuit inductance.
- Even when these vacuum devices fail to commutate the current, the current was still driven to a low value before failure.

4-2 PARAMETRIC STUDIES USING THE DEMOUNTABLE ARC CHAMBER

4-2.1. Introduction

The major objective of the demountable tests was to study the influence of different contact geometries on the arcing behavior (a) prior to field application and (b) during the interaction with the transverse magnetic field. Further, we wished to observe the influence of the orientation of bar contacts with respect to the applied magnetic field. Finally, it was our intent to investigate the differences in arcing behavior for Mode 1 and Mode 4 commutations.

The results are presented in the form of commutation limits achieved in these experiments, as well as in descriptions of the typical arcing behavior for the different contacts. Emphasis is laid on describing the influence on successful commutation of the arc appearance before and after application of the transverse magnetic field.

The commutation results obtained with the demountable arc chamber cannot be compared to results obtained with sealed devices because (a) the rise time of the magnetic field in the arcing space was much smaller in these arc chamber experiments due to the metal chamber walls, (b) the arc chamber could not be baked, and adsorbed gas layers at the chamber walls influenced interruption behavior, and (c) breakdowns occurred between the electrode stems and the metal chamber walls, having the consequence that the current bypassed the inter-electrode region.

4-2.2. Commutation Results

The results are summarized in Table 4-1. The commutation current is divided according to the mode in which commutation was achieved. Mode 1 signifies a monotonical and fast decrease of the current to zero, Mode 4 involves a forced current zero by ringing of the parallel capacitive circuit following initially unsuccessful commutation. It should be noted that higher commutation currents were obtained with Mode 4 in all instances. The one exception was with the concave bar oriented parallel to the magnetic field. Further, no Mode 1 commutation was observed when this bar was oriented perpendicularly to the applied magnetic field.

It must be noted that the commutation data of Table 4-1 must be interpreted with caution. These experiments were performed in a metal walled chamber and, in all cases of failure, a breakdown between the electrode stems and the chamber walls ultimately occurred. The experimental conditions are given in Section 3-1.4.

Table 4-1

COMMUTATION RESULTS OF DEMOUNTABLE ARC CHAMBER STUDIES

Contact	Current Variation kA	Capacitance μF	Commutation Current Mode 1 kA	Commutation Current Mode 4 kA
Cup, 10 cm diam.	1 - 10.8	200	--	--
Cup w. Cut, parallel to B	1.7 - 10	200	--	1.7 (no movie)
Concave Bar:				
parallel to B	1.3 - 12.1	200	1.9 (1.3)*	--
perpendicular to B	1.5 - 12.4	200	--	2.74 (2.74)
		50	--	2.2 (no movie)
45° to B	1.25- 12.0	200	1.5 (1.25)	2.1 (no movie)
Convex Bar, parallel to B	1.15- 6.2	100	1.15 (no movie)	1.7 (1.7)
Same with axial B	1.2 - 4.4	100	1.2 (no movie)	1.8 (1.6)

* Number in parentheses gives current value for which movie was taken.

4-2.3. Description of Arc Appearances

Cup Contacts. In all cases, the arc became diffuse in less than 1.5 ms after the initial bridge explosion. No anode spots were observed for currents below 11 kA. After B-field application, grouping of cathode spots occurred.

Cup Contacts with Cuts. The arc remained confined to the contact half where the initial bridge had formed. An anode spot formed on one corner of the contact at currents above 2 kA. After B-field application, bunching of cathode spots was observed together with movement of the cathode spots over the contact edge. At higher currents, the anode jet remained pointing along the magnetic field vector. The intensity of this anode jet subsided during the 1 ms period following field application.

Concave Bar Contacts. Usually one bridge was observed and the arc remained confined to the corresponding side of the bar. The cathode spots would tend to spread continuously in a circular fashion towards the contact center, but the arc would always suddenly become reconfined. This periodic bunching occurred over periods between 200μs and 500μs and was accompanied by small voltage spikes (compare Ref. (8) and (9). Transient anode spots formed at current levels of approximately 2kA, and persistent anode spots appeared between 2.5 and 3kA. At current levels above 4kA, it was occasionally observed that the arc suddenly distributed over the entire contact surface. As a consequence of the larger effective electrode area, the anode spot disappeared and the arc voltage was lower (see Fig. 4-9).

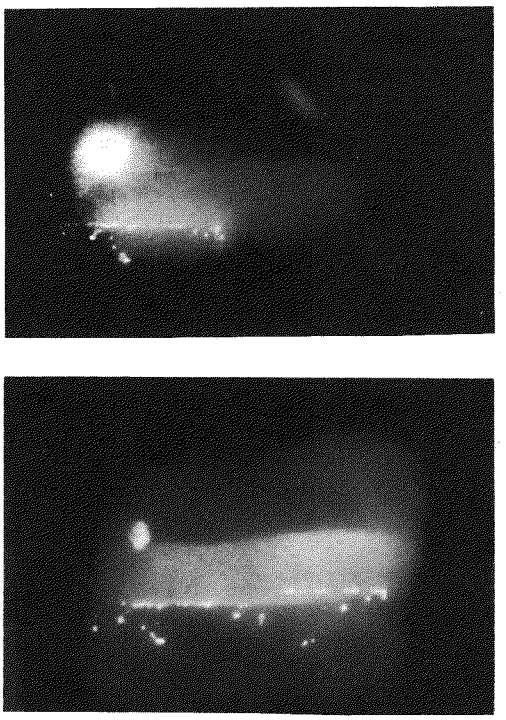

Fig. 4-9. Sudden arc expansion over entire contact, at 4kA, concave bar contact.

The anode spot reappeared around 6kA. For current values at contact separation of 2.5kA, bridge explosions were occasionally observed on both sides of the bar.

The arc observations after B-field application are split up according to the orientation of the bar contact with respect to the magnetic field.

Contacts Parallel to B

The cathode spots moved in the retrograde direction over the contact edge. Photographs from the two cameras then indicated the following sequence (See Fig. 4-10).

(a) line formation along the contact edge (b) a bunching of the cathode spots into several groups and (c) further coalescing of the cathode spots in the individual groups into single bright regions ("super-spots"). The time resolution and synchronization of the cameras was such that the (a) and (b) sequences could not be resolved with certainty. In particular, there were occasions when the group of spots formed before the cathode spots reached the contact edge.

In the cases where an anode spot was present, the radiation from the spot area subsided over a time period of several hundred microseconds. Figures 4-9 and 4-11 compare arc appearances and arc oscillograms for a Mode 1 commutation and a failure under similar conditions. The noticeable differences are that in the case of failure a brighter glow signals the release of adsorbed gas, the "super spots" persist longer on the side surface of the contact, and a glow develops which seems to be wrapped around the cathode.

Contacts Perpendicular to B. Groups of cathode spots moved in the retrograde direction over the contact edge to the bottom side of the bar. The plasma then curled around the contact edge into the interelectrode region; (see Figs. 4-12 and 4-13). This effect was more pronounced at higher currents (Fig. 4-13). No distinct difference in arc appearance was observed for Mode 4 commutation and failure under similar conditions. It should be noted that in practically all instances, application of the B-field led to an initial reduction in arc voltage as well as a reduction in the arc voltage noise (see Figs. 4-12 and 4-13).

Contacts with a 45° Angle to B. The same arcing behavior was observed with this geometry as with the contacts perpendicular to B. The preferred region for the last gathering of cathode spots was the corner of the contact which pointed in the retrograde direction with respect to the applied B-field. Comparison of Mode 1 commutation with a borderline failure (Figs. 4-19 and 4-15) shows that in the case of commutation the cathode spots formed a line of groups in the center of the contact and then disappeared within 100μs. In the case of failure, the cathode spots persisted for 400 to 600μs after application of the magnetic field, and moved during this time in the retrograde direction over the contact edge onto the bottom surface of the bar. Simultaneously a bluish glowing layer of plasma built up around the cathode. In addition to this indication of the metal vapor plasma we saw a pink glow which signals the release of adsorbed gas from the quartz envelope. At higher currents ($\sim$ 12kA) the area heated by the anode spot remained glowing for 1 ms or longer.

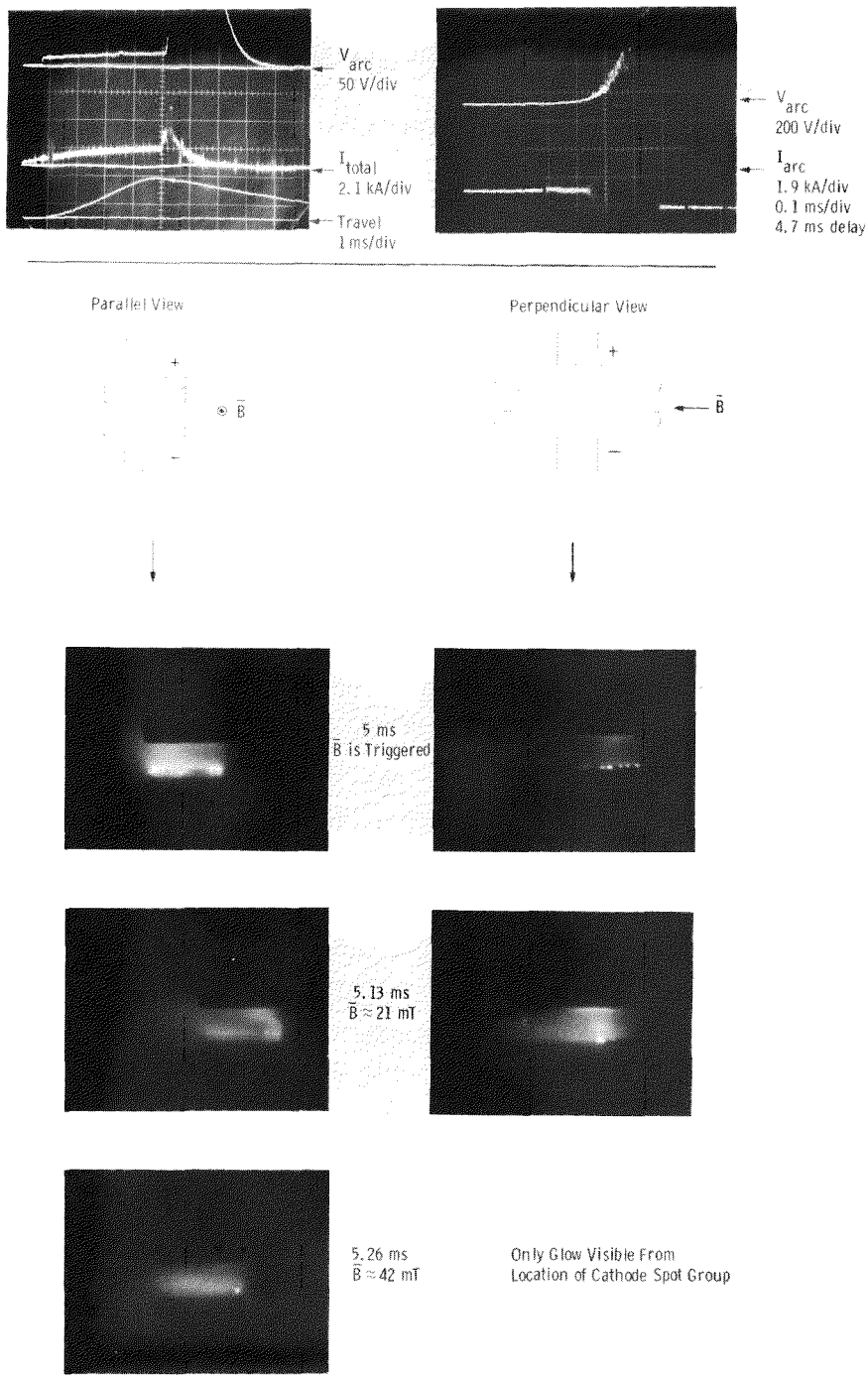

Fig. 4-10. Concave bar contact parallel to $\overline{B}$, I_{peak} = 1.3 kA.

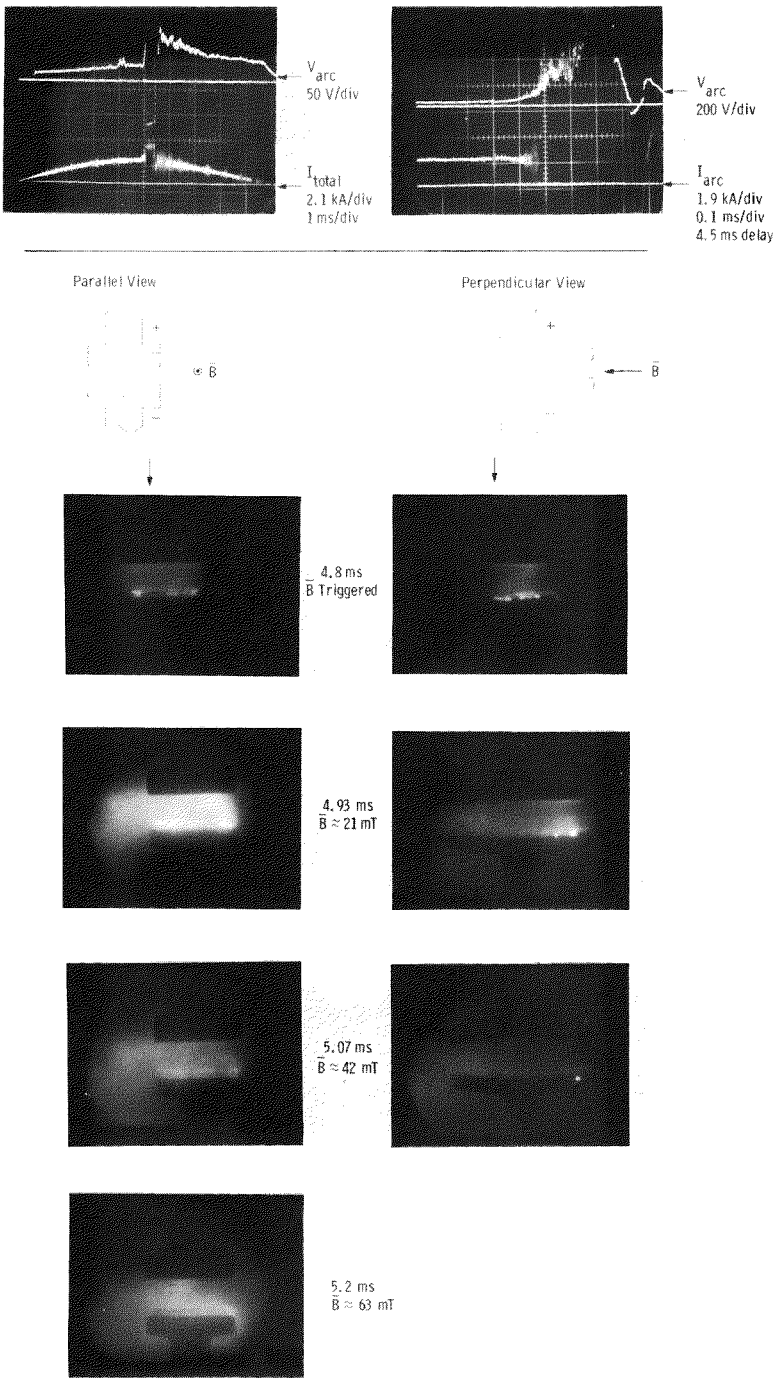

Fig. 4-11. Concave bar contact oriented parallel to $\bar{B}$, I_{peak} = 1.9 kA.

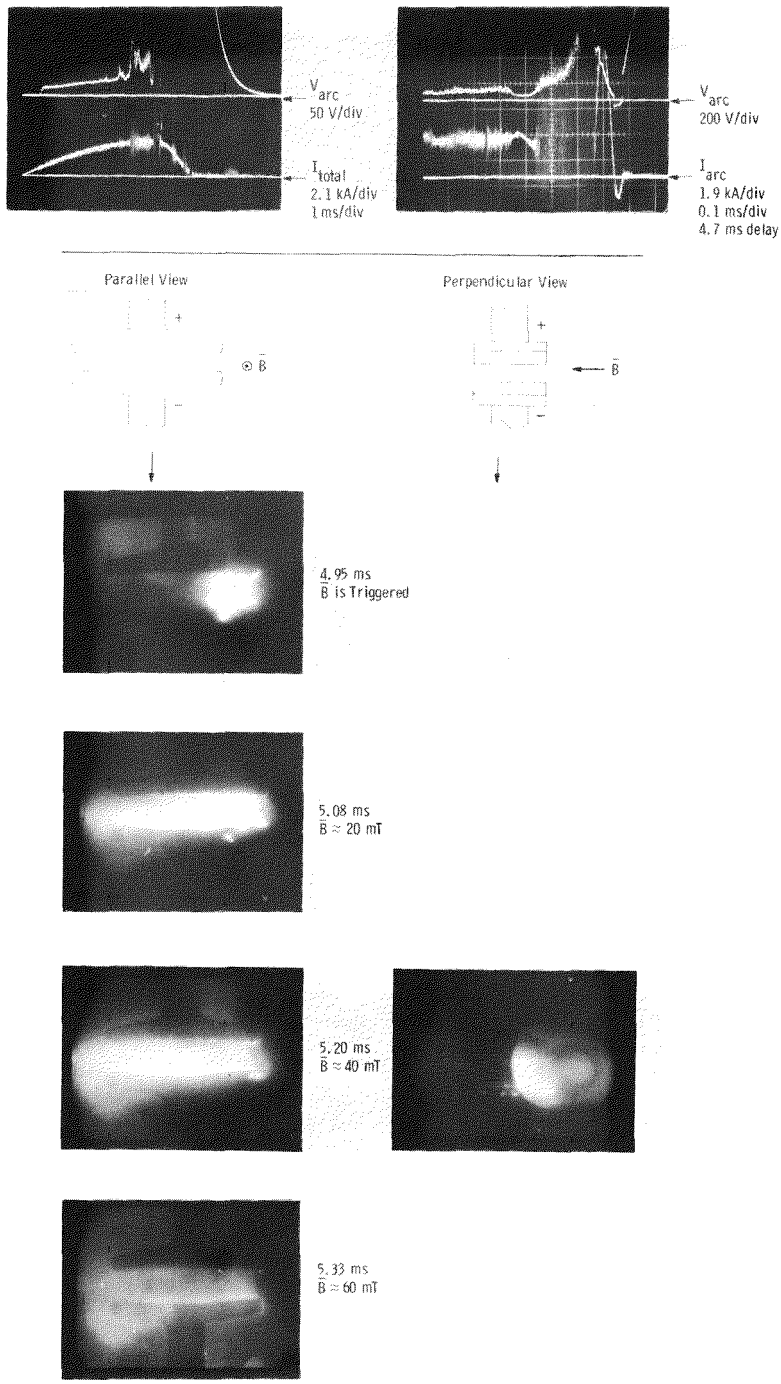

Fig. 4-12. Concave bar contact perpendicular to $\bar{B}$, mode 4 commutation at I=2.74 kA.

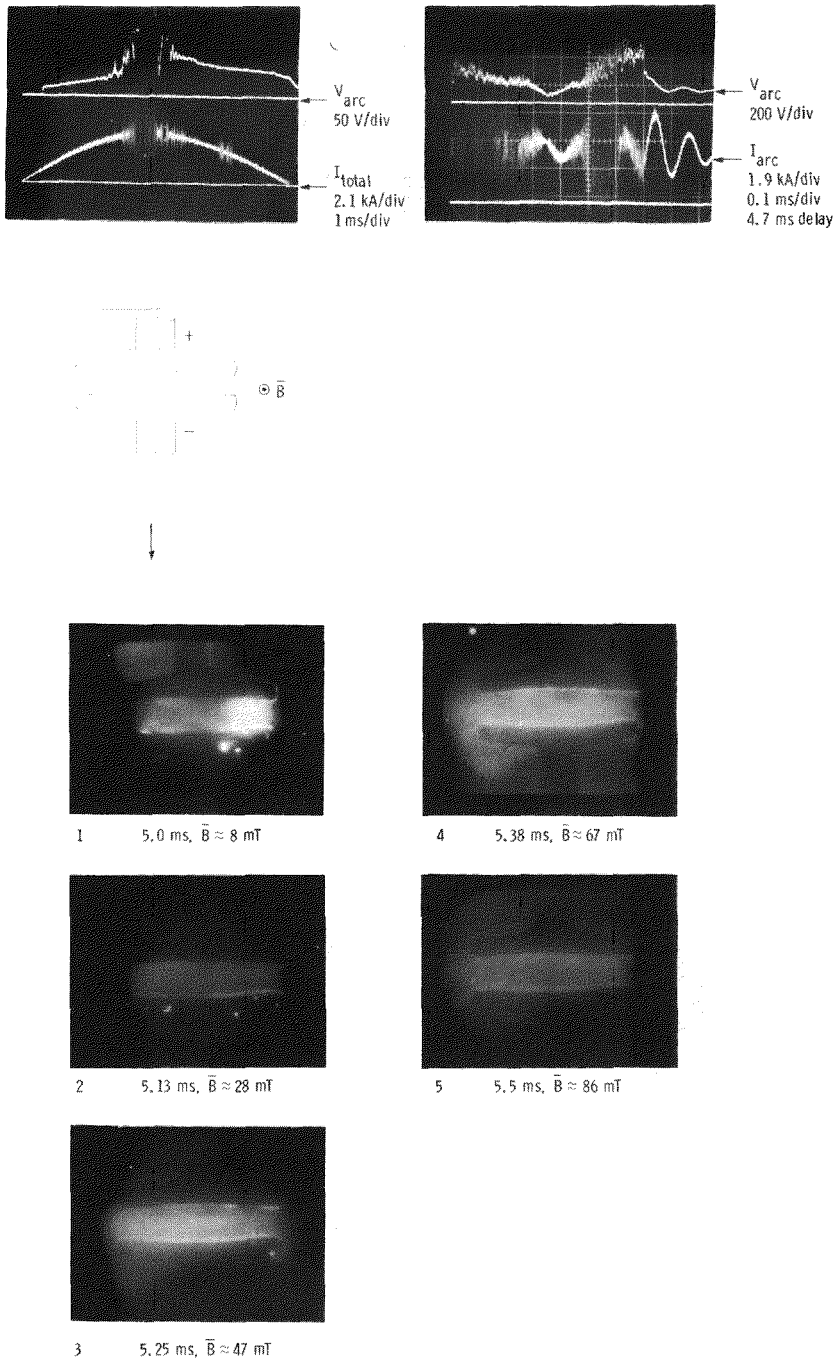

Fig. 4-13. Concave bar contact, perpendicular to $\bar{B}$, I_{peak} = 3.75 kA

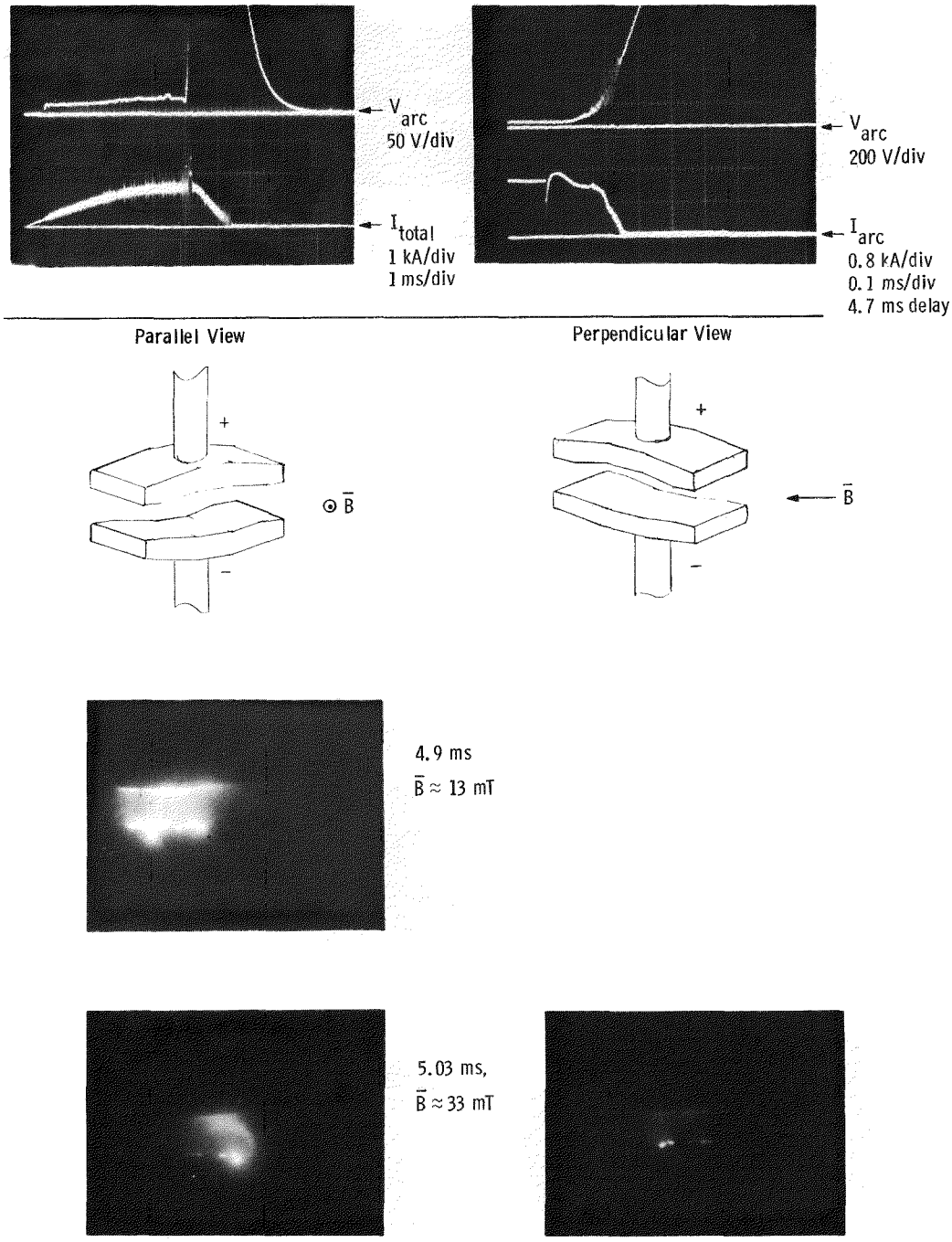

Fig. 4-14. Concave bar contact, 45° to $\bar{B}$, I = 1.25 kA

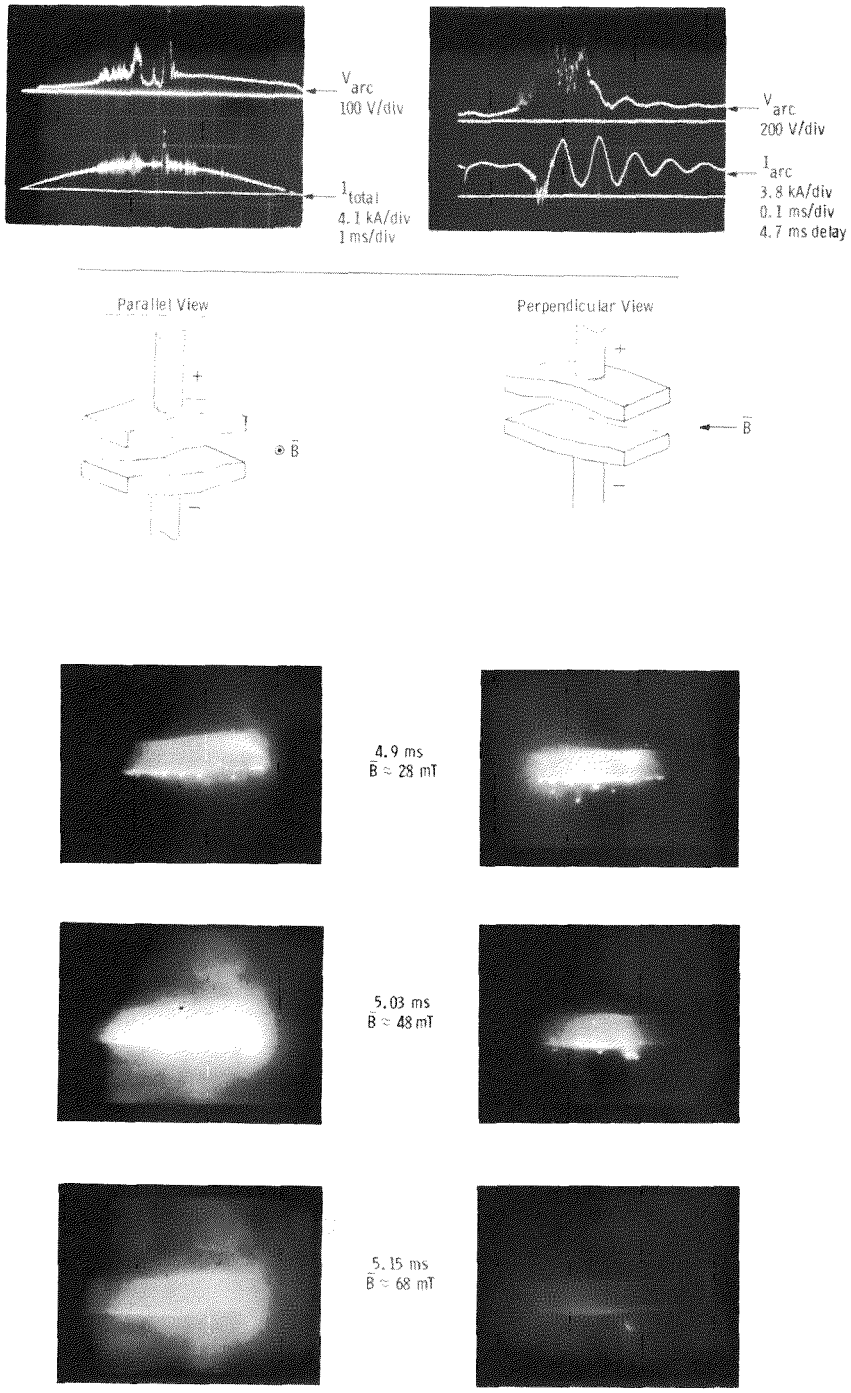

Fig. 4-15. Concave bar contacts, 45° to $\bar{B}$, I = 4.0 kA

Convex Bar Contacts, Parallel to B. With these contacts, cyclic bunching of cathode spots was also observed. However, the arc did not remain confined to one side of the bar. After application of the B-field, the cathode spots assembled in groups at the contact edge on the retrograde side (see Fig. 4-16), and subsequently moved over

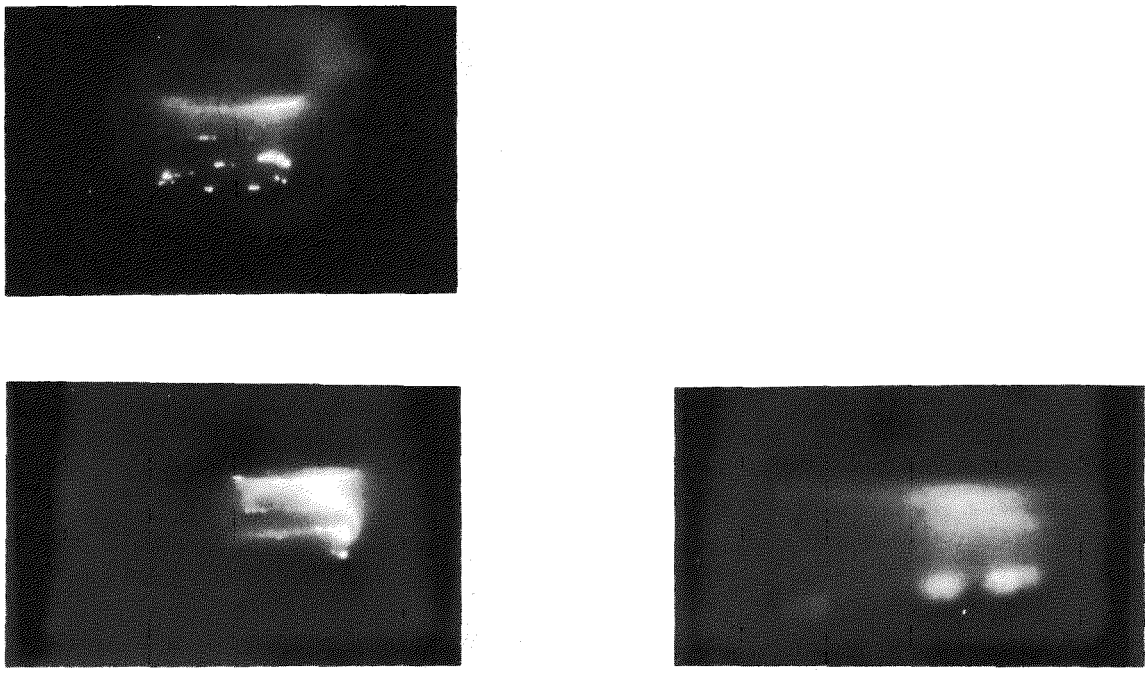

Fig. 4-16. Convex bar contact, commutation at 1.7kA.

the edge onto the side surface. In cases of failure, the cathode spots persisted on the side surface, and a glowing layer developed around the cathode. Anode spot involvement was distinct, but was probably augmented by a contaminated contact surface.

There was less cyclic bunching prior to transverse field application when the arc was subjected to an axial magnetic field. However, there were no distinct changes in arc appearance when the transverse B-field was applied.

4-2.4 Conclusions

It is difficult to arrive at definite conclusions concerning the important causes for failure or success of the commutation process. Persistence of cathode spots on the side surface, build-up of a glowing plasma layer around the cathode, and release of gas from the surrounding walls were all observed to mark the major difference between Mode 1 commutation and failure. However, the time resolution of our observations was not good enough to permit identification of cause and consequence.

There is no distinct difference in arc appearance for Mode 4 commutation and failure under comparable conditions. At higher currents, no distinct dark layer is visible in front of the anode. In the cases where Mode 4 commutation was observed, the cathode spots had moved to the side or back surface of the contact. In a previous report (ref. (1) we described a Mode 2 commutation in which the cathode spots moved over the contact edge. Our present data suggest that this motion is an insufficient condition for commutation, and that a current oscillation is also required.

We can draw several conclusions with respect to the influence of the contact geometry on commutation and arc appearance.

A. Mode 1 commutation was not observed for several contact geometries and orientations. However, a judgment based on the arc appearances prior to and following field application indicates that Mode 1 should be possible in all cases.

B. The large surface area of the cup contact prevents anode spot formation at currents up to 11kA. However, the interaction between the arc and the transverse magnetic field appears to be less pronounced than with other contacts. The radial magnetic field generated by the current flowing in the contact might be the reason for this observation. We considered that the higher magnitude and faster rise time of the transverse magnetic field in sealed devices would diminish this influence of the radial magnetic field. Consequently, the ability of anode spot prevention up to higher currents made the cup contact one choice for a practical device.

C. The cup contact with cuts is ineffective in producting useful current division. A larger amount of inductance in the parallel current paths has to be provided if parallel arcing contacts are to be considered in the future.

D. The concave bar contact does not seem to be superior to the convex bar when oriented parallel to the applied magnetic field. The arc appearance is similar in both cases, and the higher commutation current is explained by the higher parallel capacitance. The concave bar does have the disadvantage of promoting confinement of the arc to one contact half only. This leads to early anode spot formation. However, the high value of Mode 4 commutation current in the case of a concave bar oriented perpendicularly to the applied magnetic field suggests that this arrangement might prove promising for actual current limiting devices. Unfortunately, no data are available using the convex bar in the same arrangement.

E. It is difficult to compare conclusively the present results with data obtained earlier with Bruce profile contacts (1) because there was no quartz liner in these earlier experiments. Consequently, no successful commutation was observed. However, the larger contact surface area prevented anode spot formation up to currents of 14kA, and from our arc observations we cannot single out one positive feature of the bar contacts which would not be present with the Bruce profile contacts. Therefore, large area Bruce profile contacts are also recommended for practical devices.

4-3 PARAMETER VARIATIONS USING TRANSVERSE MAGNETIC FIELDS AND OSCILLATING MAGNETIC FIELD

4-3.1 Experimental Results of Parametric Study Using Conventional Field Application with Prototypes #2, #3, and #4

The experiments discussed in Section 4-1, and in this subsection, were performed with transverse magnetic fields which rose rapidly to a peak value followed by a slow decay to zero. This "conventional field" application is distinguished from the "oscillating fields" discussed in Section 4-3.2.

Comparison of Cu-Bi Electrodes (Prototype #3) with CLR Electrodes (Prototype #1). Prototypes #3 and #1 were almost identical and were equipped with 11cm diameter Bruce profile electrodes within an 18cm diameter shieldless ceramic envelope. However, the electrodes in #3 were made from Cu-Bi (0.3% Bi by weight) material. Experiments with #3 were performed at an electrode separation of 20mm and with a parallel capacitance of 50μF. Two series of tests were performed with initial rates of rise of magnetic field of 2.2 T/sec (B_{max} = B/6000) and 4.4 T/sec (B_{max} = B/24000). Data comparing this electrode material with earlier Prototype #1 data are shown in Figure 4-17. Copper bismuth has an inferior level of performance compared with CLR by about 80%.

A further disadvantage of copper bismuth over CLR is the short life. After 38 experiments the copper bismuth had shown some degradation whereas Prototype #1 was used for 61 experiments and is still in good condition.

Study of Residual Current Using Prototype #4. A special 18 cm diameter sealed device was constructed with the movable electrode insulated from the metal end. This insulation was the only difference from Prototype #1. The purpose of the experiments with this device was to study the residual current and to study the effects of greater $\dot{B}$ at the same peak magnetic field values. A sketch of this device is shown in Figure 4-18 and two sample oscillograms are shown in Figure 4-19. The electrodes are 11 cm diameter Bruce profile using CLR material. For all experiments the electrode separation was 20 mm, and the parallel circuit capacitance was 50 μF.

The oscillograms of Figure 4-19 are for the case when the insulated metal end was not connected. They show a substantial residual current. This illustrated that the residual current flows between the electrodes and that the metal end does not need to be involved.

When the metal end was connected to the movable electrode, the performance was increased by approximately 25%. The extra area improved the performance. This

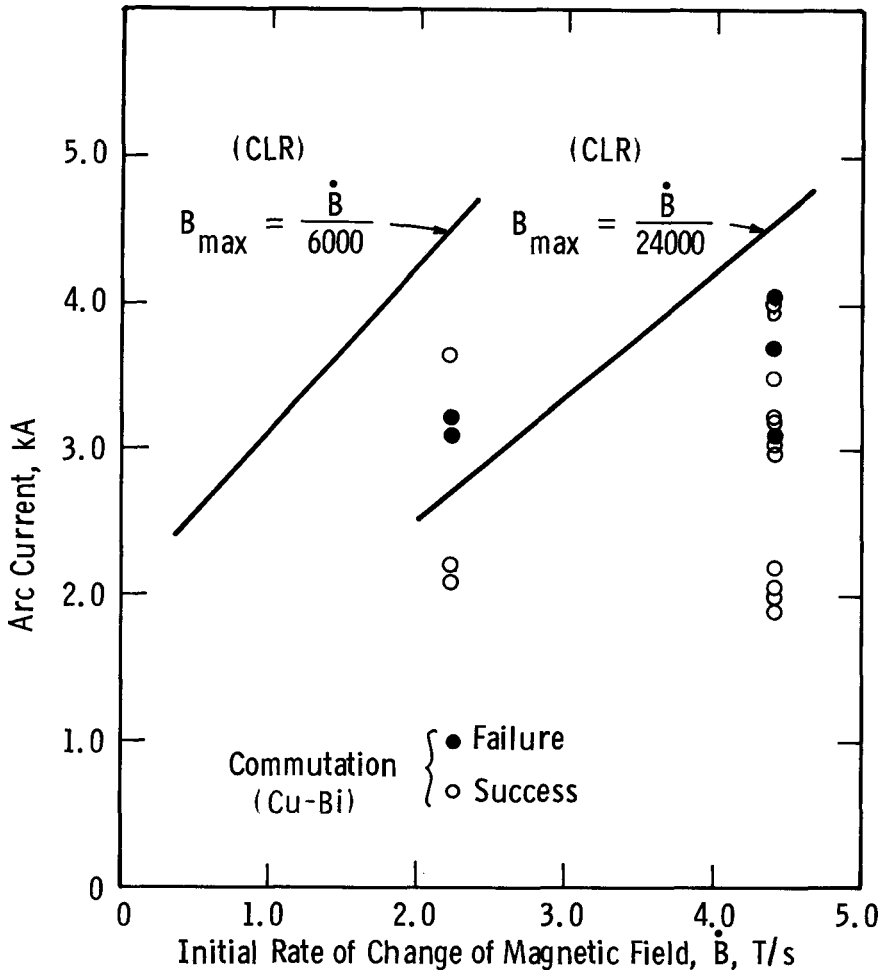

Fig. 4-17. Copper Bismuth data compared with earlier CLR results; 11cm dia. electrodes, 20mm electrode separation, 18cm. envelope (experimental points Prototype #3 full curves Prototype #1).

improvement took place regardless of whether the moving electrode was serving as a cathode or anode. When the movable electrode was the anode, approximately 10% of the current was carried by the metal end before commutation. If the device failed to commutate, this fraction increased to 30% of the total current. When the movable electrode was the cathode, less than 5% of the current was carried by the metal end before commutation. If the device failed to commutate, slightly less than 25% of the current flowed to the metal end.

Effect of Lower Inductance Magnetic Field Coils. Experiments described in Section 4-1 with CLR electrode material utilized 8 turn magnetic field coils connected in parallel. There was some evidence that a more rapidly changing magnetic field (higher $\dot{B}$) would increase the sealed device performance. Thus, we constructed two

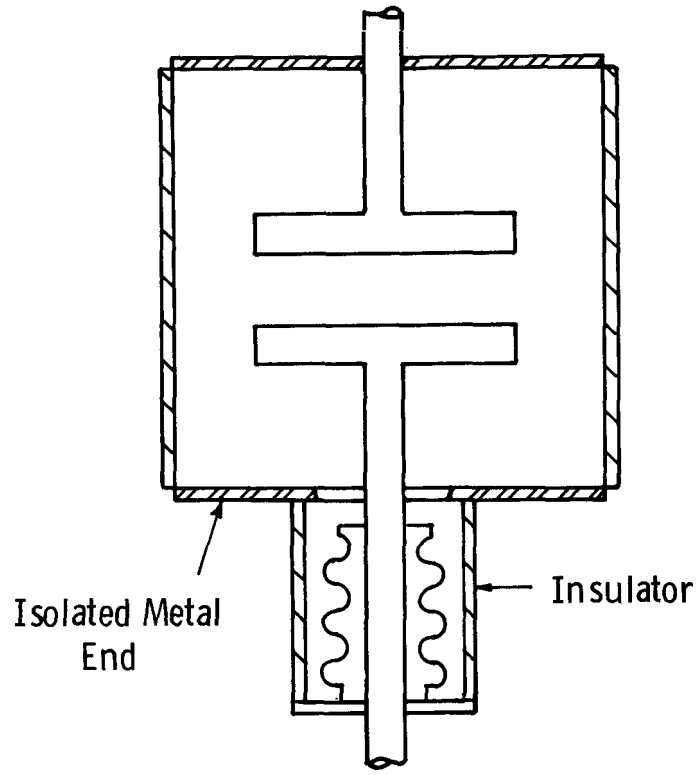

Figure 4-18. Sealed device with isolated metal end, 18cm. diameter using 11cm diameter CLR electrodes (prototype #4)

turn coils to provide a more rapidly changing magnetic field and to permit series connection to ensure equal current in each coil. Experiments with Prototype #4 with the end flange connected showed that these coils improved the performance by approximately 10% at a given peak magnetic field.

However, when $\dot{B}$ and B_{max} were increased still further (from 7700 to 9200 T/S and 0.23 to 0.28 T, respectively) we observed a decrease of performance. The new data along with comparable earlier performance information appear in Figure 4-20. The conclusion was that we had exceeded the optimum $\dot{B}$ for this external circuit. An optimum $\dot{B}$ had previously been predicted from theory (1).

In order to check that the decreased performance with increased $\dot{B}$ was not due to degradation of CLR electrodes, experiments performed at the start of the test series were repeated. These experiments yielded identical commutation data. There was no degradation after 64 experiments confirming (a) that CLR electrode material provides long device life and a stable level of performance and (b) that Figure 4-20 is realistic.

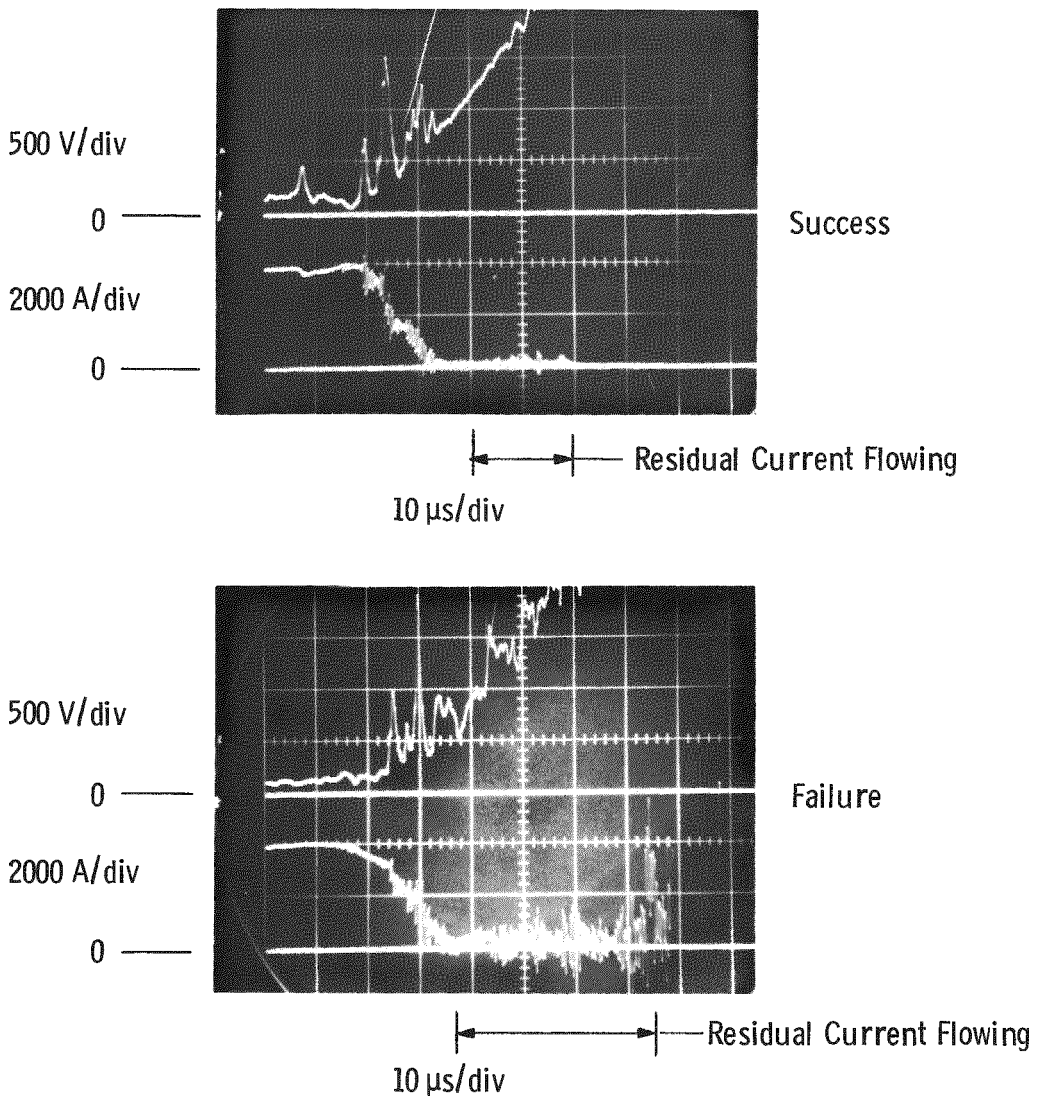

Figure 4-19. Commutation experiments with Prototype #4 showing residual current flowing to the movable electrode (metal end of sealed device isolated from the movable electrode).

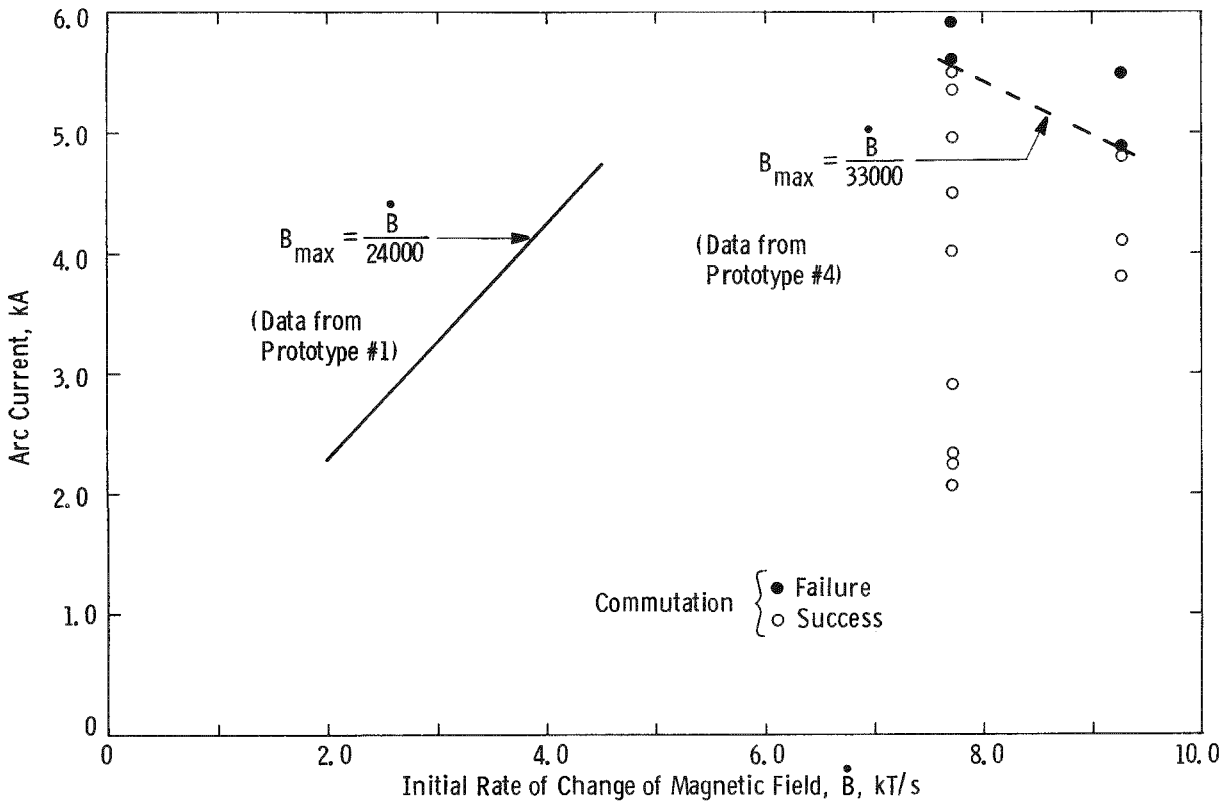

Figure 4-20. Illustration of how at 9200 T/sec the optimum $\dot{B}$ has been exceeded, 11 cm dia. electrodes, 20 mm electrode separation, 18 cm envelope diameter.

Measurements of Excursion Current Using Prototype #2. At the borderline between successful commutation and failure, a residual current of several hundred amperes can flow in the sealed device for periods of tens of microseconds. In order to further our understanding of this residual current, we measured the excursion current, I_{ex}, for a wide range of arc currents, I. This excursion current is illustrated in Figure 4-21. The data in this Figure show that the excursion current continues to increase with the circuit current. This observation suggested that auxiliary schemes to commutate current would be necessary. These auxiliary schemes included the application of a second magnetic field, oscillating magnetic fields and resonant external circuits. Experiments using these auxiliary schemes for current commutation are discussed in Section 4-3.2.

Conclusions.

- Use CLR electrode material for good performance and long device life.
- Use large area electrodes. Even stationary current collectors connected to either anode or cathode will improve performance.

- Keep the arc voltage low by using electrode materials with low gas content, rapid electrode separation, early application of magnetic field, etc.
- Use auxiliary mangetic field schemes (a second magnetic field, an oscillating magnetic field, a resonant external circuit, etc) to improve device performance.

4-3.2 Experiments Using Modulation of the Transverse B-field

Introduction

Experiments were run on both Prototype #2 and Prototype #5 to investigate the effect of a variation of the transverse magnetic field on the ability of the device to commutate. Both of these prototypes had 23 cm diameter ceramics and a length of 36 cm. Prototype #2 was equipped with 14 cm diameter Bruce profile electrodes, and Prototype #5 had concave bar electrodes with a length of 15 cm and width of 7 cm.

Two different types of experiments were run: (1) using two independent transverse fields and (2) using an oscillatory magnetic field both with and without the external circuit tuned to the 2nd harmonic of the oscillating B-field. The first

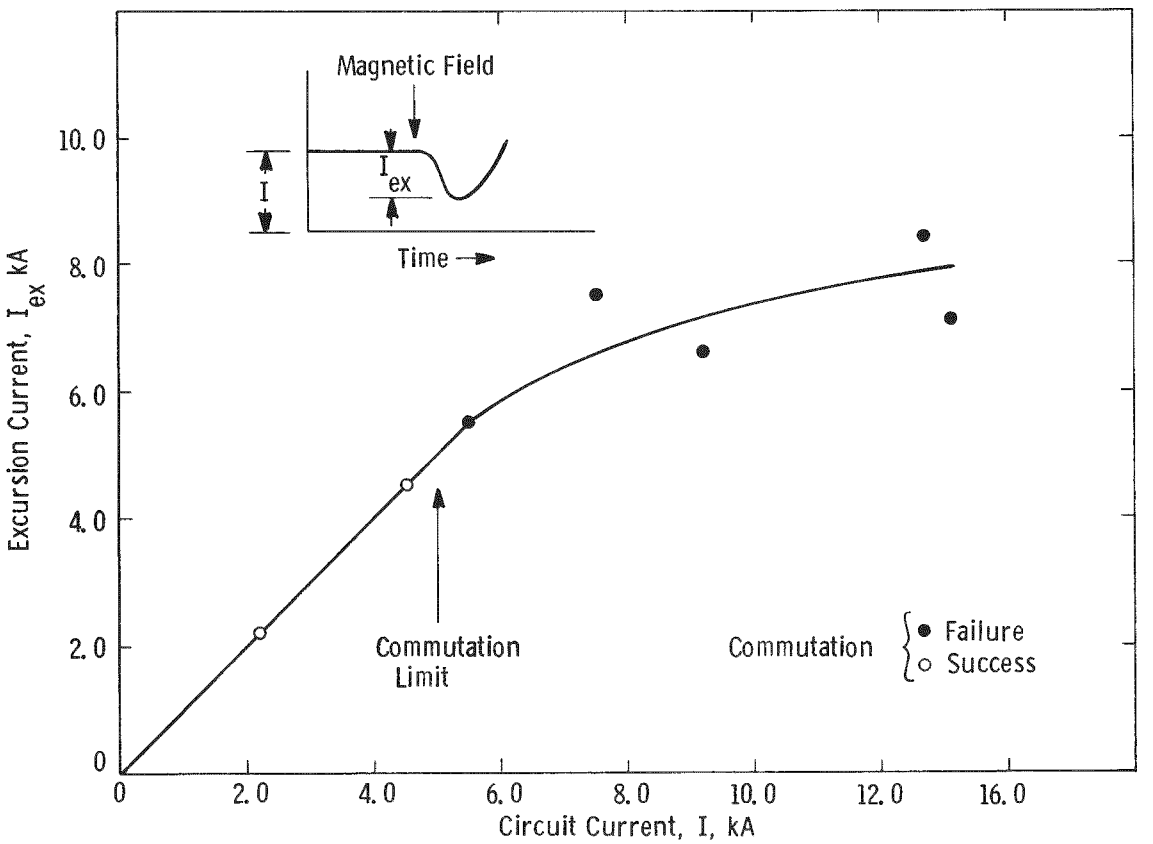

Figure 4-21. Measurements of the excursion current performance using Prototype #2. (25cm electrode separation, $\dot{B}$ = 7400 T/sec)

type experiment attempts to suppress the residual current in a Mode 1 commutation while the second type attempts to enhance this current and subsequently optimize a Mode 4 commutation.

Experiments Using Two Independent Transverse Magnetic Fields. Earlier experiments had shown that for Mode 1 commutation, a small residual current can flow through the vacuum device after most of the arc current had been commutated into the parallel network. Typically, for arcing currents below the limit of the commutation ability, a residual current of less than two hundred amperes decays to zero in some tens of microseconds. However, at the limit of commutation ability the residual current was a few hundred amperes. This current does not decay, and leads to a reignition of full current flow in the device. While the existence of this residual current is difficult to explain, its possible connection to commutation failure suggested that steps be taken to suppress it. For this purpose, a second independent transverse magnetic field was used. It was anticipated that if indeed the residual current were flowing in the arcing gap, this second field with a large $\dot{B}$ occurring at the proper time would alter conditions and quench the remaining arc plasma. The initial experiment was run with two pairs of 8 turn coils using Prototype #2. The first field, B-1, had an initial $\dot{B}$ of 100 T/sec and rose to a peak value in the gap of 0.09 T in 160 μsec. The second field, B-2, had an initial $\dot{B}$ of 5500 T/sec and rose to a peak value of 0.23 T in 70 μsec. The two coil pairs were arranged physically at right angles to prevent electrical interaction that might cause one to trigger the other or induce damaging voltages in the power supplies. The pulse size and pulse shape of the fields were held constant during the experiment and the activation of one field did not change the characteristics of the other. The parallel network was similar to that used for the earlier tests on Prototype #2 and consists of C_2 = 50 μF, R_2 = 2.3 Ω and L_2 ≈ 1.6 μH. The arcing gap was 2 cm at the time the transverse fields were applied.

Figure 4-22 summarizes the data taken with Prototype #2. The two columns on the left show the commutation ability of this device for the B-1 and the B-2 fields used independently. The data on the right show the effect of using the two B-fields together with the stronger field, B-2, delayed by the amount shown. A higher level of commutation ability is noted at a delay of about 20 μsec while the highest current commutated occurred when the fields were applied almost simultaneously. Figure 4-23 is representative of the delayed case. Figure 4-24 contrasts the failure to commutate 6 kA using the B-2 field only with the successful commutation of 6 kA using the B1 and B2 fields simultaneously. Note that the successful commutations in these Figures are both Mode 1 current commutations.

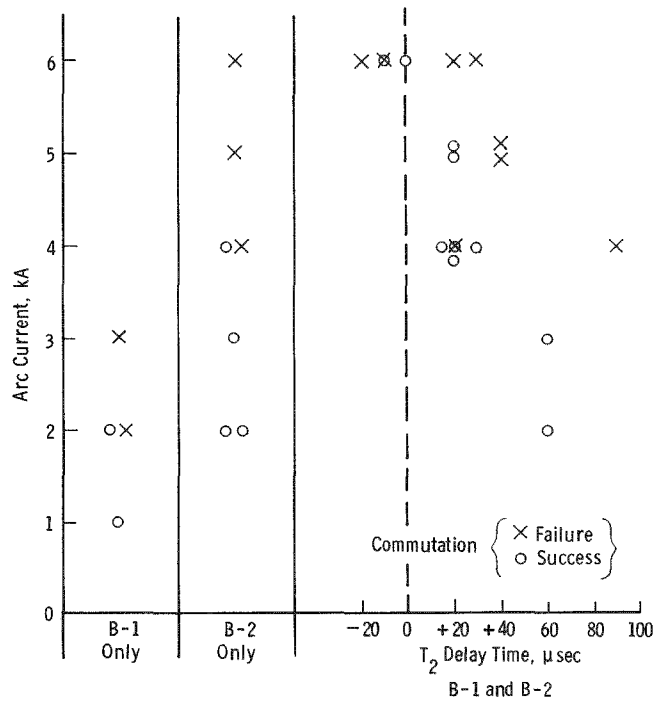

Figure 4-22. Summary of data taken to explore the effect of two independent transverse magnetic fields; Prototype #2 with C_2 = 50µF, d - 2cm.

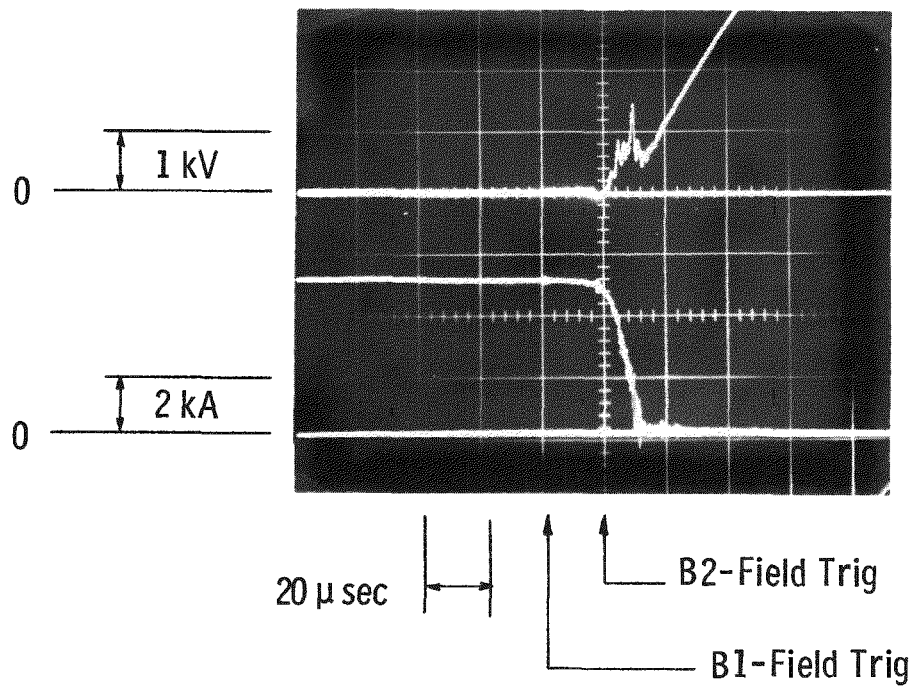

Figure 4-23. Successful commutation of 5kA from Prototype #2 using two transverse fields approx. 20µsec apart; C_2 = 50µF, d = 2cm.

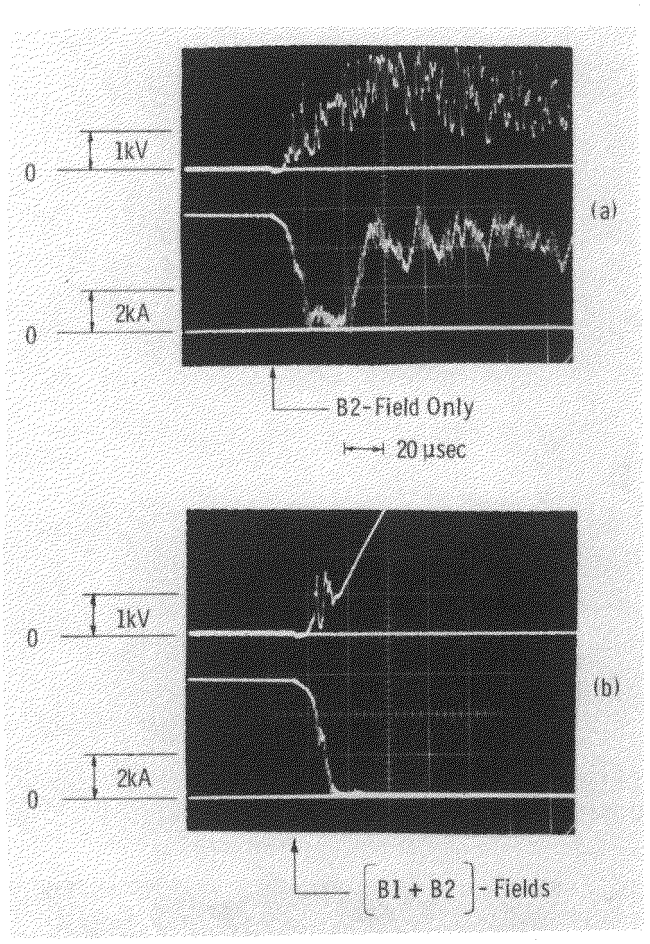

Figure 4-24. (a) Failure to commutate 6 kA with B2-field only and (b) successful commutation of 6 kA with simultaneous application of B1 + B2; Prototype #2 with C_2 = 50 μF, d = 2 cm.

A second experiment using two independent transverse magnetic fields was performed with two pairs of 2 turn coils using Prototype #5. The two transverse magnetic fields were of approximately equal strength with an initial $\dot{B}$ of 6800 T/sec for B-1 and 7200 T/sec for B-2. The peak fields were 0.2 and 0.23 T, respectively and the peak was attained in 48 μsec. The results of this experiment are shown in Figure 4-25. The B-1 field lines followed the length of the bar while the B-2 field lines followed the width of the bar (both fields were, of course, transverse to the arc current). The two left hand columns in Figure 4-25 show the response of Prototype #5 to each field independently, and it will be noted that simultaneous field application only equaled the performance with B-1 alone.

The experimental data in Figures 4-22 and 4-25 indicate only marginal improvements with double field application, and we therefore decided to investigate the effect of oscillating fields as described in the subsequent Section.

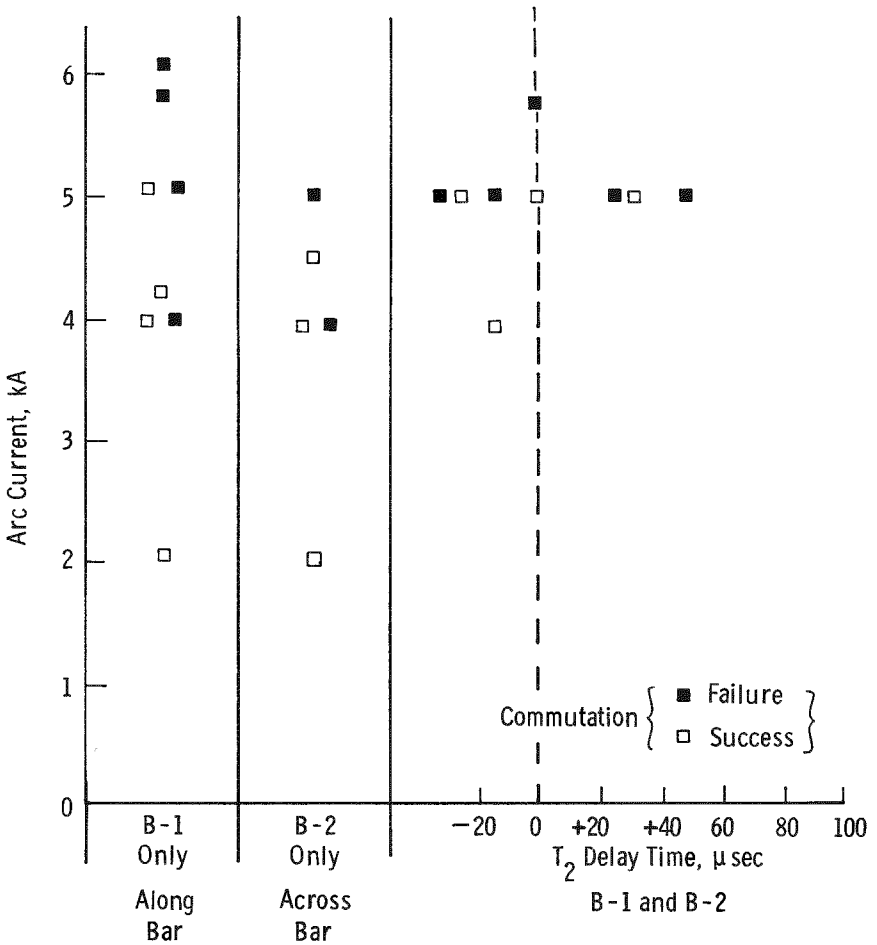

Figure 4-25. Summary of data taken to explore the effect of two independent transverse magnetic fields; Prototype #5 with C_2 = 50μF, d = 2cm.

Experiments with an Oscillating Magnetic Field. The first oscillating field experiments were performed with Prototype #5. Figure 4-26 shows a successful commutation of 8200 A with an oscillating magnetic field. It will be noted that the arc voltage is proportional to the absolute value of B, and oscillates at twice the frequency of the magnetic field circuit. This commutation took 760μsec. At lower currents much more rapid commutations were observed. For example, at 7500 A the commutation time was 140μs. The increase in commutation level using oscillating magnetic fields with prototype #5 was about 60%. This substantial improvement led us to investigate the phenomenon more fully in all subsequent experiments, and details of the theory and experiment are to be found in Sections 2-3 and 4-4 respectively.

Experiments Involving Tuning the External Circuit. Examination of the mode 4 commutation illustrated in the oscillogram of Fig. 4-26, and consideration of the current flow in the parallel circuit suggests that if this circuit were resonant at twice the frequency of the magnetic field circuit (10.2kHz) the performance could be increased. In the oscillogram of Fig. 4-26 the external circuit has a capacitance of 50μF and it is resonant at 17.2kHz.

We added inductance to the external circuit to bring the natural frequency down to 10.2kHz. We found that the extra inductance used to tune the external circuit actually reduced performance by the small amount of approximately 10%.

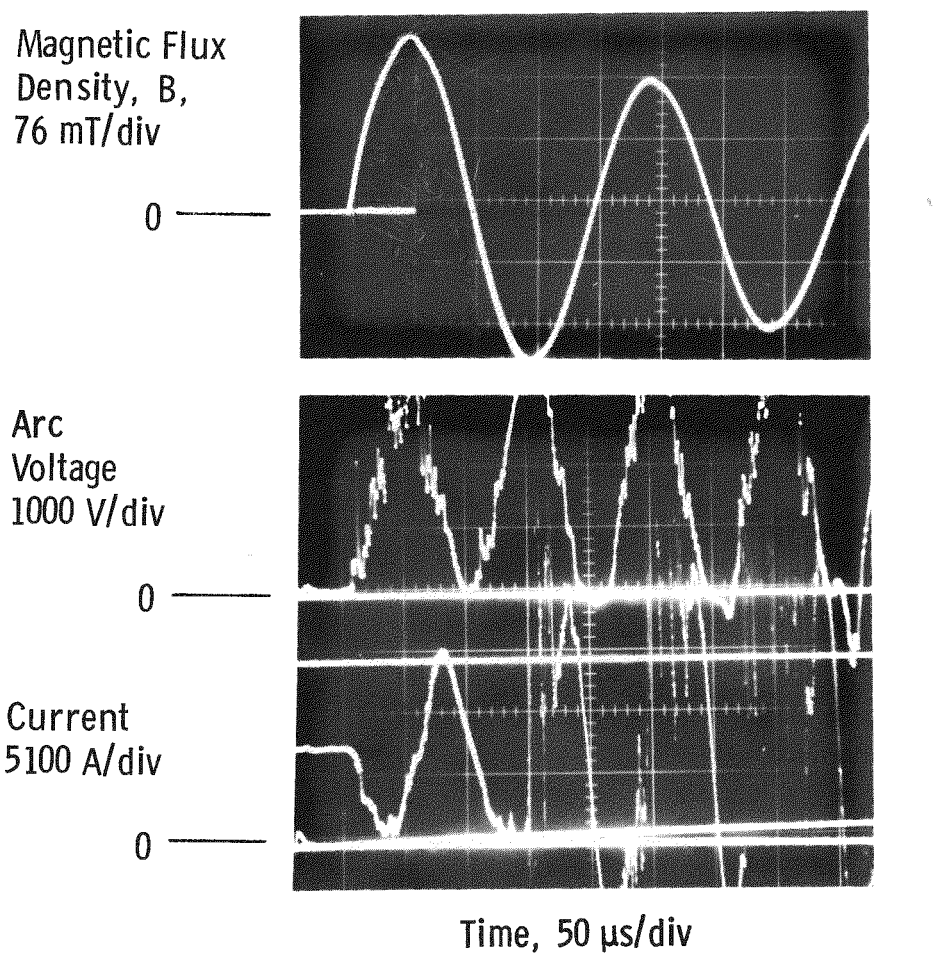

Figure 4-26. Effect of oscillating magnetic field on the arc voltage, 50μF parallel capacitance, 25mm electrode separation. Successful commutation of 8200 A.

An oscillogram of a commutation from 7400 A is shown in Figure 4-27. After the current had been commutated into the external capacitance, C_2, the voltage across C_2 rose to 15kV whereupon the protective spark gap connected in parallel with C_2 flashed over and carried current until the normal current zero. This is illustrated in the lower trace, total current, of Figure 4-27. The commutation is a simple Mode 4. Note that the external circuit is resonant at twice the frequency of the oscillating magnetic field.

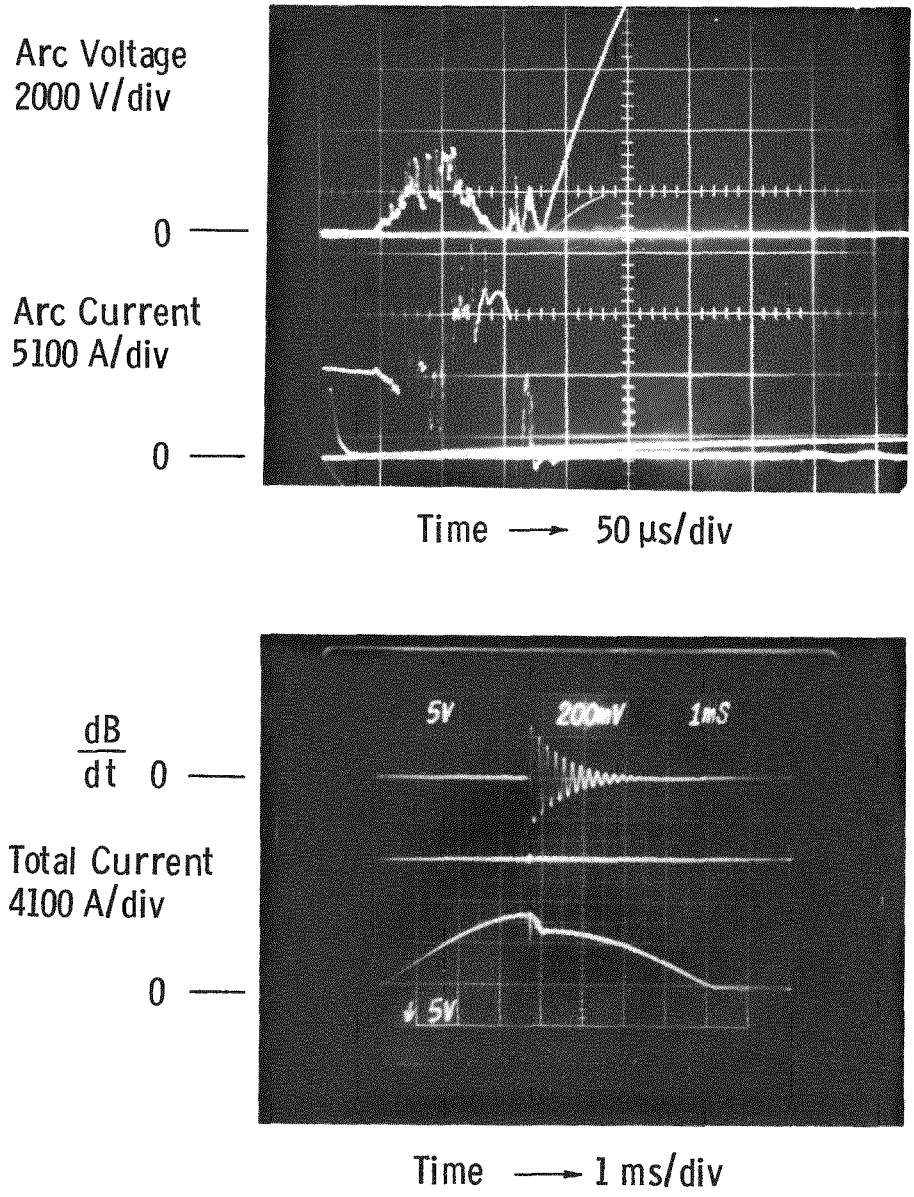

Figure 4-27. Commutation from 7400 A with external circuit tuned to 10.2kHz and the magnetic field oscillating at 5.1kHz, C_2 = 50µF, electrode separation 25mm.

Conclusions.

- Large peak magnetic fields and large $\dot{B}$ values up to 8000 T/sec should be used for maximum device performance.

- A single pair of coils is sufficient to provide the magnetic field. These coils should be positioned as close to the device as possible for maximum efficiency and field uniformity.

- An oscillatory magnetic field should be used because it promotes Mode 4 types of commutation at higher levels of current and increases device performance. For example, we observed a 60% improvement with prototype #5. A higher Q for the magnetic field circuit increased the degree of improvement. The Mode 1 type of commutation was unaffected by the oscillating magnetic field.

- The external circuit should not be tuned to the appropriate frequency by adding inductance to the parallel circuit as the extra inductance may offset the expected improvement.

- The external circuit should be tuned to the desired frequency by adding capacitance.

4-4 TUNING THE MAGNETIC FIELD AND EXTERNAL CIRCUITS; CLD's IN SERIES

4-4.1 Experimental Investigations Into the Effect of Tuning Both the Magnetic Field and the Parallel External Circuit (Prototype #5)

Introduction. In the previous section we discussed the manner in which the arc voltage oscillates at twice the magnetic field frequency. We determined that the arc voltage approximately follows the absolute value of the magnetic field. We considered that the commutation ability would be improved if the external circuit were resonant at twice the frequency of the magnetic field circuit. In these previous experiments, the natural frequency of the magnetic field circuit, 5.1 kHz, was either too low or the frequency of the external circuit, 17.2 kHz, was too high. We added inductance to the external circuit to decrease the resonant frequency. However, there was no increase in the performance; rather, we observed a small decrease of performance. We attributed the decrease of performance to the extra inductance. This seemed reasonable since larger arc voltages have to be developed to effect a given rate of change of current in the external circuit. Our objective in the present experimental series was to match the frequency of the external circuit to twice the frequency of the magnetic field without increasing the external circuit inductance. This was achieved by increasing the magnetic field frequency, and decreasing the frequency of the external circuit by adding additional capacitance.

Experimental Results. For this series of experiments we used Prototype #5 which was still in good operating condition. We started at a condition with 50 μF in the external circuit to permit comparison with earlier data. The circuit frequency was 17.7 kHz. We used separate magnetic field supplies to power each of the magnetic field coils. This permitted high peak magnetic fields, and in the 5 kV mode the magnetic field frequency was 3.3 kHz. For this combination of circuit and magnetic field, the two frequencies were furthest apart and we anticipated poor commutation ability from a tuning standpoint. In the 10 kV mode the magnetic field was closer to the circuit frequency and was 6.5 kHz. We completed our experiments with 100 μF in the external circuit which reduced the circuit frequency to 13 kHz. We again made measurements with the magnetic field frequency of 3.3 kHz, and in particular with the field coils powered by 10 kV supplies where the magnetic field frequency was tuned to half the frequency of the parallel circuit. The four test conditions are illustrated in Figure 4-28 and the parameters are listed in Table 4-2. Only condition #4 of Table 4-2 represents a match of frequencies. The other three conditions represent an orderly progression toward the desired match of frequencies.

Figure 4-29 illustrates the experimental results for two of the test conditions when there is an external parallel capacitance of 50 μF. Since we are near the optimum

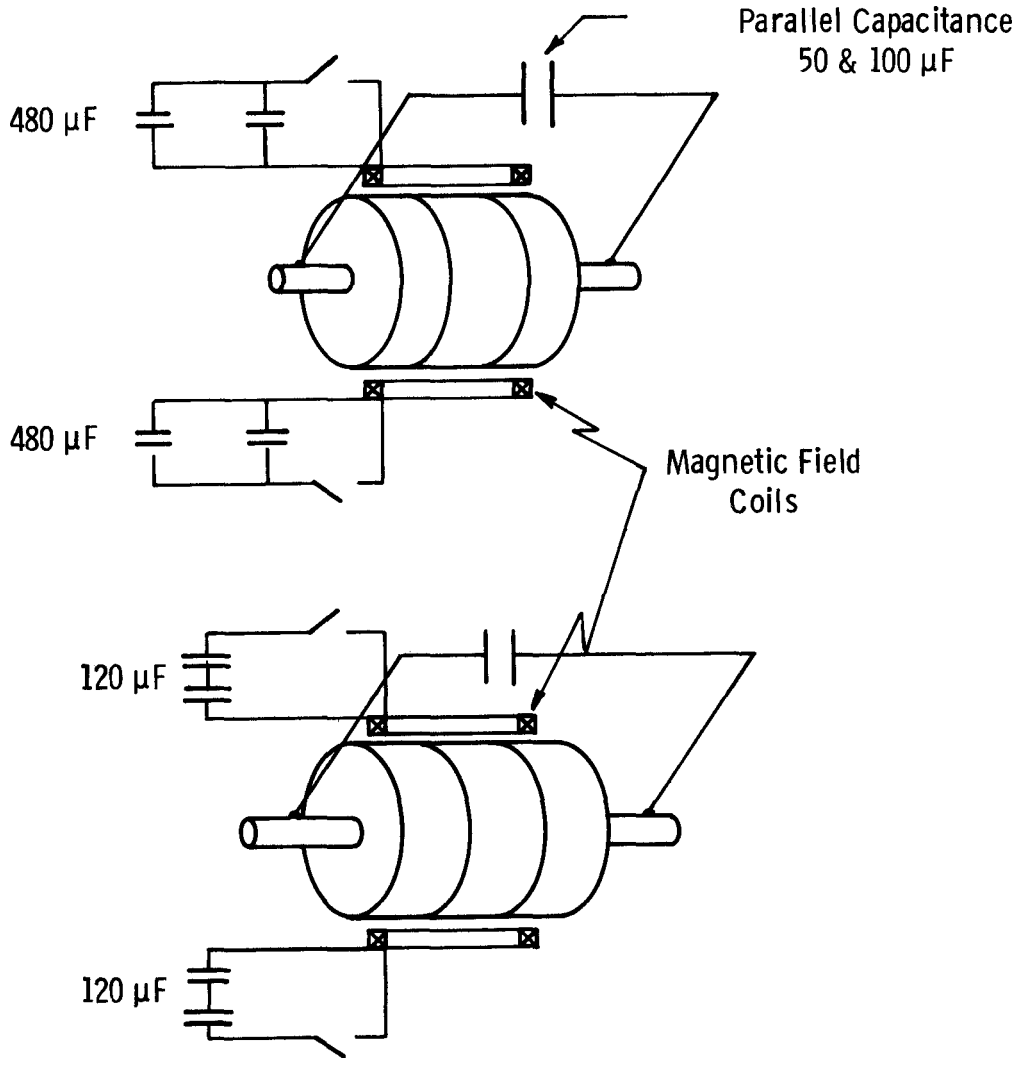

Figure 4-28. Experiments with altering the natural frequency of both the magnetic and the external circuits.

value for the rate of change of magnetic field, $\dot{B}$, the performance of the device is insensitive to changes in that parameter but the performance is somewhat greater at the lower frequency of 3.3 kHz. The reason for this improved performance is that a lower frequency magnetic field is associated with a greater peak value of B for a given $\dot{B}$.

It was impossible to compare all four experimental conditions at the same B and the same peak B. In the past we resolved this dilemma by comparing all data at the same $\dot{B}$ and being aware that greater peak B is usually associated with greater performance.

TABLE 4-2

EXPERIMENTAL CONDITIONS FOR TUNING BOTH MAGNETIC FIELD AND EXTERNAL CIRCUITS

Condition Number	Magnetic Field Circuit			External Circuit		
	Capacitance μF	Voltage Limit kV	Natural Frequency, f_B, kHz	Capacitance μF	Natural Frequency, f_e, kHz	Frequency Ratio f_e/f_B
1	480	5.0	3.3	50	17.7	5.4
2	480	5.0	3.3	100	13.0	4.0
3	120	7.1*	6.5	50	17.7	2.7
4	120	7.1*	6.5	100	13.0	2.0

*So as not to exceed the current rating of the power supplies.

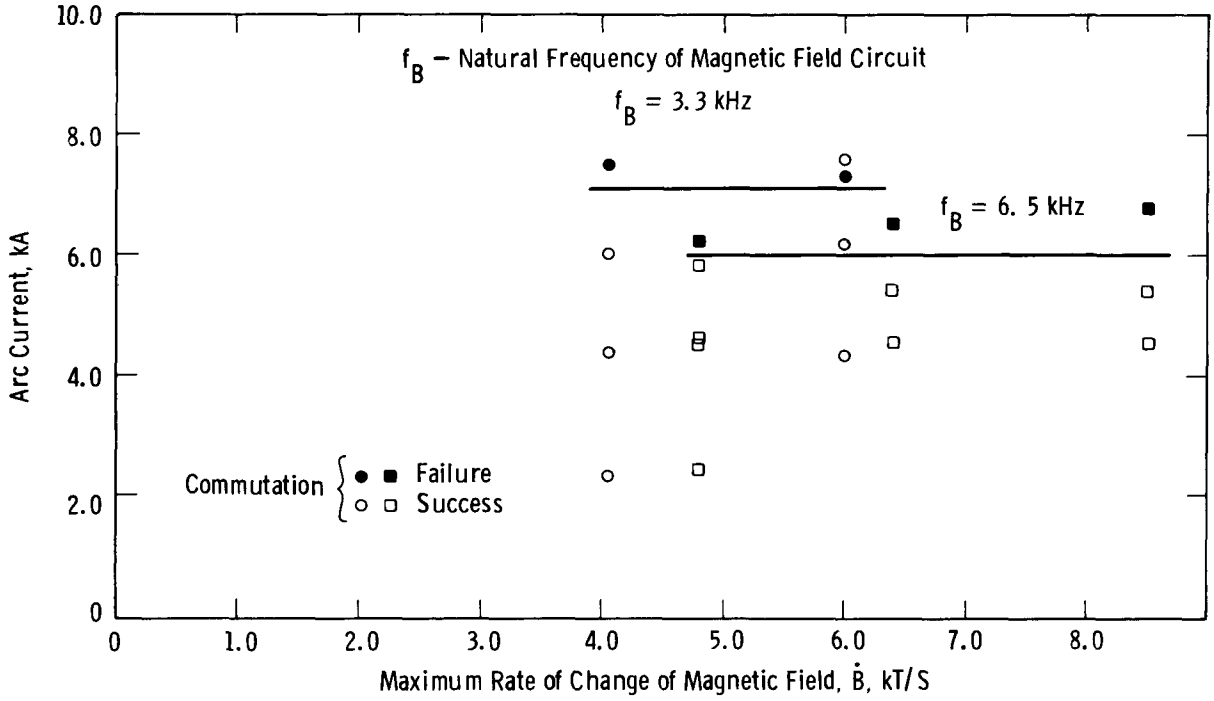

Figure 4-29. Experimental results with 50 μF of parallel capacitance, natural frequency of the external circuit is 17.7 kHz, electrode separation is 25 mm.

The optimum $\dot{B}$ for all four test conditions appeared to be between 5 and 6 kT/s, but values as high as 8 kT/s did not seriously degrade performance. We chose to compare the commutation limit for the four test conditions at 5.5 kT/s and the data are illustrated in Figure 4-30. It will be observed that tuning the external or magnetic field circuits did not have any significant effect on performance. The reason why an increase in capacitance from 50 to 100 μF did not give a more pronounced increase of performance is not clear.

Conclusions. The results of these experiments are somewhat confusing when compared to the conclusions of Section 4-3.2. However, we can conclude that an oscillating magnetic field improves device performance and that the frequency of the external circuit should be $\geq$ than twice the magnetic field frequency. Evidently, the combination of the above two improvements were not additive at least for the bar shaped contacts of Prototype #5.

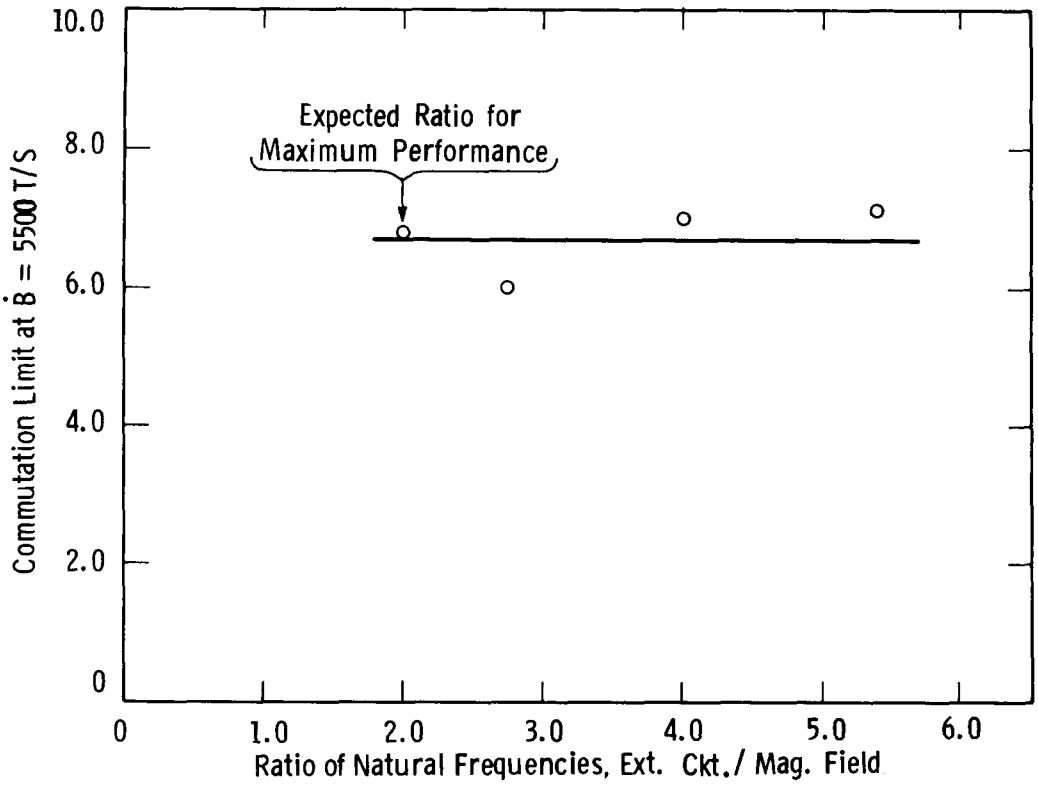

Figure 4-30. Illustration that tuning both the magnetic field circuit and the external parallel circuit didn't have any effects; at least for ratios greater than two.

4-4.2 Comparison of the Commutation Ability of Prototype #4, Prototype #5, and Their Series Combination

Introduction. The experimental setup shown in Figure 4-31 was used to compare the performance of two devices individually and then in a series combination. As we found previously, the Mode 1 commutation seemed to be limited by a persistent small residual current flowing in the device after most of the circuit current has been commutated. This residual current can lead to a reignition of the vacuum arc and commutation failure. One rationale behind the present experiments was to begin the commutation in one series device. When the residual current level was reached, a transverse magnetic field would then be applied to the second series device at the optimum time, with highest $\dot{B}$, and with maximum effect.

We also wanted to investigate whether Mode 4 commutations would be aided by a series arrangement of devices. We considered that such a series arrangement might hold off arc reignition for a longer time and this would allow capacitor C_2 to accumulate

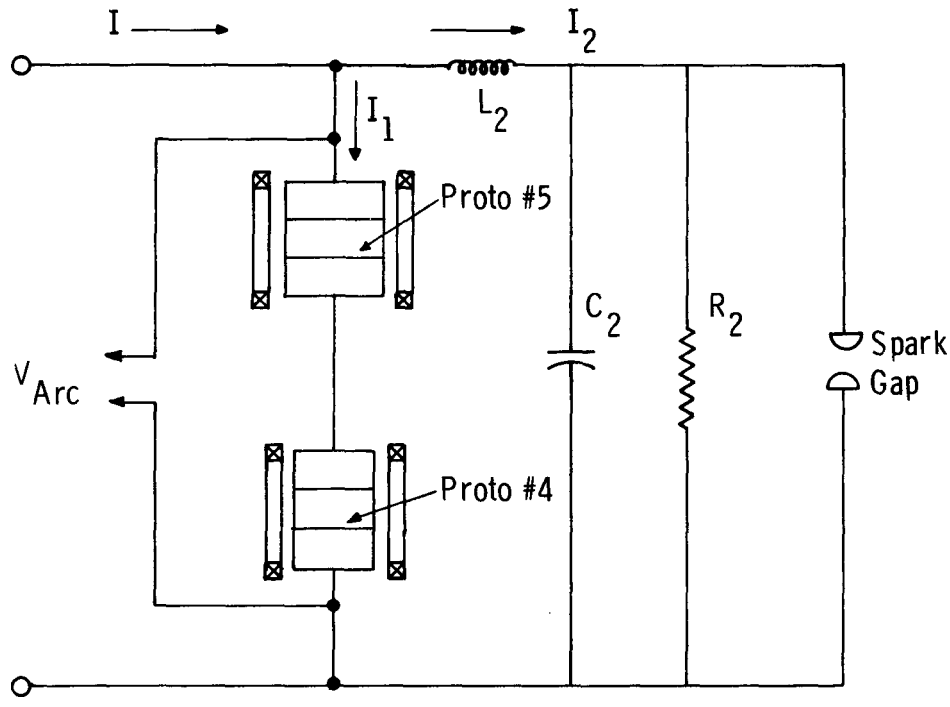

Figure 4-31. Schematic of the experimental setup used for testing two CLD's in series.

more charge. A larger charge on C_2 should lead to a more vigorous oscillation of the current in the external circuit (the loop formed by C_2, L_2 and the vacuum devices) and therefore to a more definite current zero in the device with subsequent arc extinction.

Experimental Details. Two previously used devices were used in these experiments. Prototype #4 had 18 cm diam. ceramics and was equipped with 11 cm diam. Bruce profile electrodes. Prototype #5 had 23 cm diam. ceramics and contained concave bar electrodes with a length of 15 cm and width of 7 cm. The contacts of each device were parted immediately after the start of current flow and opened with a velocity of 5 m/sec.

Identical pairs of two-turn coils were used on each device. Each pair of coils was connected electrically in series and powered by its individual 5 kV/10 kV power supply. In the 5 kV mode the power supply capacitance was 480 μF and the transverse field oscillated at a frequency of 2.5 kHz ($\tau/4$ = 100 μsec). In the 10 kV mode the power supply capacitance was 120 μF and the field oscillated at 5 kHz ($\tau/4$ = 50 μsec). In both cases the damping factor given by ln (A_1/A_2) was 0.3. Although the 28 cm

diameter field coils were identical for the two devices, the separation of these coils was different and this led to differences in the initial rate of rise of magnetic field and in the peak value of the magnetic field. The coils on Prototype #5 were separated by 28 cm and the first peak of the field was 0.18 Tesla. The coils on Prototype #4 were separated by 23 cm and gave a magnetic field with a first peak of 0.28 Tesla. All of the data were taken under these conditions which led to initial $\dot{B}$'s for #5 of 2900 T/S or 5800 T/S, and for #4 of 4400 T/S or 8800 T/S.

The two transverse magnetic fields were turned on from a common trigger pulse at a nominal time of 3.5 msec after the start of the 60 Hz current flow. The arcing gap (or gaps) was 15 mm at this time. The nominal trigger-on time was varied from 3.0 to 4.0 msec under some conditions to search for the optimum time/gap setting. A second pulse delay generator was used to vary the relative time between the start of the two fields by $\pm$ 30 μsec.

Almost all of the data were taken with the capacitor C_2 across the series combination equal to 50 μF. This produced a ringing frequency of the external circuit of 13 kHz (with a logarithmic decrement of 0.34). When C_2 was changed to 100 μF, the ringing frequency of the external circuit was reduced to 9.1 kHz with a logarithmic decrement of 0.38.

General Results. All of the data for C_2 = 50 μF are displayed in Figure 4-32. The commutation ability of each device alone is shown in the left two columns. These data were taken by operating each device separately in the setup of Figure 4-31. Both devices gave their maximum commutation performance at the larger value of $\dot{B}$. Each device showed a limit of about 6.5 kA under these conditions.

The right hand side of Figure 4-32 shows the performance of the series combination of these two devices. The relative delay of the transverse magnetic field applied to Prototype #4 was varied as indicated. The highest currents commutated for the various conditions occurred for simultaneous application of the transverse fields. The series combination shows a commutation limit of about 8.7 kA and thus an improvement of 33% greater than the individual device limits.

Discussion and Conclusions for Series Operation of CLD's. The results of these experiments using two devices in series showed a 33% improvement over the current commutation ability of one device alone. However, the conditions of the experiment were not optimum in that the two devices were physically and electrically different.

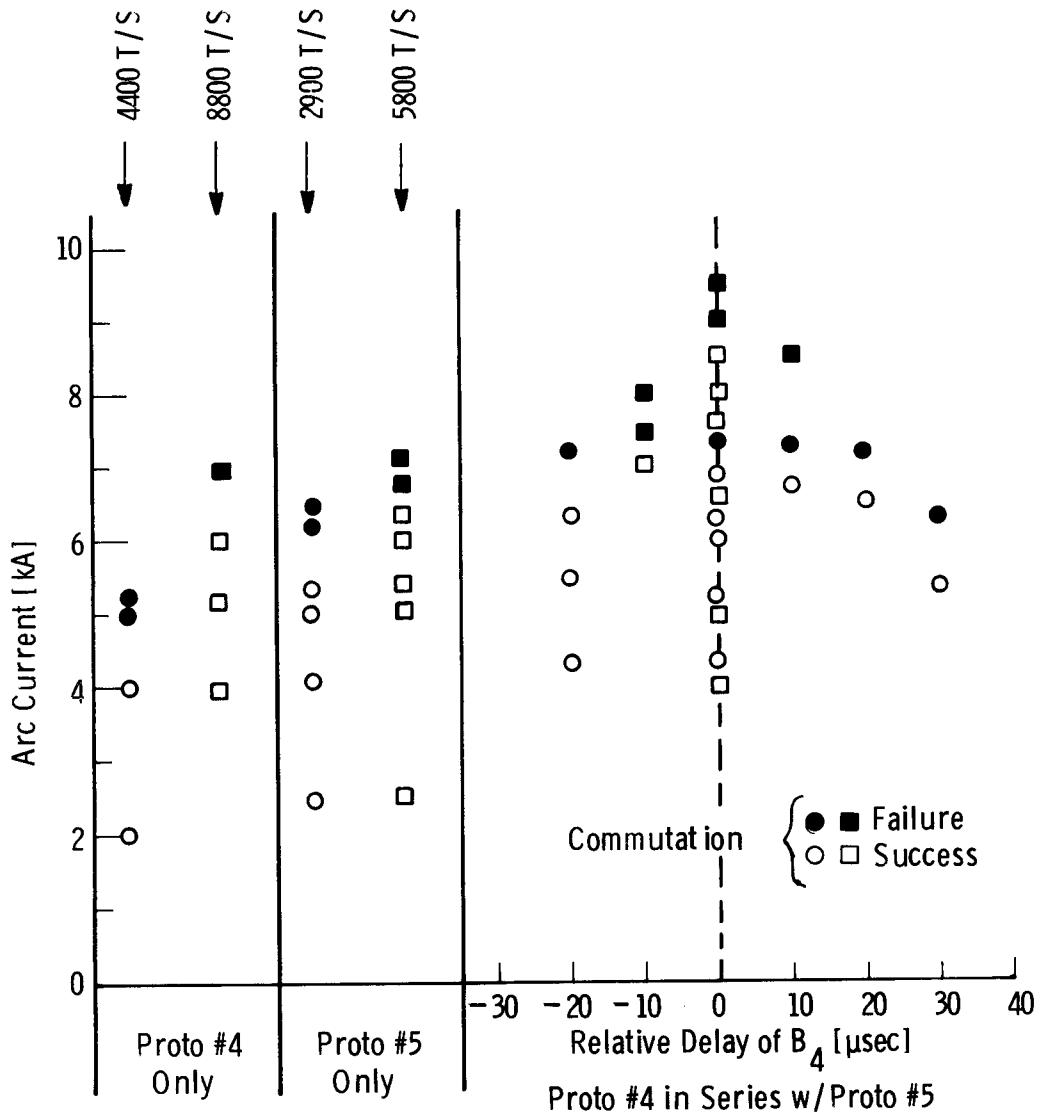

Figure 4-32. Summary of data taken to explore the effect of two devices in series: C_2 = 50μF.

Prototype #4 seemed to perform best in the Mode 1 type of commutation while Prototype #5 performed best in the Mode 4. The mode of failure of the series combination seemed to be a restrike rather than a reignition of the arc from a small residual current. We considered that the ability to withstand restrikes could be improved, with consequent improvement of commutation ability, by ensuring equal distribution of the recovery voltage between the two series devices. This distribution was not monitored in the present experiments, but an unequal distribution seems likely since the prototypes were of different sizes and designs.

4-5. EXPERIMENTS USING PROTOTYPE #7 WITH CONVENTIONAL OSCILLATING MAGNETIC FIELD APPLICATION

4-5.1 Introduction

Prototype #7 was constructed using an 18cm diameter ceramic envelope with the electrodes oriented 90^{o} from the usual configuration. A sketch appears in Fig. 4-33. It will be noted that the CLR electrodes are oriented along the long axis of the interrupter in a configuration which permits the application of relatively uniform magnetic fields, with high rates of rise, to large area electrodes. The movable electrode is 20cm long and the stationary electrode is 28cm long. This stationary electrode is partially split in order to promote the formation of parallel arc paths. Figure 4-33 shows the electrically resistive stainless steel pin used to connect and support the two halves of the stationary electrode.

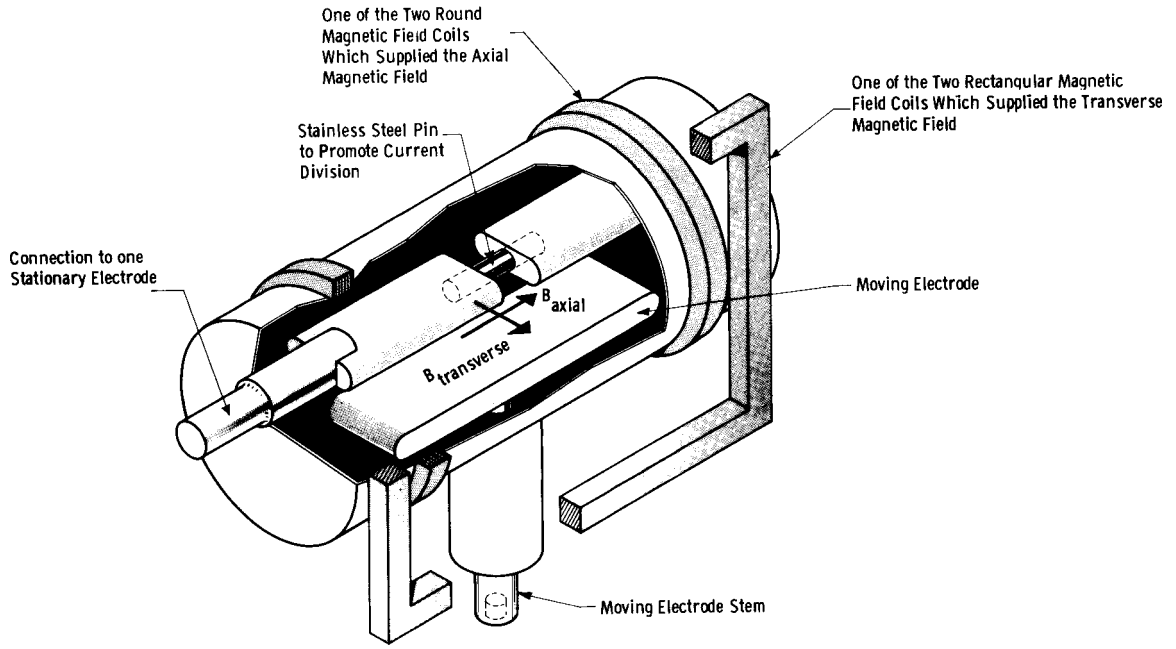

Fig. 4-33. Illustration of the magnetic field orientation for the experiments performed with the solenoidal field prototype #7.

Because of the relatively fragile construction of this device we utilized slow opening and slow closing of the electrodes. For all experiments the electrodes were separated to 20mm in 25ms by using low energy in the capacitors of the repulsion coil circuit and by connecting the coils electrically in series. Dashpots were used to provide the slow closing. The relatively long time, 25ms, to achieve maximum separation necessitated the use of D.C. keep alive techniques (1). Once the electrodes were fully separated, a half cycle of 60Hz AC current was applied. The stationary electrode was anode.

4-5.2 Experimental Results with Axial (solenoidal) Magnetic Field

An oscillating magnetic field was applied along the axis of the device utilizing the round coils shown in Fig. 4-33. Parallel capacitances of 26 and 1000μF were used. Because of the small diameter of these coils and their small spacing we achieved B and B_{max} values larger than we had previously achieved. The results of these experiments are shown in Fig. 4-34 where lines are drawn through the points of highest current commutated at each value of B. The results show an increasing commutation ability with increasing B.

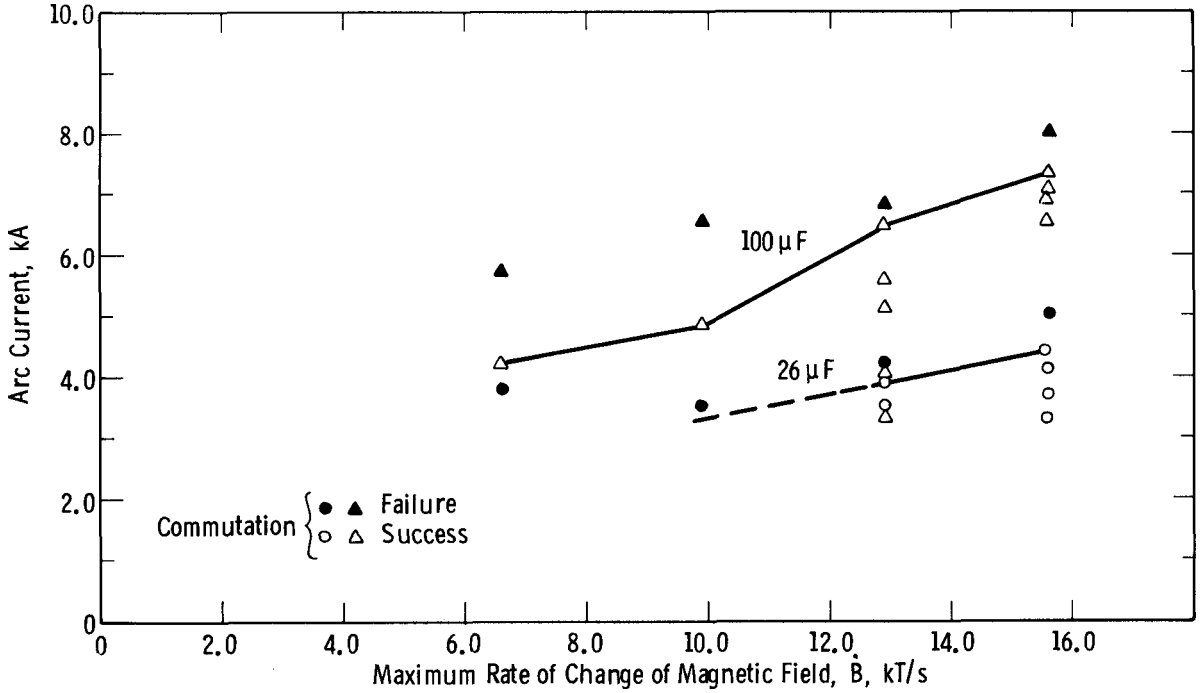

Figure 4-34. Experimental results with an axial magnetic field applied to prototype #7 with two values of parallel capacitance: 26 and 100μF. Electrode separation was 20mm. Both mode 1 and mode 4 data are shown.

Experimental results at 50μF appear in Figure 4-35. When the device was new the commutation ability was relatively independent of B, with possibly a maximum commutation ability at 10kT/s. When the device was retested after 90 experiments, there was a degradation in performance of 10%. Further, the maximum commutation ability was observed at 15kT/s.

4-5.3 Experimental Results with Transverse Magnetic Field

Prototype #7 was originally designed for an axial magnetic field orientation. The concept involved applying a field along the axis of the interrupter which would be transverse to the arcing path between the electrodes. It will be noted that a field

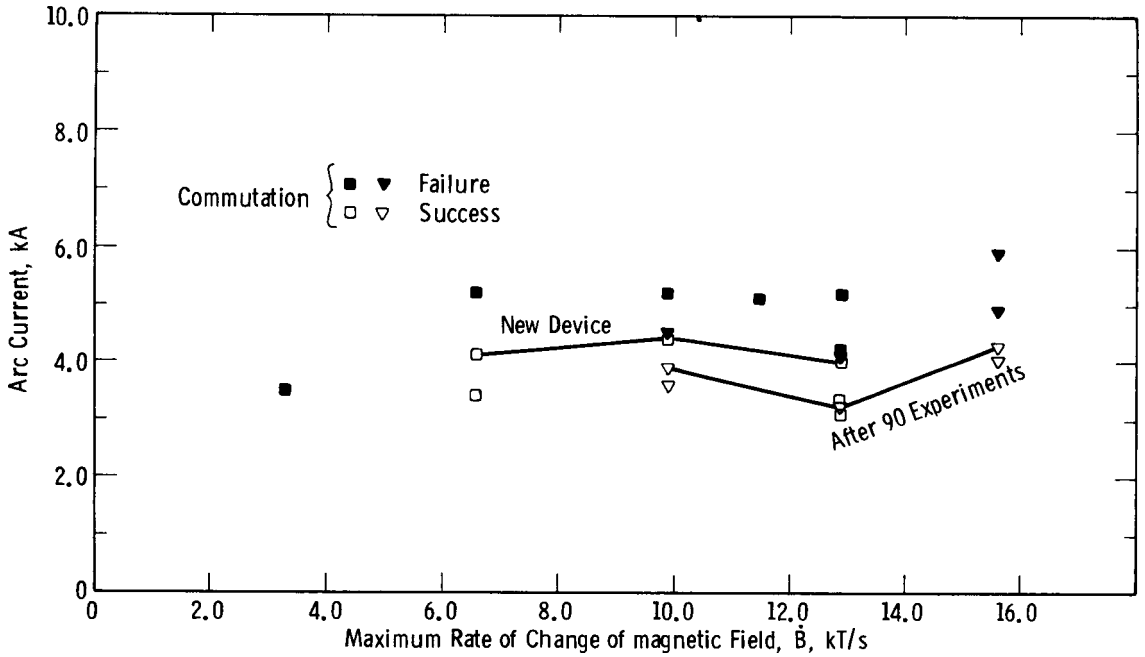

Fig. 4-35. Experimental results with an axial magnetic field applied to prototype #7 with 50μF of parallel capacitance and 20mm electrode separation. Both mode 1 and mode 4 data are shown.

can also be applied transverse to the axis of the interrupter, and that this field will also be transverse to the arc path.

In order to gain experience with devices where the magnetic field is applied across the long dimension of the electrodes, we used the rectangular coils of an earlier experimental series to apply a transverse magnetic field. The rectangular coils and their orientation with respect to the sealed device are illustrated in Fig. 4-33 The data for the experiments are illustrated in Fig. 4-36 for three values of parallel capacitance: 26, 50 and 100μF. For the transverse magnetic field there is an apparent optimum rate of change of magnetic field between 4 and 7kT/s.

4-5.4 Discussion of Test Data

Table II summarizes the data for the two directions of the magnetic field and three values of parallel capacitance. We see that the highest commutated current increased with parallel capacitance. Further, the performance with 26 and 1000μF of parallel capacitance is greater with an axial magnetic field orientation.

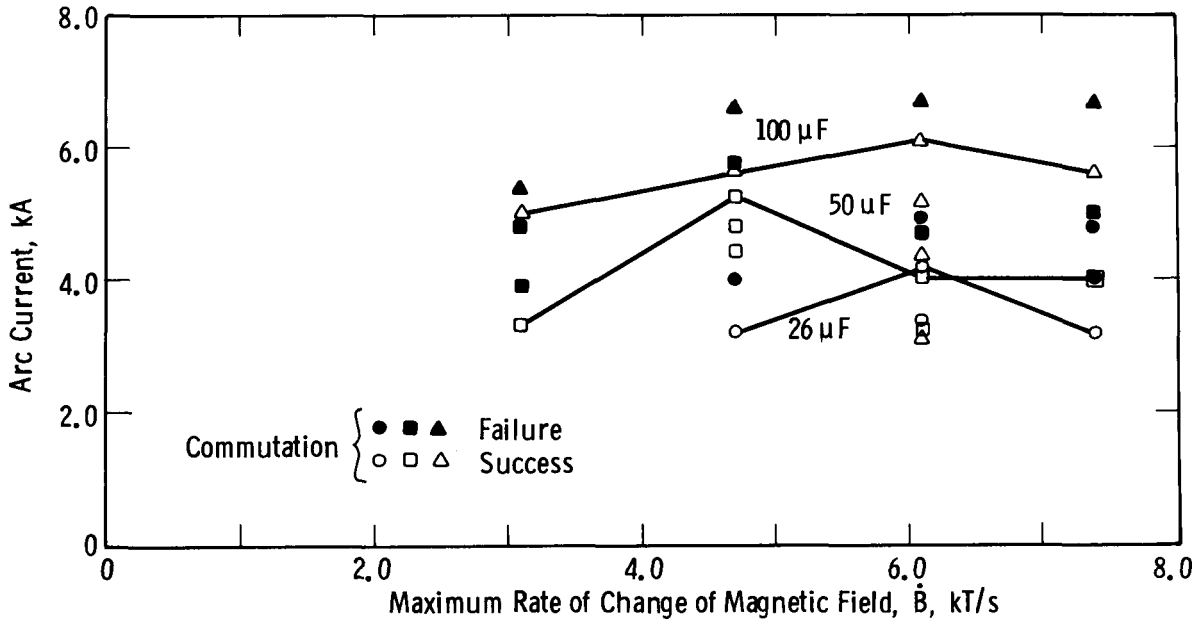

Fig. 4-36. Experimental results with a transverse magnetic field applied to prototype #7 with three values of parallel capacitance: 36, 50 and 100μF. Electrode separation was 20mm. Both mode 1 and mode 4 data are shown.

We can obtain a quantitative measure of the effect of increased parallel capacitance and magnetic field orientation by using regression techniques. Ignoring the one data point at 50μF (axial magnetic field) an equation can be fitted to the remaining five data of Table 4-3 with the form

$$I = 1.4 \times 10^5 \, KC^{0.33}$$

where I is the current in amperes, C is the parallel capacitance in farads and

$$K = \begin{cases} 1.11 \text{ for axial magnetic field} \\ 1.0 \text{ for transverse magnetic field} \end{cases}$$

Thus the performance is proportional to $C^{0.33}$ which is consistent with earlier(4-2) results, and the performance with an axial magnetic field orientation is 11% greater than with a transverse magnetic field.

In comparing the performance of Prototype #7 with other prototype devices, the initial reaction to Table 4-3 is that the performance was only moderate, particularly since the combined area of the movable and stationary electrodes was $230cm^2$. For example, we had previously commutated 5.4, 8.3 and 10kA in Prototype #5 with smaller area electrodes of $213cm^2$. However, the latter tests were performed in 23cm diameter devices.

Table 4-3

Summary of the Experimental Results
for the Solenoidal Field Device

Magnetic Field Orientation	Parallel Capacitance μF	Highest Commutated Current, kA
Axial	36	4.4
Axial	50	4.4
Axial	100	7.3
Transverse	26	4.1
Transverse	50	5.3
Transverse	100	6.1

Maximum commutation levels achieved in various prototypes as a function of electrode area, envelope diameter, and parallel capacitance are plotted in Fig. 4-37. It must be noted that the data in this figure represent the highest currents commutated from Prototypes #2, 4, 5 and 6 (Phase II) and Prototypes #2, 3 and 4 (Phase I). Many of these prototypes were tested without oscillating the magnetic field, and this qualifies the comparison with Prototype #7. In general the lines in Fig. 4-37 connecting data for the same diameter envelopes have a positive slope signifying increased performance with increasing electrode area. However, when we compare the solid points (23cm diameter envelope) to the open points (18cm diameter envelope)

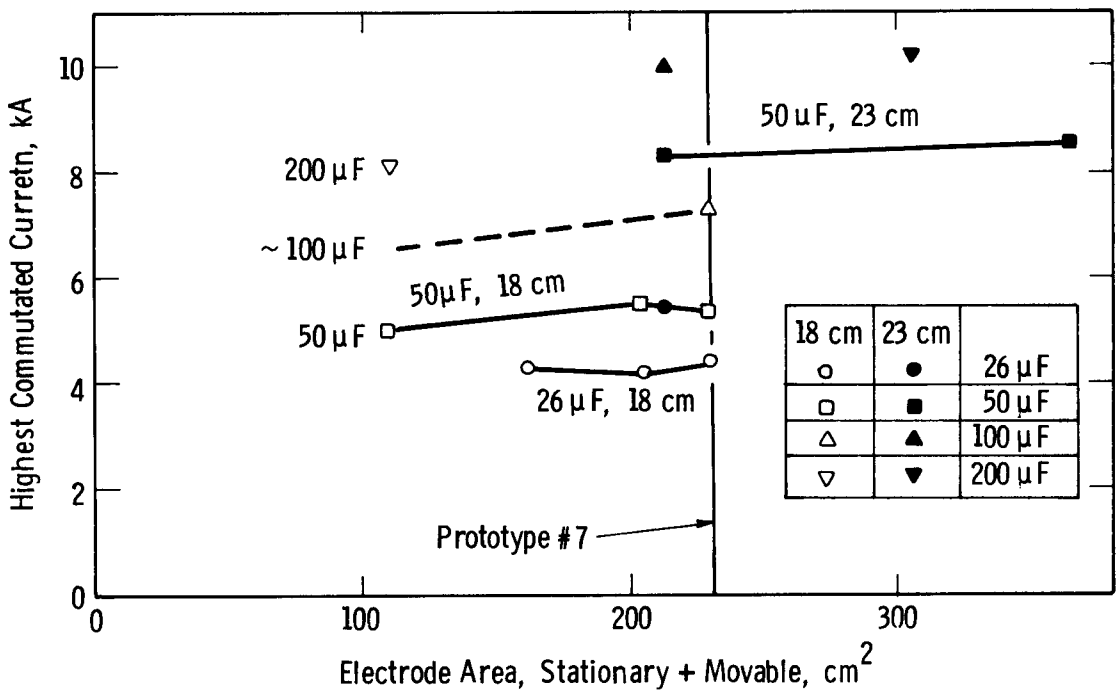

Fig. 4-37. Experimental data showing larger envelope diameter has been more effective for increasing device performance than has increased electrode area.

for a given parallel capacitance we see a marked improvement with envelope diameter. Since envelope diameter appears to be a dominant parameter, we should judge the performance of Prototype #7 by comparing the commutation ability with that of other 18cm devices. On this basis, Prototype #7 commutated a higher current than any other 18cm device at parallel capacitance levels of 26 and 100µF. At a capacitance level of 50µF, Prototype #5 with Bruce profile electrodes commutated 5.5kA compared with 5.3kA for Prototype #7.

4-5.5 Conclusions

The novel design of Prototype #7 allowed the exploration of current commutation at higher values of $\dot{B}$ with our existing power supplies. The design of this Prototype also allowed for a much larger contact area in an 18cm dia. envelope. Moreover, these tests showed that:

- Values of $\dot{B}$ greater than 8 to 10 kT/sec did not lead to high commutation capability at least with 50µF of parallel capacitance.

- The commutation ability of this novel prototype deteriorated after about 90 test shots.

- The larger area of the electrode did not produce a greater commutation ability.

- The highest current commutated by Prototype #7 was about equal to that of other 18cm dia. devices.

- The data seemed to confirm the idea that large envelope diameter is more important than large electrode diameter.

4-6 EXPERIMENTS WITH VARIATION OF DEVICE GEOMETRY AND CIRCUIT PARAMETERS

4-6.1 Experiments using Prototype #8 with a Third Low Mass Arc Initiation Electrode

Introduction

In a practical current limiting device the electrodes must be separated a distance of 20 to 30mm in 1 to 1.5ms. With the large and massive electrodes needed to maintain a diffuse arc, the forces required to achieve this separation are quite large. These forces could be reduced if the device contained two large and massive electrodes which were permanently separated by the required spacing, with a third low mass arc initiation electrode to carry the continuous current. Prototype #8 was designed to implement this concept and a schematic is shown in Fig. 4-38. Items 1 and 2 are the two relatively large CLR electrodes and item 3 is the movable arc initiation electrode which was also made of CLR. Item 4 is the current carrying support structure for electrode 1 and item 5 is a flexible connector to carry the current from electrode 1. The envelope is 23cm in diameter and the electrodes are 15cm diameter Bruce profile. Electrode 3 has only 48% of the mass of electrode 2. Electrode 2 is typical of electrode and stem designs used in previous prototype vacuum interrupters whereas electrode 3 represents a reduced mass arc initiation electrode.

We can make an approximate calculation of the advantage to be gained by using an electrode with 48% of the mass. With a constant acceleration, a, an electrode of a given mass, m, could be moved a distance s in a time t_1 where

$$t_1 = \frac{2s}{a} \qquad (1)$$

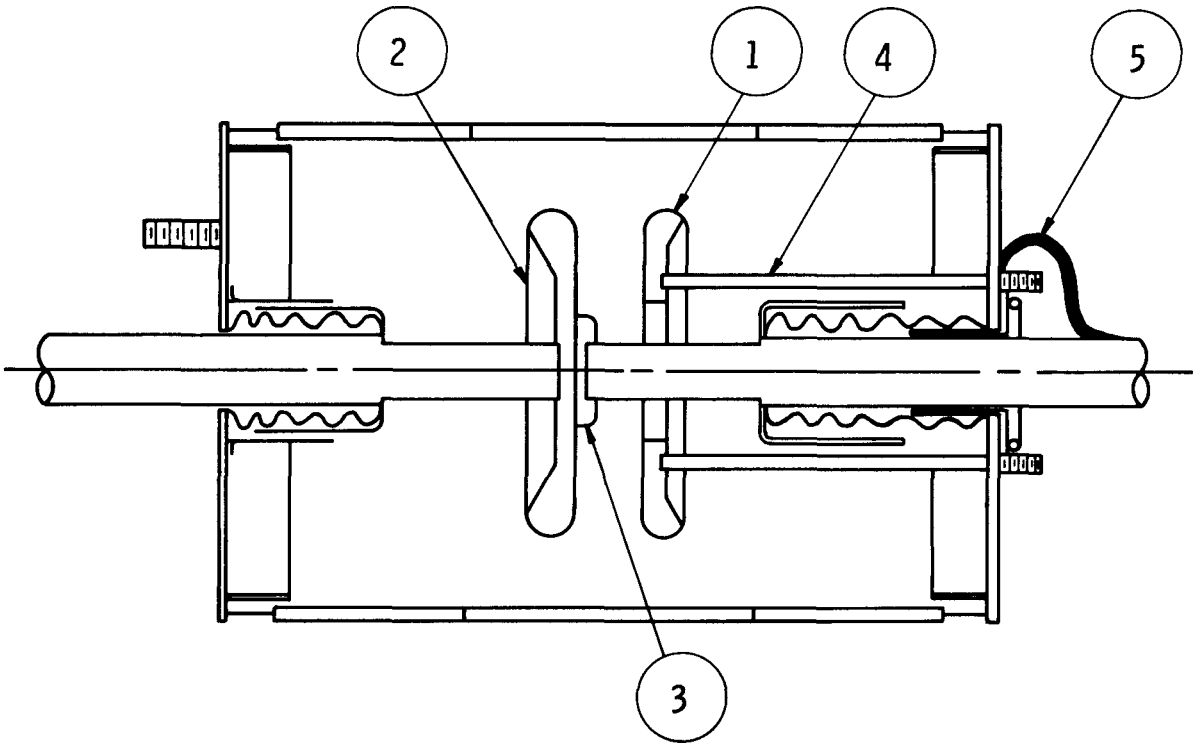

Fig. 4-38 - Schematic of Prototype #8 with the low mass bridging electrode

If instead we have a mass of 0.48m, it would accelerate by the same force at a larger acceleration, $\frac{a}{0.48}$. We would achieve the same distance or separation, s, in a time t_2 where

$$t_2 = \frac{2s.\ 0.48}{a} = 0.69t_1$$

Hence, 48% of the mass reduces the time to achieve a given separation by the square root of the mass reduction, 69%

Objectives of the Experiments

The objectives of this series of experiments was to keep the large movable electrode stationary and move only the low mass electrode. The large electrodes, items 1 and 2 of Fig. 4-38, were separated by 20mm for all experiments. Electrode 3 was

withdrawn through a hole in electrode 1, and could be separated from electrode 2 a distance greater than 20mm.

First we delayed the opening of the low mass electrode in such a manner that the desired separation was achieved at the crest of the current. This technique has the advantage of minimizing damage to the device if it should fail to commutate the current. Following this series of experiments, we eliminated the delay so the desired separation was achieved with a slightly rising current immediately prior to current crest.

Finally we applied the magnetic field approximately 2ms after the start of the current to achieve true fault current limitation. In the past experiments we had either used a direct-current keep alive technique to maintain the arc to achieve true fault current limitation or we had commutated near the crest of the current.

Figure 4-39 shows an oscillogram of the travel of the low mass electrode. This

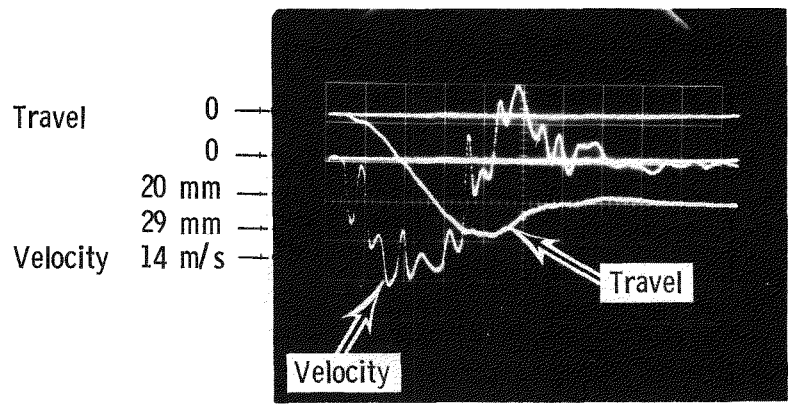

Fig. 4-39 - Typical travel and velocity oscillogram for the small electrode of Prototype #8. There was 20mm separation in 2.6ms (2.1ms + 0.5ms of dead time)

oscillogram is typical of all 38 experiments. We achieved a maximum velocity of 14m/s without damage to either the actuator or the bellows. We considered this quite an accomplishment.

Experimental Results

When we commutated at the crest of the current utilizing delayed opening we could commutate only 8.6kA. We even had some failures to commutate at 8.6kA. When we eliminated the delay and applied the magnetic field immediately prior to current crest we could commutate 10kA and an oscillogram is shown in Figure 4-40. The electrode spacing is 20mm.

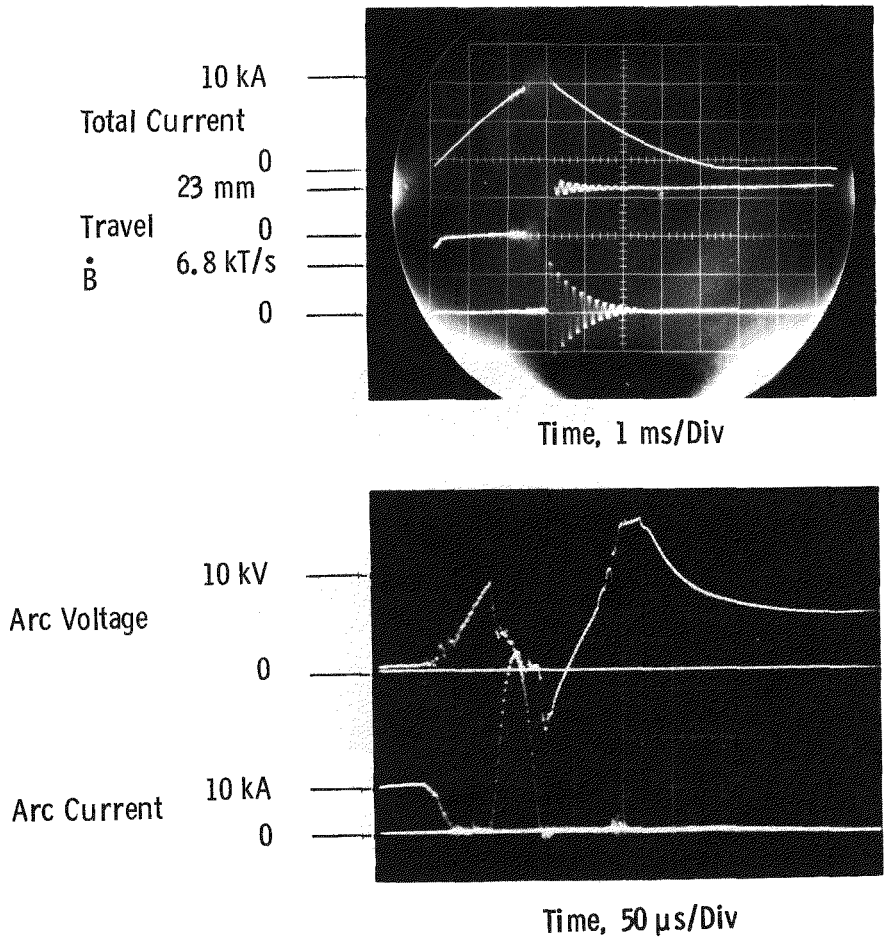

Fig. 4-40 - Oscillogram of a 10kA commutation using Prototype #8 with the small electrode the cathode. C = 50µF, separation 23mm, R - 3.33Ω

When we applied the magnetic field 2.2ms after the start of current we commutated 8.5kA. Here the small electrode was only separated by a distance of 12mm from the opposing electrode. Because of concern about the asymmetry of the device design, we ran experiments with the small electrode connected both as anode and the cathode. There was no detectable change in commutation characteristics.

Discussion of the Experimental Results

The performance of Prototype #8 was definitely inferior with delayed opening. Comparing oscillograms with and without delay we saw that:

- With delay the current was fluctuating before the magnetic field was applied. This signified a higher and more fluctuating arc voltage prior to the application of the magnetic field. With or without the delay, the arcing times were identical.

- Without the delay, the application of the magnetic field resulted in a larger and more rapidly rising arc voltage.

One possible implication of the above was that one should open as quickly as possible when a fault is detected, and that a mechanism design with significant dead time was undesirable. A further possible reason for the observed behavior was that when electrodes are separated at low currents, the cathode spots spread out quickly and a diffuse arc is formed. Separating electrodes at high currents may result in a constricted arc column with a consequent decrease in current commutating ability(7).

Conclusions

Although we could not commutate 10kA at 2.2ms after the start of current, we could commutate 8.5kA. This was a relatively large current for an electrode separation of only 12mm. With Prototype #2 we commutated 6.4kA into 50μF using 26mm electrode separation. This same 23cm diameter device commutated 10.2kA into 200μF using 20mm electrode separation. Prototype #8 commutated 10kA into 50μF with 15cm diameter Bruce profile electrodes separated by 20mm. We considered that the rapid electrode separation used in experiments with Prototype #8 was the reason for the improved performance. These experiments also indicated that a low mass bridging electrode can be used in a current limiting device to improve the effective speed of electrode separation.

4-6.2 Experiments using Prototype #9 with Cup Electrodes

Introduction

Experiments with Prototype #6 and the demountable arc chamber showed that the cup electrode design was useful for maintaining a diffuse arc and for high current commutation. Prototype #9 was constructed with 15cm diameter cup electrodes in a 23cm diameter envelope.

Objectives of the Experiments

The first objective of these experiments was to compare the cup electrode geometry with other electrode designs. These electrodes are quite massive, and in order to compare with earlier data at the same electrode separation we had to stress the actuator and coupling to its limit. Coupling breakage had been a problem in the past with less massive electrodes. In order to reduce the stress on the actuator and coupling, the repulsion coils were electrically connected in series; further the high voltage capacitor of the two stage power supply was only charged to 1150V but the high energy capacitors were charged to 1030V, a relatively high voltage. The combination of these two parameter changes resulted in a relatively low acceleration at the beginning of the stroke with a relatively long dead time of 0.5ms. However, the large available energy resulted in a continued acceleration, and we were able to achieve the desired 21mm in 4.2ms without breaking the coupling or actuator.

The second objective of this series of experiments was to investigate the effect of a series connected standard vacuum interrupter. The purpose of this series device was to interrupt the current if the current limiting device induced current oscillations severe enough to produce zero crossings. A secondary purpose was to gain experience for eventual application in 72kV or higher voltage circuits. The standard vacuum interrupter had arc shields and electrodes which permit high current interruption and high voltage withstand. Hence, the current limiting device would force the current to zero, but the standard interrupter would hold off the subsequent high voltage transient. A schematic of the test circuit is shown in Figure 4-41. The series connected vacuum device had no magnetic field coils.

The third objective of these experiments was to use iron cores in series with the vacuum device in order to reduce the rate of change of current after a current crossing. This would facilitate current commutation. Schematics of the two

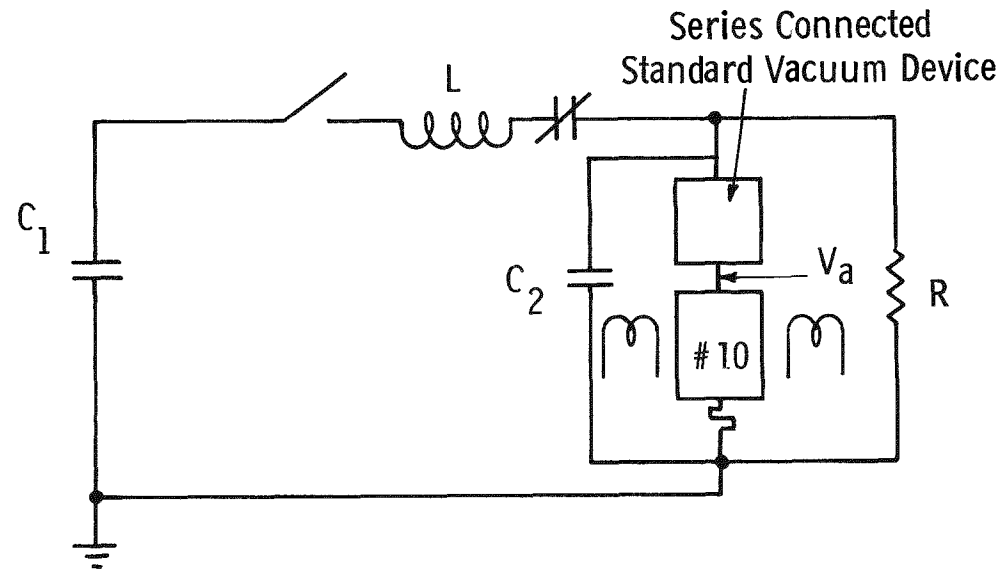

Fig. 4-41 - Circuit for prototype #9 experiments with series connected vacuum device.

circuits used to investigate the effect of the iron cores are shown in Fig. 4-42. In Fig. 4-42a the iron cores are in series with the vacuum device. Here, when I_{Fault} is being commutated from the vacuum device into the capacitance, the iron cores are in the circuit to reduce the rate of change of current after the current crosses zero. In Fig. 4-42b the iron is not in the capacitor circuit and neither helps nor hinders the commutation. Further there was a spark gap connected in parallel with the capacitor which protected the capacitor by limiting the voltage to 10kV. This spark gap continued the flow of current through the iron cores. In Fig. 4-42b the current in the iron cores did not go to zero until well after the commutation was complete.

Experimental Results

Figure 4-43 shows the commutated current as a function of capacitance. The data are consistent with past results which showed that the current which can be

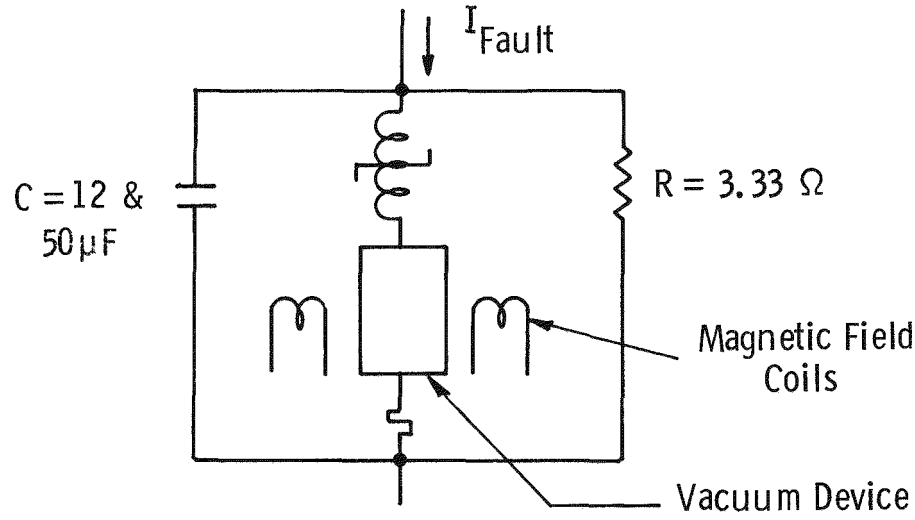

a) Iron in the Capacitor Circuit

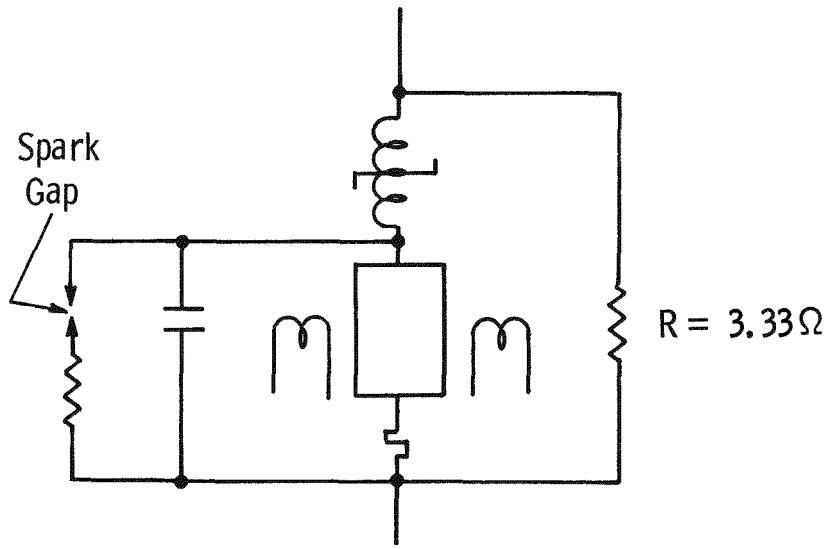

b) Iron not in the Capacitor Circuit

Fig. 4-42 - Schematics of the two circuits used to evaluate the effect of saturable iron cores in the capacitor-vacuum device circuit.

commutated was proportional to the capacitance raised to the 0.4 power. At each level of capacitance we commutated a record high current. An oscillogram of the 12kA commutation into 50μF is shown in Fig. 4-44. We will comment later on the strange behavior of the arc current and arc voltage during the first half cycle of magnetic field (the first 100μs).

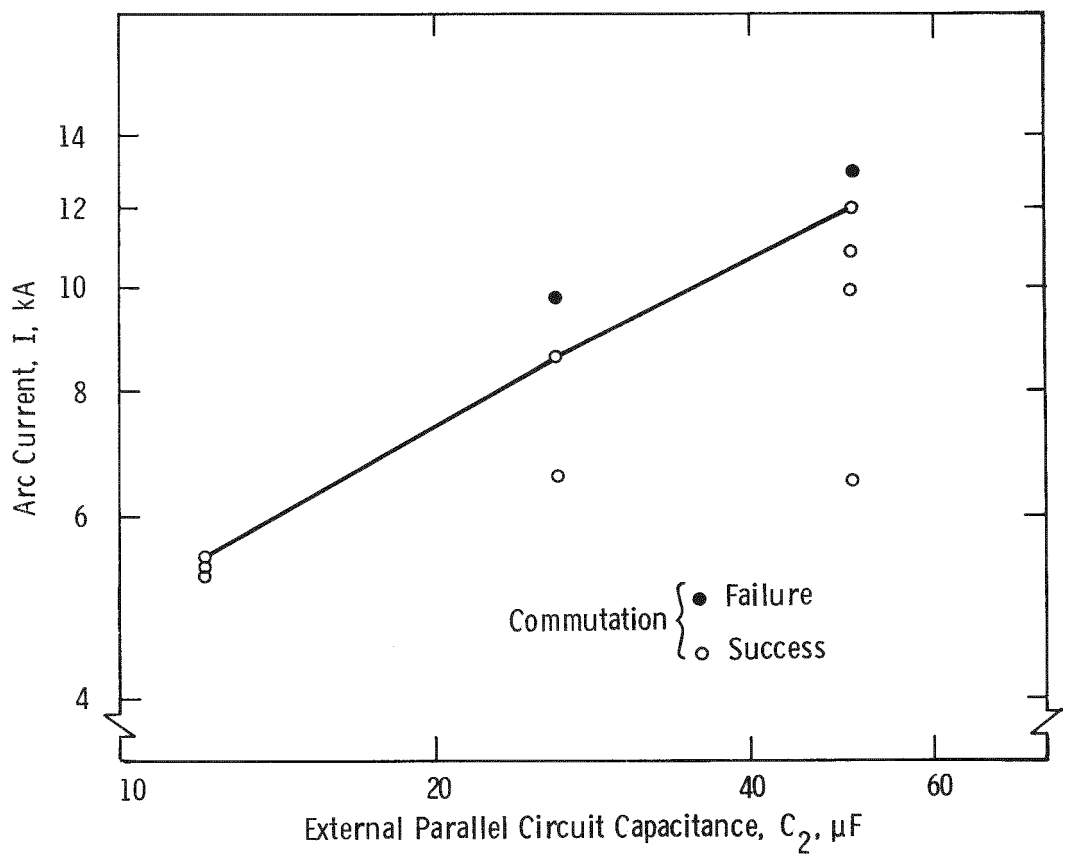

Fig. 4-43 - Experimental data for Prototype #9 with 15cm. dia. cup electrodes separated to 21mm in 4ms. and with standard vacuum interrupter connected in series at 26 and 50μF only. B = 6.8kT/s. There was no iron in the capacitor circuit. Data are consistent with $I \sim C_2^{0.4}$

Table 4-4 shows data with and without iron cores in the circuit. With the iron cores in the capacitor circuit the device performance is approximately 85% of the value without the cores.

Table 4-4

EXPERIMENTAL RESULTS WITH PROTOTYPE #9 WITH AND WITHOUT IRON CORES IN THE CIRCUIT

Iron Cores	Parallel Capacitance μF	Highest Success kA	Lowest Failure kA	Mode
Yes	12	4.3	5.5	4
No	12	5.5	---	4
Yes	50	9.8	11.0	4
No	50	11.0*	12.0	1

*We commutated 12kA earlier in the experimental series with a standard vacuum interrupter connected in series.

With the standard vacuum interrupter, a type WX-32598, 18cm diameter device, connected in series we commutated 12kA, see Fig. 4-44. However, there were failures to commutate 13kA. The corresponding currents without the series connected vacuum interrupter are 11 and 12kA. The series connected vacuum interrupter appeared to have increased the performance by 1kA or approximately 9%.

By pushing the actuator even harder we increased the electrode separation without any change in other parameters. While we could commutate 12kA with an electrode separation of 21mm we could not commutate 10.8kA with 26mm of electrode separation even though slightly larger arc voltages were developed: 5.7kV at 26mm vs 5.2kV at 21mm.

Conclusions

For each value of capacitance, we commutated the highest current levels achieved up to this time. This illustrated that the 15cm diameter cup electrodes were superior to any electrode design we had used, and were even superior to the 15cm diameter Bruce profile electrodes used in Prototype #8.

The oscillograms (see Fig. 4-44 for instance) showed that the arc current (and the arc voltage) are little affected by the application of the magnetic field during the first 100μs for the initial experiments. However, the arc current and arc voltage were immediately affected by the magnetic field in later experiments. It should be noted that the series connected vacuum interrupter was not responsible for the lack of oscillations. On the other hand, experiments with the demountable arc chamber showed the arc was slow to respond to the application of the magnetic field when cup electrodes were used. We consider that the occasional lack of immediate response of the arc current and arc voltage to the application of the magnetic field was a peculiarity of the cup electrode design. However, this phenomenon did not adversely affect the prototype's performance.

The initial experiments with iron cores were performed without background work to determine the optimum usage of these devices. The cores were not insulated from each other. Further, in their present mode of operation they add inductance to the capacitor circuit and this extra inductance is responsible for the somewhat reduced performance. Further discussion of the cores appears in Appendix D.

We again found that high current commutation ability was somewhat reduced by large electrode separations. However, we appreciated that current commutation in a 72kV circuit would require relatively large electrode separations of about 2cm in order to withstand the high recovery voltages (see Section 6). Future experiments were performed in high voltage circuits to duplicate the necessary recovery conditions.

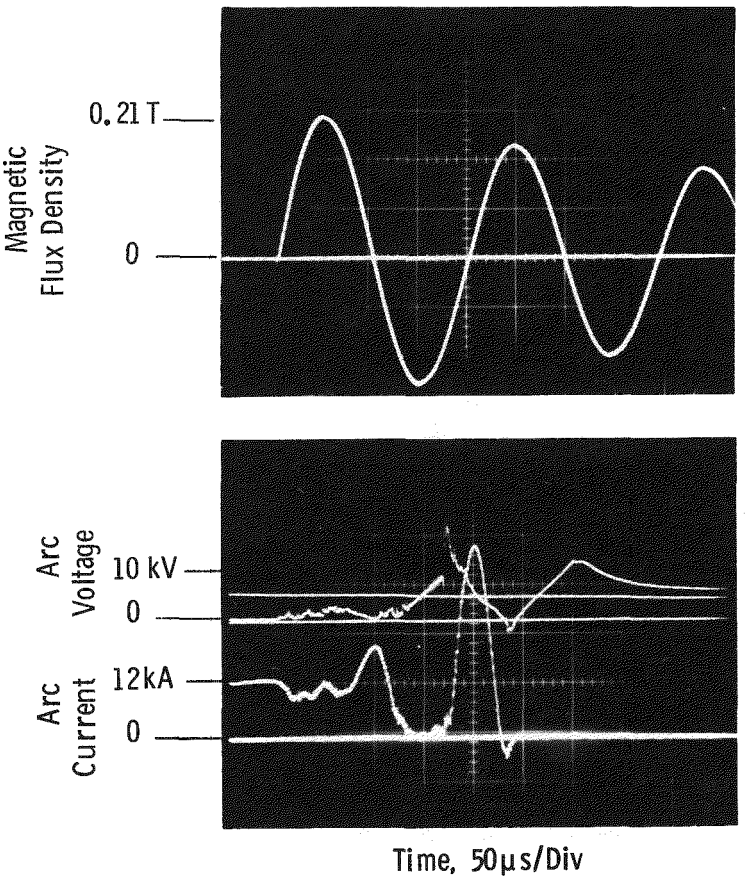

Figure 4-44. Oscillogram of a 12kA current commutation, using 15cm diameter cup electrodes in a 23cm diameter device. 50μF parallel capacitance, 21mm electrode separation and $\dot{B}$ = 6.8 kT/s. Standard 18cm dia. vacuum interrupter connected in series

4-7 HIGH VOLTAGE CIRCUITS AND SERIES VACUUM INTERRUPTER

4-7.1 Study of a Vacuum CLD with Peak Recovery Voltage of 50kV

Practical current limiting devices in 72kV circuits must withstand initial peak recovery voltages ranging from 50kV to 70kV. As discussed in Section 6, the exact peak voltage will depend on the degree of current limitation required as well as the network parameters of the circuit in which the CLD is installed.

In the studies of Sub-sections 4-1 through 4-6 we used experimental setups that provided realistic initial rates of rise of the recovery voltage. However we limited the peak voltage to approximately 15kV by means of a spark gap. In the present experiment we used capacitors rated at 50kV and explored the performance of a CLD with peak recovery voltages up to 50kV. The objectives of the experiment were: (1) to devise means to obtain high recovery voltages (2) to find the highest current that could be commutated by Prototype #9 under high recovery voltages conditions and (3) to use a standard vacuum interrupter in series with Prototype #9 for comparison purposes.

Experimental Approach (Dual Capacitor Banks)

The experimental setup used for these initial high recovery voltage tests is shown in Fig. 4-45. This arrangement is similar to circuits used for previous CLD tests except that the capacitor, C_s, was part of an 80kJ capacitor bank located about 30 meters from the test cell housing the CLD and its associated equipment. One frame of this bank carrying 36 units of 0.88μF each (making C_s = 31.7μF) was connected by means of a coaxial cable. The inductance, L_s, was the distributed inductance of the entire external circuit with inductances of about 8μF each in the coax line, in the connecting bus at C_s, and in the connecting cables, which were non-coaxial, at the CLD. The total inductance was L_s = 24.2μH. The resulting frequency of the external circuit was thus 5.74kHz; the inherent Q of this circuit was 8.5 with R_s approaching infinity, and the Q was reduced to 3.4 with R_s = 5Ω.

Prototype #9 (23cm diam. ceramic, 15cm diam. cup electrodes) was used for the CLD. This device had previously been evaluated in low voltage circuits as discussed in Section 4-6.2. An 18cm diam. standard vacuum interrupter was in series with the CLD.

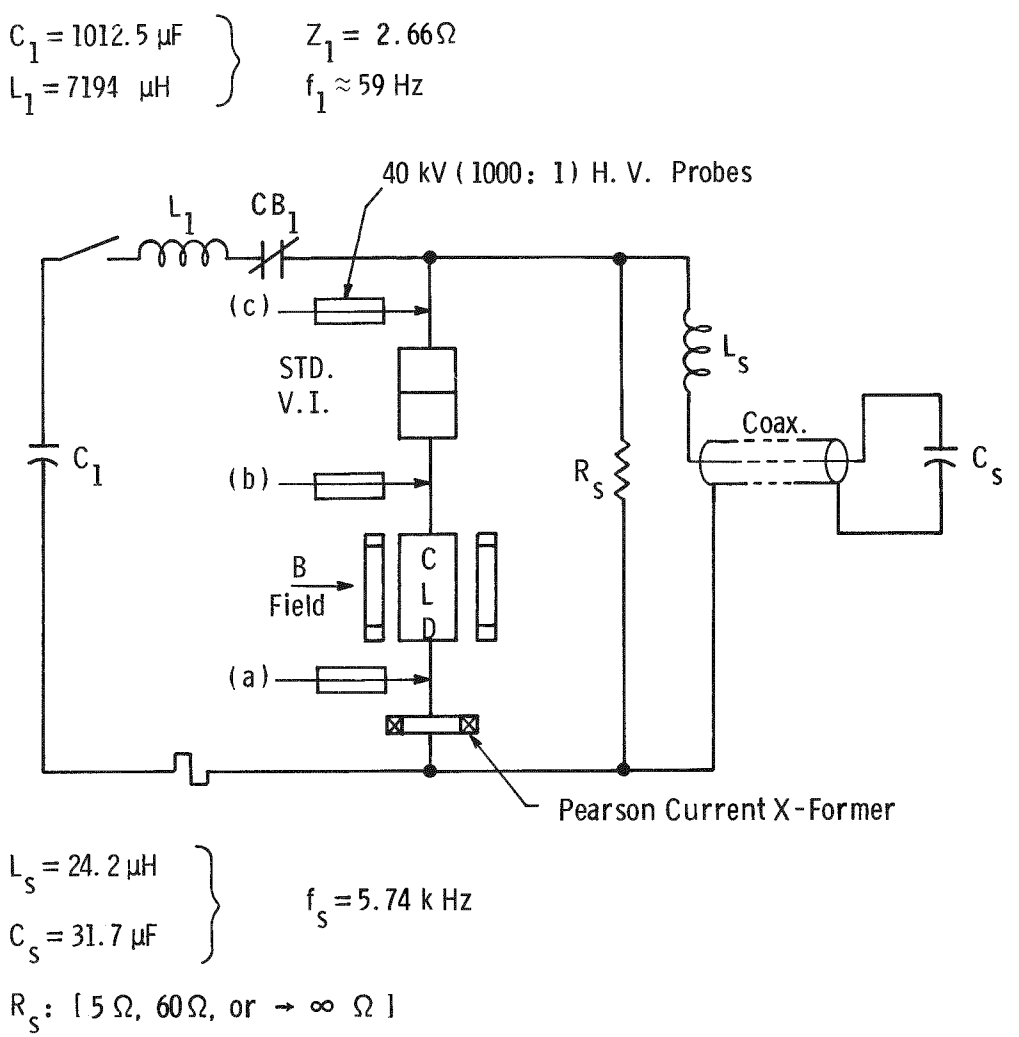

Fig. 4-45. Circuit for high voltage tests using dual capacitor banks

Results and Discussion

Because of the low ringing frequency (5.74kHz) of the external circuit, due to the large value of L_s, the frequency of the oscillating transverse magnetic field was set at 2.5kHz for most of the experiments. This arrangement produced an initial

$\dot{B}$ of 2900 T/sec and a B_{max} of 0.185T. A small amount of data was also taken with the frequency of the B field set at 5kHz. However, a precise limit of the current commutation ability under this condition was not determined due to instrumentation problems. A value of less than 4kA would seem to be the limit based on the charging voltage of C_1 and the circuit impedance. These data, when compared with a limit of 6.1kA found for a B field frequency of 2.5kHz, suggest that the frequency of the external circuit must be at least twice the frequency of the oscillating B field for maximum Mode 4 performance of the CLD.

A summary of the data taken without opening the V.I. in series with the CLD is shown in Fig. 4-46. For all the data, with $R_s = 60\Omega$ or $R_s \to \infty$, the peak recovery voltage was reached in approximately 600μsec. For the data with $R_s = 5\Omega$, the peak recovery voltage was reached in approximately 400μsec. The number near each data point is the time duration in microseconds for the current commutation to be completed. Thus all of the commutations were type Mode 4 except the three at the lowest current value (1.3kA) which were type Mode 1. In all the data taken in these experiments, none of the failures to commutate could be attributed to a recovery voltage restrike. The failure at 6.8kA was caused by the lack of a forced current zero.

Finally, the vacuum interrupter in series with the CLD was opened in synchronism with the CLD under the condition of $R_s = 60\Omega$ and for arcing currents of 3.2kA. All combinations of the voltages across the devices were measured with the two H.V. Probes as shown in Fig. 4-45. In five tests, the total recovery voltage of 40kV divided with 34kV across the V.I. and 6kV across the CLD. The positions of the two H.V. Probes had no effect on this result. We must assume that the effective capacitance across the open CLD was approximately 6 times the capacitance across the open vacuum interrupter. Alternatively, the effective resistance of the CLD was a factor of 6 lower. In any event the standard interrupter "protected" the CLD by withstanding 85% of the peak recovery voltage.

Conclusions

In this first attempt to use a CLD with high recovery voltages, we chose to use the Dual Capacitor Banks concept. The second capacitor bank was located about 30 meters from the CLD. The large amount of inductance in the connecting cables led to reduced performance. In this setup with $C_s = 31.7\mu F$, and $\dot{B} = 2900$ T/sec the maximum current commutated was 6.1kA. In a previous experiment using Prototype #9, Subsection 4-6 , with $C_s = 26\mu F$ and $\dot{B} = 6800$ T/sec, a maximum current of 8.6kA

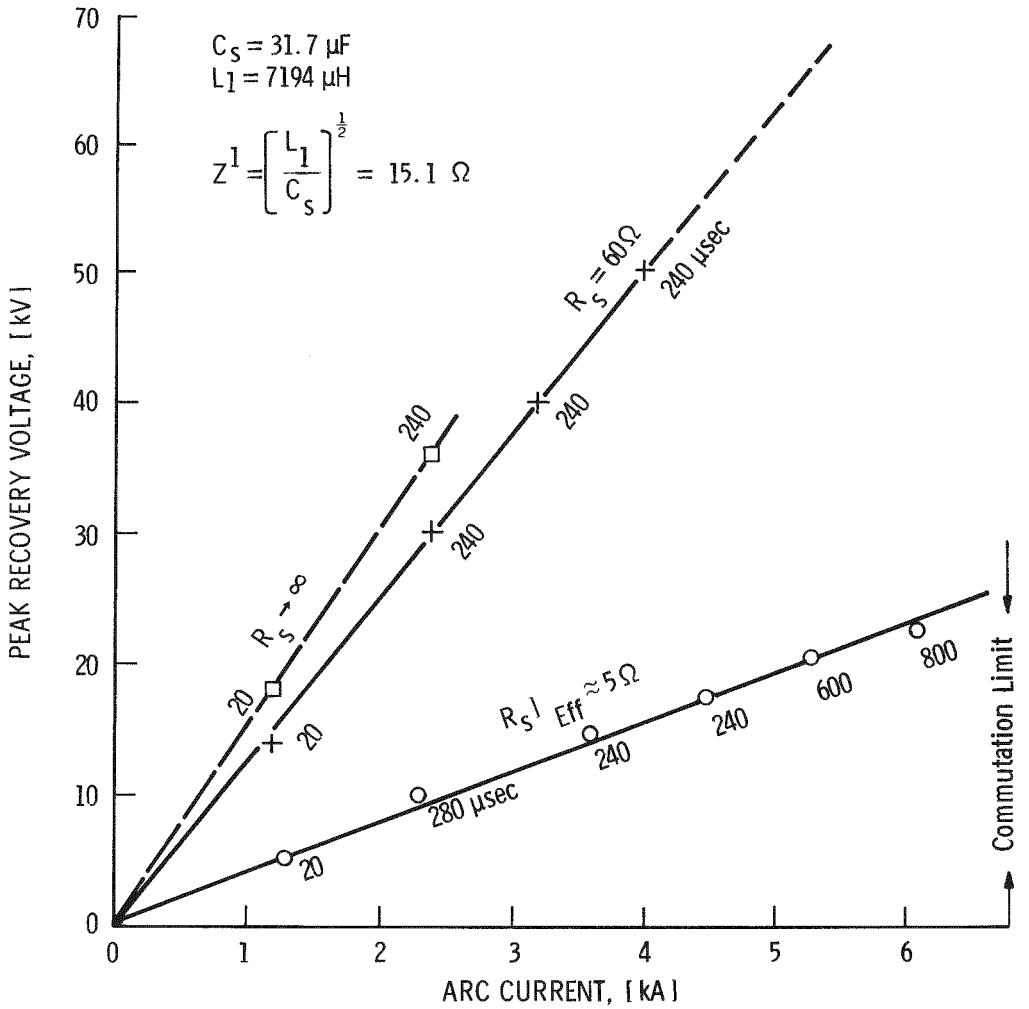

Fig. 4-46. Peak recovery voltage vs. arcing current. Freq. of external circuit: 5.74kHz ; Freq. of B-field: 2.5kHz; $\dot{B} \simeq 2900$ T/sec
$B_{max} \simeq 0.19$ T

was commutated. The two experiments also differed in that the oscillating B-field in the present experiment was 2.5kHz (in order to be less than half the ringing frequency of the external circuit) while the previous experiment used an oscillating B- field of 5kHz. This was less than half of the frequency of its external circuit. Nonetheless, the Dual Capacitor Banks concept is a viable means to test CLD prototypes with high recovery voltages.

Moreover, the experiment met its primary objective of producing a peak recovery voltage of 50kV after commutating a current of 4kA. No restrikes or reignitions were experienced and therefore these figures are neither a voltage nor a current limit for the CLD in this experimental setup.

Additionally, we showed that with a standard vacuum interrupter operating in series with the CLD, 85% of the peak recovery voltage appeared across the standard vacuum interrupter. Specifically the standard interrupter withstood 34kV (not a limit) while the CLD withstood 6kV. Since the CLD alone withstood a peak recovery voltage of 50kV (again not a limit) we can conclude that the series combination should be capable of withstanding significant recovery voltages.

4-7.2 Experiments with Prototype #10 in Circuits Limited to 20kV or Less and Without a Series Connected Vacuum Interrupter

Previous experiments had shown a consistent increase of current commutating ability with increased envelope diameter. For example, we achieved greater performance using 23cm diameter devices, with relatively small area electrodes, than we did with 18cm diameter devices. In order to capitalize on this observation we constructed an even larger diameter 30.5cm device. It incorporated 15cm diameter Bruce profile electrodes made of CLR material.

The first objective of this experimental series was to investigate the effect of larger envelope diameter keeping other parameters as constant as possible.

An immediate difficulty concerns the magnetic flux density. With a larger envelope the magnetic field coils must be placed further apart, and the magnetic flux density reduces approximately as the reciprocal of the coil separation. Further, the profile of the magnetic flux density in the region of the electrodes will be different. In order to maintain the profile of flux density we used larger diameter magnetic field coils. However, the size of these coils further reduced the peak magnitude and rate of change of the magnetic flux density. In order to compensate we used two separate magnetic field power supplies, one for each coil.

This enabled us to maintain as closely as possible both the magnetic flux density and the rate of change of flux density.

Selection of Magnetic Field Power Supplies

The supplies could not be connected electrically in parallel since they would have been damaged by the large circulating current. Further they could not be connected electrically in series since they would be damaged by the voltage. We therefore connected each supply to a separate coil and triggered them at the same time. Even though the supplies were limited in the current they can deliver, the separate coils presented a lower inductance and we were therefore able to increase $\dot{B}$. This approach had three disadvantages: the impedance of one coil was not large enough and excessive currents could have been drawn if the capacitors of the power supply had been charged to the full value, the two circuits would not oscillate at exactly the same frequency, and the magnetic flux produced by one coil would not remain synchronized with the other for long periods.

We also investigated using one power supply to deliver current to both coils connected electrically in series. This has the advantages of a better impedance match and a guarantee that the current in each coil is identical. The results of experiments with the different magnetic field power supplies and with different charging voltages are presented in Table 4-5. Basically there was a slight advantage to using two independent supplies, and subsequent experiments were performed with this arrangement.

Comparative Commutation Data

Figure 4-47 shows the circuit for experiments with Prototype #10. There was a spark gap (not shown) in parallel with C_2 to limit the voltage to 10kV (50μF) or to 20kV (26μF). The results are shown in Table 4-6 and comparative data are shown for other prototypes. The interruption performance at 50μF was disappointing, although the commutation level at 26μF was reasonably high.

Examination of the oscillograms showed that Prototype #10 easily forces a current zero but subsequently conducts again during voltage re-application. An example of this behavior is shown in Fig. 4-48. Here the current had been forced through zero several times. Typically the voltage across the vacuum device would rise to 4 to 6kV, and conduction would resume with a collapse of the voltage.

Table 4-5

EXPERIMENTS WITH THE MAGNETIC FIELD; NO SERIES CONNECTED VACUUM INTERRUPTER

Number of magnetic field power supplies used	Field Coil Power Supply Capacitor charging voltage, kV	Parallel Circuit Capacitance μF	Peak magnetic flux density T	Rate of change of magnetic flux density kT/s	Time of magnetic field application after start of current, ms	Highest current commutated kA	Lowest failure kA
1	9.9	50	.14	4.0	4.0	7.8	8.7
2	2.5	50	.05	1.6	4.0	---	7.8
2	5.0	50	.09	3.3	4.0	8.4	---
2	8.0	50	.14	5.2	4.0	8.3	---
1	5.0	26	.08	2.2	4.0	---	5.0
1	7.0	26	.11	3.0	4.0	5.0	---
1	9.9	26	.14	4.0	4.0	7.7	9.0
2	8.0	26	.14	5.2	4.0	7.7	8.9

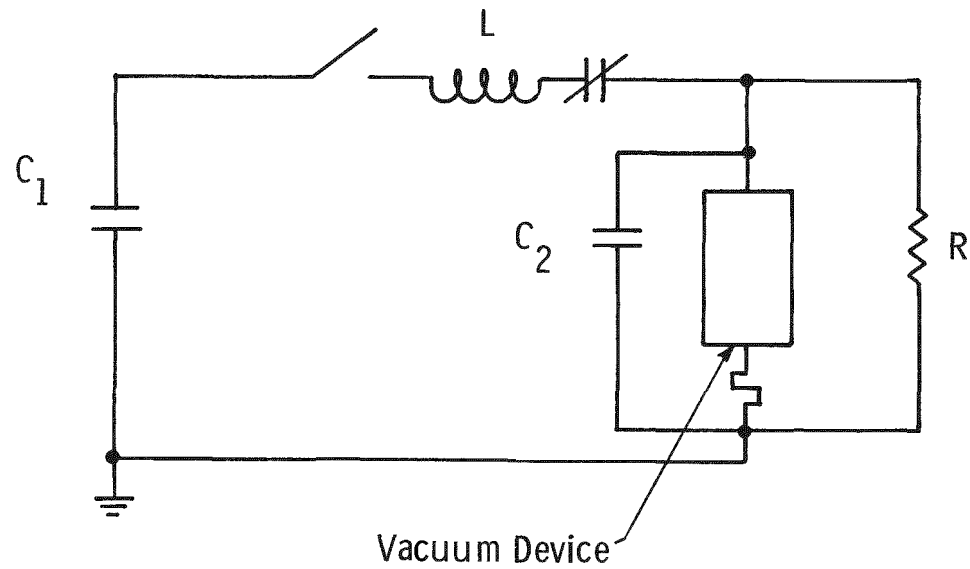

Fig. 4-47. Circuit for experiments with Prototype #10

With 26μF of parallel capacitance we commutated 7.7kA. Results of experiments with other devices at 26μF appear in Table 4-6, and comparison of the data show a consistent increase of performance with envelope diameter.

Effect of Electrode Separation on Commutation Ability

The above experiments were performed at an electrode separation of 2 to 2.1cm. We performed an experiment to determine whether even larger electrode spacings would increase commutation ability, and to do this we charged the capacitors in the actuator power supply to a higher voltage. We achieved an electrode separation of 25mm without changing any of the other parameters such as time of field application, the peak value of the field, and the rate of change of magnetic field. The results are presented in Table 4-7. Basically, at this current level the performance was insensitive to electrode separation.

Table 4-6

COMPARISON OF THE PERFORMANCE OF THE 30.5cm DIAMETER PROTOTYPE #10 WITH PROTOTYPES OF SMALLER DIAMETER

Device; Prototype Number	Parallel Capacitance μF	Envelope Diameter cm	Electrode Diameter cm	Magnetic Flux density B,T	Electrode Design	Rate of Change Ḃ, kT/s	Electrode Separation mm	Current Commutated kA
10	50	30.5	15.	0.14	Bruce	5.2	21	8.3
9	50	23	15	0.21	Cup	6.8	21	11.0
8	50	23	15 (5 cm bridging electrode)	0.21	Bruce	6.8	20 and 23	10.0
2	50	23	14	0.23	Bruce	7.4	21	5.9
10	26	30.5	15	0.14	Bruce	5.2	21	7.7
5	26	23	15 x 7	0.23	Bar	7.2	24	5.4
7	26	18	28 x 5	0.4	Bar	15.6	20	4.4

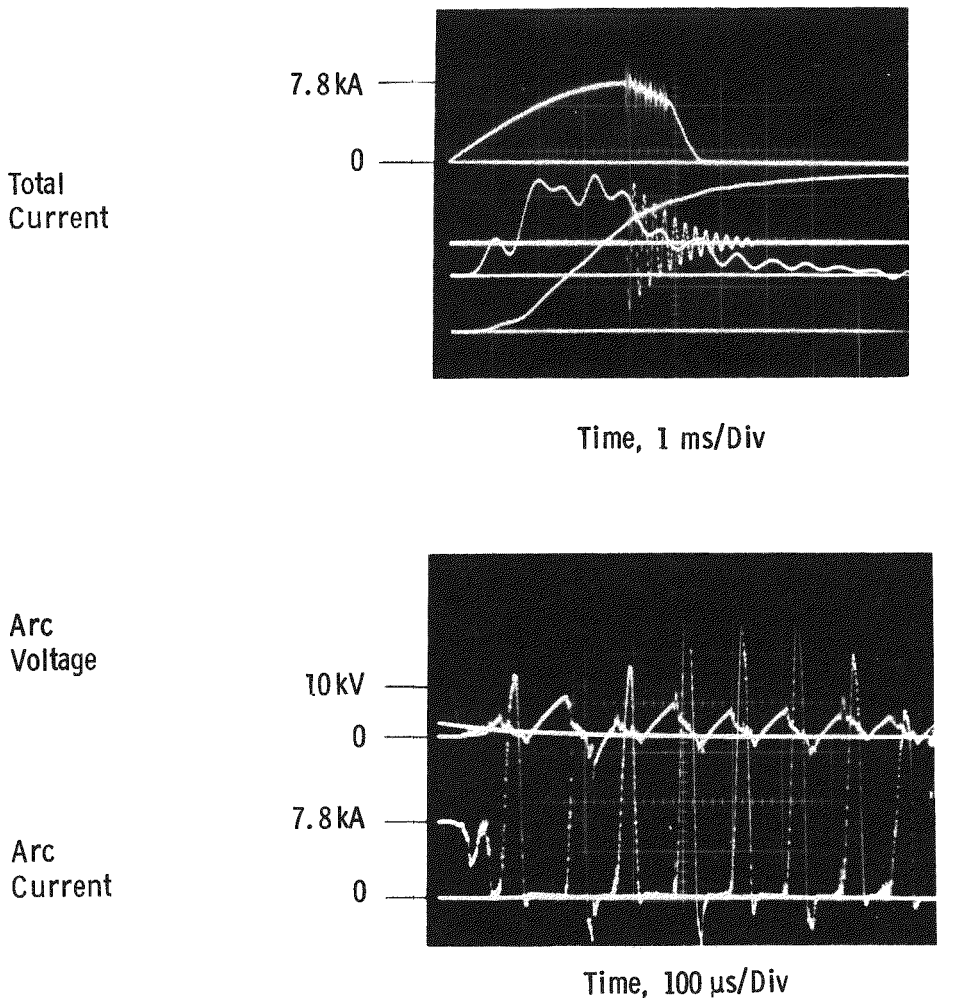

Fig. 4-48. Prototype #10, 50µF parallel capacitance, 20mm electrode separation, B = 4kT/s, NO series connected vacuum interrupter

Table 4-7

STUDY OF THE EFFECT OF GREATER ELECTRODE SEPARATION;NO SERIES CONNECTED VACUUM INTERRUPTER

Voltage used in actuator Power supply	Electrode Separation mm	Peak Magnetic flux density T	Rate of change of magnetic flux density, kT/s	Time of magnetic field application after start of current, ms	Parallel capacitance μF	Highest current commutated kA	Lowest failure kA
1300/850	20.6	0.14	5.2	4.0	26	7.7	8.9
1350/1070	25.1	0.14	5.2	4.0	26	7.8	8.8

Conclusions

- High $\dot{B}$ was attained using two power supplies
- The large diameter envelope of Prototype #10 produced many current zeros with the oscillating B-field
- The need for a series vacuum interrupter was very evident
- Prototype #10 showed that an electrode separation of 20mm was adequate

4-7.3 Experiments with Prototype #10 with a Series Connected Standard Vacuum Interrupter

Low Voltage Circuits

The current oscillations induced by Prototype #10 suggested that a series connected standard vacuum interrupter could be used to interrupt the current and withstand the voltage. Indeed, with a series connected interrupter we were able to commutate a maximum current of 14.5kA, Fig. 4-49. Under the same conditions but without the series interrupter we had been limited to 8.3kA. Figure 4-50 shows the circuit diagram for this experiment and the circuit location where the arc voltage, V_a, was measured. As soon as the current was interrupted by the series connected vacuum device, the arc voltage across Prototype #10 collapsed. The series device withstood the recovery voltage.

This commutation of 14.5kA with 50μF of parallel capacitance was a record high current level. We believe the improvement was the result of the larger envelope diameter. Confirming this we commutated 9.2kA with 26μF of parallel capacitance.

We considered that the reduced ability of the device to withstand large restored voltage was not a shortcoming of the larger diameter envelope, rather it is a function of the difficulty of processing such a large device. The Division which manufactures these vacuum devices worked on the problem and subsequent devices had the seasoning treatments given Prototypes 8 and 9.

All of the data used to compare the effect of a series vacuum interrupter as a function of parallel capacitance appear in Fig. 4-51.

High Voltage Circuits

The purpose of this experiment was to determine the current commutating ability of Prototype #10 under high recovery voltages conditions.

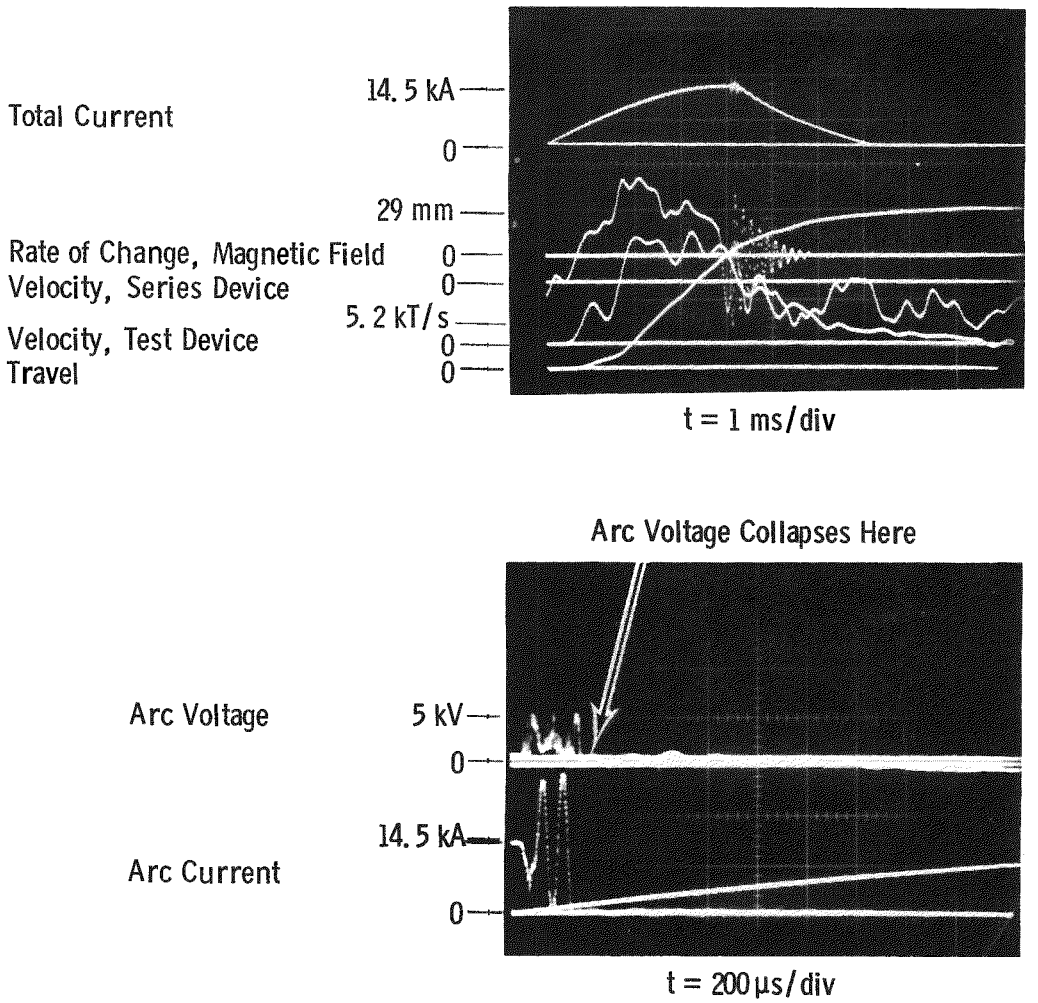

Fig. 4-49. Oscillogram of largest current commutated into 50µF of parallel capacitance. Electrode separation is 21mm, prototype #10 with conventional vacuum interrupter connected in series, 30cm dia. device with 15cm dia. Bruce profile electrodes, R = 3.33Ω

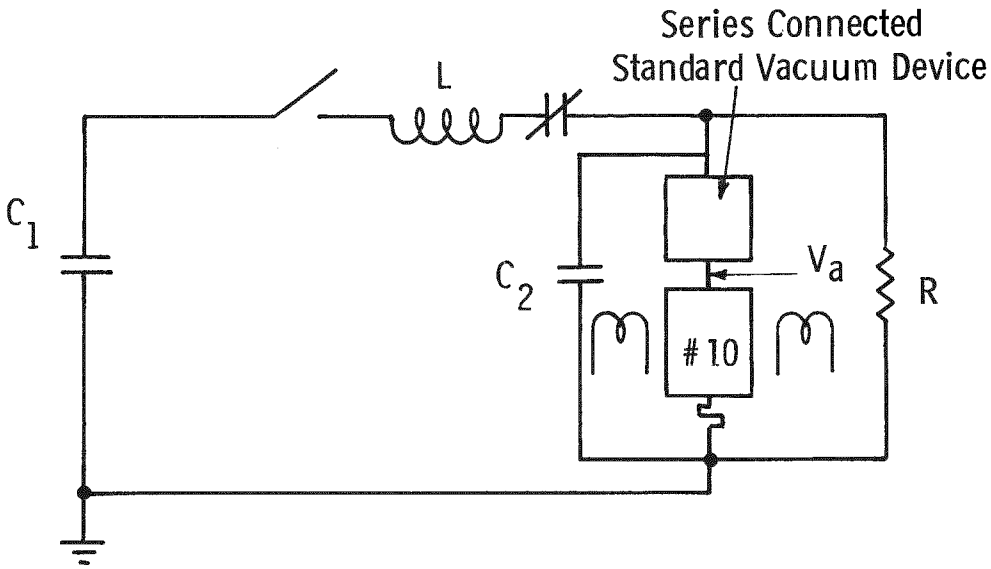

Fig. 4-50. Circuit for prototype #10 experiments with series connected vacuum interrupter

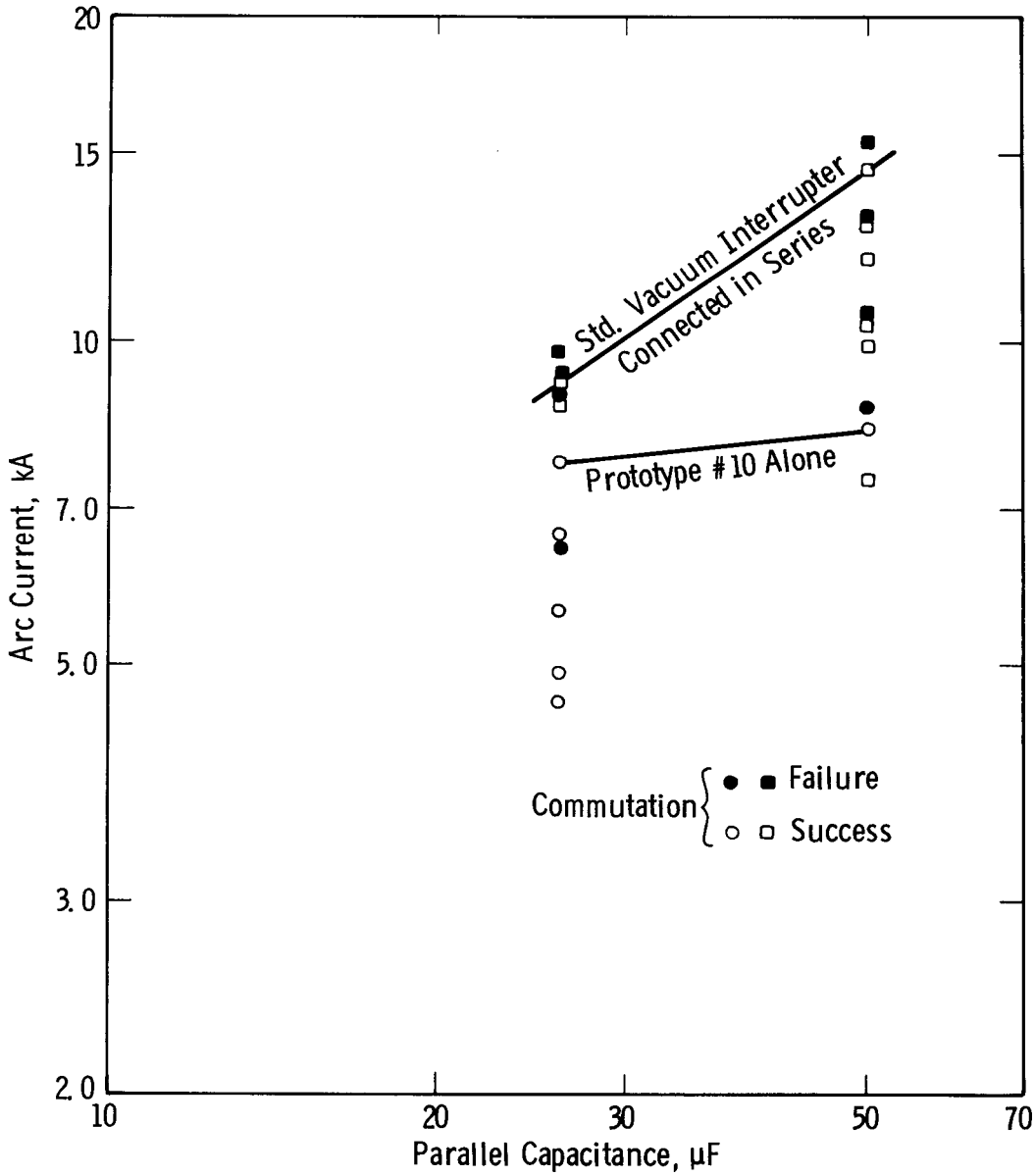

Fig. 4-51. Experimental results showing improvement resulting from the use of a standard vacuum interrupter connected in series with the test device. Electrode separation was 21mm, B was 5.2kT/s, $\dot{B}_{max}$ was 0.14T and all commutations were Mode 4

The experimental setup was similar to that described in Section 4-7.1. Here a 50kV capacitor bank was coupled in parallel to the CLD by means of a 30m length of coaxial cable. In the present experiment several beneficial changes were made. (1) The equipment under test was moved into a test cell adjacent to the parallel capacitor bank. (2) Two parallel coaxial cables were used, each about 5.5m long. (3) Each coaxial cable was connected to half of the capacitors whereby the center conductors were tied to the high side of the capacitors and the sheaths were tied to the frame or low side of the capacitor bank. (4) The parallel coaxial cables were tightly coupled to the series combination of VI and CLD.

The results of the above changes produced an effective capacitance of 31.7μF in the external circuit that showed a ringing frequency of 16.3kHz. The effective inductance of this circuit was 3μH. (In the previous setup the ringing frequency was 5.7kHz and the inductance was 24μH). Since the frequency of the oscillating B-field was 5.9kHz, we achieved a high voltage external circuit having a resonant frequency greater than twice the frequency of the oscillating B-field. Thus, on the basis of our understanding of the best conditions for Mode 4 commutation, this new setup allowed us to use the largest $\dot{B}$ available while at the same time the external circuit frequency was equal to or greater than twice the frequency of the B-field.

This new circuit performed well up to a commutation current level of 4.5kA with a recovery voltage of 29kV. Unfortunately, following this commutation we experienced a flashover of the isolation coupler to the actuator rod of Prototype #10. The resulting damage to our electronic timing, control and measurement circuits was extensive. The problem with the coupler was solved by a rearrangement of the vacuum interrupter and CLD, and alternate electronic equipment was substituted. However these changes compromised our ability to record the commutation process on the high sweep speed oscilloscope. Nonetheless, we proceeded to demonstrate a current commutation of 7.5kA with a recovery voltage of 45kV. Failures to commutate at 8 and 8.5kA were recorded. While our data were incomplete, these failures appeared to be caused by the absence of a forced current zero rather than a reignition due to a rising recovery voltage.

Conclusions

We had gained additional experience with the use of a remote capacitor bank for use as the parallel capacitor in our CLD circuit. Our experience suggested that this method could be improved further such that it would prove viable for a practical device. We had demonstrated the commutation of 7.5kA (31.7μF) with a peak recovery voltage of 45kV.

4-7.4 Experimental Investigation into the effect of a Spark Gap Connected in series with either the Parallel Capacitor or Resistor

Current oscillations produced by varying the applied magnetic fields were giving the highest commutation levels. We explored two potential methods of enhancing this oscillation using Prototype #10 without a series connected vacuum interrupter. In the first technique, a spark gap was connected in series with the parallel capacitance. This spark gap prevented charge buildup on the capacitor during electrode separation. Further, the spark gap isolated the capacitor during the initial period of high arc voltage associated with magnetic field application. The concept was to flashover the spark gap at a relatively high arc voltage, with a consequent rapid increase of capacitor current and corresponding decrease in arc current. The second technique involved connecting a spark gap in series with the parallel resistor. Here the concept was to keep the dissipative resistor element out of the parallel circuit until a high arc voltage had been developed in the device.

Effect of the Spark-gap in Series with the Parallel Capacitor

A circuit schematic is shown in the inset diagram of Fig. 4-52. The spark gap in series with the 26μF capacitor was set for various flashover voltages, and the corresponding current commutation level was recorded. The data appear in Fig. 4-52, and indicate a reduction in commutation ability with increasing flashover voltage. We concluded that the energy dissipated in the spark gap offsets the potential advantage of a more rapid current transfer to the capacitor.

Effect of the Spark-gap in Series with the Parallel Resistor

Here the commutation level increased very slightly by about 3%. This confirms that the parallel capacitor has the major influence on commutation ability, and that the resistor only plays a significant role following commutation.

Conclusions

Neither a spark gap in series with the parallel capacitor not the parallel resistors improved the level of current commutation.

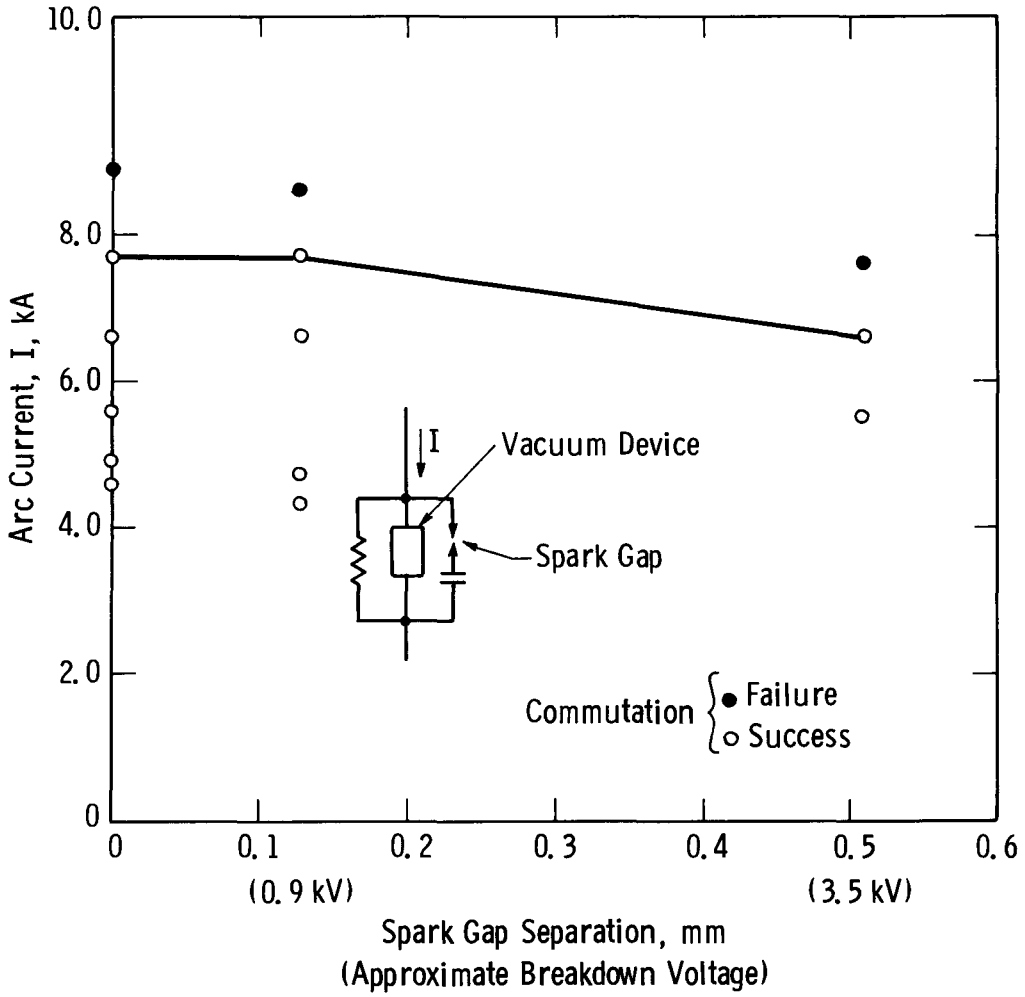

Fig. 4-52. Effect of spark gap in the capacitor circuit, Prototype #10, C = 26μF, electrode separation 21mm, R = 3.33Ω, Mode 4 commutations only

4-8 DUAL ACTUATION; COUPLING TO A HV CAPACITANCE BANK

4-8.1 Experiments using Prototype #11 in the High Voltage Circuit

Past experience had shown that high levels of current commutation were associated with (a) the cup contact geometry [as used in Prototype #9; see Section 4-6.2] and (b) with larger diameter ceramic envelopes [as used in Prototype #10, see Section 4-7.3]. The cup contact geometry can sustain an arc in the diffuse or quasi-diffuse mode to higher currents than any other contact geometry that we have observed for CLD purposes. The use of a larger diameter ceramic envelope, while using the same diameter contact, simply removes the arc from the adverse effects of the wall when the arc plasma is subjected to the transverse magnetic field. Thus Prototype #11 was built with 15cm dia. cup contacts in a 30.5cm diam. ceramic envelope. An additional important feature built into Prototype #11 was the use of two movable contacts, as shown in Fig. 4-53. By using a repulsion coil actuator on both ends, we had the capability of obtaining the desired contact separation of 2cm in a shorter time than with Prototype #9.

Prototype #11 was the second 30.5cm dia. CLD built. Extra care was taken in the vacuum processing and voltage seasoning of this device. Before power testing, Prototype #11 was given a 60Hz voltage withstand test. The device held off 70kV rms for seven minutes with the electrodes held 2cm apart. Higher voltages and longer times were not attempted since the above withstand was more than adequate for the planned tests.

Objectives of the Experiment

The first objective in testing Prototype #11 was to make a direct comparison with the results obtained with Prototype #9 such that the increased envelope diameter (from 23cm to 30.5cm) could be evaluated. This objective included the use of the oscillating transverse magnetic field, the use of a H.V. (50kV) recovery voltage, and the use of a standard vacuum interrupter in series with the CLD.

The second objective was to evaluate the effect of more rapid electrode separation by means of the dual actuation of the two movable electrodes.

The third objective was to improve the circuitry to provide a 50kV recovery voltage using a capacitance of C = 48μF while at the same time providing an external circuit with a ringing frequency $\geq$ 2 times the frequency of the oscillating magnetic field.

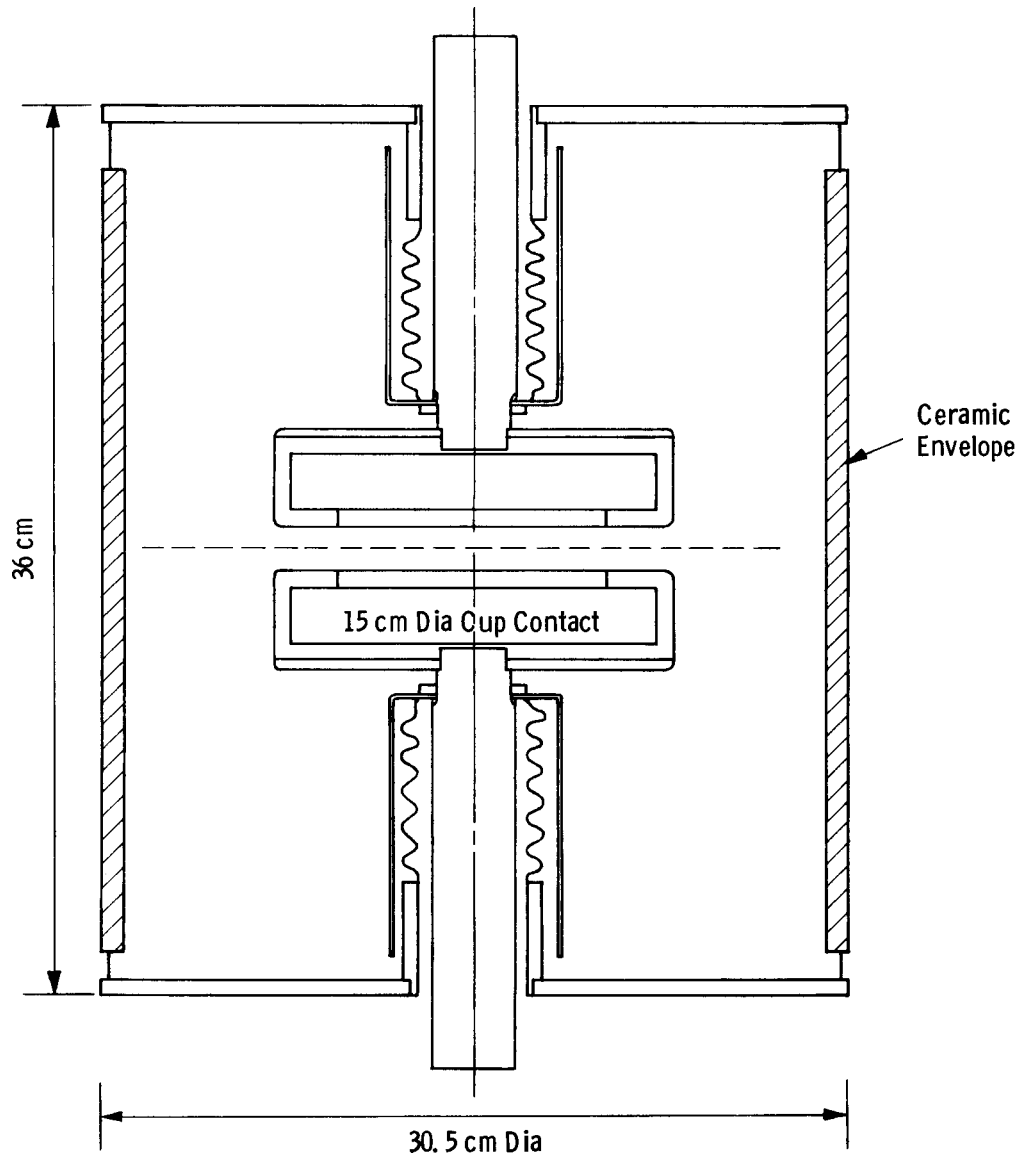

Fig. 4-53. Schematic of Prototype #11 with two movable cup contacts

All three of the above objectives were met using the schematic circuit shown in Fig. 4-54. The value of the stray inductance, L, was minimized since it is critical in obtaining a high ringing frequency in the external circuit. The value of the resistance, R, was selected to limit the recovery voltage to 50kV once the source impedance (not shown) had been selected.

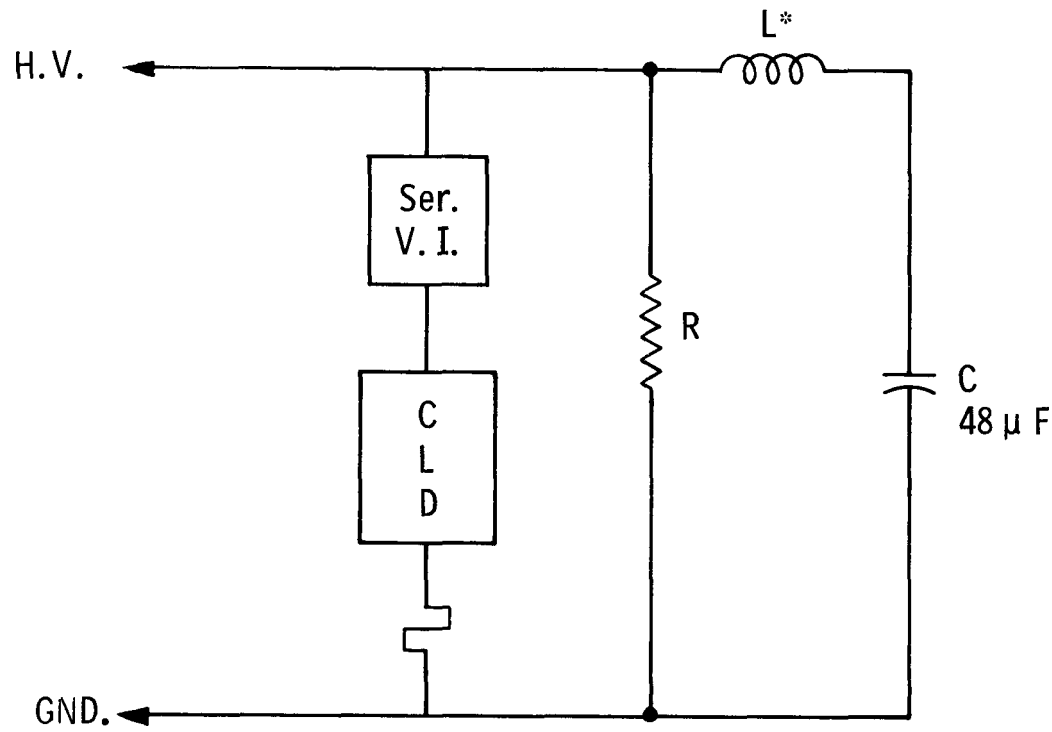

Fig. 4-54. Schematic circuit for testing Prototype #11

Experimental Results and Discussion

The required circuit conditions were realized by the tightly coupled circuit shown in some detail in Fig. 4-55. The high ringing frequency resulted from the use of as many coaxial cables in parallel as needed to reduce the cable inductance. At the same time the capacitance was divided into tightly grouped units. For the case at hand, each of the capacitors, C, was made up of a rack of 18 units with individual values of 0.88μF. These units were connected in parallel to give $C \approx 16\mu F$. The remaining stray inductance was associated with the bussing of the series vacuum interrupter and the CLD. Here aluminum plates of 15 or 20cm width were used to make the electrical connections. The resulting value of L* was about 2.2μH which, with $3C = 48\mu F$, gave a ringing frequency of 15.5kHz. Since the B-field frequency was 5.8kHz, we had met the condition for the frequency of the external circuit being greater than twice the B-field frequency.

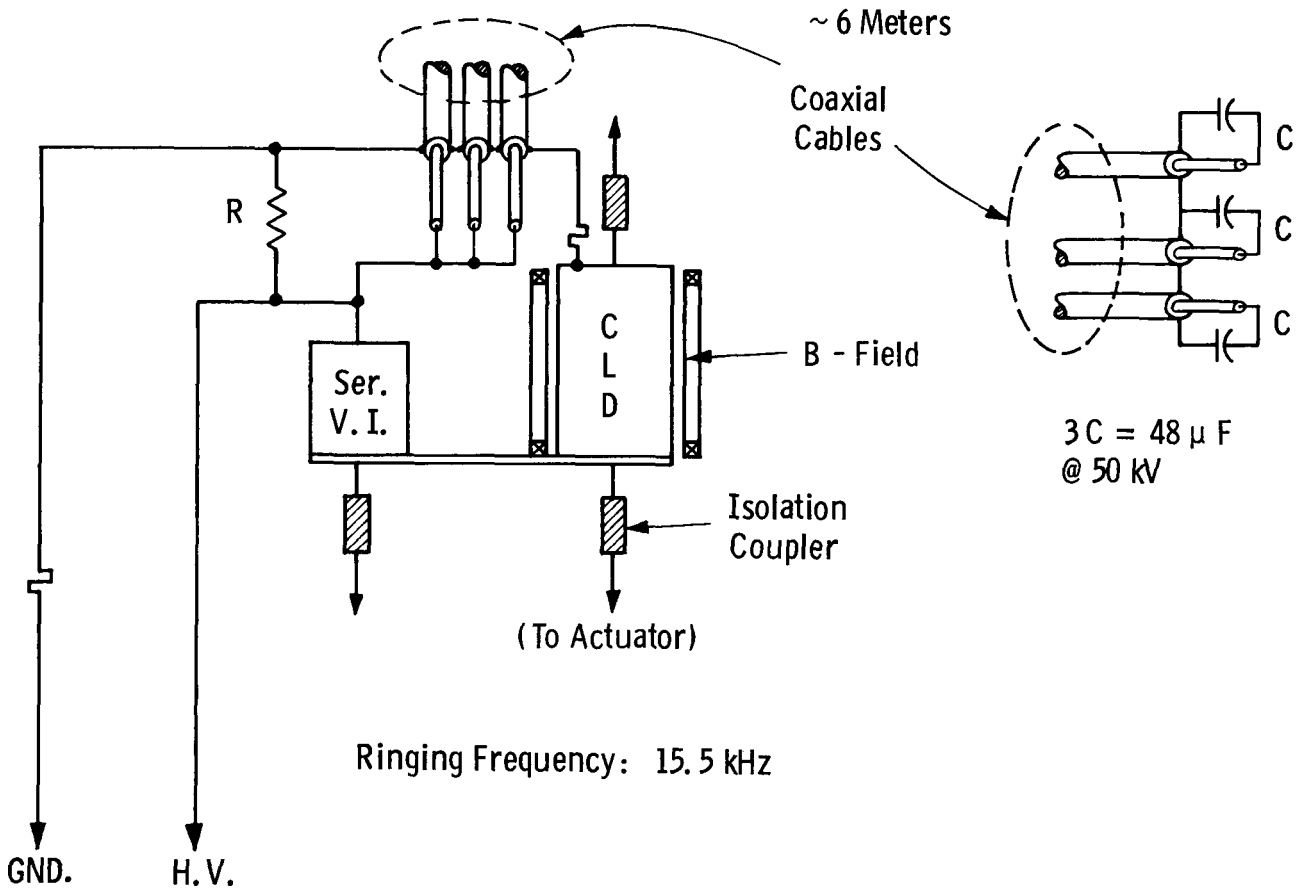

Fig. 4-55. Tightly coupled circuit for high voltage tests using remote capacitor banks

Tests were then begun to compare Prototype #11 with Prototype #9. One electrode of #11 was held fixed while the other was separated to a gap of 20mm in 4msec. The series vacuum interrupter was opened at the same time. After eight successful test shots we had achieved current commutation of 7.8kA with a peak recovery voltage of 38kV. The next test shot was a failure at 8.8kA. The test records were not clear so an attempt was made to commutate at a lower current which also failed. Inspection of the Prototype #11 showed that it had lost its vacuum and the testing had to be terminated.

The cause of the failure was the abrasive rubbing of the movable contact stem against its bellows. This opened a pinhole in the bellows. The rubbing of the bellows

occurred over one half the cylindrical area of the stem and with a length comparable to the stroke. This led us to believe that the bellows was undergoing a swivel-like motion. This type of motion and failure was not observed in Prototype #9 whose construction was identical. Further, we had never experienced this phenomenon in previous prototypes nor in the hundreds of vacuum interrupters we had dealt with over the years.

Conclusions

The remote capacitor bank concept had been demonstrated for a realistic arrangement of circuit components. We concluded that we were able to design H.V. circuits for capacitor values of interest without compromising the desirable high ringing frequency.

The unexpected failure of Prototype #11 meant that double actuation experiments would have to be delayed. We concluded that experience with double actuation should be gained immediately, and we therefore decided to continue our experiments using the circuit designed for Prototype #11 but substituting Prototype #8. We further concluded that a new Prototype (#12) should be built with a similar geometry to #11 but with better stem/bellows design.

4-8.2 Experiments using Prototype #8 with Dual Actuation in a H.V. Circuit

The vacuum failure of Prototype #11 led us to reuse the 23cm diam. Prototype #8 with the objective of gaining immediate information on dual actuation in a H.V. circuit. Prototype #8 has two movable electrodes; a 15cm diam. Bruce profile electrode, and a 5cm diam. lower mass electrode. For these experiments, both of the movable electrodes were actuated by using a repulsion coil mechanism on each movable stem. The mating plane of the movable contacts was set at 10mm from the large stationary contact. Then, by moving the two movable contacts in opposite directions a distance of 10mm each, a gap of 20mm was attained. At full gap the plane of the arcing surface of the small contact was in the plane of the arcing surface of the large stationary contact. By this means we had a condition wherein two 15cm diam. Bruce profile contacts were effectively spaced by a gap of 20mm.

Figure 4-56 shows the curve of the relative separation of the contacts as a function of time. A gap of about 20mm could be reached in about 1.5msec. This was the fastest effective gap separation we had achieved to date. Previously, the fastest separation to 20mm had been achieved with Prototype #8 by moving the smaller electrode only. This second fastest opening to 20mm required 2.1msec and is shown for comparison by an "X" in Fig. 4-56.

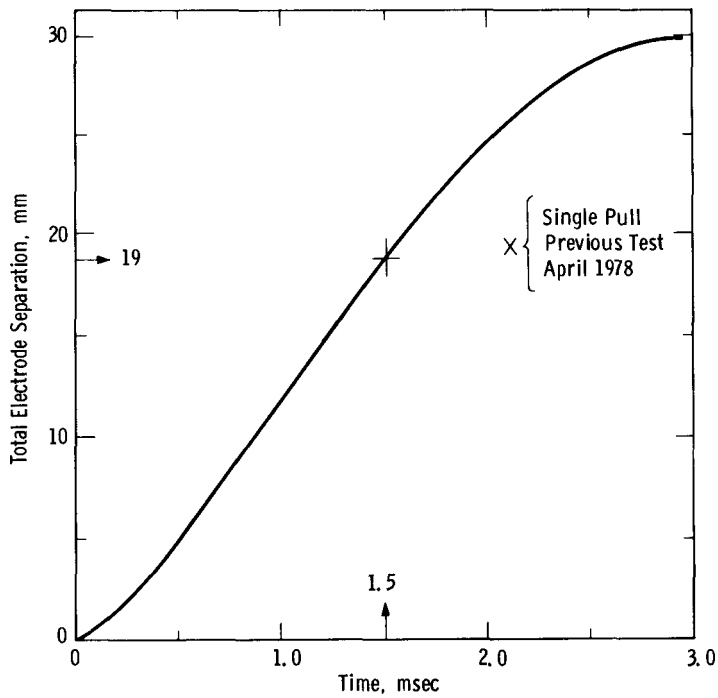

Fig. 4-56. Travel curve for experiments with Prototype #8

Experimental Objectives and Approach

The experimental objectives for dual actuation of Prototype #8 in a H.V. circuit were specifically: (a) to gain experience with dual actuation, (b) to find the commutation limit of this prototype in a H.V. circuit and (c) to compare the new results with previous results taken at slower contact separation with lower recovery voltage.

The experimental approach was identical to the setup described in Section 4-7.1. The circuit is shown in Fig. 4-54 where it will be noted that a series vacuum interrupter was used. Some details of how the circuit was tightly coupled to the remote H.V. capacitor are shown in Fig. 4-55.

Experimental Results and Discussion

Fast separation of the contacts to the desired gap of 20mm was tested in two distinct ways: (1) The contacts were parted as early as possible and the current was commutated by applying the transverse B-field on the rising wave; and (2) the parting of the contacts was delayed to a later time so that the commutation took

place at the crestof the 60Hz wave. We will discuss these two techniques separately.

Effect of Reduced Arcing Time with Electrode Separation at Low Currents

The minimum time to part the contacts (deadtime) was 0.7msec. The contact separation time and also the arcing time was 1.5msec. Therefore, the earliest time that the B-field could be applied to cause commutation with a 20mm gap was 2.2msec after the a.c. current zero. The largest current commutated under these conditions was 10kA. Figure 4-57 shows oscillograms for this case. The recovery voltage of 47kV was measured across the resistor, R, (see Fig. 4-54) and was, therefore, divided between the interrupter and the CLD. [The series interrupter was left closed for one test at the 6kA level and a recovery voltage of about 28kV appeared across the CLD alone. The recovery voltage limit for Prototype #8 was not, however, pursued further during these tests].

In previous tests with Prototype #8 (Sub-section 4-6), a current of 10kA was also commutated on a rising current. In this previous test, the commutation took place after an arcing time of 2.1msec and the recovery voltage was about 16kV. Evidently neither the shorter arcing time of 1.5msec nor the use of a H.V. remote capacitor bank had reduced the current level that Prototype #8 could commutate.

Some additional remarks on the details of Fig. 4-57 are in order. In the bottom oscillogram, both the current and voltage traces suffer from an oscillation that was shown to be a pickup signal from the oscillating B-field. This unwanted pick-up was a direct result of the tight circuit coupling necessary to reduce the stray inductance, L*.

An unexplained phenomenon was seen on all oscillograms taken of current commutation on the rising current wave for which the recovery voltage was greater than about 35kV. This phenomenon will be discussed relative to the traces of Fig. 4-57. Note that the recovery voltage rose to a value of 47kV in 380μs which is consistent with calculation. Then, about 60μsec later in this case, a dip is seen in the recovery voltage followed by a declining voltage that goes to zero in about the same time that it rose to its peak. One might suppose that the backup breaker, which was a vacuum interrupter with a gap at this moment of only 3mm, arced-over, and allowed the energy stored in the 48μF capacitor to return to the inductor of the L_1C_1 source supplying the circuit current. This hypothesis might explain the behavior of the recovery voltage. It does not however, explain the lack of

a comparable oscillation in the trace of the circuit current, shown in the top oscillogram of Fig. 4-57, nor the long time duration of the circuit current after current commutation. Further analytical and experimental work was needed to fully explain these observations.

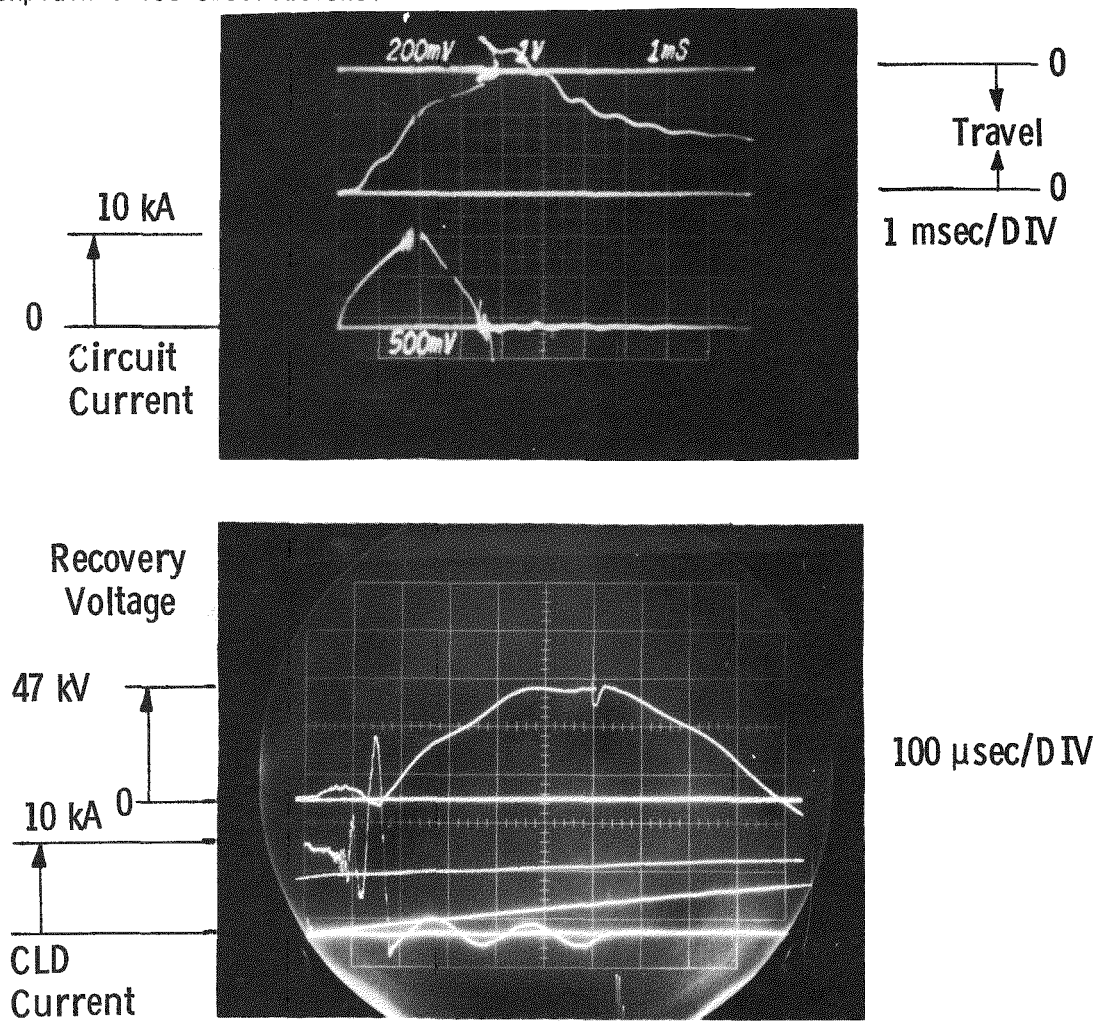

Fig. 4-57. Effect of reduced arcing time; Prototype #8 was opened to a gap of 20mm in 1.5msec; current at contact separation was 3.2kA

Effect of Opening at Higher Current

The second technique involving fast contact separation involved delaying the contact separation to higher current levels. The separation time and therefore the arcing time was held constant at 1.5msec. Of course, the deadtime of 0.7msec remained. By adding an additional delay of 2.2msec to the actuator trigger source,

current commutation was tested at the crest of the 60Hz wave. The highest current commutated with this method was 6.4kA and an oscillogram is shown in Fig. 4-58. The current at the instant of contact separation was 6kA. The recovery voltage rose to a peak of 33kV in the expected time of 380μsec and then remained constant for the remainder of the observation time of 500μsec. (Actually the recovery voltage decays via the parallel resistance, R = 80Ω, with an RC time constant of about 4msec.). Attempts were made to commutate 7.8kA, but these failed due to the lack of definite current zeros rather than restrikes associated with the recovery voltage.

Previous tests with Prototype #8 were not performed at contact separation currents as high as 6kA. Thus a direct comparison is not possible. The highest contact separation current in the previous tests was 4.7kA which resulted in marginal commutation of 8.6kA. These previous successes had recovery voltages of about 15kV.

From the above results, we were led to consider whether it is possible, with 15cm diam. Bruce profile contacts, to part the contacts at currents $\geq$6kA and expect to produce a diffuse arc in 1.5msec. A diffuse arc was thought to be necessary in order for the transverse B-field to interact properly with the arc plasma in order to produce the initial high arc voltage. We do not have direct observations of vacuum arcs for the present condition, i.e., for parting contacts at currents of the order of 6kA and separating to 20mm in 1.5msec. However, some insight is gained from the data shown in Fig. 4-59, where the arc appearance is shown on a plot of electrode gap versus instantaneous current. This figure is taken from ref. (7).

Figure 4-59 shows the physical arc appearance for 10cm diameter electrodes separated with an average speed of about 3m/sec during an a.c. half cycle. The diagram is a composite of observations made with electrode separations at different points on the current wave. An individual sequence is shown by the dashed curve. Here the arc starts in a constricted form, changes into a jet column form at longer spacings, and becomes diffuse at a current level of 20kA prior to current zero. Of particular interest to the present study is the arc form following electrode separation at current levels of 5 to 10kA. At these currents, the arc has some of the characteristics associated with a column although there is a subsequent rapid transition to the diffuse form. It must be remembered that the present electrode separation speed was 13m/sec and hence the data of Fig. 4-59 may not be relevant. On the other hand the present data, together with Fig. 4-59

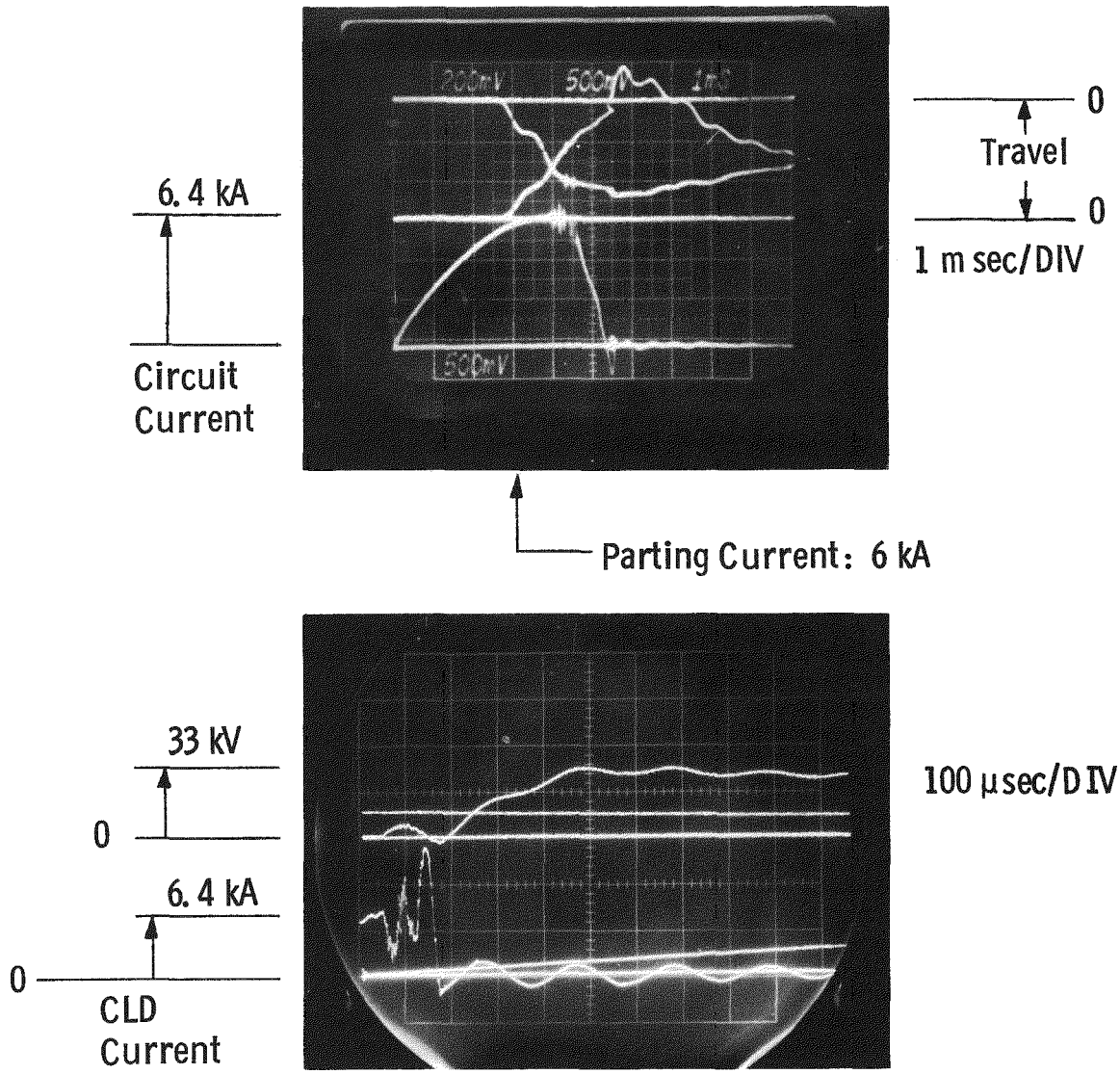

Fig. 4-58. Effect of opening at higher current; 6.4kA was the largest current commutated with 6kA at contact separation; prototype #8 opened to a gap of 20mm in 1.5msec

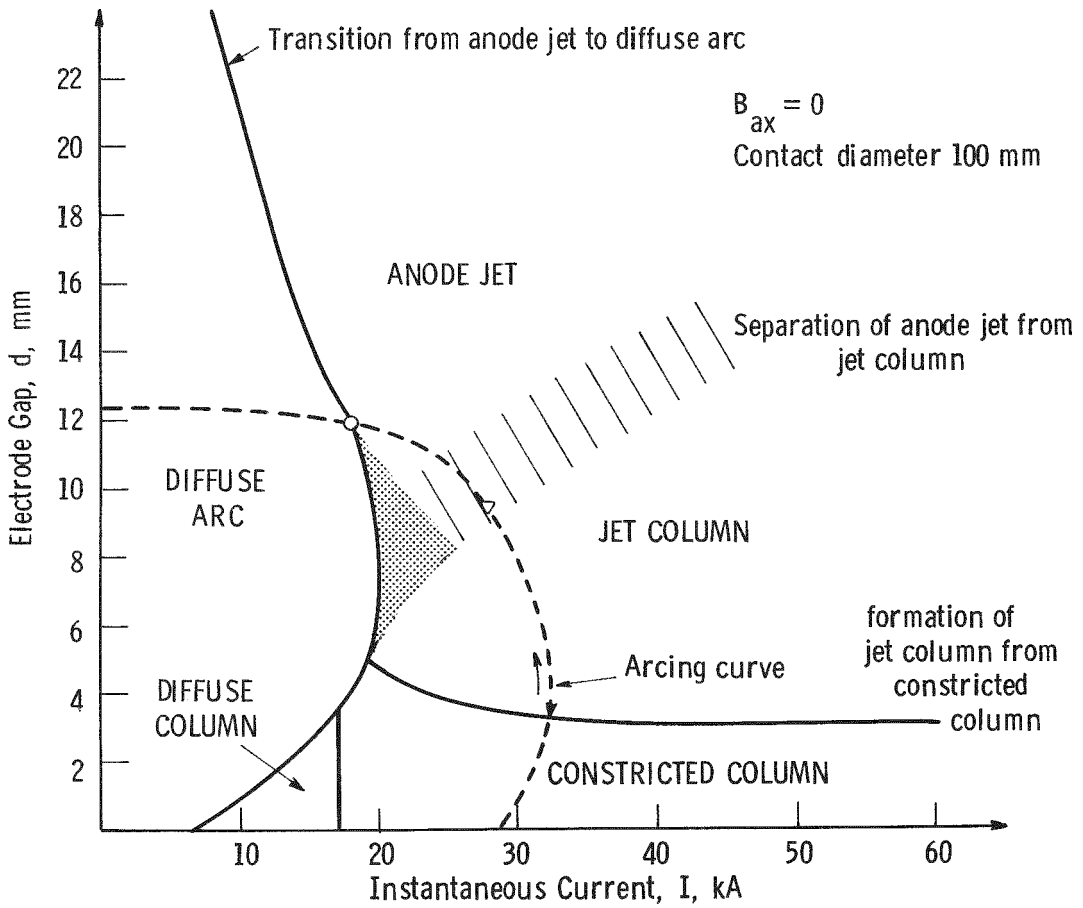

Fig. 4-59. Physical arc appearance as a function of current and electrode gap, for one half cycle of arcing, 50-60Hz, contact diameter 100mm, $I_{sep} > 7kA$

suggested that the possible arc column formed at 6kA might be affecting the current commutation.

Conclusions

Dual actuation, i.e., acceleration of both contacts in opposite directions, was a viable way to explore current commutation on the time scale needed for a practical device. We had demonstrated that a contact separation of 20mm can be attained in 1.5msec; at least for moderate to light contacts.

With dual actuation, and with a H.V. remote capacitor bank, the current commutation limits of Prototype #8 were about the same as previously found for single contact actuation in a lower voltage circuit. In the present study 10kA (using 48μF) could be commutated when the contact separation current (rising wave) was 3.2kA. However, only 6.4kA could be commutated when the contact separation current was 6kA. We concluded that neither rapid contact separation nor high recovery voltage would decrease the performance of our current limiting devices when the current level at contact part was less than 6kA.

4-9 OPENING SPEED AND SEPARATION CURRENT

4-9.1 Experiments using Prototype #12 in the High Voltage Circuit

High levels of current commutation were achieved using the cup contact geometry in Prototype #9 in a 23cm diameter envelope. For example, 12kA was commutated in a 12kV circuit as described in Subsection 4-6. We attributed this commutation to the presence of a diffuse or quasi-diffuse arc mode at relatively high currents with the cup contact geometry.

Additional tests were performed with Prototype #12 which had high speed welded bellows with a larger inside diameter and greater lateral stiffness. The larger inside diameter increased the clearance between the stem and the bellows while the increased lateral stiffness prevented impact between the stem and the bellows. This device had similar cup electrodes to Prototype #11 with both electrodes movable. Prototype #12 was tested with two actuators, operated simulataneously, in order to simulate higher speed operation than #11. The latter prototype was tested with electrode separation to 2cm in 4ms.

4-9.2 Objectives of the Experiment

The primary objective of the experimental series was to gain commutation experience with cup electrodes during the simulation of rapid electrode separation. In particular, the capability of reaching a desired electrode separation in a short time permitted us to explore the effect of separating the electrodes at high current. The experiments with Prototype #8 previously indicated reduced performance when Bruce profile electrodes were separated at a high current level of 6kA.

A further objective was to gain additional experience using a series connected standard vacuum interrupter at recovery voltages of the order of 50kV.

4-9.3 Actuator Achievements

An oscillogram of the electrode separation as a function of time for both upper and lower electrodes is shown in Fig. 4-60. Here an electrode separation of 20mm was achieved in 2.8ms (or 2.2ms plus 0.6ms of dead time) with each electrode moved 10mm. The mass of each electrode and stem was 3.7kg. We ran a total of 11 experiments before the coupling on one actuator failed. Prior to this failure we established a commutation limit of 8.3kA with a recovery voltage of 42kV.

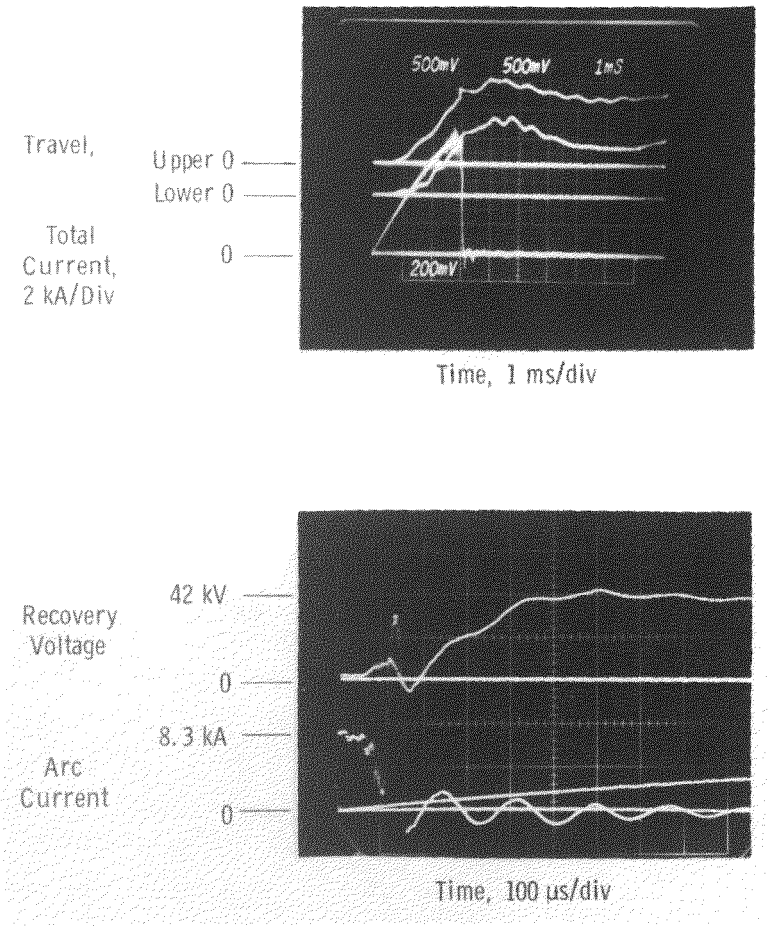

Fig. 4-60. Commutation of 8.3kA with 42kV recovery voltage C_2 = 48µF, L* = 2.2µH, R = 80Ω, prototype #12, electrode separation of 20mm, separation current, 2.8kA

Subsequent experiments were run with the actuators subjected to a lower level of stress, and a total of 37 additional experiments were run without actuator failure.

4-9.4 Erratic Performance of Prototype #12

A part of the seasoning process during the manufacture of these vacuum devices is to subject them to a high alternating 60Hz voltage. The limit of the apparatus at the Industrial and Government Tube Division (I.G.T.D.) is 156kV rms. Prototype #12 withstood this maximum voltage without incident, and this demonstrates superior initial performance.

When Prototype #12 arrived at the R&D Center it was again subjected to high alternating 60Hz voltage. This had been standard quality control for all prototypes.

The purpose of this procedure was to ensure that the device had retained a good vacuum. However, Prototype #12 broke down at 20kV.

The device apparently had a slow leak, and we decided to essentially pump the gas molecules by repeated breakdown. This imbeds the molecules in the electrodes. We held the a.c. voltage steady until the breakdowns ceased. We then increased the voltage until voltage breakdown started. With repetition of this technique we improved the level of voltage withstand to 73.8kV at which level no further improvement was possible. Thus Prototype #12 started off as a marginal device with barely adequate voltage withstand capability.

Another symptom of the apparent slow leak of air was the high arc voltage. Figure 4-61 is an oscillogram which shows that the arc voltage was 500V and erratic when the arc current was only 12kA.

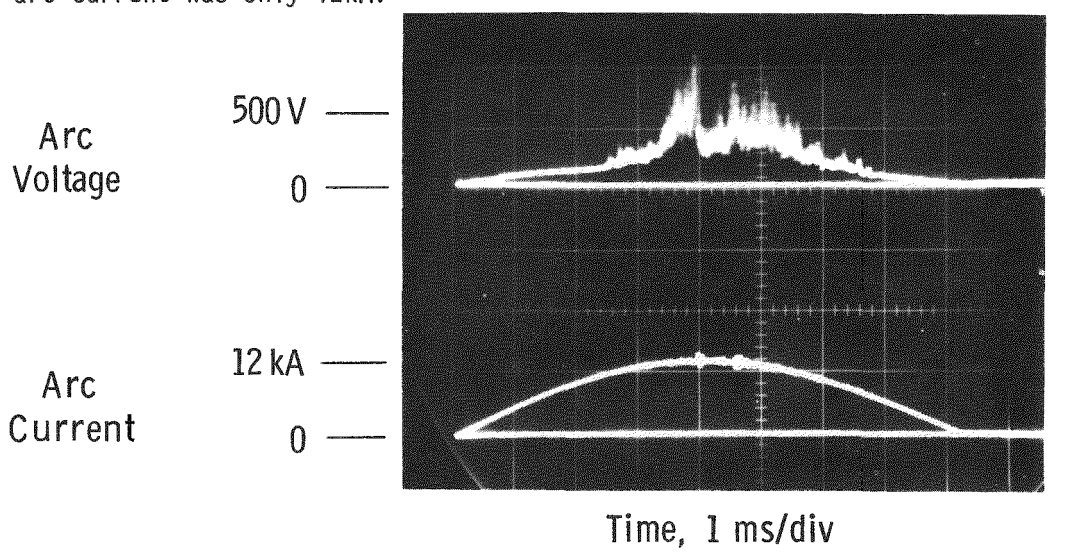

Fig. 4-61. Arc voltage of prototype #12 with no magnetic field applied. Electrode separation 14mm at 2.7ms after start of current

4-9.5 Experimental Results and Discussion

A total of five commutation test conditions were used for the experiments with Prototype #12. This prototype was connected in series with a conventional interrupter. The first condition involved operating the actuators at their limit to obtain the desired 20mm electrode separation as soon as possible after current initiation. The next two test conditions involved using a smaller electrode

separation to reduce the arc voltage at the time of magnetic field application. Electrode separations of 14 and 10mm were selected. These smaller electrode separations had the further benefit of reduced stress on the actuator.

The remaining two test conditions involved delaying the electrode separation so that a constricted, high current arc would be present at the moment of electrode separation. Here the field was applied at spacings of 14 and 19mm.

The highest currents commutated along with other data are presented in Table 4-8.

With a fast electrode separation of 20mm in 2.2ms we commutated 8.3kA with a recovery voltage of 42kV. An oscillogram from this experiment appears in Fig. 4-60. However, the arc voltage was high and we could not commutate 8.8kA. The upper electrode actuator failed during the exploration of this current limit.

We repaired the actuator and operated it at a lower electrode acceleration for the dual purposes of (a) reducing the actuator stress with a stroke of 14mm in 2.1ms (2.1ms + 0.6ms of dead time) and (b) achieving a lower arc voltage at the time of magnetic field application. At this condition we commutated 10.4kA with a recovery voltage of 51kV. We attributed the improved performance to the reduced arc voltage and to the improved internal vacuum in the interrupter as a consequence of repetitive arcing. At 51kV the voltage measuring circuit failed, and we were unable to record the recovery voltage. Figure 4-62 is an oscillogram from a subsequent experiment at 10.2kA but with 40Ω of parallel resistance and consequently slightly lower recovery voltage.

When the electrode separation was reduced to only 10mm, the commutation level was significantly lower at 7.3kA.

The fourth and fifth test conditions involved delaying the operation of the actuators in such a manner that the electrodes separated at high current. A comparison of the commutation levels in Table 4-8 for conditions (1 and 2) and (4 and 5) indicated that the separation of cup electrodes at high current did not reduce their performance. In fact, for condition 5 we observed the highest current commutation we have yet achieved in the high voltage circuit. Figure 4-63 is an oscillogram of this 11.0kA current commutation. Since we did not observe any failures to commutate during test condition 5 we concluded that 11kA was not a current limit. Rather, 48kV represents a voltage limit for our present capacitor bank and this limited the experiment. We attributed the good performance during condition 5 to a steady

TABLE 4-8

HIGHEST CURRENT COMMUTATED AT EACH TEST CONDITION
PROTOTYPE #12, 48μF OF PARALLEL CAPACITANCE

Test Condition	Was the time of opening delayed to increase the current at electrode separation	Commutated Current kA	Recovery Voltage kV	Electrode Separation mm	Separation Current kA	Time of Magnetic Field Application ms	Current Limiting Resistance R, Ω	Figure which shows the relevant oscillogram
1	No	8.3	42	20	2.8	2.8	80	4-60
2	No	10.2	47	14	3.8	2.7	40	4-62
3	No	7.3	36	10	2.5	2.3	40	- - -
4	Yes	7.5	35	14	10.4	6.3	40	- - -
5	Yes		48	19	13.0	6.0	40	4-63

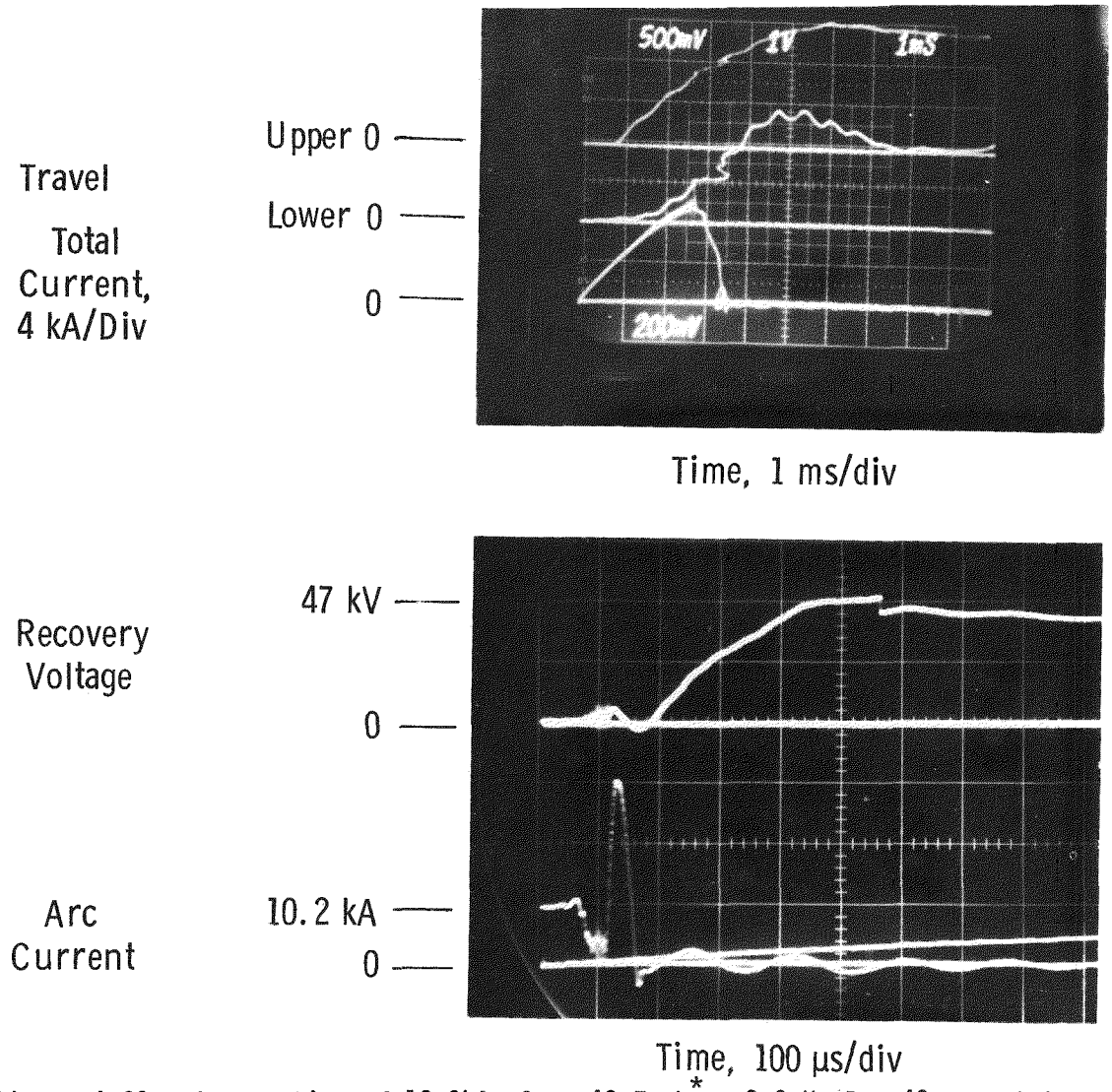

Figure 4-62. Commutation of 10.2kA; C_2 = 48µF, L^* = 2.2µH, R - 40Ω, prototype #12, electrode separation of 14mm, separation current, 3.8kA

improvement in the condition of Prototype #12. It should be noted that the multiple zero voltage sweeps in Fig. 4-63 are the result of a malfunction of the back-up breaker. This resulted in multiple oscilloscope triggers when the series devices reclosed following commutation.

Finally, a comparison of conditions 4 and 5 showed that the performance with 19mm of electrode separation was superior to that at 14mm. This indicates that greater current commutating ability should be observed at larger electrode separation provided the arc voltage remains low.

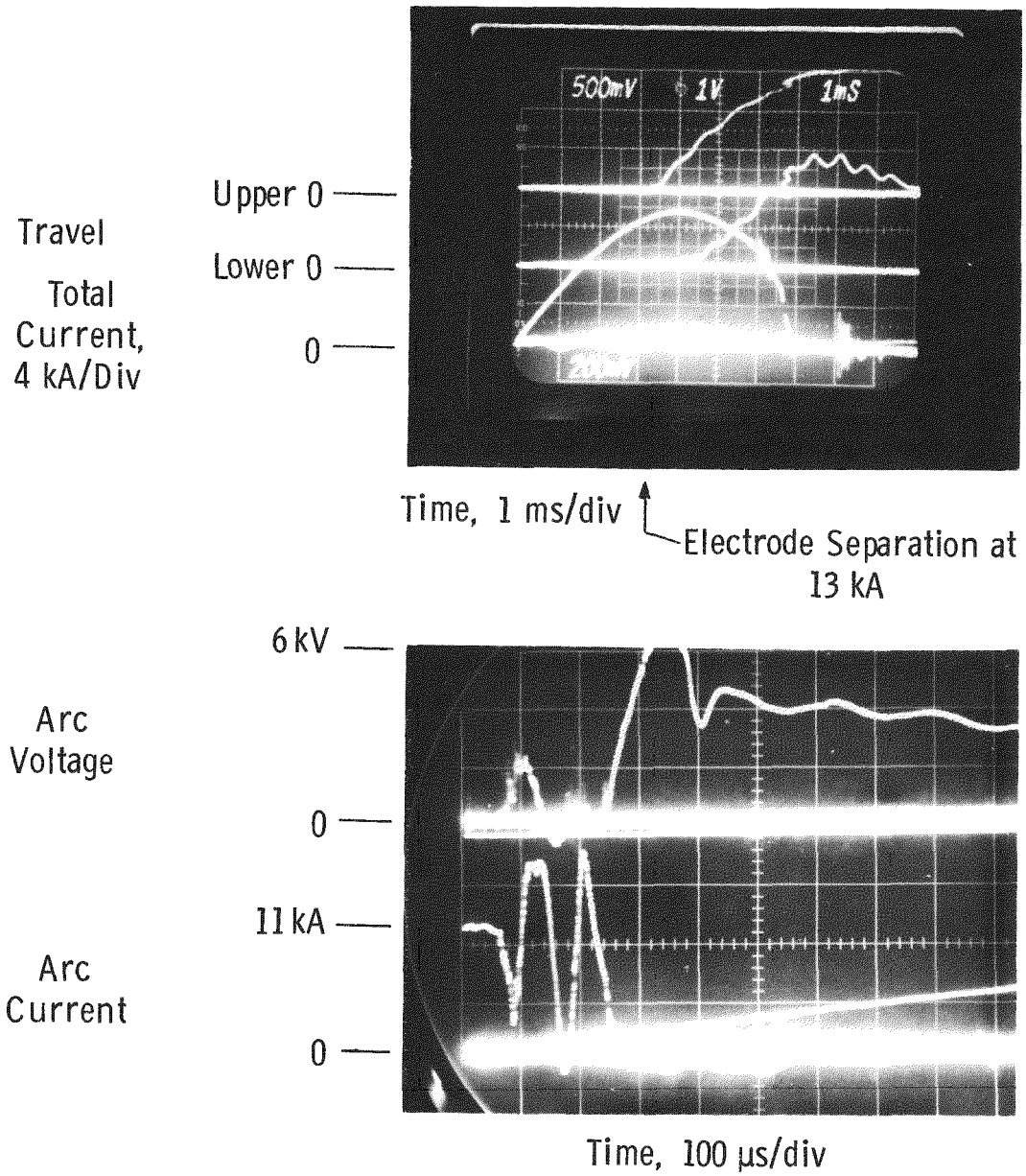

Fig. 4-63. Commutation of 11kA with a recovery voltage of 50kV; C_2 = 48µF, L^* = 2.2µH, R = 40Ω, prototype #12, electrode spearation of 19mm, separation current, 13kA

4-9.6 Conclusions

- Even with a vacuum device of questionable vacuum integrity we were able to commutate a high current of 10.4kA with a record high recovery voltage of 51kV. Further, we commutated 11kA against a recovery voltage of 48kV. We considered that the series connected vacuum device improved the ability to withstand the recovery voltage.

- We operated the actuator 11 times at maximum acceleration to move 3.7kg of electrode plus stem through 10cm (20cm total separation of two electrodes) in 2.2ms (2.8ms including dead time). A reduced level of acceleration permitted reliable operation without incident.

- The high speed welded bellows, with a larger inside diameter and greater lateral stiffness, were effective in preventing contact between the bellows and electrode stem during more than 60 experiments.

- With magnetic field application at a time of 2.8ms following contact part, the cup electrodes retained a high level of commutation performance (11kA) even when the electrodes were separated at currents as high as 13kA. By contrast, the Bruce profile electrodes of Prototype #8 were limited to 6kA when the field was applied at a time of 1.5ms following contact part at a current level of 6kA. It seemed possible that cup electrodes were associated with a more rapid transition to a diffuse arc from a columnar arc, and this could explain the better results with Prototype #12.

4-10 HIGH SPEED SEPARATION; HIGH VOLTAGE CIRCUITS

4-10.1 Introduction

In the previous experiments in Phase 2, systematic changes were incorporated into each new CLD prototype to move toward higher commutation currents. Likewise, systematic changes were made to provide the optimum oscillating magnetic field and to improve the external circuit such that recovery voltages typical of a 72kV device could be used. Finally, the contact separation speed needed for a practical CLD was gradually approached. In the final two prototypes, #13 and #14, these features were combined into the two best candidates which were then tested under conditions approximating a 72kV circuit.

Features of Prototype #13. A schematic of prototype #13 is shown in Fig. 4-64. It has a 30.5cm diameter envelope and two 15cm diam. stationary Bruce profile electrodes, Item 1. These two electrodes are separated by a gap of 20mm which is not adjustable. These electrodes are mounted on cylinders, Item 3, attached to the end plates. Two 5cm diam. movable bridging electrodes, Item 2, move through the stationary electrodes. The design is somehwat similar to Prototype #8 which was equipped with one stationary Bruce profile electrode and one 5cm diam. movable bridging electrode.

A second feature of Prototype #13 was the first use of small diameter stainless steel electrode stems. These stems were 1.6cm in diameter and were lighter than the 3.2cm diam. copper stems used in Prototype #8. The stem diameter and material changes provided a 52% reduction of the moving mass.

Features of Prototype #14. Prototype #14 also had a 30.5cm diam. ceramic envelope. The design was similar to Prototype #12, as shown schematically in Fig. 4-53. However, the two movable 15cm diam. cup contacts had less mass and the electrode stems were made of stainless steel. By comparison with Prototype #12, the mass that had to be moved was reduced by 40%.

4-10.2 Experimental Objectives and Approach

The experimental objectives for these two prototypes were basically the same; to achieve high speed electrode separation, and to find the limits of current commutation with the recovery voltage rising to $\sim$ 50kV. For Prototype #13, the goal for the reduced mass bridging electrodes was an electrode separation of 20mm in approximately 1.1msec (plus dead time) by means of dual actuation. This compares

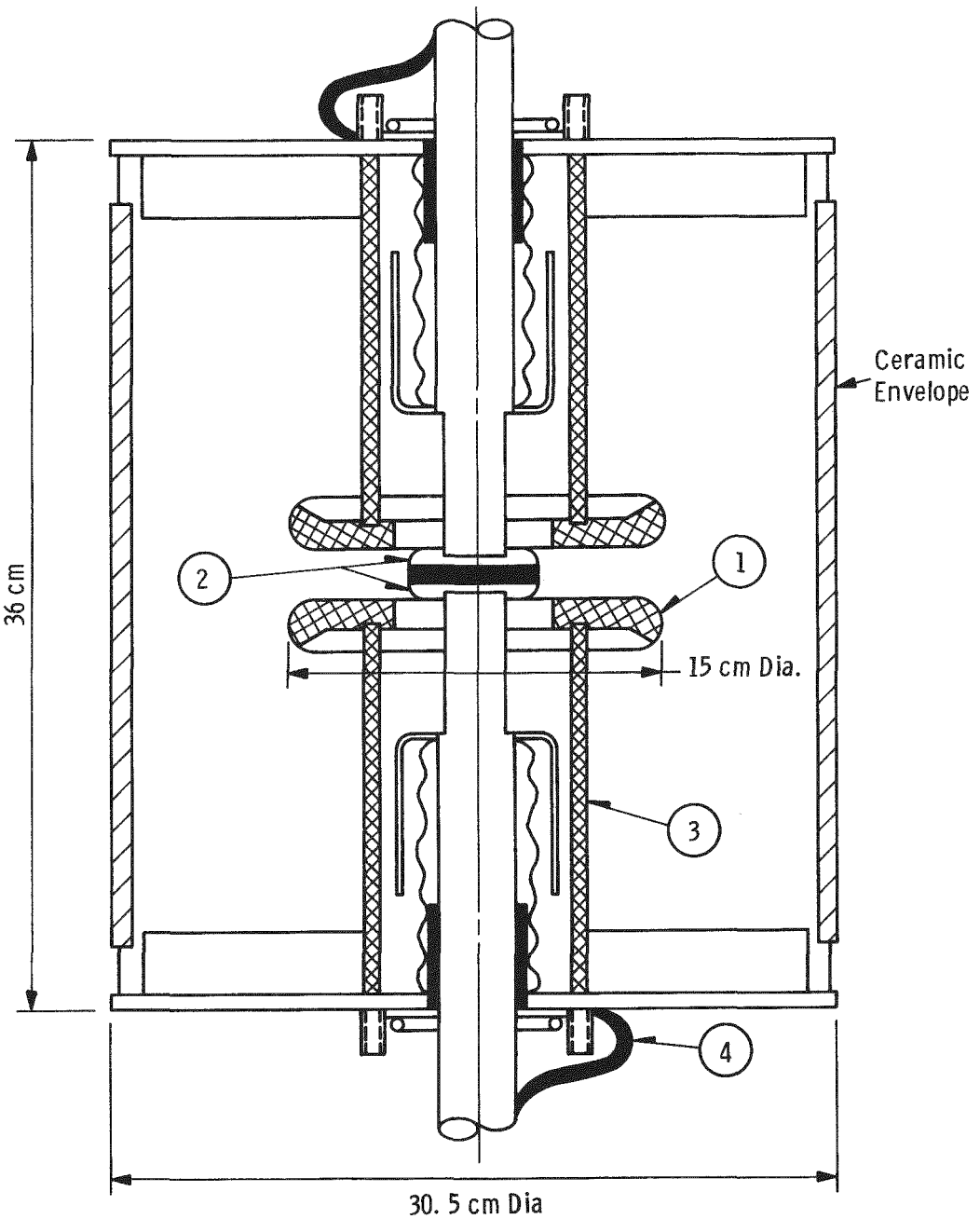

Figure 4-64. Schematic of Prototype #13 with two movable bridging electrodes

with 19mm in 1.5msec for Prototype #8 using dual actuation (see Fig. 4-56). For Prototype #14, the goal for the reduced mass cup electrodes was 20mm in 1.8msec (plus dead time) by means of dual actuation. This compares with 20mm in 2.2msec for Prototype #12 where damage to the actuators occurred after eleven operations.

The experimental approach is shown in the schematic of Fig. 4-54 and is identical to the setup described in Section 4-8.1. Details of how the circuit was tightly coupled to the remote H.V. capacitor are shown in Fig. 4-55. Again a series-connected standard vacuum interrupter was used to improve the recovery voltage withstand capability.

A further objective of these experiments was to compare the current limiting ability of these two different configurations both on a rising current wave at a comparatively low separation current and at high separation currents. This comparison is more meaningful when the contact separation time is appreciably less than a quarter cycle of the 60Hz wave. Finally, the overall performance of these two prototypes was to be compared to previously tested prototypes.

4-10.3 Experimental Results and Discussion

Before these two prototypes were tested for current commutation ability, each was given a 60Hz voltage withstand test. Prototype #13 withstood 75kV (rms) for 5 minutes with no "spits" and no measurable current flow. On the other hand Prototype #14 drew a current of 4.5 milliamps at 75kV (rms). After several minutes, with no change in this current flow, the test was stopped. One side of the ceramic envelope from end flange to end flange was too hot to touch. Evidently, electrical leakage on the inside of the ceramic was the cause of the heating. Thus Prototype #14 was of questionable integrity before the power testing began.

A summary of the power tests is given in Table 4-9. Sample data are presented in Figures 4-65, for Prototype #13. Referring to Table 4-9, the highest current commutated with #13 at an opening speed of 20mm in 1.4msec was 8kA. This was not a limit of the CLD but of the actuators. At the reduced speed of 20mm in 1.6 or 1.8msec, the current of 9kA (46kV recovery voltage) was a limit when the separation current was low (2.5kA) Likewise the current of 11kA (50kV recovery voltage) was a limit for the higher separation current of 7.6kA. In this latter case a type of resistor voltage grounding was used which may account for the somewhat better performance. More work would have to be done to prove this point.

TABLE 4-9

Highest Currents Commutated with High Speed
Separation and High Recovery Voltage

Prototype No.	Time on Rising Wave of Contact Separation msec	Separation Current kA	Opening Speed Gap/Time mm in msec	Commutated Current kA	Recovery Voltage kV
13	0.5	2.5	20 in 1.6	9.0	46
13	3.6	8.0	20 in 1.4	8.0	31
13	2.2	7.6	20 in 1.8	11.0	50
14	0.6	2.6	20 in 1.8	10.0	47
14	2.4	8.5	20 in 1.8	12.0	49

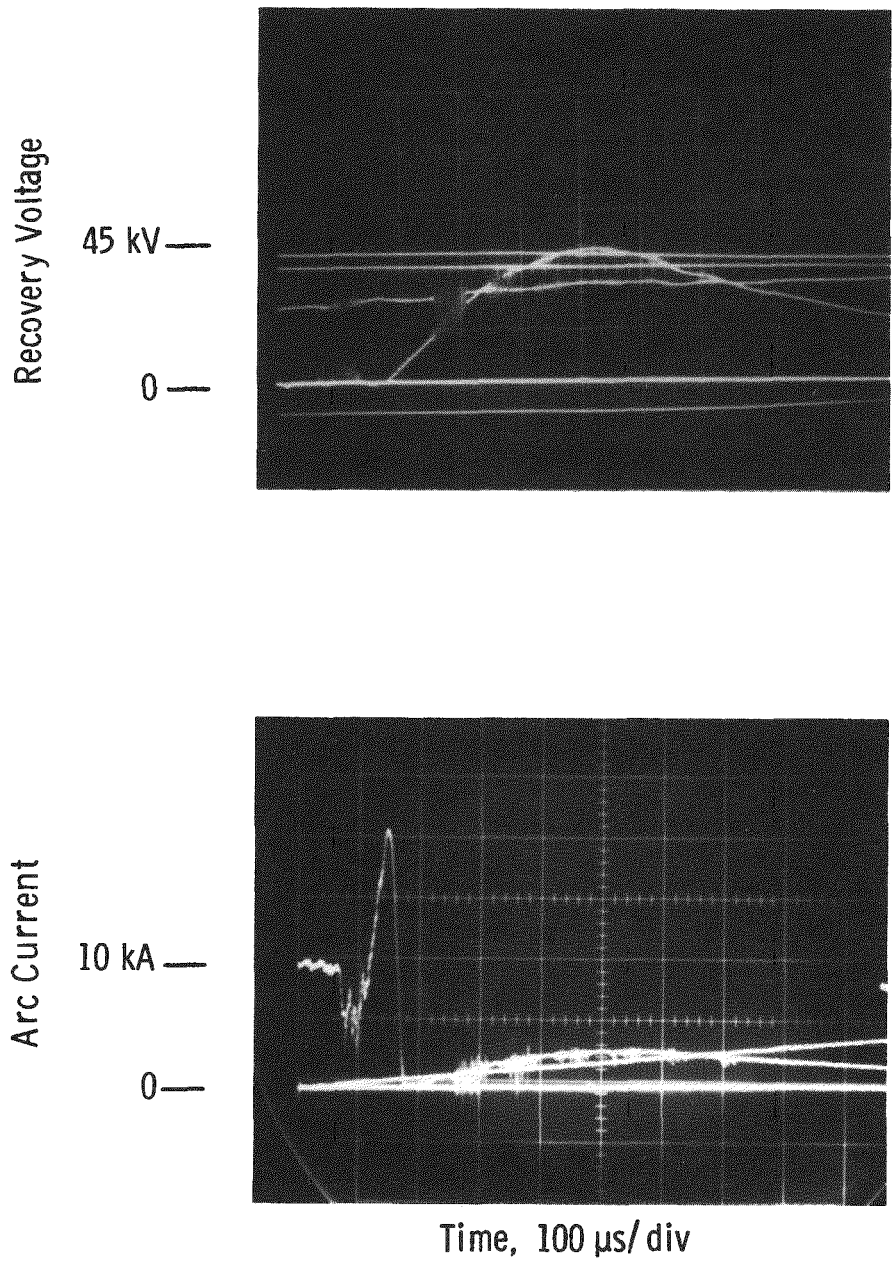

Figure 4-65. Recovery voltage and arc current for Prototype #13; 10kA was commutated after separation of the contacts at a current of 7kA and opening to a gap of 20mm in 1.8ms

Figures 4-66 and 4-67 present data for Prototype #14 when its contacts were opened at a high separation current while Fig. 4-68 shows typical results for low separation current. Referring to Table 4-9, the highest currents commutated under these two conditions are shown. At a separation current of 8.5kA, a current of 12.0kA was commutated (49kV recovery voltage) At the lower separation current of 2.6kA, a current of 10kA was commutated (47kV recovery voltage). This 10kA commutation may not be a true limit because Prototype #14 had suffered from a large current surge just prior to obtaining this data point. In fact the device became gassy and when tested with 400V dc across its opened electrodes, a glow discharge was observed.

4.10.4 Experimental Conclusions

At first sight, a direct comparison of the Prototypes can be made by noting from Table 4-9 that the test conditions of the 1st and 3rd rows for Prototype #13 are nearly the same as those in the 4th and 5th rows for Prototype #14. The voltage grading, referred to above, was also used in the test for Prototype #14 recorded in the 5th row. To the extent that conditions were the same, it would appear that Prototype #14 had a 10% higher capability than #13.

Some specific conclusions can be reached.

- Both prototypes seemed mechanically capable of opening at high speed. The limitation to a speed higher than 20mm in 1.4msec was set by the actuators.

- Contact separation at higher currents did not reduce the performance. This conclusion confirmed the results from Prototype #12 (see Sec. 4-9) and ruled out the tenative, contrary conclusion reached with Prototype #8 (see Sect. 4-8.2).

- The higher opening speeds used here did not reduce the performance but rather might have increased performance. For instance, Prototype #12 with cup contacts had a limit of 11kA (50kV recovery voltage) at a speed of 20mm in 2.4ms. In contrast, Prototype #14 with reduced mass cup contacts but otherwise of similar design, now showed a limit of 12kA (49kV recovery voltage) at a speed of 20mm in 1.8ms.

- Grading the voltage between the series connected vacuum interrupter and the CLD showed a definite improvement in the commutation capability. The reasons for this improvement are not clear at present, and the method needs to optimized. However, it is worth noting for future work.

- Finally, Prototype #14 (cup contacts) was shown to have internal wall leakage before testing and finally went gassy after only 17 test shots. We might well conclude that this type of CLD should be capable of higher currents. For example, 14.5kA was the limit for the cup contacts in Prototype 10 but with a low recovery voltage.

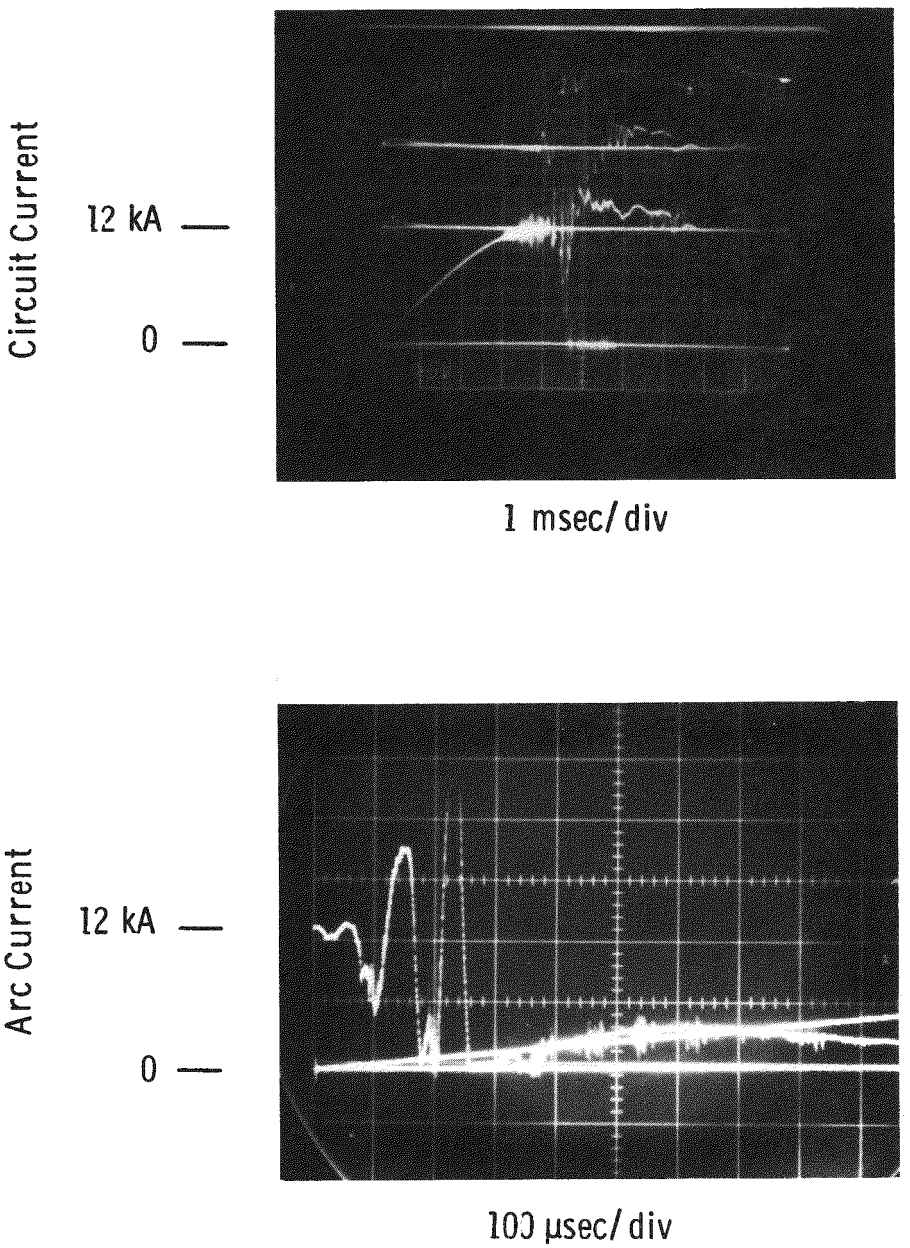

Figure 4-66. Circuit current and arc current in Prototype #14; 12kA was commutated after separation of the contacts at 8.5kA and opening to a gap of 20mm in 1.8ms

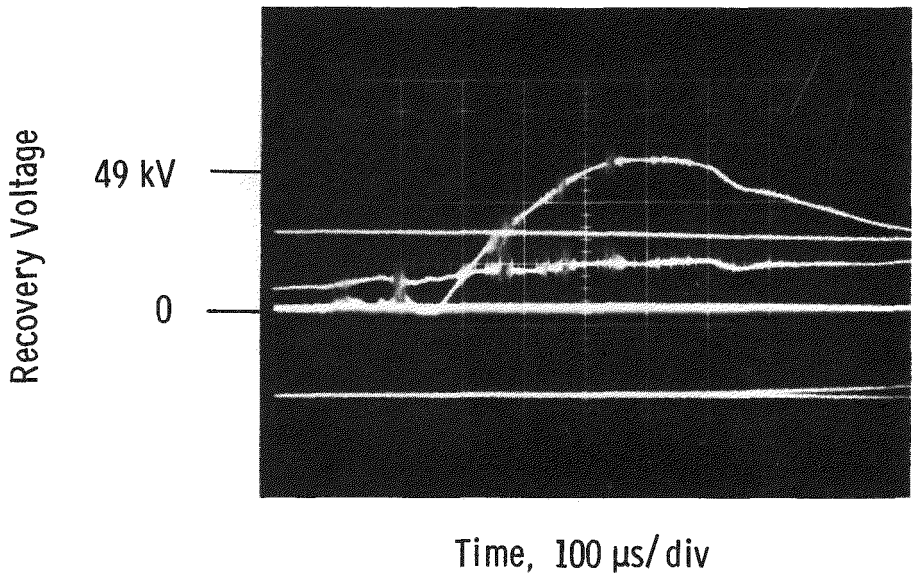

Figure 4-67. Recovery voltage following the commutation of 12kA using prototype #14 with 50µF of parallel capacitance. The initial slope is 2.4 x 10^8 V/s and the peak voltage of 49kV reached in 310µs

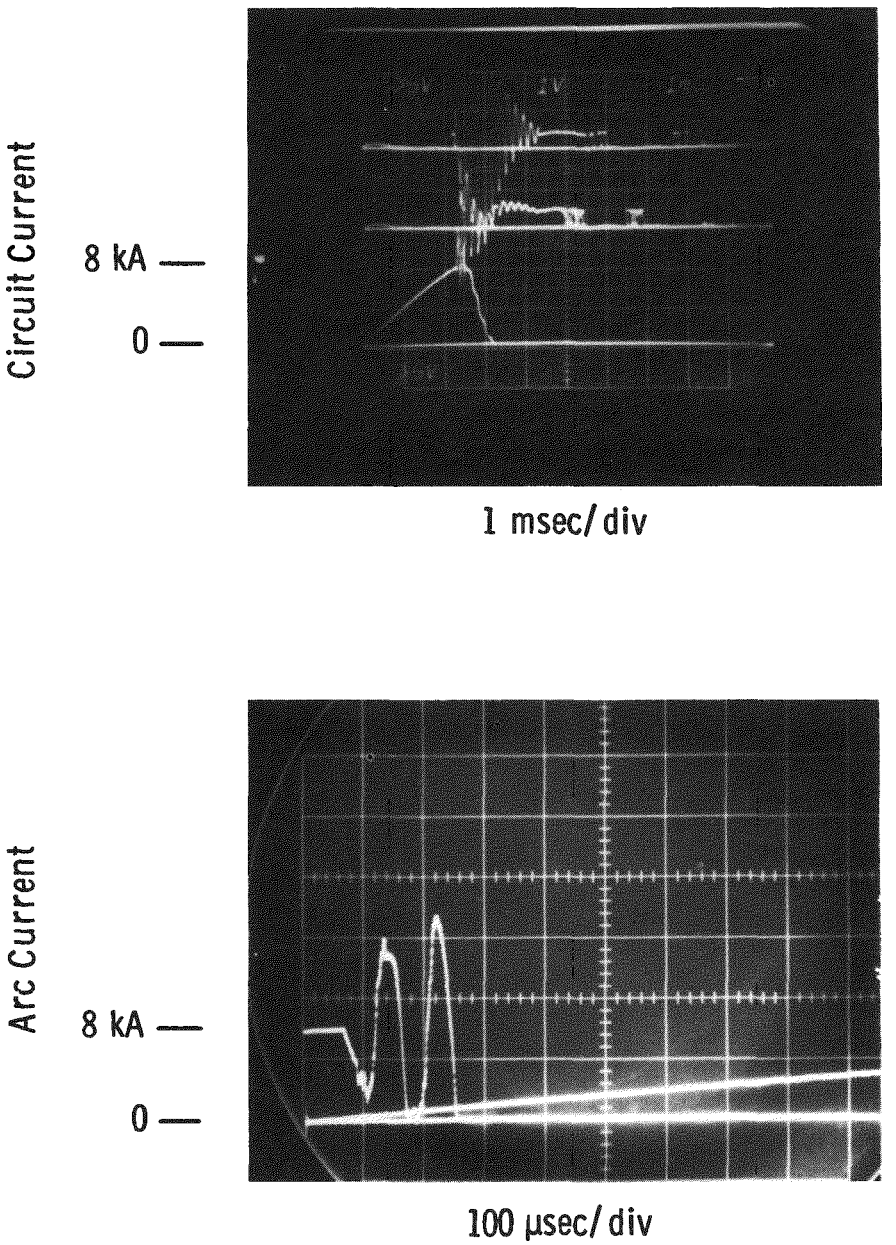

Figure 4-68. Circuit current and arc current in Prototype #14; 8kA was commutated after separation of the contacts at 3kA and opening to a gap of 20mm in 1.8msec.

Section 5

IMPLICATIONS OF EXPERIMENTAL DATA FOR A 72kV DEVICE

5-1 INTRODUCTION

From a review of the Experimental Results (Section 4) we can arrive at certain conclusions about the parameters (see Section 3.2) that were investigated. In particular we will discuss these parameters as they apply to a 72kV current limiting device. The parameters are not independent of one another. Thus the interaction between parameters has been considered in concluding the optimum characteristics of any one parameter.

5-2 DEVICE PARAMETERS

5-2.1 Electrode configuration - Our first choice is the 15cm diam. cup contacts that were used in Prototype #14. The second choice is low mass bridging contacts surrounded by disk or Bruce profile electrodes such as those used in Prototype #13.

As explained in Section 4-10.4, the cup contacts commutated the largest current (12kA) at a recovery voltage (49kV) representative of a 72kV circuit. Further, the cup contacts hold promise of yet higher commutation ability (also in Section 4-10.4). All three of the large cup Prototypes (namely #11, #12 and #14) suffered from various difficulties in manufacture (see Sections 4-8.1, 4-9.4 and 4-10.4) which were not related to the cup design. However, despite these problems, Prototype #14 showed the best overall performance. The test data from Prototypes #11, #12 and #14 are discussed in sections 4-8.2, 4-9 and 4-10. The cup electrode configuration is more massive than the bridging electrodes of our second choice Prototype #13 (section 4-10.1), and the use of the cup configuration in a practical circuit would depend on the availability of improved actuators. Even with Prototype #13 the opening time to 20mm was limited by the actuator design to 1.4ms, (see Section 4-10, Table 4-9).

5-2.2 Envelope - The envelope should be as large as possible. The largest practical choice at this time is 30.5cm. diam. ceramic. The device must be equipped with shielded bellows of a design suitable for high speed operation.

Experiments using these large 30.5cm diam. prototypes are discussed in sections 4-7 through 4-10. Care must be taken in the manufacture of these large volume devices to assure good outgassing and high surface resistance on the inside of the ceramic. The causes of less than perfect performance of three of the five large devices have been identified and are discussed in sections 4-8.2, 4-9 and 4-10.

5-2.3 Arcing Gap - A gap of 20mm at the time of transverse magnetic application gives the most consistent high current commutation.

The gap need not be larger than 20mm as the series connected vacuum interrupter will withstand most of the recovery voltage (see Fig. 4-63 of Section 4-9.5). A gap of 20mm was also shown theoretically (Section 2-2.2) and experimentally (Section 2-2.3) to lead to reasonable values of B_c and $\dot{B}$.

5-3 CIRCUIT PARAMETERS

5-3.1 Parallel Circuit - The capacitor of the parallel circuit should be $\sim 50\mu F$ for current commutation levels of 12 to 14kA. This capacitor must be tightly coupled such that the stray inductance is minimized.

The importance of reducing the stray inductance of the parallel circuit is discussed in sections 4-7.1 and in Appendix D-1.3. We accomplished a reduction in inductance by the use of many parallel coaxial cables as discussed in Sections 4-7.3 and 4-8.1. The reduction of stray inductance was sufficient to raise the resonant frequency of the parallel circuit to 15kHz even though the high voltage capacitor was some 6 meters removed from the current limiting device.

5-3.2 Transverse Magnetic Field - An oscillating magnetic field is needed for high current commutation. Its natural frequency f_1 should be less than or equal to half of the frequency of the parallel circuit, f_2. The value of $\dot{B}$ should be about 8000 T/s. The magnetic field should be provided by two coils, one on either side of the current limiting device. These field coils should be connected electrically in parallel both to minimize the inductance and to ensure that the currents in each coil are in phase. Only enough capacitance should be used to maintain the desired ringing frequency, f_1, less than or equal to half f_2.

The need for an oscillating transverse magnetic field is discussed in Sections 4-3.2, 4-4 and 4-7. Additional information appears in Appendix B which shows a growing oscillation of current until a current zero occurs and commutation is

actuated. The need for f_1 to be less than or equal to half f_2 is discussed in Section 4-7.1. An analysis of the effect of the ratio of f_1 to f_2 could be performed using the empirical model of the arc voltage discussed in Appendix C. An optimum value for $\dot{B}$ of 8000 T/s is indicated by Fig. 4-20 of Section 4-3.1. As discussed in Section 3-1.3, we used two turn magnetic field coils having a mean diameter of 38cm. separated by a distance of 36cm. to accomodate the insulation between the coils and the 30.5cm diam. device.

5-3.3 Series Vacuum Interrupter - The addition of a series connected vacuum interrupter is a necessity for providing the high voltage withstand during the recovery voltage period.

The performance improvement associated with using a series connected standard vacuum interrupter to provide the high voltage withstand is discussed in Section 4-7.1. The experiments with prototypes #13 and #14 discussed in Section 4-10 indicate that increased performance was obtained by an elementary form of voltage grading.

5-4 OPERATIONAL PARAMETERS

5-4.1 Actuators - The electrodes must be separated to 20mm in 1.5ms including dead time.

The required times for the sensor and the actuator are discussed in Section 6. A total actuation time of 1.5ms is assumed in that Section, but if this time were greater than 1.5ms, the fault current rating of the device would have to be reduced. Conversely, if this time were shortened, the rating could be increased. The time period of 1.5ms includes dead time which for our repulsion coil actuators is approximately 0.5ms. Hence the electrodes would have to be separated in 1.0ms. A discussion of the device design to accomodate the stresses required appears in Section 6-2.4.

We have used dual actuation to simulate the arc effects using the presently available repulsion coil actuators. Using dual actuation we have achieved an electrode separation of 20mm in 1.4ms as discussed in section 4-10. This separation time of 1.4ms simulates an actuator with a dead time of 0.1ms.

5-4.2 Separation Current - The current at the time of contact separation does not affect the subsequent commutation current level in the range of 12kA.

Experiments which showed a reduction of commutating ability when the opening of the electrodes of Prototype #8 was delayed and the separation current was increased are discussed in Section 4-6.1 and in Section 4-8.2.

However, the subsequent experiments discussed in Section 4-10 with Prototypes #13 and #14 confirm that the current at the time of contact separation does not affect the subsequent commutation current level. The commutated currents used in all these experiments were in the range of 9 to 12kA and the separation currents ranged up to 8.5kA.

Section 6

CONSIDERATIONS WHICH AFFECT RATING

6-1 INTRODUCTION

At Westinghouse, we have been simulating fault currents in the laboratory and commutating these fault currents into a parallel connected resistive circuit. During these experiments the vacuum device has been subjected to realistic recovery voltages of approximately 50kV with a rate of rise of recovery voltage of 2.5×10^8 V/s. The vacuum device is only part of a fault current limiter which includes a sensor, actuator, transverse field tube and series vacuum interrupter. In this part of the final report we will look at the individual components and in the last sections, 6-5 and 6-6, we will put the components together, making reasonable assumptions about their operations, and estimate a potential rating for the fault current limiting system.

Section 6-2 discusses actuator speed considerations. We compare what we have achieved in the laboratory during Phase I and Phase II of this project with what is required of an actuator in a practical system. We further discuss the limitations imposed by electrode acceleration on electrode stem design.

In Section 6-3 we discuss the sensor and actuator as a system. One sensor design is described in Reference (10). It uses both current magnitude, I, and rate of change of current, di/dt, to sense a fault. Once both limits have been exceeded the device waits for a period of time, called the discrimination time, before the actuator of the current limiting device (CLD) is triggered.

We have been simulating symmetric fault currents in the laboratory, and an example of a symmetric fault current as a function of time is shown in Figure 6-1. The numbers 1 and 2 which appear in the Figure will be described below in more detail. There has been concern that an asymmetric fault may be more difficult to limit because the sensor would give a trip signal too late. An example of an asymmetric fault is shown in Figure 6-2.

In section 6-4 we calculate the needed parallel resistance to limit the fault current and from this we determine the steady state voltage which will be applied to the 50μF capacitor bank. From this voltage we calculate the size and cost of this capacitor bank. A transient analysis shows that the peak voltage is not much greater than the steady state voltage. We continue in section 6-4 to compare the recovery voltage used in the laboratory with the voltage a vacuum device will be subjected to as a part of a fault current limiting system.

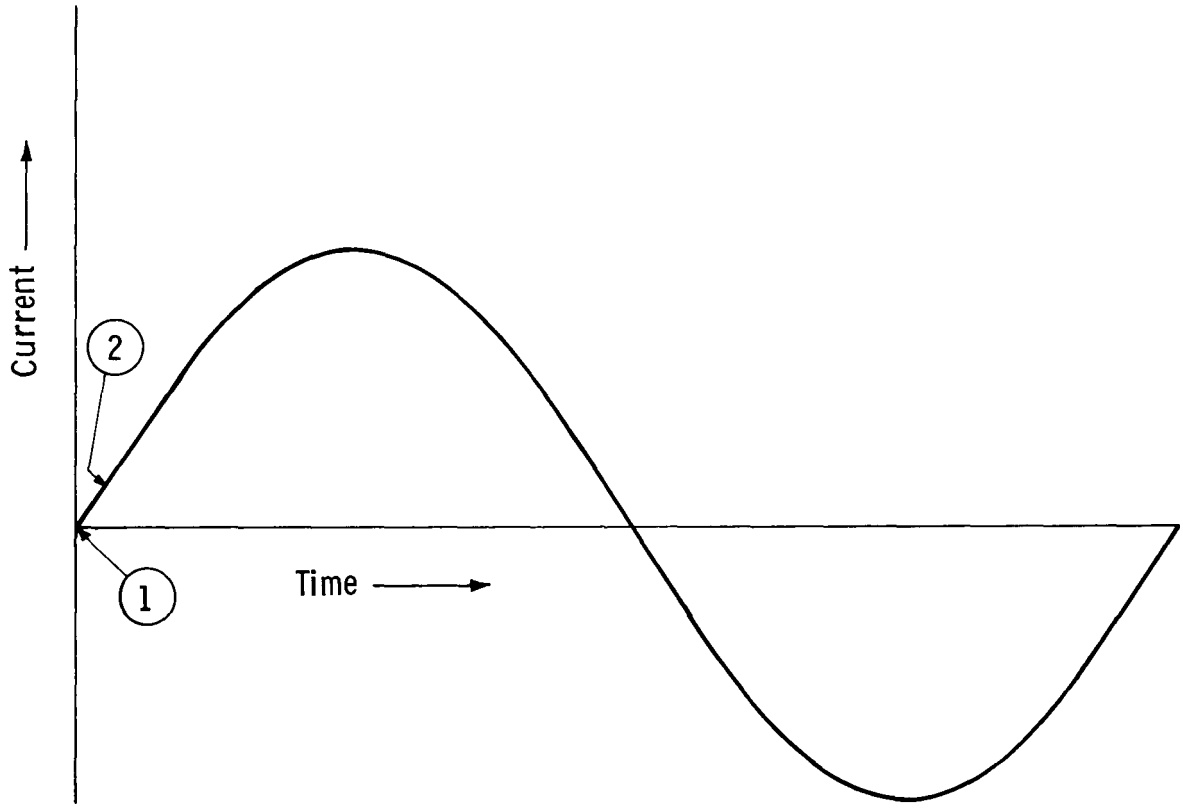

Figure 6-1. Symmetric fault current, $\alpha = 0$.

In Section 6-5 we consider a current limiting device application. In the first part of this section we make a preliminary investigation of the effect of sensor characteristics on prototype rating. In all cases we are considering that the magnetic field can force a current zero at current levels $\leq$ 14.5kA (the highest commutation current we have achieved to date). For the first calculations, Sub-section 6-5.3, we assume that the sensor is tripped for the dual conditions of I $\geq$ 3kA, in a system with an available symmetric fault capability of 15kA rms, and di/dt $\geq$ di/dt at the 3kA level in a 15kA rms symmetric fault. It is shown that this di/dt criterion is

inadequate. A second approach is considered in Sub-section 6-5.4 where we look at a practical circuit and determine an appropriate di/dt criterion. The current limiter is assumed to be located in a 72kV substation with two high voltage lines (e.g. 230kV) coming in and several 72kV lines leaving. Within the substation the current limiter is assumed to be located at the secondary terminals of one of the transformers and/or at the tie breaker location. In either location we consider the available symmetrical fault current is 15kA rms and the current must be limited to the equivalent of a 7.5kA rms symmetrical fault. Analysis of this circuit shows the need for a lower di/dt trip value, and the implications of this criterion relative to operation of the vacuum limiter in the system described above are discussed in Section 6-6.

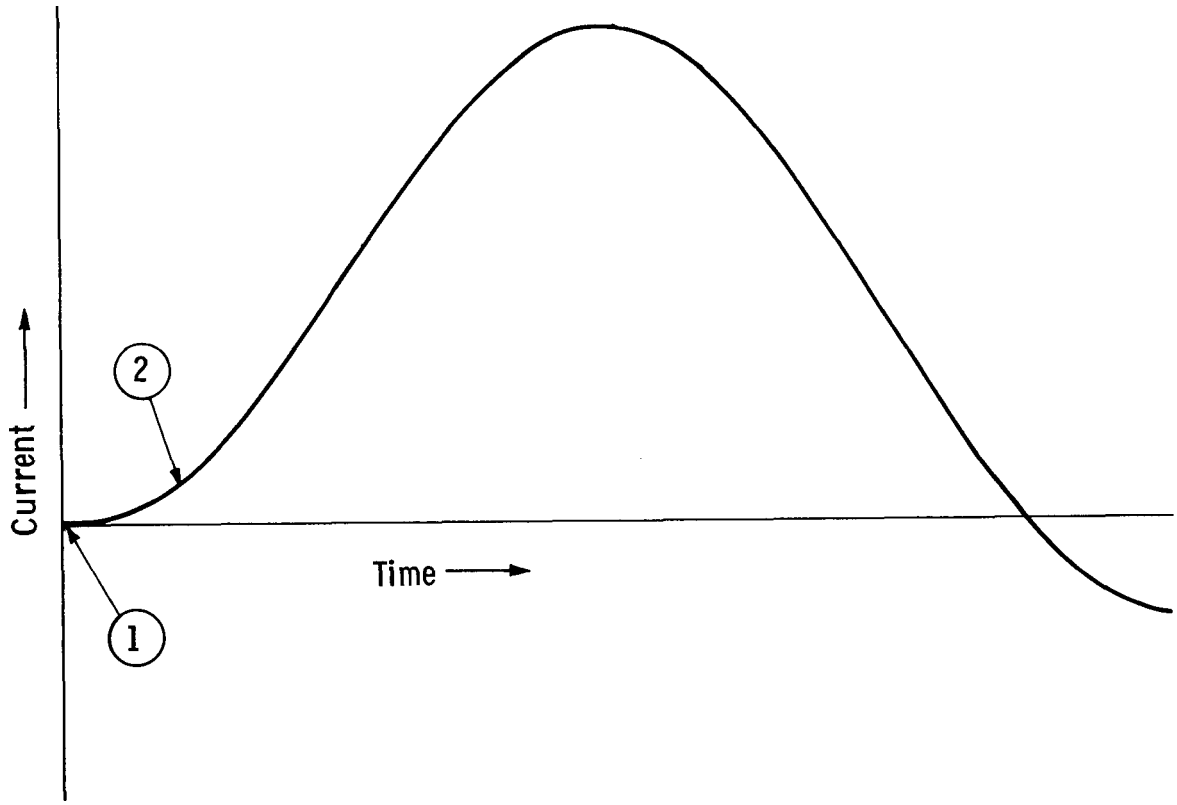

Figure 6-2. Fully asymmetric fault current, α = 1.

6-2 ACTUATOR SPEED CONSIDERATIONS

6-2.1 Introduction

In a practical current limiter the electrodes will have to be separated a distance of 20 to 30mm in 1.5ms or less. This requires a sophisticated actuator, and the

high accelerations also influence the design of the vacuum device. Westinghouse is not involved with the design of an ultra-high speed actuator. However, we have considered the potential stresses on the vacuum device, and the influence this will have on the stem designs. In Section 6-2.2 we give the Westinghouse background on high speed current limiter operation. A brief Summary of the actuator specifications requested by Westinghouse appears in Section 6-2.3 and this is followed in Section 6-2.4 by calculations of the stem diameter required to meet the actuator specifications. Section 6-2.5 discusses the levels of acceleration which have been encountered in previous Phase I and II experiments.

6-2.2 Background

In Appendix C of the Phase I final report (1) we discussed the need for parting the contacts of the vacuum device to a spacing of 30 mm in a time period of about one millisecond. As a realistic design goal we relaxed the requirement to 30 mm in 2.0 ms. The achievement in Phase I is outlined in Table 6-1. The actual device being operated was a standard vacuum interrupter with a metallic arc shield. The moving mass was only 2 kg, and no current was passing through the device at the time of the experiment. After each operation the actuator required minor maintenance such as re-attachment of the cushion pads which were positioned between the movable coil drive plate and the three shock absorbers. We achieved a maximum velocity of 17 m/s. Further, the repulsion coil actuator was quite efficient with a conversion of stored electrical energy to mechanical (kinetic) energy at an efficiency of 16%.

Table 6-1

ACHIEVEMENT IN PHASE I
(ONE TIME ACTUATION)

Mass =	2 kg
Power Supply Energy =	1800 J
Maximum Velocity =	17 m/s
Kinetic Energy =	290 J
Efficiency =	16%
Achievement:	20 mm in 2.0 ms
	(including dead time)
	or
	20 mm in 1.5 ms
	(not including dead time)

Our high speed achievement during the first 18 months of Phase II is shown in Figure 6-3. There we moved 1.8 kg a distance of 20 mm in 2.1 ms. This represents a working level of stress on the Westinghouse repulsion coil actuator, and we were able to perform 38 experiments before the actuator needed repair. Later, during experiments with Prototype #13 with stainless steel stems and 52% reduction of the moving mass, we achieved an electrode separation of 20 mm in 1.4 ms + 0.5 ms of dead time moving two electrodes. We were able to perform seven experiments before the actuator needed to be repaired.

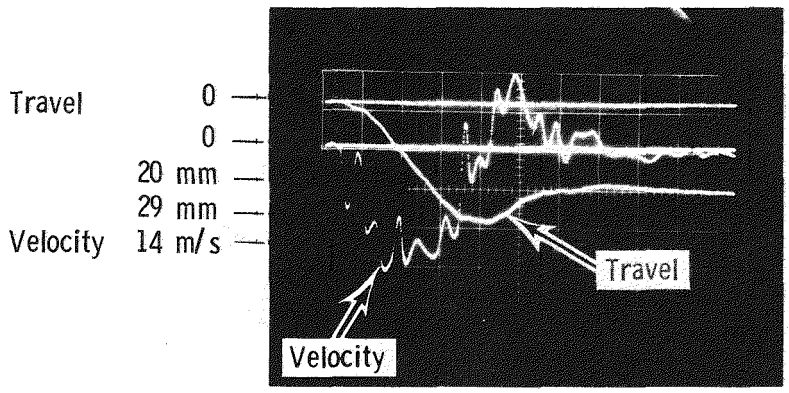

Figure 6-3. Typical travel and velocity oscillogram for the small electrode of Prototype #8. There was 20mm separation in 2.6ms (2.1ms + 0.5ms of dead time).

The minimum electrode separation time is limited, in part, by mechanical damage to the vacuum device. At high accelerations, the yield stress of the stem material will be approached, and this will lead to stem deformation. We will focus on this failure mechanism in Section 6-2.4. However, it should be noted that other failure mechanisms can occur. For example, the insulated coupling between actuator and stem has to survive the rapid acceleration. Further, the rate of change of acceleration (jerk rate) must be kept to a minimum to avoid undesirable oscillations in the moving and stationary parts. Finally, the electrode could separate from the stem.

6-2.3 Actuator Specifications

The Westinghouse Repulsion Coil Actuator has been described in the Phase I Final Report (1) and has been used for all our experiments with vacuum arc current commutation. This actuator is an efficient, reliable and moderate speed device. It could be redesigned and strengthened to increase its operating speed and reliability, but that is beyond the scope of the present project.

In order to obtain a high speed actuator for our use, the Electric Power Research Institute issued a Request For Proposal (RFP 564-2) in March, 1978. In the initial specifications, the actuator to be supplied was required to move a mass of 3.5 kg a distance of 30 mm in 1.5 ms or less. Further, it was required to move a smaller mass, 2.0 kg, a distance of 30 mm in 1.0 ms or less. Westinghouse responded with a solid propellant actuator design and Gould/ITE responded with a combination repulsion coil and high pressure piston design.

From the responses to the RFP, it was apparent that the requirements of 30mm in 1.5ms and 30mm in 1.0ms entailed extremely sophisticated actuator designs. Accordingly, we reduced the specification to 20mm/1.5ms and 20mm/1.0ms. Despite this reduction in specification, the actuator still proved too expensive to justify development at this stage in the project. In the next Section we will show that the attainment of electrode spacings of 20 to 30mm in times of 1 to 1.5ms places difficult, but not impossible, design requirements on the electrode stem.

6-2.4 Limitations Imposed by Electrode Acceleration on Electrode Stem Design

Table 6-2 illustrates the g values required to achieve a given separation in a given time. The required acceleration increases linearly with separation, but inversely as the square of the time period. Notice particularly the last two lines of Table 6-2 where the acceleration is more than doubled when the required time period is shortened from 1.5 to 1.0 ms.

We can calculate the maximum allowable acceleration by looking at the construction of the vacuum device. In practice, it is necessary to select three or four places along the electrode stem where the stem might fail. The stress is then calculated at each of the points relative to the mass to be moved and the cross sectional area. The maximum allowable stress σ_y, which can be developed in the OFHC copper stems is 7×10^7 N/m^2. The relation between stress and force is

$$F = \sigma_y A \qquad (6\text{-}1)$$

where A is the cross sectional area of the electrode stem at the expected point of failure. The relation between acceleration and force is

$$a = \frac{F}{M} \tag{6.2}$$

where M is the mass being accelerated by the force developed in the section where failure might occur.

The strength of the electrode stem can be increased by increasing the diameter. However, the allowable acceleration does not increase linearly with the cross sectional area because the mass to be moved increases as the stem diameter increases. The first column of Table 6-3 presents the results of calculations

Table 6-2

Acceleration Required as a Function of
Different Electrode Separation Requirements

$S = 1/2\ a\ t^2$ where S is the electrode separation, a is the uniform acceleration and t is the time.

S, mm	time, ms	minimum acceleration required, multiples of the acceleration of gravity, g's*
30	1.0	6100
30	2.0	1530
20	1.0	4100
20	1.5	1800

*Acceleration of gravity is 9.807 m/s^2

using an OFHC copper stem 24cm long moving an electrode mass of 2.6kg. For a design goal of 4000g's (20mm in 1.0ms) it will be noted from Table 6-3 that unreasonable stem diameters are required. However, a copper stem diameter of between 3.8 and 5cm would prove adequate for separating the contacts a distance of 20mm in 1.5ms.

Table 6-3

Calculation of Allowable Acceleration as
a Function of Stem Diameter

- Stress Considerations; Yield Strength of Fully Annealed OFHC Copper is 7×10^7 N/M^2

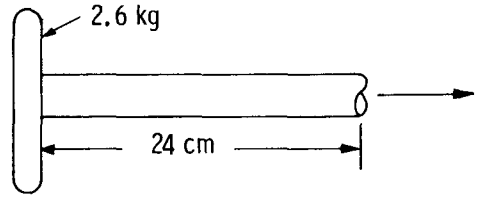

Stem Diameter	OFHC Copper	Copper, St. Steel Reinforced		All St. Steel Stem
		St. Steel Core Diameter		
1.9 cm	633 g	0.95 cm	1100 g	2600 g
2.5 cm *	980 g	1.3 cm	1700 g	4100 g
3.8 cm *	1600 g	1.9 cm	2800 g	6600 g
5.0 cm	2100 g	2.5 cm	3600 g	8700 g
25.4 cm	3200 g	12.7 cm	5600 g	13000 g

* Practical Stem Diameter

In the right hand column of Table 6-3 we have also listed the maximum accelerations which could be used with stainless steel stems. Here the allowable yield stress is 2.9×10^8 N/m^2. A stem diameter of 2.5cm would permit an acceleration of 4000 g's. In fact, a stainless steel construction would satisfy all of the acceleration requirements in Table 6-2. On the other hand, stainless steel has a high resistivity, and this stem would only prove suitable for experimental prototypes. Furthermore, at the high accelerations of 4000g, we would anticipate problems with both the coupler and the joint between the stainless stem and the electrode.

In order to combine the high yield stress of stainless steel with the high electrical conductivity of copper, it would be practical to reinforce a copper stem. The third column of Table 6-3 shows the diameter of the reinforcing rod, and the overall acceleration which can be withstood by the larger diameter copper rod with this reinforcement. For a copper rod diameter of 3.8cm, the maximum acceleration is 2800g and this would readily permit electrode separation to 20mm in 1.5ms.

6-2.5 Levels of Acceleration used in Previous Experiments

It is instructive to compare the levels of acceleration used in previous experiments with the calculated maximum allowable acceleration.

Prototype #10 used a Bruce profile electrode design which represents a moderate mass of 4.1kg. The calculated maximum acceleration of the movable electrode, using Eqs. 6-1 and 6-2, is 1200g's. In our experiments we used an average acceleration of 550g's over a period of 1.5ms. Consistent with calculation, this level of acceleration did not damage the device.

Prototype #8 used a low mass, 5cm diameter bridging electrode. The mass to be moved was 1.8kg and the calculated maximum acceleration is 2600g's. In our experiments we used an average acceleration of 1430g's for 1.0ms. Again we did not damage the device at this level of acceleration.

Finally, Prototype #9 used a cup electrode design. This design exhibits superior performance over the Bruce profile electrode for a given electrode and envelope diameter. Unfortunately, the cup electrodes are more massive. The movable electrode of Prototype #9 is 5.3kg and this extra mass reduced the maximum allowable acceleration to 930g's. The device was not damaged.

6-3 SENSING AND OPERATING TIME PERIODS

It is instructive to look at the time periods involved with the current limiter sensor and actuator system. Each time period is a critical part of the total time to act upon the increasing fault current. In order to develop a high speed limiter, there has to be a concerted effort to shorten each time period to arrive at a balanced and efficient final design.

The first time period involves the sensing of the fault. The present detector designs(10). use level of current, I, and the rate of change of current, di/dt, to detect the fault. Both set conditions must be exceeded before the discrimination time, the second time period is started. The purpose of the discrimination time is to prevent nuisance tripping. A switching surge may cause both I and di/dt to be exceeded without producing a real fault where the current limiting device should act. We assume a discrimination time of 0.2ms.

The third time period is the "dead time" which follows the trip signal from the sensor. This is the time associated with build up of current in the repulsion coils or, in pneumatic systems, the build up of pressure in the chamber. During this period the electrodes will be stationary.

The fourth time period is the time required to separate the contacts of the vacuum device. An excessive effort to shorten this time period will result in both an expensive actuator and an expensive vacuum device which has to be constructed to survive the high accelerations. These four time periods added together must be minimized or the fault current will have reached damaging levels before the device acts. Further, if the current is too large, the vacuum device may not commutate.

Reducing each time period represents a cost, and each period must be reduced to the minimum consistent with an optimized overall cost and reliability.

6-4 CIRCUIT RECOVERY VOLTAGE

6-4.1 Introduction

Most of the Phase II experiments have used parallel capacitance of 50μF and it is worthwhile to consider the size and cost of such a capacitor in a practical 72kV circuit. Let us consider two levels of fault current 20 and 24kA peak which are limited by a resistor to a value of 10 to 12kA. In order to simplify the calculation, we assume that the steady state voltage developed across the current limiting resistor R in Fig. 6-4 is the limited fault current, I_L, multiplied by R. Then the crest voltage V_C, across the capacitor is related to the three phase line to line circuit voltage, V_{LL}, the potential fault current, I_p, and limited fault current, I_L, by the following equation:

$$V_C = RI_L$$

where

$$R = V_{LL} \sqrt{\frac{2}{3}\left(\frac{1}{I_L^2} - \frac{1}{I_p^2}\right)}$$

where I_p is the crest value of the potential fault current and I_L is the crest value of the limited fault current. V_{LL} is the rms line to line voltage.

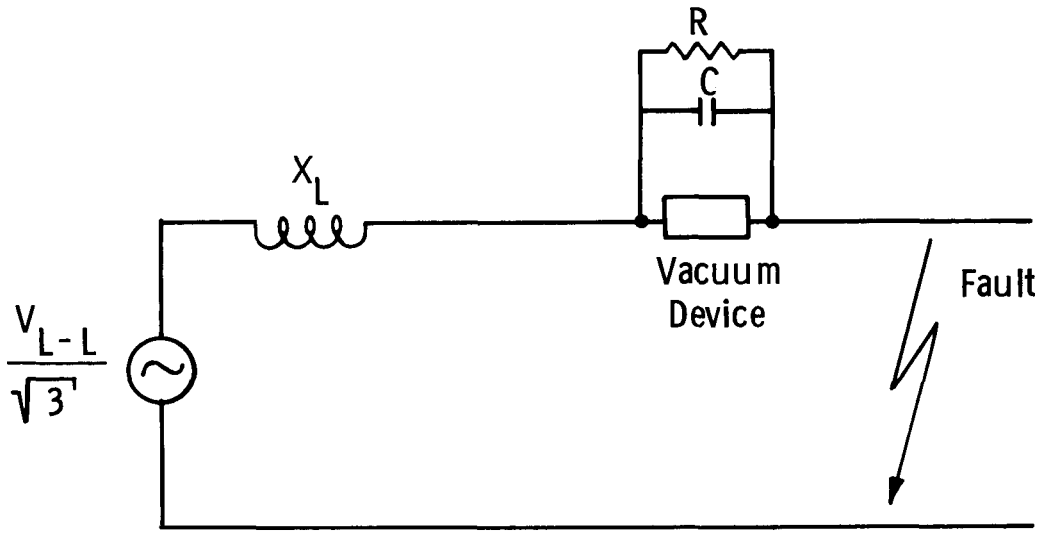

X_L ~ Equivalent Source and Line Reactance

R ~ Current Limiting Resistance

C ~ Current Limiter Capacitance

Figure 6-4. Basic current limiter circuit for recovery voltage analysis.

6-4.2 Steady State Analysis

The size and cost of the 50μF capacitor bank is a function of its voltage rating. We will assume that a 50kV over-voltage lasts for 30 cycles and that the duty cycle is 12 such over-voltages per year. According to N.E.M.A. specifications, the allowable over-voltage is then 2.4 times the crest value of the capacitor rated voltage. To provide a safety factor we will use only a factor of two. Thus, the capacitor rated voltage is

$$\frac{50kV}{2 \times \sqrt{2}} = 17.7kV \text{ (rms)}$$

For the required 50μF capacitance, 27 capacitors each having a value of 1.85μF with a 17.7kV voltage rating would be necessary. The size of each capacitor would be 15cm thick x 57cm high x 34cm deep plus the height of the bushing, and the cost of the capacitor bank per phase would be about $15,000.

The above calculations reinforce the need to reduce the magnitude of the parallel capacitance. In particular, the physical size of the three 50μF capacitor banks for a practical three phase limiter could prove a major obstacle to device application.

6-4.3 Transient Analysis

A transient analysis was made of a single phase simplified circuit shown in Fig. 6-5. The basic differential equation for the voltage in the circuit of Fig. 6-5 is

$$LC \frac{d^2V_c}{dt^2} + \frac{L}{R} \frac{dV_c}{dt} + V_c = e(t)$$

where $e(t) = E_m \cos(\omega t + \theta)$.

Assuming the potential fault current, (I_p), is symmetrical, θ is the electrical angle from current zero to the time where the fault current, (I_p), is limited by being commutated into the R C network. This angle θ is

$$\theta = \text{arc sine } (I_L/I_p)$$

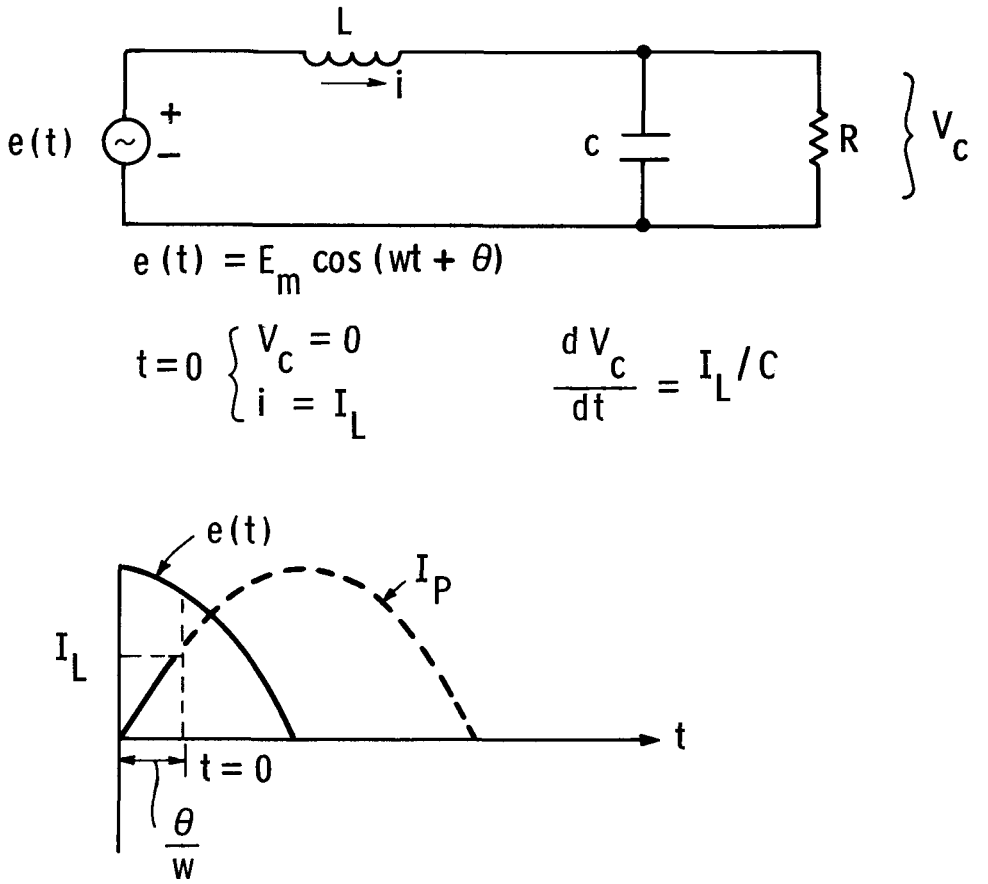

Fig. 6-5. Schematic of the equivalent circuit for analyzing voltage across the capacitor (C) - Resistor (R) network of current limiter. The figure shows (1) the initial conditions when current is commutated from the CLD to the R-C network, and (2) the relation of the potential fault current to the source voltage waveforms.

Using the initial conditions at instant of current commutation, (t = 0), where $V_c = 0$ and $\frac{dV_c}{dt} = \frac{I_L}{C}$, the solution to the differential equation was solved and the voltage, V_c, versus time was solved for four different cases. The transient voltage across the capacitor bank, V_c, as a function of time following the instant of current commutation is shown in Fig. 6-6.

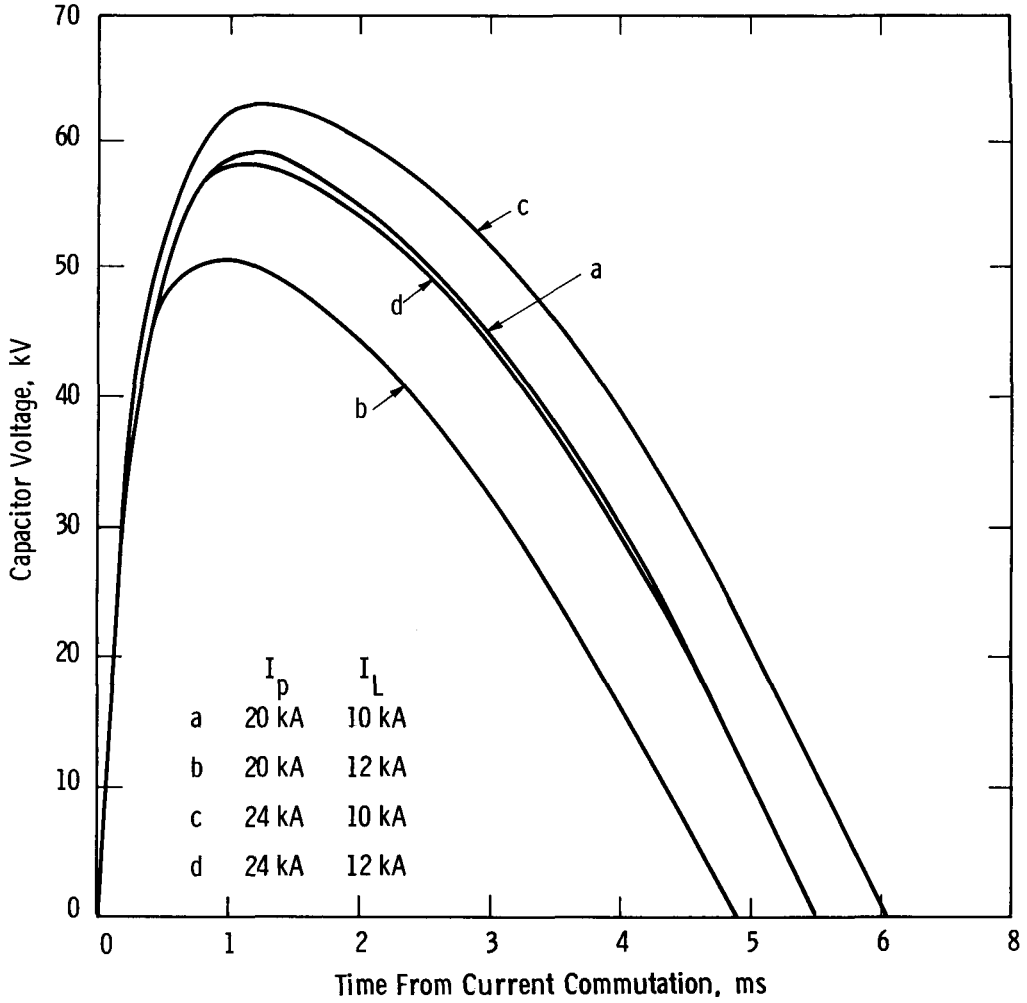

Fig. 6-6. The transient voltage waveforms which develop across the current limiter R-C network as a function of time from the instant of current commutation in the CLD. Waveforms are shown for different peak fault currents I_p and limited current, I_L.

The results of the peak transient voltage are given in Table 6-4.

Table 6-4

Peak Transient Voltage Across Capacitor Bank for 72kV Current Limiter

Potential Fault kA(pk)	Limited Fault kA(pk)	Current Limiting Resistance, ohm	Peak Transient Voltage kV	Peak a.c. Voltage kV
20	10	5.09	58.9	50.9
20	12	3.92	50.9	47.0
24	10	5.34	62.9	53.4
24	12	4.24	58.2	50.9

The worst case is the one in which a potential fault of 24kV(pk) is limited to 10kA. Here a transient voltage of 63kV can develop across the capacitor bank. Since this voltage is only 18% above the peak a.c. value and lasts for less than one millisecond, this overvoltage should not overstress the capacitor bank. Besides, according to the transient voltage analysis described in reference (1) on a 145kV current limiter, the effect of the system in which the current limiter is connected lowers the transient voltage. Therefore, it is expected that the transient voltage would also be lower than that shown in Table 6-4 because of the system effects.

A similar analysis was performed assuming the potential fault current is asymmetrical. The results show that the peak transient voltage is lower than for the symmetrical current case.

6-4.4 Recovery Voltage Comparisons

The needed recovery voltage impressed upon a vacuum device in a 72kV circuit appears in Fig. 6-6. We do not have a 72kV power circuit in our laboratory but we can simulate the recovery voltage. The recovery voltage appearing across prototype #14 when it commutated 12kA appears in Fig. 4-67. This recovery voltage should be compared with curve b of Fig. 6-6 and such a comparison appears in Table 6-5. Also shown in Table 6-5 for comparison is a 12kA commutation using prototype #12. This recovery voltage is shown in Fig. 4-44 of Section 4-6.2.

Referring to Table 6-5 we see that the current being commutated and the initial part of the recovery voltage curve for both the high voltage and low voltage experiments are identical to the calculated required recovery voltage. However the source voltage in a power circuit changes with time as a cosine function. Our experimental circuit has a low and steady voltage so we must compensate in the high voltage experiment by increasing the value of the parallel resistance to 27Ω. In the low voltage experiment we could use the appropriate parallel resistance because we limited the voltage to 11.5kV. Because of the small L and large parallel R in the H.V. experiments, we reached the peak voltage in 0.31ms rather than the desired 0.95ms. Hence the Westinghouse experiments may have been more severe than necessary. The time to peak for the low voltage experiment notes only the time at which the spark gap limited the voltage. As far as the peak magnitude, the Westinghouse 49kV is a good simulation of the desired 50.9kV.

Table 6-5

RECOVERY VOLTAGE COMPARISON

	Current Being Commutated, kA	Initital Rate of Rise, V/s	Source Voltage, kV	Parallel Resistance, Ω	Time to Peak, ms	Peak Magnitude, kV
Calculated, Curve b, Fig. 6-6	12	2.4×10^8	59 cos (wt + ϕ)	3.92	0.95	50.9
High Voltage Experiment with Prototype No. 14	12	2.4×10^8	0.4 and steady	27	0.31	49
Low Voltage Experiment with Prototype No. 12	12	2.4×10^8	0.0	3.33	0.059	Limited to 11.5kV

6-5 EXAMPLE OF A CLD APPLICATION

6-5.1 Introduction

In this section we look at a current limiting device application and we analyze the transient current which flows through a current limiting device. The underlying purpose is to bracket the limits on a possible rating for such a device. We look at different degrees of asymmetry to the fault current and we use realistic fault sensing and actuation times to determine the level of current which must be commutated by the vacuum device. These calculated currents will be compared with currents we have commutated in the laboratory.

We will first look at the equation for the fault current as a function of time and second we consider some fault sensing conditions. In subsections 6-5.4 through 6-5.6 we evaluate a practical circuit to determine a di/dt fault current sensing criterion when the fault current could be as high as 15kA rms symmetrical. Subsection 6-5.7 is a repeat of the analysis when the fault current is 10kA rms.

6-5.2 Background Equations

The equation for the fault current i as a function of the time, t, following the fault is given by Greenwood (11) as

$$i = \frac{V_m}{\sqrt{R^2 + (\omega L)^2}} \left[\sin\left(\omega t + \theta - \arctan\left(\frac{\omega L}{R}\right)\right) - \sin\left(\theta - \arctan\left(\frac{\omega L}{R}\right)\right) e^{\left(\frac{-R}{L} t\right)} \right] \qquad (6\text{-}3)$$

where V_m is the source voltage, R the source resistance, L the source inductance, ω is the circular frequency of the source and θ is the angle in the voltage cycle at which the fault occurs. We can simplify by substituting

$$\alpha = -\sin\left[\theta - \arctan\left(\frac{\omega L}{R}\right)\right]$$

$$I_m = \frac{V_m}{\sqrt{R^2 + (\omega L)^2}} \quad ,$$

and

$$\beta = \frac{R}{L}$$

into Eq. 6-3. Here I_m is the maximum current of a symmetric fault. After substitution we obtain

$$i = I_m \left[\sin (\omega t - \arcsin \alpha) + \alpha\, e^{-\beta t}\right] . \qquad (6\text{-}4)$$

Differentiating Eq. 6-4 with respect to time we obtain

$$\frac{di}{dt} = I_m \left[\omega \cos (\omega t - \arcsin \alpha) - \alpha\, \beta\, e^{-\beta t}\right] . \qquad (6\text{-}5)$$

When $\alpha = 0$ we have a symmetric fault current and when $\alpha = 1$ we have a fully offset asymmetric fault current, α can have any value between -1 and +1. Figure 6-1 is a plot of Eq. 6-4 when $\alpha = 0$ and Fig. 6-2 is a plot of this equation for $\alpha = 1$. $\frac{\omega L}{R}$ of the source is assumed to be 15.

6-5.3 Sensor Set at I = 3kA and di/dt (3kA)

Consider the situtation of having a fault of 15kA rms symmetric and just barely detecting this fault. By barely detecting we mean that the di/dt level is set to just detect and trip when the current level reaches 3kA. For example, if the fault occurs at point 1 in Fig. 6-1 (t = 0), the detection will occur at point 2. For a 15kA symmetrical fault

$$I_m = \sqrt{2}.15 \times 10^3 = 21.2\text{kA},$$

$$di/dt = 8 \times 10^6 \text{ A/s at point 1 (from Eq. 6-5)}$$

and

$$di/dt = 7.92 \times 10^6 \text{ A/s at point 2 when the current reaches 3000A } (\tfrac{\omega L}{R} = 15).$$

If we let 7.92×10^6 A/s be the trip level we can calculate if the trip signal occurs with a fully asymmetric fault ($\alpha = 1$). With any degree of asymmetry, $\alpha > 0$, there is a direct current component which decays with time:

$$i_{dc} = I_m\, \alpha\, e^{-\beta t}$$

from Eq. 6-4. Whenever i is greater than zero, by Eq. 6-5, the di/dt is reduced everywhere by

$$- I_m\, \alpha\, \beta\, e^{-\beta t} .$$

Hence the greatest slope when $\alpha = 1$ and $0 \leq t \leq 8ms$ is 7.52×10^{-6} A/s which occurs at t = 4.2ms after the fault. This greatest slope is less than the trip level of 7.92×10^{6} A/s. Thus we will never obtain a trip signal from our sensor, and the sensing condition is inadequate.

6-5.4 Evaluation of a Practical Circuit to determine a di/dt Criterion

The current limiter is considered to be located in a typical 72kV substation with two high voltage lines (e.g., 230kV) coming in and several 72kV distribution lines leaving. Within the substation the current limiter could be located either at the secondary terminals of one of the transformers or at a tie breaker location. Fig. 6-7 is a line diagram of a substation showing the positions in the system where the current limiter could be located. Position A is the transformer secondary terminals and position B is the bus tie breaker position.

We assume the maximum symmetrical available fault current, I_A, is 15kA rms for either position A or B. The available major loop peak current is

$$I_{PA} = 2.7^{*} I_A - 40.5kA$$

For the sake of our calculations we have assumed that the current must be limited to no more than one half of the available major loop peak current. Hence

$$I_L = \frac{40.5}{2} = 20.2kA \quad .$$

*Dodds (10) cites ANSI C37.06 which gives the factor 2.7

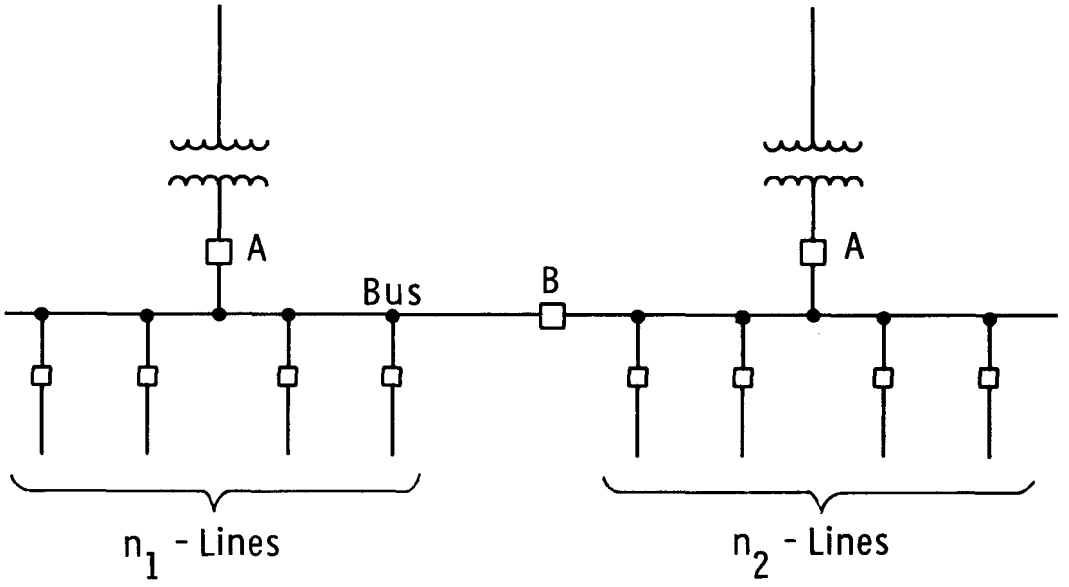

Figure 6-7. Typical substation where the Fault Current Limiter would be applied

[Location A - Transformer secondary position
Location B - Bus Tie position]

A comparison of the fault currents in question appears in Fig. 6-8. Curve 1 is a 15kA symmetric fault ($\alpha = 0$) and curve 2 is the corresponding asymmetric fault ($\alpha = 1$). Curve 3 is a 7.5kA symmetric fault ($\alpha = 1$). Any fault current has to be limited to values less than curve 4.

We can use the magnitude, I, and the slope of the current to detect the fault. The greatest slope, di/dt, when $\alpha = 1$ and the fault current is 7.5kA, can be calculated from Eq. (6-5):

$$(di/dt)_{max} = 3.76 \times 10^6 \text{ A/s.} \qquad (6\text{-}6)$$

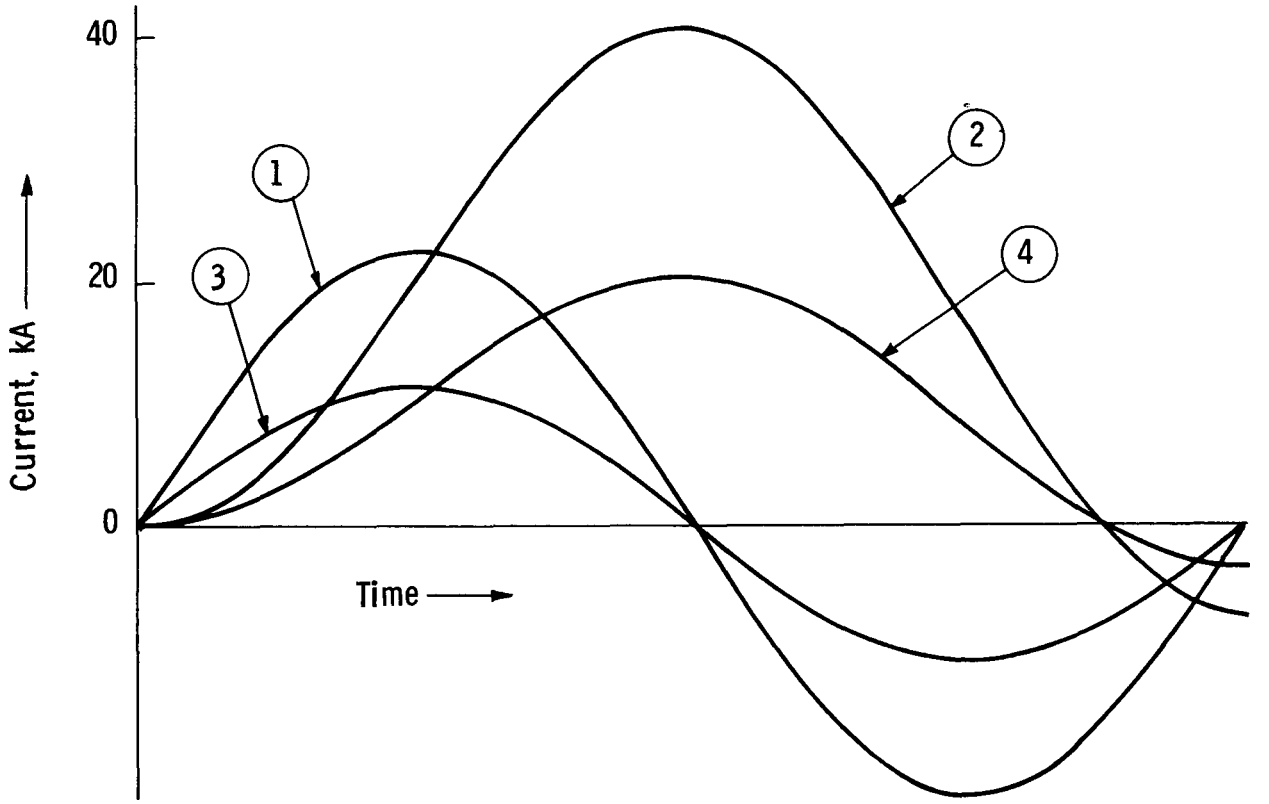

Figure 6-8. Comparison of 7.5 and 15kA$_{rms}$ symmetric and asymmetric fault currents

This maximum slope occurs approximately 4.2ms after the fault. This is the highest reasonable setting for the fault current sensor in order to be able to at least detect a potentially damaging fault ($I_{PA} \geq 20.2$kA). Other criteria could be used. For example, Dodds et al (10) suggest detecting a current that is 6 times the normal maximum continuous load current. The maximum continuous load current, I in such a system could be as high as 2.0kA. The maximum rate of change of this load current, di/dt, is

$$\frac{di}{dt} = 2\ \pi\ 60\ (2.0 \times 10^3) = 7.5 \times 10^5\ \text{A/s}. \qquad (6\text{-}7)$$

For this we could set our sensor to trip when di/dt exceeds 6 times the slope from Eq. (6-7)

$$(\frac{di}{dt}) = 6 \times 7.5 \times 10^5 = 4.5 \times 10^6\ \text{A/s}.$$

If we set the detector to 6x normal current we could have an undetected potentially damaging fault current. However, if we set the detector to 5x maximum continuous load current, still a reasonable setting, the two criteria coincide at the value calculated in equation 6-6.

6.5.5 Implications of a Sensor Set for I = 3kA and di/dt = 3.76×10^6 A/s

If we have our sensor set to trip at I = 3kA and di/dt = 3.76×10^6 A/s we can calculate what level of current the CLD must commutate for two cases of $\alpha = 0$ and $\alpha = 1$. The following discussion assumes that there is a maximum 15kA rms symmetric fault current available from the source. Referring to Fig. 6-1, for $\alpha = 0$ the fault occurs at point 1, t = 0, and the current reaches a level of 3kA at point 2, t = 0.377ms. The di/dt = 7.92×10^6 A/s at this point so we have an alarm and we start our discrimination time. After a pause of 0.2ms we find I > 3kA and di/dt > 3.76×10^6 so the sensor issues a trip signal to the actuator at 0.577ms. After an additional 1.5ms the electrodes have reached the desired separation, the magnetic field is applied and it reaches the critical value at t = 2.07ms after the occurrence of the fault. At this time the current has a value of 15kA, and is commutated into the parallel resistance.

For the case of $\alpha = 1$ we can refer to Fig. 6-2 where the fault is asymmetric. The fault occurs at point 1, t = 0, and the current reaches 3kA at t - 1.62ms, point 2. At this time the rate of change of current, di/dt is 4.1×10^6 A/s. Since both I and di/dt have exceeded the limit, we start the discrimination time. After 0.2ms the sensor issues a trip signal to the actuator and, after an additional 1.5ms (t = 1.62 + 0.2 + 1.5 = 3.32ms), we apply the magnetic field. At this instant the current is 12.9kA and it is commutated into the parallel resistance with resulting limitation.

A summary of all of the above data appears in Table 6-6 together with the case for $\alpha = 0.5$. For this case, a higher current must be commutated than for either the symmetric or the asymmetric fault.

We have demonstrated commutation of 14.5kA in the laboratory and it is instructive to see the time at which the current equals this value. This time appears in Table 6-6 and shows how small the combination of actuator and sensor times must be to permit the CLD to commutate before the fault current exceeds 14.5kA. Basically, the commutation level of our present 15kA rms device would have to be improved if the sensing criteria were unchanged, with the discrimination time remaining at 0.2ms

and electrode separation in 1.5ms. Alternatively, the potential device rating would have to be reduced from 72kV/15kA to about 72kV/12kA.

Table 6-6

Requirements for Commutation of 15kA Fault Current with a Detection Level of 3kA ($\omega L/R=15$)

$\frac{(\omega L)}{R} = 15$

α	t_2, for 3000A, ms	di/dt at t_2, A/s	Time of Commutation, ms	Current to be Commutated, kA	Time at which Current reaches 14.5kA, ms
0	0.38	7.9×10^6	2.08	15.0	2.0
0.5	0.43	7.2×10^6	2.13	15.9	1.943
1.0	1.62	4.1×10^6	3.32	12.9	3.55

6-5.6 Implications of a Sensor Set for I = 5kA and di/dt = 3.76×10^6 A/s

If we reduce the sensitivity of the fault current sensor to a current level of 5kA, the limiter would have to commutate higher currents in a 15kA rms circuit. The corresponding data for the 5kA trip level appear in Table 6-7. The currents which must be commutated range from 16.1 to 17.9kA. These currents are beyond those so far demonstrated in the laboratory with 50μF of parallel capacitance.

Table 6-7

Requirements for Commutation of 15kA Fault Current with a Detection Level of 5kA($\omega L/R=15$)

α	Time, t_2, after current zero for start of discrimination period, ms	di/dt at t_2, A/S	Time after current zero for field application and commutation, ms	Current to be commutated, kA	Time at which current reaches 14.5kA, ms
0.	0.63	7.8×10^6	2.33	16.3	2.00
0.5	0.70	7.5×10^6	2.40	17.9	1.94
1.0	2.06	5.1×10^6	3.76	16.1	3.55

In order to use this detection scheme, it would be necessary to increase the amount of parallel capacitance from 50μF to perhaps 100μF. Alternatively, the sensor discrimination time and actuator opening time would both have to be reduced.

6-5.7 Implications of a Sensor Set for I = 3kA or 5kA and di/dt = 3.76 x 10^6 A/s in a Circuit with a Maximum Fault Current Level of 10kA rms Symmetrical

It is instructive to apply the same di/dt criterion (3.76 x 10^6 A/s) with sensor fault levels of 3kA and 5kA in a circuit with a lower potential fault of 10kA rms symmetrical. As would be expected, the current levels attained at reasonable times following fault current detection are lower than observed in Sections 6-5.5 and 6-5.6 and the calculated data appear in Table 6-8.

Table 6-8

Requirements for Commutation of 10kA Fault with Detection Levels set at 3 and 5kA

Detection Level, kA	α	Start of discrimination period t_2, ms	di/dt at t_2, A/s	Time of Commutation, ms	Current to be commutated, kA	Time at which current would reach 14.5kA, ms, if the FCL was not activated
3	0	0.57	5.2 x 10^6	2.27	10.7	--*
3	1.0	2.32**	3.8 x 10^{6**}	4.02	12.0***	4.52
5	0	0.96	5.0 x 10^6	2.66	11.9	--*
5	1.0	2.51	4.0 x 10^6	4.21	13.0	4.52

* The current never reaches 14.5kA (10kA x $\sqrt{2}$ = 14.14kA)
** The discrimination period does not start until di/dt exceeds 3.8 x 10^6 A/s
*** This would have been 10.2kA if we used I only to sense the fault

6-6. IMPLICATIONS FOR A PRACTICAL CURRENT LIMITING DEVICE

In order to associate a prototype current limiter with a particular rating it is necessary to know (a) the maximum current which can be reliably commutated from the device (limiter characteristics) (b) the time for the actuator to separate the contacts (actuator characteristics) (c) the time for the sensor to detect the fault plus the sensor discrimination time (sensor characteristics). Further, it is necessary to understand the overall circuit and the level of protection required (circuit characteristics).

The present study is preliminary in nature, but serves to indicate some of the important time considerations. For example, it is inadequate to specify that a sensor should be triggered at a given current level in symmetric fault, and that the sensor should trigger at this same di/dt level for an asymmetric fault. Further, for a given sensing level and di/dt, the fully asymmetric wave may not require the highest commutation level. A fault with $\alpha = 0.5$ may be more exacting.

The present prototype would prove adequate for operation in a system with a 10kA rms maximum available symmetrical fault current, with an electrode separation time of 1.5ms and a sensor set to trigger at a 3kA level ($di/dt > 3.8 \times 10^6$ A/s). However, the prototype would be unable to handle a 15kA r.m.s. fault under these same conditions. In fact, for the particular circuit studies, the potential rating would be between 72kV/10kA and 72kV/15kA.

Section 7

CONCLUSIONS

We have developed a current limiting device in which the continuous current is carried by closed "in line" electrodes. When a fault is detected, we have shown that it is feasible to separate the electrodes a distance of 2cm in 1.4ms, and subsequently commutate the current into a parallel current limiting resistor via the application of a high frequency transverse magnetic field. With a conventional vacuum interrupter connected in series with the current limiting device, and with a 50μF parallel capacitor, we have shown that it is possible to commutate currents of 12kA into the parallel resistor against recovery voltages of 50kV. Currents of 14.5kA were commutated at lower circuit voltages.

The major conclusions relative to high current, high voltage commutation performance are:

- use large diameter electrodes within large diameter (30.5cm) ceramic electrodes.
- use cup type electrode configurations or plain disk electrodes equipped with a light bridging electrode.
- use a series connected vacuum interrupter to withstand the recovery voltage following commutation into the parallel circuit.
- minimize the inductance associated with the leads to the parallel circuit.
- use a high frequency high amplitude oscillating magnetic field
- it is feasible to design vacuum devices with stems and bellows capable of the rapid accelerations associated with electrode spacings of 2cm in 1.5ms
- the sensor should detect both di/dt and current level before tripping the actuator. Further, the discrimination time should be minimized.

In determining a rating for the present device, we have considered a fault current limiter applied at either a transformer secondary terminal or in a tie breaker position. We have assumed that the sensor is set to trigger at a 3kA level and $di/dt > 3.8 \times 10^6$ A/s, that the sensor has a discrimination time of 0.2ms, and that the actuator subsequently opens the electrodes to 2cm in 1.5ms. We conclude that in a 72kV circuit with an available fault of 10kA r.m.s., application of the present system would reduce the peak fault current by half. With a slightly

reduced discrimination time and/or actuation time, the limiter would produce the same proportionate effect in a 72kV circuit with an available fault current of 15kA r.m.s.

Section 8

RECOMMENDATIONS FOR FUTURE WORK AT 145kV

We have developed a vacuum current limiting system comprising a transverse field device, a series conventional vacuum interrupter, and a parallel capacitor and resistor network. This system is shown in Figure 1-1. We have established that the system is capable of commutating fault currents of 12kA instantaneous in simulated 72kV circuits. In Section 6 we have shown that this fault current limiter could be applied at either a transformer secondary terminal or in a tie breaker position to limit faults in circuits with r.m.s. values of 72kV/10kA to 72kV/15kA.

We consider that the fault current commutation limit, and reliability, could both be improved by additional experimental and theoretical investigations. A further goal would be reduction in the magnitude of the parallel capacitance. We further consider that the system shown in Figure 1-1 should be evaluated as a module for a 145kV device, with two of the modules connected in series for 145kV operation.

Our specific recommendations for future work on this vacuum-arc current limiter concept involve three parallel efforts.

- Experimental evaluation of additional prototypes.
- Analysis to determine the recovery voltage associated with a 145kV module and the overall 145kV rating.
- Conceptual design of a prototype 145kV three-phase current limiting device.

With respect to experimental evaluation, the present work indicates that future prototypes should be made with 30.5cm diameter ceramic envelopes, and with two movable electrodes to permit simulation of high speed actuation. Further, all experiments should involve a series conventional vacuum interrupter, and should be performed in a high voltage circuit which simulates one half of the recovery voltage associated with a 145kV system. Prototype variables would include electrode shape, including split electrodes to force multiple bridge points, and also electrode materials. Additional variables would be the use of saturable reactors and magnetic field waveshapes.

With respect to circuit analysis, the first objective would be to assist the experimental program by determining the recovery voltage associated with one module in a 145kV circuit. A second objective would be to establish a rating for the overall 145kV device. This would involve analysis of circuits requiring fault current limiters with due consideration of the current commutation characteristics of the device under development. The analysis would also require an assumption of the high speed actuator and the sensor characteristics. At this stage we would not recommend an exhaustive study of system interactions using, for example, analog computer studies. Rather we recommend an analysis which focusses on identifying circuit applications without determining the detailed interaction between the current limiter and the protected circuit. The rating analysis should include factors such as the location of the current limiter relative to transformers and the types of circuit devices to be protected. Other considerations should include duty cycle requirements, protection requirements, coordination with system devices, and qualitative effects on system stability.

With respect to a conceptual three-phase design, we recommend the layout of an overall 145kV current limiting device. This device would be designed to meet the rating developed from the research evaluation of prototypes, and also the circuit analysis. The layout should be performed by personnel who are familiar with the packaging of capacitor banks and vacuum apparatus. However, research personnel would have to cooperate in selecting the type of vacuum devices required for 145-kV duty. For example, it may be reasonable to use two of the 72-kV devices shown in Figure 1-2 connected in series. This would involve two transverse field devices and two conventional interrupters. A possible disadvantage with this system would be the capacitor connection to the midpoint of the two stages. The arc currents in each stage would not necessarily be equal during magnetic field application, and in particular the arcs could extinguish at different times. This would result in uneven distribution of the recovery voltage during commutation. An alternative consideration would be use of a single transverse field device in series with three conventional interrupters, with a capacitor connected in parallel with the series arrangement. The decision between these two configurations will involve analysis of the parallel circuit, layout considerations for minimizing inductance in the parallel capacitor circuit, and cost considerations. The overall layout should include the transverse field devices, the series vacuum interrupters, the magnetic field coils and associated power supplies, the capacitor banks, the insulators, and the mounting platform. Reasonable assumptions would have to be made concerning the space and power required

by the sensors and high speed actuators. The layout should include all the necessary power supplies and control circuitry for a functional device.

This recommended Phase 3 program would terminate with a final report which would summarize the progress, provide specifications which would permit the design and fabricating of a high-speed actuator, and contain a specific design of a prototype 145-kV three-phase CLD having an established objective rating.

Section 9

REFERENCES

1. C. W. Kimblin, J. G. Gorman, F. A. Holmes, J.V.R. Heberlein, P. R. Emtage, R. E. Voshall, P. G. Slade, "Development of a Current Limiter using Vacuum Arc Current Commutation; Phase 1: A feasibility study for using arc instability in vacuum for current limitation", E.P.R.I. Final Report EL-393 on Project 564-1, March 1977.

2. C. W. Kimblin, "Erosion and ionization in the cathode spot regions of vacuum arcs", J. Appl. Phys., 44, 7, pp. 3074-3081, July 1973.

3. W. D. Davis and H. C. Miller, "Analysis of the electrode products emitted by d.c. arcs in a vacuum ambient", J. Appl. Phys., 40, pp. 2212-2221, April 1969.

4. M. P. Reece, "A review of the development of the vacuum interrupter", Phil. Trans. R. Soc. London, A, 275, pp. 121-129, 1973.

5. A. N. Greenwood and T. H. Lee, "Theory and Application of the Commutation Principle to HVDC Circuit Breakers", Trans. IEEE PAS-91 (1972) pp. 1570-1574.

6. R. W. Warren, "Experiments with Vacuum Interrupters used for Large D.C. Current Interruption", Los Alamos Scientific Laboratory Informal Report, LA-6906-MS, October, 1977.

7. J.V.R. Heberlein and J. G. Gorman, "The Columnar Metal Vapor Arc under the Influence of an Axial Magnetic Field", Proc. 5th Intrnl. Conf. on Gas Discharges, Liverpool, England, pp. 281-284, September 1978.

8. C. W. Kimblin, et.al.; "Developmental studies of a current limiter using vacuum arc current commutation", Symp. Proc. New Concepts in Fault Current Limiters and Power Circuit Breakers, E.P.R.I. EL-276-SP Special Report, April 1977.

9. R. Webster, et.al.; "The Characteristic Behavior of a High Current Vacuum Arc", University of Liverpool, Arc Discharge Research Project, Report ULAP-T41, December 1975.

10. T. H. Dodds, et.al., "Development of Fault Current Limiters for Electric Power Systems (Final Report of Research Project 281-1)", EPRI Report TD-130, March 1976.

11. A. Greenwood, Electrical Transients in Power Systems, Wiley-Interscience, 1971.

Appendix A

THE PLASMA STRUCTURE

A-1 INTRODUCTION

This Appendix presents a calculation of the shape of a cylindrical plasma in a transverse magnetic field, when all the current comes from a uniform array of cathode spots aligned parallel with the field lines, as in Figure 2-1b.

The first two of the following sections treat the classical theory of conduction in a dilute plasma subject to a magnetic field, and the current distribution in a non-uniform cylindrical plasma. Subsequent sections obtain the shape and height of the plasma boundary, and some other results.

A-2 THEORY OF CURRENT FLOW

An electron in a dilute plasma subject to a reasonably large magnetic field makes many revolutions between collisions with the ions of the plasma. Consider its motion in the absence of collisions under crossed electric and magnetic fields, $\underline{E} = (E_x,0,0)$, $\underline{B} = (0,0,B_z)$; the equations of motion are

$$m\dot{v}_x = -eB_z v_y - eE_x \quad ,$$

$$m\dot{v}_y = eB_z v_x \quad ,$$

$$m\dot{v}_z = 0 \quad ,$$

where $\underline{v}$ is the electron velocity, and e and m are the electron's charge and mass, respectively. The solutions are

$$v_x = A \sin \omega_c t \quad ,$$

$$v_y = A \cos \omega_c t - E_x/B_z \quad ,$$

$$v_z = \text{const} \quad , \qquad \text{(A-1)}$$

A being a constant of integration and ω_c the cyclotron frequency

$$\omega_c = eB_z/m \quad . \tag{A-2}$$

It will be seen, from Eq. (A-1), that the electron rotates with arbitrary amplitude at frequency ω_c, and in addition drifts with a mean velocity $\bar{v}_y = - E_x/B_z$ in the y-direction, which is perpendicular to both the electric and magnetic fields; there is no current parallel with the electric field. However, when scattering occurs the electron orbit is displaced on average in the direction of the electric field; therefore, as a result of scattering, some current does flow in the direction of the electric field. The magnetic field changes our normal picture of conduction, where electron flow is parallel with the electric field and is retarded by scattering; here, no flow along the electric field would occur if there were no scattering.

Conduction under magnetic fields has been extensively investigated. If there were no magnetic field, one would have

$$E_x = \sigma^{-1} j_x$$

where $\underline{j}$ is the current density, and σ is the conductivity,

$$\sigma = ne^2\tau/m \quad , \tag{A-3}$$

n being the electron density and τ the scattering time. When a field B_z is present, one must add to E_x the electric field needed to produce the drift current $j_y = -ne\bar{v}_y$; the relation between field and current is now

$$E_x = \sigma^{-1} j_x + \frac{1}{ne} j_y B_z \quad ,$$

$$E_y = \sigma^{-1} j_y - \frac{1}{ne} j_x B_z \quad ,$$

$$E_z = \sigma^{-1} j_z \quad . \tag{A-4}$$

When there is no current along the y-direction, one has

$$E_y = -\omega_c \tau E_x = - \frac{1}{ne} j_x B_z \quad . \tag{A-5}$$

This transverse field, E_y, is the Hall field, and it acts in the right direction to cause a current to flow along the x-axis even if there were no scattering. In fact, the magnetoresistance vanishes altogether and the current in the x-direction is given by

$$j_x = \sigma E_x \quad .$$

A-3 THE CURRENT DISTRIBUTION

It will here be shown that the electron current lies in a thin layer adjacent to the retrograde edge of the plasma. Since most of the cathode spots lie near a single line along the z-axis across the cathode, we may take $j_z = 0$ provided that there are many spots. The electric fields and currents lie in the x-y plane of Figure 2-1b and the relation between them is given in Eq. (A-4). Terms involving the plasma conductivity σ are large only near the origin, where n is large.

From the quasistatic condition $\underline{\nabla} \times \underline{E} = 0$ one finds

$$\sigma^{-1} \left(\frac{\partial j_x}{\partial y} - \frac{\partial j_y}{\partial x} \right) = \frac{B_z}{en^2} \left(j_x \frac{\partial n}{\partial x} + j_y \frac{\partial n}{\partial y} \right) . \tag{A-6}$$

where the relation $\underline{\nabla} \cdot \underline{j} = 0$ has been used. Since σ^{-1} is small compared with B_z/en (except near the origin), we see that $\underline{j} \cdot \underline{\nabla} n$ must be small in most of the plasma. The current is therefore parallel with $\underline{\nabla} n$ except where $\underline{\nabla} \times \underline{j}$ is large.

Further, the condition $\underline{\nabla} \cdot \underline{E} = \rho/\varepsilon_o$, where ρ is the charge density, gives

$$\frac{\partial j_x}{\partial y} - \frac{\partial j_y}{\partial x} = \frac{1}{n} \left(j_x \frac{\partial n}{\partial y} - j_y \frac{\partial n}{\partial x} \right) - \frac{en\rho}{\varepsilon_o B_z} .$$

Therefore, $\underline{\nabla} \times \underline{j}$ cannot be large except where ρ is large or the plasma density varies rapidly at right angles to the current flow. Both conditions are met near the edge of the plasma. Nearly all of the current flow is therefore adjacent to the plasma boundary.

To find which edge supports the current we shall presume a "rigid" plasma such as that sketched in Figure 2-1b, where the plasma density is not perturbed by the current flow and the Hall field. Assume that each spot emits ions with velocity u_i isotropically into a hemisphere; on taking account of both radial and z components of velocity, and averaging along the length of the row of spots, one obtains for the plasma density

$$n = I_i/2eu_i r\ell \quad , \tag{A-7}$$

r being the cylindrical radius and I_i the total ion current emitted by a length ℓ of spots ($\ell >> r$). The plasma boundary is the plane $x = 0$, so we expect the current to be localized in this plane, with j_y the greatest component of current.

At great distances from the origin Eq. (A.6) then yields

$$\frac{\partial j_y}{\partial x} = -\frac{\sigma B_z}{en^2} j_y \frac{\partial n}{\partial y} = \frac{2\sigma B_z \ell u_i}{I_i} j_y \, \mathrm{sgn}(y) \quad ,$$

where sgn(y) is the sign of y. Therefore,

$$j_y \sim e^{x/\delta} \quad , \quad y > 0 \quad , \tag{A-8}$$

$$j_y \sim e^{-x/\delta} \quad , \quad y < 0 \quad ,$$

$$\delta = I_i / 2\sigma B_z u_i \ell \quad .$$

A more careful analysis shows that the two solutions for j_y are in fact linked; i.e., at great distances the current has the form $j_r \sim e^{-r\theta/\delta}$, where θ is the angle measured from the negative y-axis. It follows that the current is restricted to a thin skin on the "retrograde" side of the plasma.

The calculated current thickness is very small. A typical plasma conductivity is of order $3 \times 10^3 \, \Omega^{-1}\mathrm{cm}^{-1}$, and the ion velocity u_i is of order 10^6cm/sec. For a 5kA arc, I_i = 500A, on electrodes of diameter ℓ = 10cm in a field B_z = 0.05T, one obtains $\delta = 10^{-3}$cm. In practice, the spot density will not be constant along the row of spots, so j_z will not be zero; this introduces an extra term in Eq. (A-6), and weakens the above derivation. The current thickness will be greater than is calculated, and the argument has been presented primarily to show in what direction the current must flow. The actual thickness of the region occupied by the current has little effect on the subsequent discussion, provided this thickness is small compared with the interelectrode spacing.

A-4 THE PLASMA BOUNDARY

Ions initially within the region of current flow on the retrograde side of the plasma are subject to an intense Hall field accelerating them away from the cathode. The region occupied by the ions therefore bends upwards away from the cathode. Since total charge separation must be small, the sheet of electron current must also bend upwards, as in Fig. A-1a and will now intercept the trajectories of ions that were before unaffected by the current. There is a large Hall field within the region of current flow, and therefore a rapid variation in potential. The potential must be sufficient to reduce the normal component of ion velocity to zero, since otherwise ions would penetrate through the boundary

and the plasma would extend beyond its presumed limits. After falling to zero, the normal component of ion velocity is reversed, with the result that the ion is specularly reflected from the envelope.

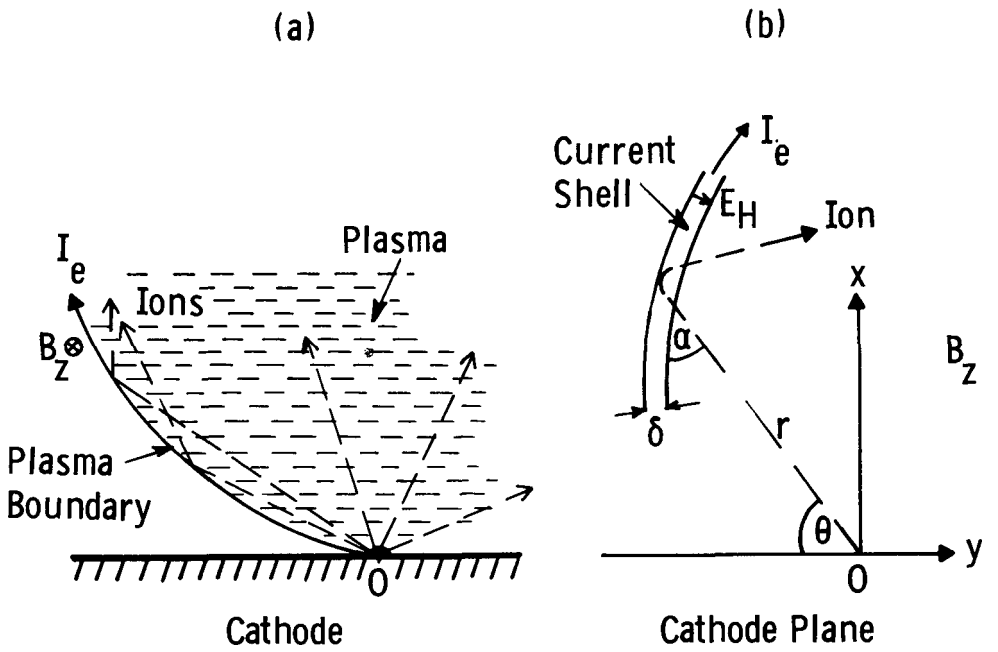

Figure A-1. (a) Bending of the retrograde plasma boundary in a magnetic field. (b) Coordinates used in calculating the plasma envelope.

In this section we shall multiply the ion density by a factor f that is intended to make allowance for multiple reflections; the factor will be calculated in the following section. This factor, which really involves momentum changes rather than densities, can be estimated in the case of a circular boundary as follows. Ions incident on the surface between θ and $\theta + d\theta$ come after 0,1,2,... reflections; those that suffer n-1 reflections were originally emitted in the range of angles between θ/n and $\theta/n + d\theta/n$, so they are fewer in number by a factor 1/n than those directly incident, and carry a normal momentum that is less by the same factor. For small angles and a circular boundary, therefore,

$$f \simeq \Sigma \frac{1}{n^2} = \frac{\pi^2}{6} \simeq 1.65 \quad .$$

More detailed calculation shows that, for a circular boundary, f changes from 1.65 to 2.5 as one goes from low to high angles of incidence. It will be taken that f is constant round the boundary, and only its mean value will be calculated.

The charge density incident on the boundary is given by Eq. (A-7); within the skin of current this density must be doubled, since each ion traverses the region twice, and also we must multiply by the factor f described above. The effective density within the region of current flow is therefore

$$n = fI_i/eu_i r\ell \quad . \tag{A-9}$$

Let an ion emitted at an angle θ to the negative y-axis meet the plasma boundary at an angle α, a distance r from the origin, as in Figure A-1b. If the potential that accelerates the ion into the plasma is V_i, the boundary potential required to reflect it from the boundary is

$$V_b = V_i \sin^2\alpha \quad .$$

The current density within a skin of thickness δ is

$$j = I_e/\ell\delta$$

The Hall voltage across the skin is therefore

$$V_H = E_H\delta = jB_z\delta/ne = I_eB_zu_ir/I_if \quad .$$

On equating this with V_b one obtains

$$r = r_H \sin^2\alpha \tag{A-10}$$

$$r_H = \frac{I_i}{I_e}\frac{V_if}{u_iB_z} \quad .$$

The solution to the equation between r and α is the cardioid

$$r = r_H \sin^2\theta/2 \quad . \tag{A-11}$$

The peak height of the envelope is reached at $\theta = 120°$, and here one has

$$x_H = \left(\frac{3}{4}\right)^{3/2} r_H \simeq 0.65\ r_H \quad . \tag{A-12}$$

When the plasma reaches this height, it has either intercepted the anode already, or it must extend tangent to the anode, with electron current crossing the gap between plasma and anode (see below).

The calculated plasma structure is shown in Figure 2-2. The plasma boundary, given by Eq. (A-11), is bent in the Amperian direction, and continues parallel with the anode after the maximum height is reached. Within it lies another calculated

curve, the envelope of all first reflections from the boundary. All reflections lie between the outer boundary and the reflection envelope, and give rise to a dense region adjacent to the boundary. Shown also in Figure 2-2 are contours of approximately constant density that were obtained by a ray tracing procedure; the densities chosen are arbitrary, and abrupt changes in density are expected only at the outer boundary and at the reflection envelope.

A-5 PLASMA HEIGHT AND THRESHOLD FIELD

The greatest height reached by the plasma can be calculated in a manner that is only weakly dependent on the geometry of the plasma boundary. This calculation is equivalent to finding the factor f that was introduced in Eq. (A-9).

In most of the plasma the conductivity σ is very great. Therefore from Eq. (A-4), the component of current normal to the cathode is

$$j_x = -neE_y/B_z = -\bar{Z}en_iE_y/B_z = -\dot{p}_y/B_z \quad ,$$

where p_y is the ion momentum in the y direction. The total electron current across any plane is $-I_e$, so on integrating j_x over all volumes up to the greatest height d_H of the plasma one obtains

$$-\int j_x d^3\underline{r} = I_e d_H = B_z^{-1} \int \dot{p}_y d^3\underline{r} \quad .$$

Therefore,

$$d_H = \dot{P}_y/I_eB_z \quad , \tag{A-13}$$

where $\dot{P}_y$ is the total rate of change of ion momentum. The total radial momentum of ions emitted at angles between θ and $\theta + d\theta$ is

$$dp_r = \frac{1}{2} \frac{I_iV_i}{u_i} d\theta \quad .$$

The geometry of the surface must now be taken into account. Ions traveling initially at an angle θ to the y-axis travel at an angle 2θ after their first reflection. The change in y-component of momentum, for first reflections, is proportional to $(\cos\theta - \cos 2\theta)$; this form for $\dot{p}_y$ holds from $\theta = \theta_o$, where second reflections occur, to $\theta = 2\pi/3$, where the surface reaches its maximum height. However, only ions for which $\theta > \theta_o$ undergo only one reflection on the rising part of the surface, the value of θ_o being approximately 75°. All other ions undergo two or more reflections and emerge almost parallel with the y-axis;

for these ions the change in momentum is $(1 + \cos\theta)$. We find

$$\dot{P}_y = \frac{I_i V_i}{2u_i}\left[\int_0^{\theta_o}(1 + \cos\theta)d\theta + \int_{\theta_o}^{\frac{2\pi}{3}}(\cos\theta - \cos 2\theta)d\theta\right]$$

and hence the plasma height is

$$d_H = 1.43\,\frac{I_i}{I_e}\,\frac{V_i}{u_i B_z} \quad . \tag{A-14}$$

On comparison with Eqs. (A-10) and (A-12), one finds that the numerical factor corresponds to $f = 2.20$, which is a reasonable value.

The threshold field B_c for the beginning of arc extinction when the electrode separation is d_o is the value of B such that $d_H = d_o$. In the case of Cu, where $V_i = 30V$, $\bar{Z} = 2$, and $I_e/I_i = 11$, one finds from Eq. (A-14)

$$B_c = 0.034/d_o \quad , \tag{A-15}$$

where d_o is measured in centimeters and B_c in Tesla.

A-6 RAPIDLY RISING MAGNETIC FIELDS

When the plasma is subject to a rapidly rising magnetic field, the boundary of the plasma contracts fast. The pressure exerted on the ions rises, partly because they gain in normal momentum through being reflected from a moving surface, and partly because their momentum must be changed in a shorter time. An approximate analysis shows that the rate of change of momentum obeys the following rule

$$\dot{P}_y(v) = \dot{P}_y(0)(1 + v\overline{u^{-1}}) \quad ,$$

where v is the rate of change of the mean length of the ion trajectories within the curved part of the boundary, and $\overline{u^{-1}}$ is the mean reciprocal of the radial component of ion velocity, $\overline{u^{-1}} = \pi/2u_i$. The length of the cardioid is $\frac{3}{2}\,d_H$, and the mean ion trajectory is somewhat shorter than this, so we obtain

$$\dot{P}_y(v) \simeq \dot{P}_y(0)(1 + 2\dot{d}_H/u_i) \quad .$$

From Eq. (A-13) one now obtains

$$B_c(\dot{B}) = B_c + \tau_f \dot{B} \quad , \tag{A-16}$$

where

$$\tau_f = 2d_o/u_i \tag{A-17}$$

is the mean time of flight of ions from cathode to anode, and B_c is given by Eq. (A-15)

A-7 CURRENT TO THE ANODE

During extinction the upper plasma boundary must be plane and parallel with the anode, as sketched in Figure 2-5. In the coordinates of Figure A-1 the boundary is

$$r = d_H/\sin\theta, \quad \theta > 120°$$

where d_H is the peak height of the plasma, which is reached at $\theta = 120°$.

The total electron current $I_e(\theta)$, which flows in a sheath parallel with the anode, must decrease as θ increases beyond 120°, because a constant current would bend the surface down away from the anode and the plasma region would become charged. From the argument leading to Eq. (A.10) we find that the sheath current required to maintain a stable boundary at d_H is given by

$$I_e(\theta) = I_o \frac{\sin^3\theta}{\sin^3\theta_1} \quad , \theta > \theta_1 = 120°.$$

where I_o is the total current from a line of spots of length ℓ.

The decrease in I_e results from a current flowing from plasma to anode. The current density is

$$j = -\frac{\partial I_e}{\ell \partial y} = -\frac{3\, I_o \sin^4\theta \cos\theta}{\ell d_o \sin^3\theta_1}$$

This is a monotonically decreasing function when $\theta > 120°$, so the peak value of j occurs at $\theta = \theta_1 = 120°$. This peak is

$$j_{max} = \frac{3\sqrt{3}}{4} \frac{I_o}{\ell d_o} \quad .$$

A-8 DISCUSSION

The above argument differs from that presented in our final report on Phase I in that the details of current flow and plasma structure are considered; the plasma height is calculated directly, rather than being estimated from the mean force on an ion. This correction is necessary, because the two calculations differ by almost a factor of three.

Appendix B

CIRCUIT ANALYSIS TO UNDERSTAND
THE MODE 4 TYPE CURRENT OSCILLATIONS

B-1 INTRODUCTION

When we are commutating relatively small currents or operating with a heavily damped magnetic field, the current in the sealed device is usually forced directly to zero. This is called a Mode 1 type of commutation and is illustrated in Figure B-1. When the

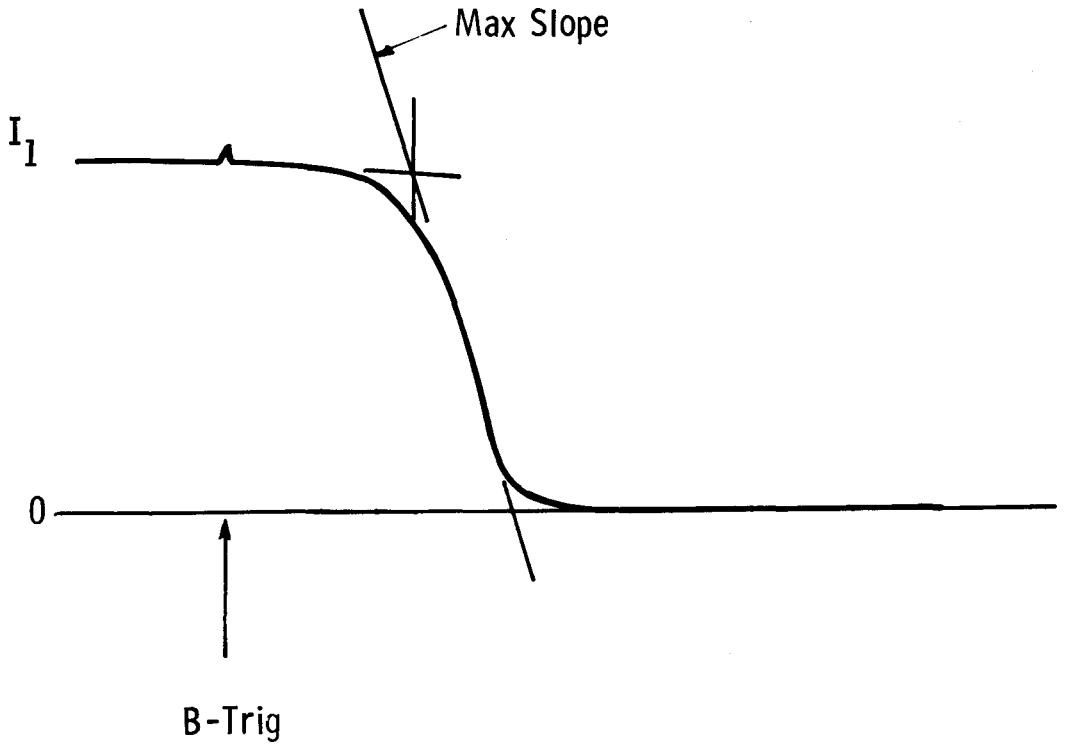

Figure B-1. Illustration of a mode 1 commutation

device is new, or when we are using an oscillating magnetic field and are operating near the limit of the device, the arc current may fail to fall directly to zero and the current will subsequently increase. The arc current may then oscillate back towards current zero with a successful commutation on the second attempt. This is

called a Mode 4 commutation and is illustrated in Figure B-2. This process may continue a third time with the current oscillations growing until a commutation is achieved

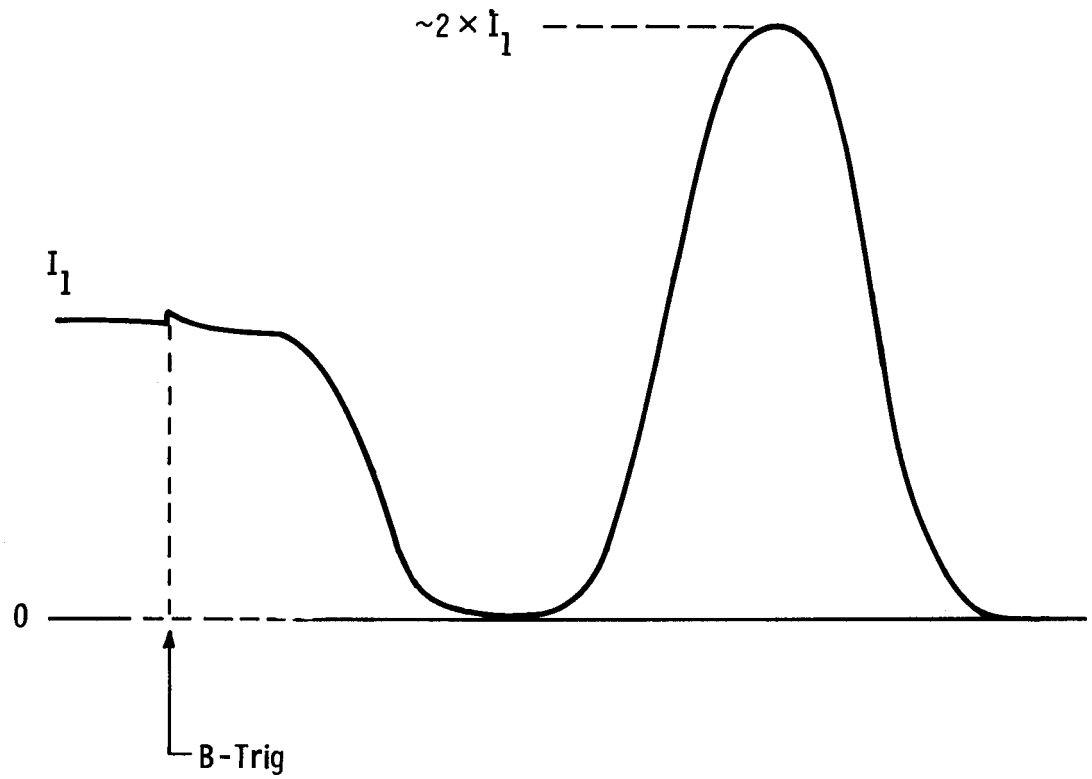

Figure B-2. Illustration of a mode 4 commutation

The oscillograms of Figure 2-11 illustrate two experiments where the current was forced toward zero three times before successful commutation was achieved. These two oscillograms are not unusual and we have occasionally seen four and five excursions before successful commutation is achieved. Greater than five excursions usually leads to a failure.

In Figure 2-11 the current crosses zero after the second excursion and again after the third excursion. The arc voltage also changes sign. The final commutation

takes place from a negative current. We have analyzed the two oscillograms of Figure 2-11 with the objective of approaching an understanding of this oscillatory phenomenon.

B-2 CIRCUIT ANALYSIS USING THE LABORATORY MINICOMPUTER

Figure B-3 shows the equivalent circuit which was used for the analysis. It is assumed that the current to be commutated, i_c, does not change during the approximately 300 microsecond period required for final commutation and that the current

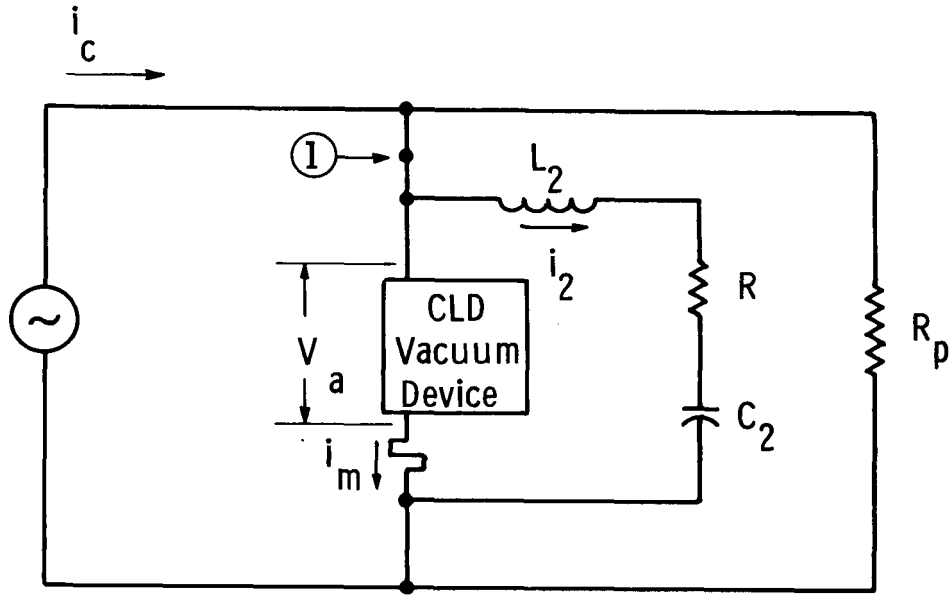

Figure B-3. Equivalent circuit used for the analysis where i_c is the commutated current, V_a is the measured arc voltage, C_2 is the parallel capacitance and i_m is to be calculated as a function of time.

flowing through R_p is small compared with i_c during this period. We are therefore, interested in the inner circuit comprising the vacuum device, L_2, R and C_2. Here C_2 is the parallel capacitance, L_2 is the lumped representation of the inductance of the connecting leads, the measuring shunt, and the capacitor, and R is the lumped representation of the resistive components of the parallel circuit.

We obtain approximate values for the circuit parameters C_2, L_2 and R using a simple procedure. The value of the parallel capacitance, C_2, is known and is 100μF in Figure 2-11. The value of L_2 was determined by charging capacitor C_2 to a low voltage of 6V with the electrodes of the vacuum device separated and with the main circuit disconnected at point 1 of Figure B-3.

The electrodes were then closed to initiate a current i_m in the measuring shunt. An example of an oscillogram showing i_m under these conditions is shown in Figure B-4. The current, i_m, oscillates at a frequency, f, and L_2 is determined

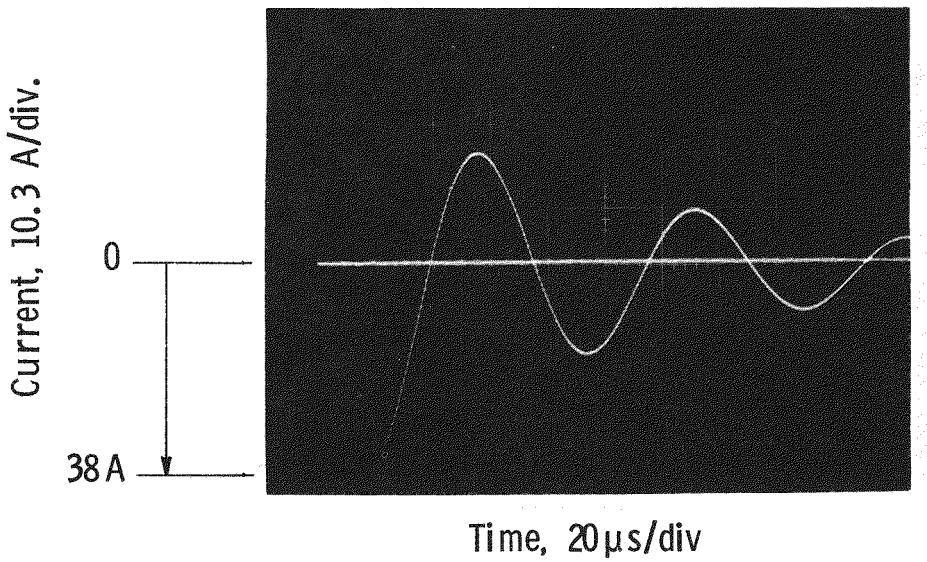

Figure B-4. Illustration of oscillating current in the external circuit, used to determine L_2 = 1.5μH and R = 29 mΩ.

from the relation:

$$L_2 = \frac{1}{(2\pi f)^2 C_2}$$

The current i_m decays with time, and this permits calculation of R where:

$$R = 2f L \ln \left(\frac{i_n}{i_{n+1}}\right)$$

where i_n and i_{n+1} are the peak values of i_m from cycles n and n+1, respectively.

The differential equation for this circuit is

$$V_a = L_2 \frac{di_2}{dt} + R\, i_2 + \frac{1}{C} \int_0^t i_2\, dt \quad . \qquad \text{(B-1)}$$

We wrote a computer program which numerically integrates Eq. (B-1) using the parameters R, L_2 and C_2 obtained by the above procedure and the arc voltages, V_a obtained from our laboratory manual digitizer. Figure B-5 is a plot of the arc voltages from the upper oscillogram of Figure 2-11 obtained from the manual digitizer and used as input to the computer program. These points can be connected by

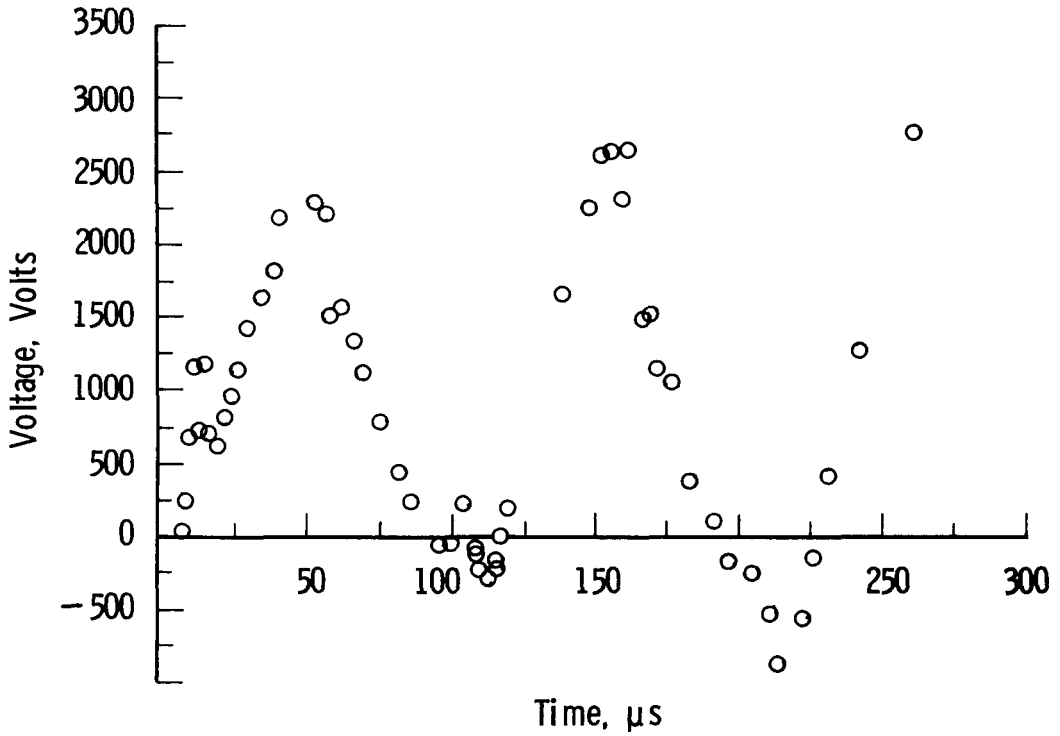

Figure B-5. Arc voltage from upper oscillogram of Figure 2-11 used as input for computer program.

straight line segments to reconstruct the arc voltage trace. Figure 2-12 shows a comparison of the calculated current compared with the measured current (symbols). Figure 2-13 shows a similar comparison for the lower oscillogram of Figure 2-11.

Examination of Figures 2-12 and 2-13 shows substantial agreement between the circuit analysis and the measured current. In the case of Figure 2-12 the computer indicates a commutated current of 8.8kA versus 8.6kA measured. Further, prior to the successful commutation, there are three excursions of current, with each excursion greater than the previous one. Finally, the calculated curves show that the current was negative on two occasions. Figure 2-12 shows some disagreement

as to the time when commutation took place (225μs vs 260μs) whereas Figure 2-13 shows excellent agreement with the time of commutation (210μs). Here the computer calculated a commutation current of 10.5kA which compares well with the 10.0kA measured. The arc functions as an oscillator to drive increasing current oscillations in the inner circuit of Figure B-3 until successful current commutation is achieved.

Appendix C

REGRESSION ANALYSIS TO OBTAIN AN EMPIRICAL MODEL FOR THE ARC VOLTAGE

C-1 INTRODUCTION

Curve fitting or regression analysis (C-1, C-2) was used to obtain an equation which represents the arc voltage as a function of important parameters. The resulting equation or model is useful for future estimation of the current behavior in another circuit. A model of the arc voltage is useful for predicting the behavior of a current limiter with a series connected vacuum interrupter, with a saturable iron core in the circuit, or with some other frequency of oscillation of the magnetic field.

C-2 ANALYSIS

The data used to understand current oscillations in Appendix B are in the form of arc voltage, V_a, current in the arc, I, and magnetic flux density, B, as a function of time. If we consider that the arc voltage is the dependent variable and current and magnetic flux density are the independent variables we can try several forms of equations to see which best fits the data. The equations which were used are

$$V_a = B0 + B1(|B|) + B2\ I \quad , \tag{C-1}$$

$$V_a = B0 + B1(|B|) \text{ and} \tag{C-2}$$

$$V_z = B0(|B|)^{B1} \tag{C-3}$$

Equation C-1 was a reasonable fit to the data with a coefficient of determination, R^2, of 0.64 and 0.81 of each of the two oscillograms in Figure 2-11. This means that the use of equation C-1 could account for 64 and 81 percent of the variance. An equation with $R^2 = 1$ would be a perfect fit to the data. After using equation C-1 we calculated the partial F statistics (C-1, C-2) for the current and for the magnetic flux density. The partial f statistics show the effect of each term in the model as if it were added last. The F statistic for the current was small indicating that it should be dropped from the model; that equation C-2 is the better choice. Equation C-2 could account for 54 and 80 percent of the variance; unfortunately the intercept at B = 0 was negative (a negative arc voltage) and significant. A negative intercept suggests an equation with curvature such as

equation C-3 would be a better fit. Taking the logarithm of both sides of C-3 we have

$$\log (V_a) = \log(B0) + B1 \log(|B|)$$

and we can use linear techniques to determine B0 and B1. The form of Eq. C-3 which fitted the logarithm of the data from the upper oscillogram of Figure 2-11 was

$$V_a = 7.8 \times 10^3 B^{1.05} \qquad (C\text{-}4)$$

and for the lower oscillogram was

$$V_a = 5.4 \times 10^3 B^{1.1} \quad . \qquad (C\text{-}5)$$

a plot of the arc voltage data along with a plot of equations (C-4) and (C-5) are presented in Figure C-1 and C-2. These equations have the advantage of a zero intercept at B = 0, but they account for only 56 and 69 percent of the variance. A

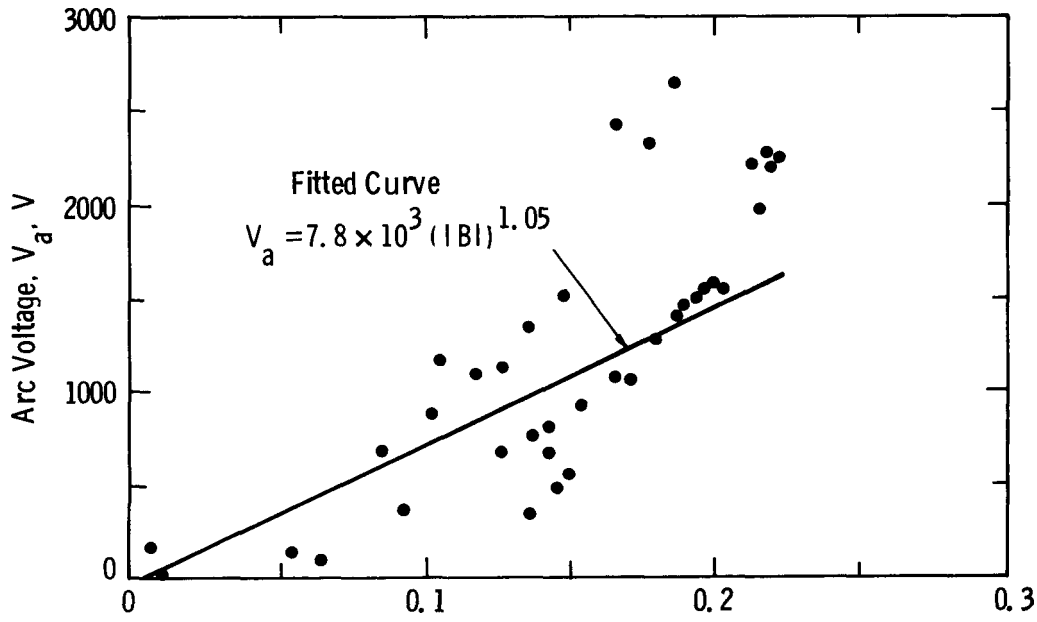

Figure C-1. Plot of the arc voltage data from the upper oscillogram in Figure 2-11 showing an early attempt to fit the data with an equation of the form $V_a = B0\ (|B|)^{B1}$.

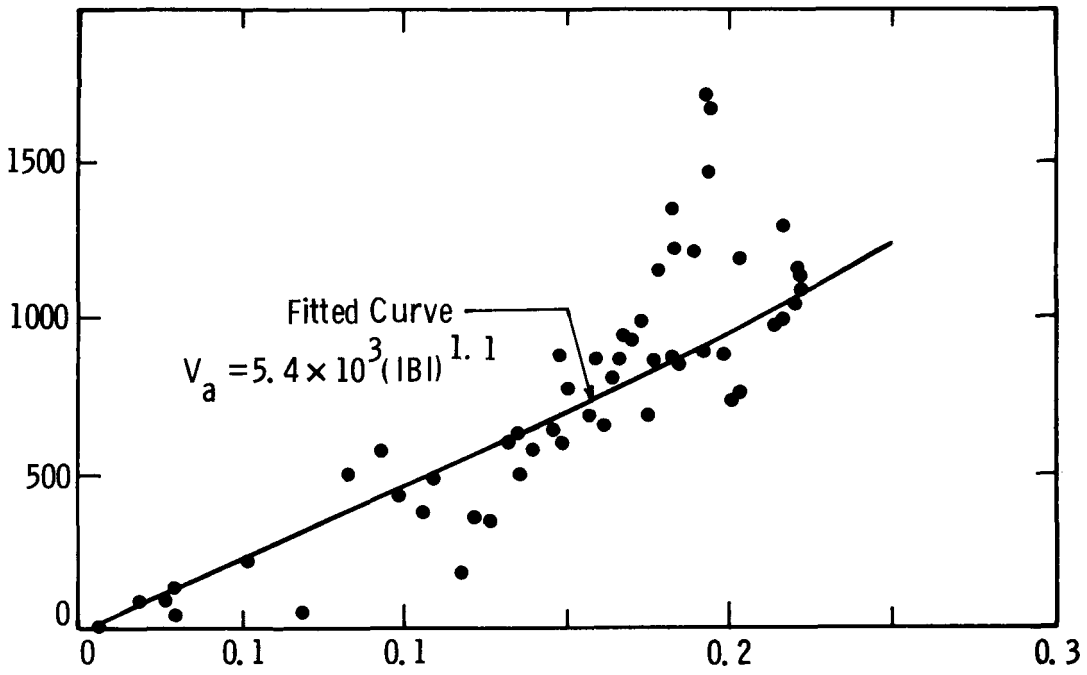

Figure C-2. Plot of the arc voltage data from the lower oscillogram in Figure 2-11 showing an early attempt to fit the data with an equation of the form $V_a = BO(|B|)^{B1}$.

non-linear regression fit to the data would improve the fit, but the scatter of the data and the lack of reproducibility from experiment suggested that a simple approach would be sufficient.

Theory predicts an equation of the form

$$V_a = BO\ B^2 \quad . \tag{C-6}$$

The B^2 term can be treated as the dependent variable and linear techniques used to determine BO. This approach works quite well and the results for the upper oscillogram of Figure 2-11 are:

$$V_a = 4.6 \times 10^4\ B^2 \tag{C-7}$$

which accounts for 67 percent of the variance results for the lower oscillogram of Figure 2-11

$$V_a = 2.8 \times 10^4 B^2 \qquad \text{(C-8)}$$

which accounts for 68 percent of the variance.

A plot of equation C-7 is compared with the data in Figure 2-14, and C-8 is compared with the data in Figure 2-15.

REFERENCES

C-1 N.R. Draper and H. Smith, Applied Regression Analysis, John Wiley and Son, N.Y., 1966.

C-2 I. Miller and J. E. Freund, Probability and Stastics for Engineers Prentice-Hall Inc. Englewood Cliffs, N.J. 1965.

Appendix D

DETAILED EXPERIMENTAL RESULTS

D-1 EXPERIMENTAL RESULTS OF PARAMETRIC STUDY USING PROTOTYPES #1 AND #2

D-1.1 Effect on Commutation to 10kA of the Magnetic Field Parameters

The schematic diagram in the upper right hand corner of Fig. D-1 illustrates the electrical circuit used for supplying the magnetic field. A capacitor bank C_3

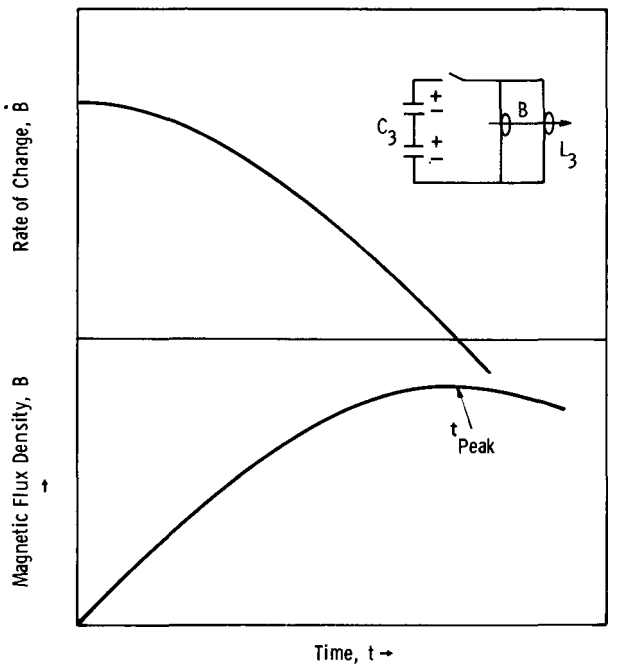

Figure D-1. Illustration of how magnetic field, B, and $\dot{B}$ change with time

is initially charged to some voltage, V_0, and at the proper time the switch is closed allowing the capacitor bank to discharge into the two coils with an inductance of L_3. The two coils are mounted on either side of the vacuum device.

The lower curve illustrates how the magnetic field, B, builds up as a function of time. It can be approximated (since the resistive component of the circuit is

is small and there is no metal surrounding the vacuum device) by

$$B \cong B_{max} \sin \omega t$$

where B_{max} is the maximum magnetic field flux density, ω is the circular frequency of the L_3C_3 circuit:

$$\omega = \frac{1}{\sqrt{L_3C_3}}$$

and t is the time. The rate of change of magnetic flux density, $\dot{B}$ is the derivative of equation (1) with respect to time:

$$\dot{B} \cong B_{max} \omega \cos \omega t$$

The value of B_{max} is directly proportional to the voltage on the capacitors in the capacitor bank. We have varied $\dot{B}$ for sealed device experiments in the past, but this has been accomplished by adjusting the voltage on the capacitor bank, C_3. Unfortunately, B_{max} is also varied by this procedure.

These experiments on two sealed vacuum devices were the first time we had varied $\dot{B}$ independently of B_{max}. We can connect the two capacitors in the capacitor bank in either series or parallel or we can connect the coils on either side of the vacuum interrupter in series or parallel. We can, therefore, vary the ratio ω between $\dot{B}_{max}$ and B_{max} by a factor of four. Table D-1 illustrates the four ways we can connect C_3 and L_3 to achieve three different levels of the two parameters $\dot{B}$ and the time to the peak B, t_{peak}. The upper curve of Fig. D-1 illustrates how $\dot{B}$, initially large and nearly constant, eventually falls to zero when time, t, reaches t_{peak}.

Figure D-2 illustrates the performance of prototype #1 with the 11cm diameter electrodes. The dark symbols represent the lowest failure and the open symbols are the highest success. We see that the performance increased as $\dot{B}$ was increased, consistent with earlier test data. The square symbols correspond with the test condition of the last line in Table D-1, i.e., 70μs to the peak magnetic field. The circles correspond to the first line of Table D-1, i.e., 280μs to the peak magnetic field. Here the peak magnetic field, $\dot{B}_{max}$, was larger for a given B and the performance is superior. Hence, both $\dot{B}$ and B_{max} should be large to achieve maximum performance. It should be recognized that for a given $\dot{B}$, B_{max} being large corresponds with a long duration magnetic field so that the improved performance with larger B_{max} may well be the result of the longer duration of magnetic field. The other

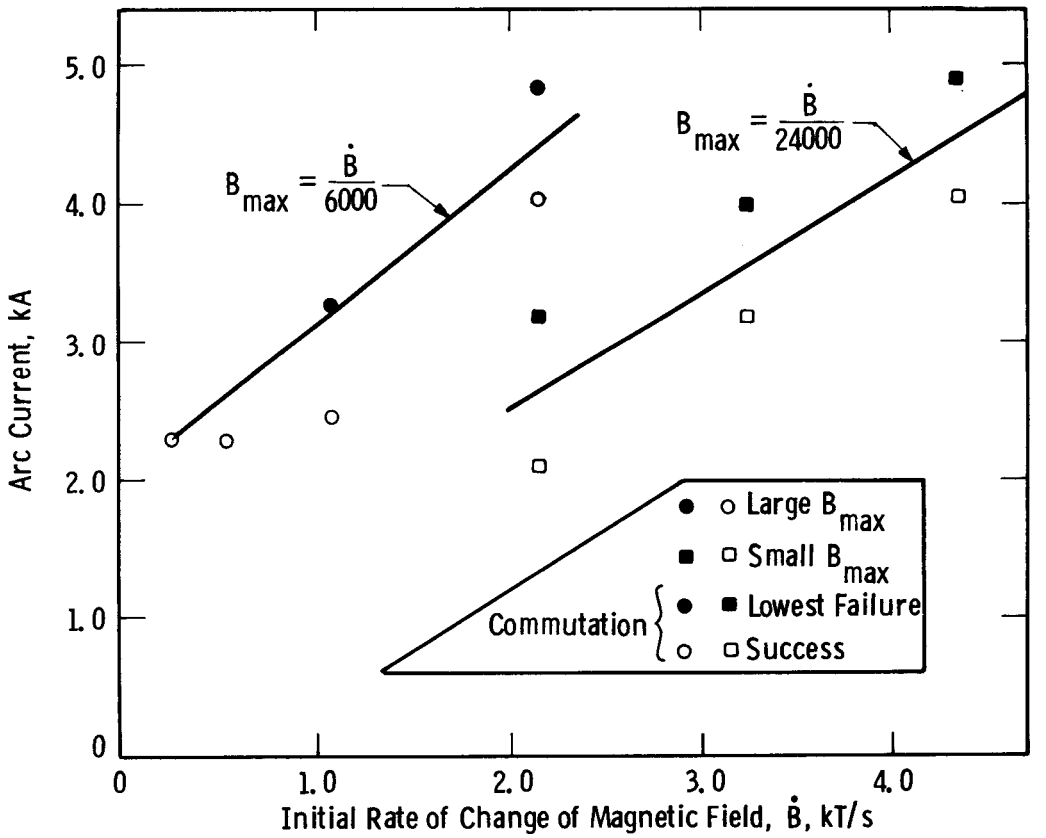

Figure D-2. Test data from interrupter #1 illustrating that both $\dot{B}$ and B_{max} should be large to achieve maximum performance, C_2 = 50μF, 11cm electrodes

two conditions described in Table D-1, where the time to peak magnetic field is the intermediate value of 140μs, produced intermediate levels of performance.

Table D-1

MAGNETIC FIELD

Capacitance	Coils	Max B, T	Max $\dot{B}$, kT/s	Time to peak B, T_{peak}, μs
Parallel	Series	0.224	1.35	280
Parallel	Parallel	0.224	2.7	140
Series	Series	0.224	2.7	140
Series	Parallel	0.224	5.4	70

Prototype #2 equipped with larger, 14cm diameter electrodes exhibited the same behavior when both $\dot{B}$ and B_{max} were varied, although we used fewer combinations of the variables. These data are illustrated in Fig. D-3 where the "Small B_{max}" data correspond to peak magnetic field being achieved in 70μs and "Large B_{max}" data correspond to 140μs. For all the data in Fig. D-3 the magnetic field coils are connected in parallel.

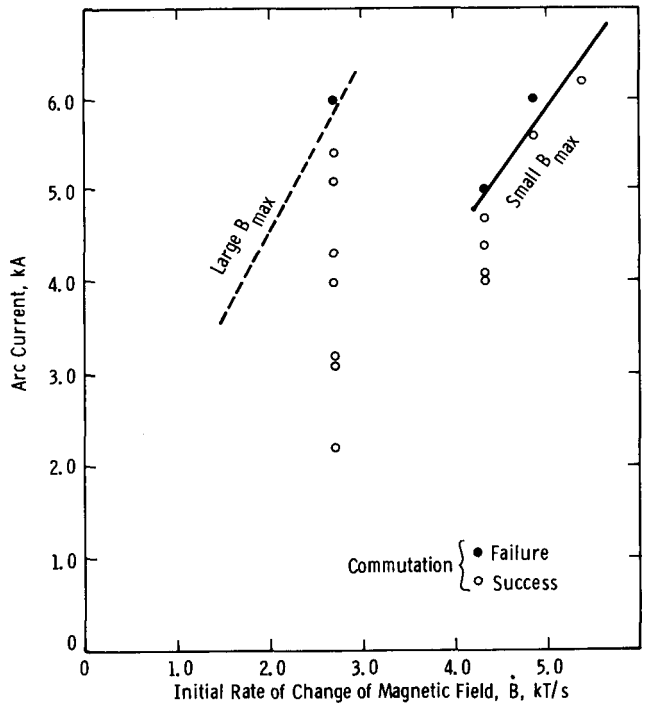

Figure D-3. Test data from interrupter #2 with 14cm dia electrodes, C_2 = 50μF

D-1.2 Effect on Commutation of Larger Capacitance and Larger Electrode Diameter

Figure D-4 illustrates how increased parallel capacitance increased the commutation ability. The slopes of the two curves both suggest the performance is proportional to the square root of capacitance. The larger electrode diameter of Prototype #2, 14cm, improved the performance. In fact a 22 percent increase of electrode diameter resulted in approximately a 35 percent increase of performance. The upper line traces the performance for the larger electrodes at a 20mm gap. At 10.4kA the greatest capability was achieved at an electrode gap of 20mm. However, when the device was operating in the vicinity of 6kA with 14cm diameter electrodes, greater performance was achieved at greater gap. The device diverted 6.2kA at 33mm gap but only 4.4kA at 20mm gap.

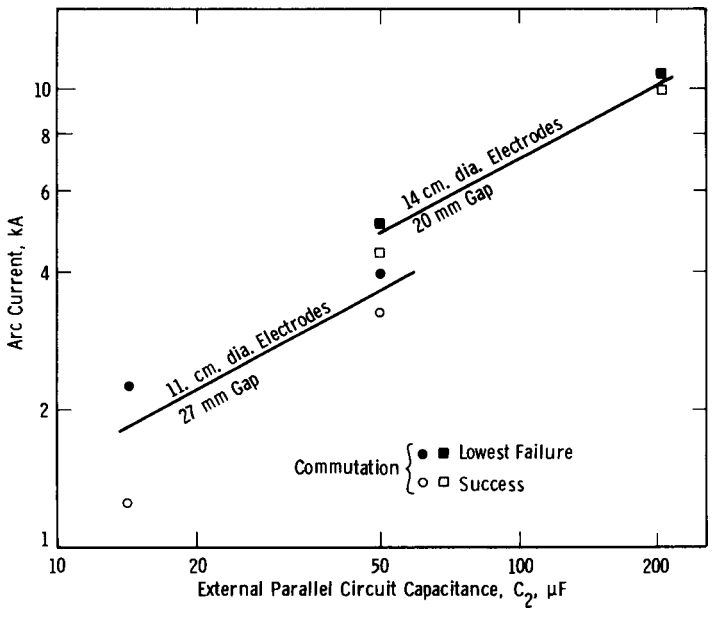

Figure D-4. Illustration of how increased parallel capacitance and larger electrode diameter both improve commutating ability

It should be noted that the sealed device with the larger electrode diameter also had larger envelope diameter. Thus, some of the increased performance could be associated with the larger envelope. A further note is that the sealed device with the larger electrodes had quite a considerable arc voltage. We observed a 500V arc voltage at 10.5kA prior to field application. Prototype #1 with the smaller diameter electrodes had arc voltages less than 50V at currents up to 6kA. The large arc voltage of interrupter #2 did not appear to impair the performance.

D-1.3 Effect of External Circuit Inductance

Past experiments and theory both suggest that reduced inductance in the external circuit will improve performance. The first experiments were conducted keeping the inductance of the external circuit to a practical minimum. As an example, copper sheets were used to connect the capacitors to the vacuum device. There are still ways to reduce inductance of the external circuit, but a reduction to 50% of its present value would be difficult. Rather than spending the time to accomplish this, we chose to deliberately increase the inductance of the external circuit. We reasoned that if the performance were relatively unchanged by doubling the inductance, no major change in commutation performance would be anticipated from a significant reduction of the inductance. Theory further suggests that the greatest inductance effect should be observed with the largest parallel capacitance.

Experimental data when the external circuit inductance was increased are shown in Fig. D-5. Note that an increase of external circuit inductance by a factor of

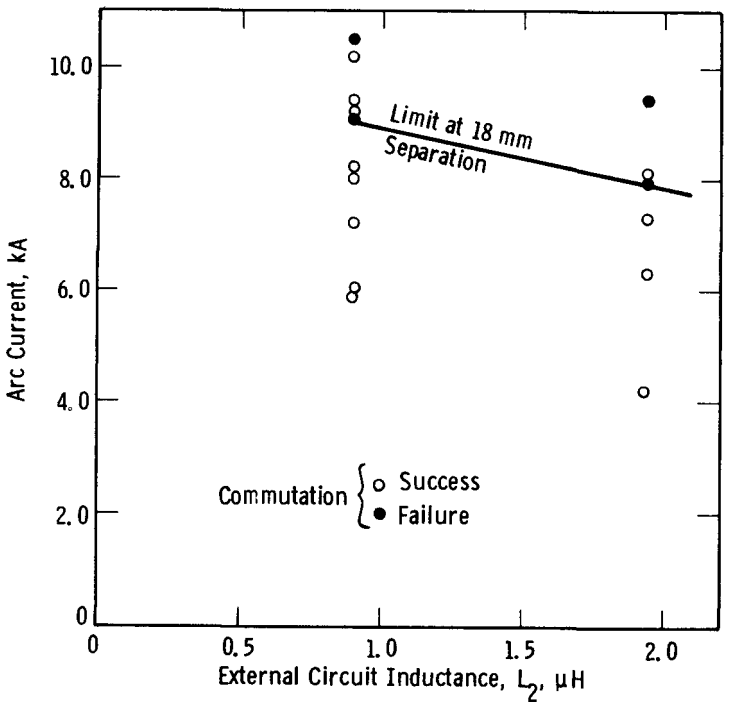

Figure D-5. Illustration of modest increase of current commutation limit when C_2 = 200μF and L_2 is decreased from 1.9μH to 0.9μH

2.1 produced only a modest decrease of current commutation limit. This suggests that reducing the inductance by half would give only a modest increase of current commutation limit at 200μF.

Figure D-6 presents data at 50μF where an increase of external circuit inductance by a factor of 3.4 had no effect. These data suggest that a further reduction of external circuit inductance would not improve device performance with 50μF of parallel capacitance. Figure D-6 also shows the effect of larger electrode separation when the current level is 6kA and the electrode diameter is 14cm. Here, larger electrode separation is beneficial.

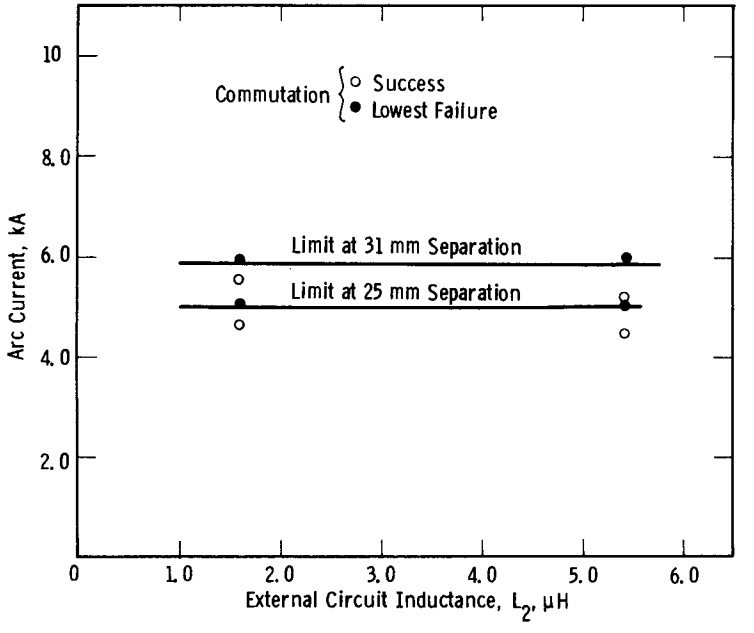

Figure D-6. Illustration that current commutation limit is not a function of external circuit inductance, C_2 = 50μF

D-2 EXPERIMENTS ON PROTOTYPE #7 WITH A PRELIMINARY ALIGNING MAGNETIC FIELD

The use of an aligning magnetic field was first proposed in the second quarter of Phase II. The concept was to apply a sub-threshold magnetic field for a short time (∿ 100μs) followed by a rapidly rising field which extinguishes the arc with current commutation. The initial aligning field was supposed to position the cathode spots prior to main field application. This concept was tested in Prototype #7 with the fields oriented in the axial direction.

The magnetic field profile was achieved using two power supplies connected to the same magnetic field coils as shown in Fig. D-7. Power Supply #1 was turned on first,

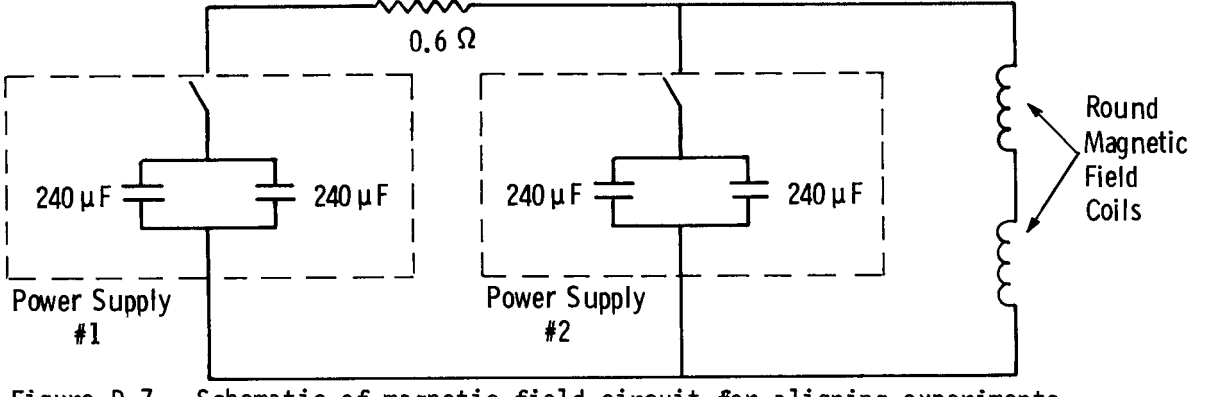

Figure D-7. Schematic of magnetic field circuit for aligning experiments

and the 0.6Ω resistor limited the current to provide a sub-threshold magnetic field, typically 27mT. After a time delay of about 100μs, the second power supply was turned on, and this supplied the oscillating magnetic field to extinguish the arc. The final magnetic field profile is shown in Fig. D-8.

The experimental objective was to apply an aligning field with a magnitude slightly below the threshold field. This threshold field is the magnitude of field required to bend the plasma out of contact with the anode with resulting arc voltage rise and arc current reduction. It was necessary to establish first the magnitude of this threshold field, and the initial experiments were therefore conducted with an

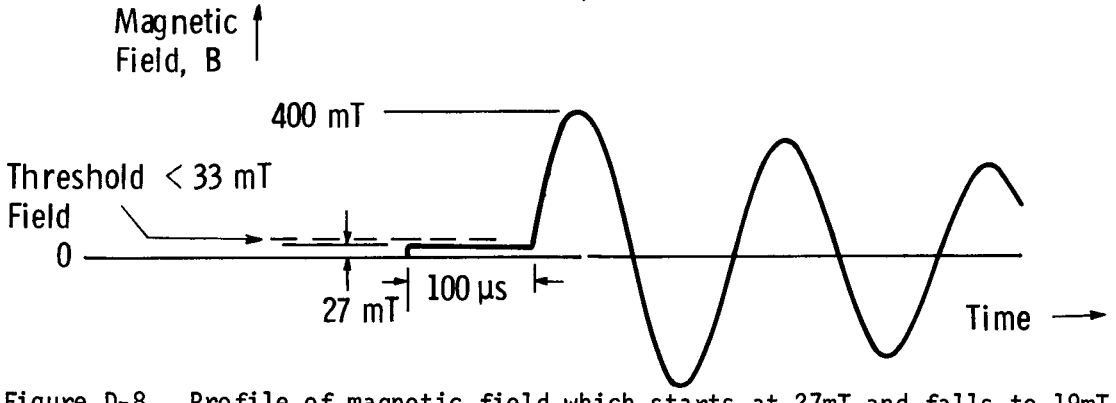

Figure D-8. Profile of magnetic field which starts at 27mT and falls to 19mT in 100μs when main field of 400mT is applied

aligning field of 33mT. This aligning field was applied without the subsequent oscillating magnetic field, and caused an arc current reduction when applied to a 5.3kA arc. The aligning field was then reduced to 27mT, and this magnitude of field did not initiate arc current commutation. Thus the threshold field had a value between 27 and 33mT which is consistent with Eq. A-15 in Appendix A.

Once the level of the threshold field had been established, the performance of the device with and without the aligning magnetic field of 27mT was established. Selected data from this series of experiments appear in Table D-2. The parallel capacitor was 50μF in all cases. It will be observed that the aligning field did not affect the device performance. Further, the commutations were mode 4 with one mode 1 commutation at 2kA.

We also investigated lower levels of the sub-threshold magnetic field (18 and 22mT) and shorter duration of the sub-threshold magnetic field (30 vs 100μs). However, neither change improved device performance.

Table D-2

Selected Data from the Aligning Field Experiments
(the profile of the field is shown in Figure 13)

Experimental Condition (Aligning field applied?)	B_{max} T	$\dot{B}$ kT/s	Mode of Commutation	Commutation Limits, kA	
				Highest Success	Lowest Failure
Yes	0.4	7.4	4	4.2	5.8
No	0.4	7.4	4	5.3	5.7

D-3 EXPERIENCE GAINED WITH SATURABLE REACTORS

D-3.1 Introduction

The method we are pursuing to limit fault currents involves a rapid decrease in the arcing current through the CLD. The desired commutation of this current into the limiting impedance can occur only if (1) the arc extinguishes when the arcing current goes to zero and (2) a deionization time is provided such that the arc does not reignite during the rising recovery voltage. Most of our experiments have relied on the transverse magnetic field to provide the deionization time. However, our data indicate that in many cases at the higher currents the time available for deionization apparently is not sufficient and that additional methods should be considered. One such method, first demonstrated by Greenwood and Lee (Ref. D-1), uses a saturable reactor to reduce the rate of change of current, dI/dt, as the current approaches zero. In effect, the amount of plasma in the vacuum gap is gradually reduced and therefore the deionization time is smaller when the current zero is reached. More recently Warren, (D-2) has shown that a saturable reactor, used in this way, can be viewed as a nonlinear impedance which isolates the vacuum device from reignition voltages during the critical deionization time. Warren further showed that the saturable reactor can be constructed in a simple manner by threading cores, wound from a 0.1mm strip of silicon steel, onto an insulated copper rod.

Our first attempt at using silicon steel cores in a CLD circuit produced a negative result (see Section 4-5.2). Some insights into this failure were gained but we felt that more experience was needed to judge whether a saturable reactor would increase the commutation ability of our CLD's. A special circuit was set up for this purpose as described below.

Figure D-9 shows a current counterpulse circuit which we used to explore the properties of the saturable reactor L_s. The circuit current, I_1, was generated in the usual way by discharging capacitor C_1 through the inductors L_1, L_s and a standard vacuum interrupter VI. The counterpulse current, I_2, was generated by discharging capacitor C_2 by means of switch S_2 which was an ignitron in this case. The counterpulse current was applied at the current crest of I_1. Since $L_1 >> L_2$, almost all of the counterpulse current flows through VI and L_s in the opposite sense to I_1. With the proper choice of initial charging voltage on the capacitor C_2, the current I_t can be forced to zero and the arc in VI can be extinguished. The current I_1 is thus commutated into C_2 which charges in the opposite direction and provides a recovery voltage across VI.

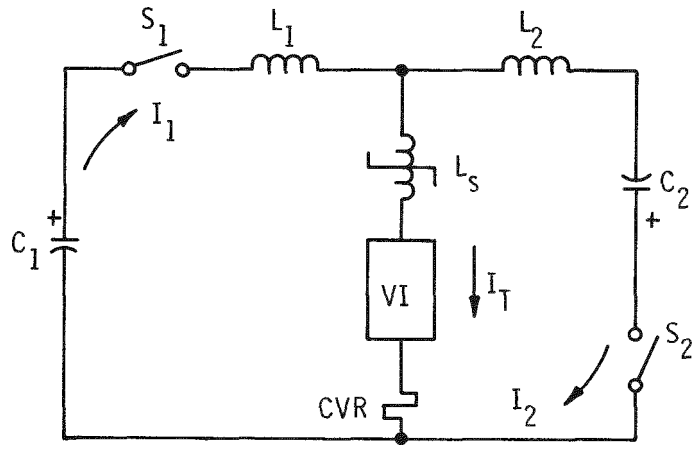

Figure D-9. Current counterpulse circuit used to explore the properties of the saturable reactor, L_s

D-3.2 Experimental Results and Discussion

A direct test was made of the saturable reactor by observing the waveform of the counterpulse current alone. Capacitor C_2 was charged to about 2kV with the contacts of the vacuum interrupter remaining closed, and the resulting oscillatory current was recorded by means of the current viewing resistor, CVR. Figure D-10a shows the

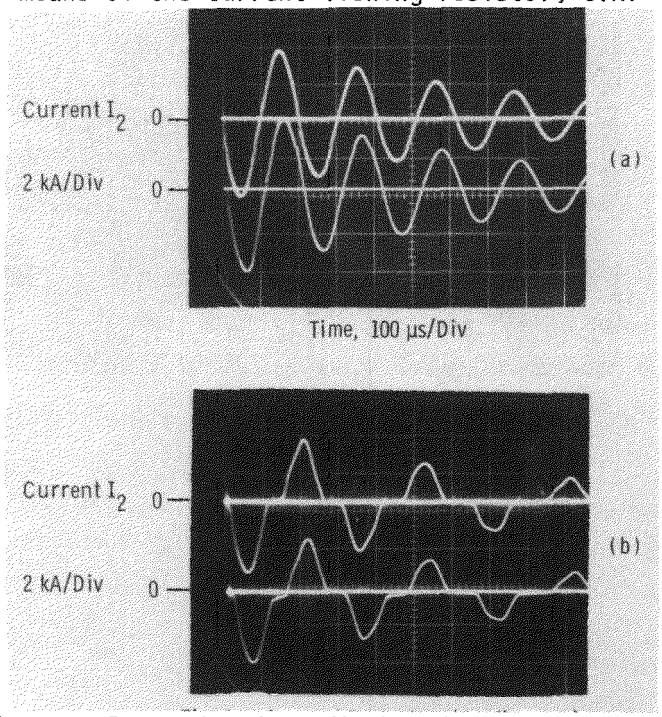

Figure D-10. Current I_2 produced by discharging capacitance C_2 through inductor L_2 and closed V.I. when (a) L_s was shorted out, and (b) L_s was a part of the resonant circuit

current I_2 when L_s was shorted out of the circuit. A decaying oscillatory current is seen having a half period of about 100μsec. With L_s in the circuit, the observed waveform is shown in Fig. D-10b. Note that the first half cycle was not affected by the presence of L_s. However, as the current approaches a low value, an abrupt decrease in dI/dt takes place that lasts for about 40μsec. Since the voltage on the capacitor, C_2, was about 2kV at this time, the now unsaturated L_s exhibits a flux change, $\Delta \phi = V \Delta t$, of $(2 \times 10^3 V)$ $(40 \times 10^{-6}$ sec) = 0.08 V-sec or 0.08 Webers. This agrees well with the value calculated for the mass of iron used. When the iron became saturated the current again oscillated for a half cycle followed by a slightly longer dwell time since the voltage on C_2 was now somewhat smaller. This behavior continued as the current decayed.

Two questions are raised by the oscillograms of Fig. D-10. First, the upper and lower traces of Fig. D-10b do not agree in all details of the current behavior around current zero. This is because the upper trace was recorded differentially while the lower trace was recorded single ended. Second, the current traces show a good deal of harmonic distortion following the first half cycle. The reason for this distortion should be investigated in future experiments.

Figure D-11 shows the effect of the saturable reactor under current counterpulse

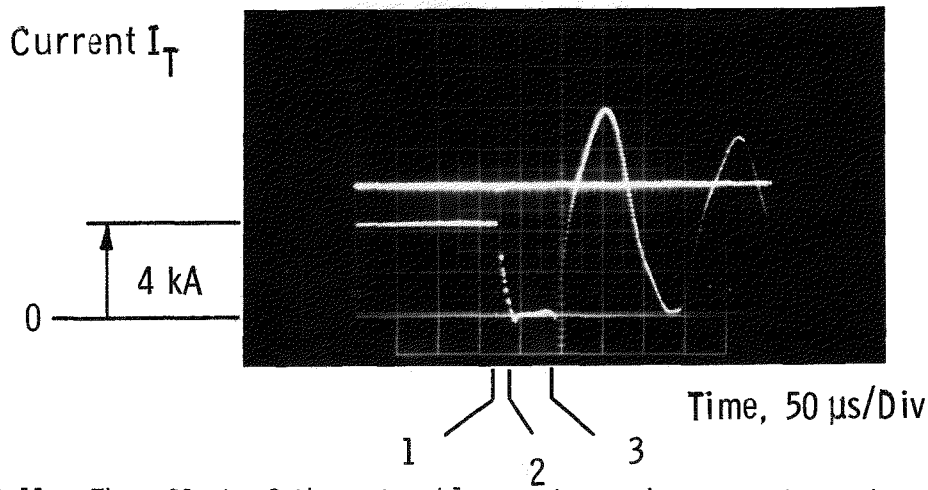

Figure D-11. The effect of the saturable reactor under current counterpulse conditions with VI closed; the current is held near zero for about 50μsec

conditions. Again the contacts of the vacuum interrupter remained closed. A circuit current of 4kA was generated by discharging capacitor C_1. At time (1) the switch S_2 was closed and current I_2 flowed counter to I_1 in L_s. A current zero was produced at time (2). From time (2) to (3) the saturable reactor remained

in its unsaturated state and produced a dwell time of about 50μsec. At time (3) the iron cores came out of saturation and an oscillatory current followed. The 50μsec dwell time agrees with calculations based on a flux change of 0.08 Webers.

Figure D-12 shows an oscillogram of a 7kA current through the arcing VI that was

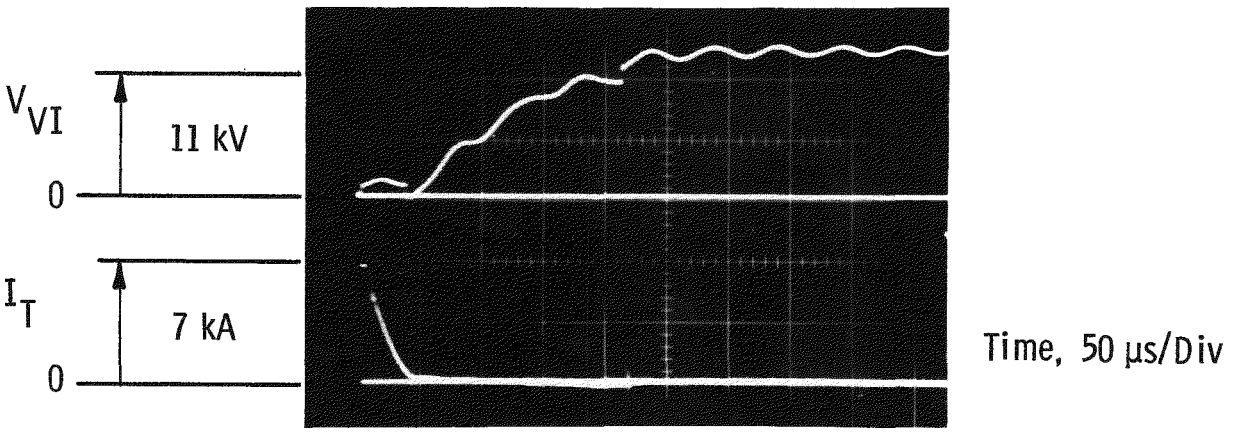

Figure D-12. An arcing current in VI of 7kA was counterpulsed to zero in about 30μsec; the recovery voltage across the vacuum interrupter reaches a peak of 11kV

counterpulsed to zero in about 30μsec. The saturable reactor was in the circuit for this test. Currents as high as 20kA were successfully forced to zero, with current commutation into the parallel capacitor, using this same circuit.

D-3.3 Conclusions and Recommendations

The results discussed above show that a saturable reactor could be beneficial for increasing the commutation limits of our CLD's. The main benefits are (1) a much lower dI/dt as the current approaches zero (2) an increased dwell time that should allow the deionization of the arc plasma and (3) an impedance to hold off, temporarily, circuit voltages prior to current zero. These benefits should be available in our Mode 4 type of commutation each time the current is forced to a current zero by the action of the oscillating transverse magnetic field. Some disadvantages exist however. The added inductance of the saturated cores, while only a few microhenries, will decrease the resonant frequency of the external circuit and might require the use of a lower frequency for the oscillating magnetic field. This in turn might mean a $\dot{B}$ lower than optimum. Further, in a practical current limiter, the effect of an in-line saturable reactor on the continuous through current would have to be considered. This could represent an energy loss, and also distort the current waveform.

REFERENCES

D-1. A. N. Greenwood and T. H. Lee, "Theory and Application of the Commutation Principle to HVDC Circuit Breakers", Trans. IEEE PAS-91 (1972) pp. 1570-1574.

D-2. R. W. Warren, "Experiments with Vacuum Interrupters used for Large D.C. Current Interruption", Los Alamos Scientific Laboratory Informal Report, LA-6906-MS, October, 1977.